UNIVERSIDADE FEDERAL DO RIO GRANDE DO SUL
CURSO DE PÓS-GRADUAÇÃO EM GEOCIÊNCIAS

Metalogênese dos depósitos hidrotermais de metais-base e Au do Ciclo Brasiliano no Bloco São Gabriel, RS.

Marcus Vinícius Dorneles Remus

Orientador:

Dr. Léo A. Hartmann

Comissão Examinadora:

Dr. Jair C. Koppe (Escola de Engenharia - UFRGS - RS)

Dr. Jorge S. Bettencourt (IG - USP - SP)

Dr. Moacir B. Macambira (IG - UFPA - PA)

Tese apresentada como requisito parcial para obtenção do título de Doutor em Ciências

1999

Remus, Marcus Vinícius Dorneles
Metalogênese dos depósitos hidrotermais de metais-base e Au do Ciclo Brasiliano no Bloco São Gabriel, RS. / Marcus Vinícius Dorneles Remus - Porto Alegre : UFRGS, 1999.
170 p. il.

Tese (Doutorado) - Universidade Federal do Rio Grande do Sul. Instituto de Geociências. Curso de Pós-Graduação em Geociências, Porto Alegre, RS - BR, 1999.

1. Geoquímica. 2. Metalogênese 3. Depósitos Hidrotermais. 4. Geoquímica Isotópica 5. Sulfêtos de Cobre. 6. Fonte dos Metais.7. Geocronologia SHRIMP I. Título.

Catalogação na Publicação
Renata Cristina Grün CRB10/1113

Dedicação:

À esposa Rosimeri, à minha família e às pessoas que torceram para que esse trabalho tivesse êxito

A formulação e finalização dessa tese foi um desafio constante ao longo destes anos pois em vários momentos defrontei-me com fronteiras desconhecidas, aparentemente insuperáveis. Os limites pessoais foram na medida do possível superados com esforço e muito suor. No final o produto da recompensa: a tese pronta para a crítica... , e também o aprendizado de uma coisa que não falha nunca: aprender.... aprender tudo que for possível aprender das ciências nesta vida e nas próximas vidas, durante talvez 2000 anos, até chegar a hora de começar a tarefa de compreender porque habitamos a terra...

SUMÁRIO

AGRADECIMENTOS

A elaboração dessa tese foi possível graças ao apoio de diversas pessoas e instituições que de alguma maneira contribuiram para a sua construção.

À esposa Rosimeri pela paciência, companheirismo e apoio incansável nas diversas tarefas e desafios enfrentados durante o desenvolvimento desse trabalho.

O autor agradece ao Conselho Nacional de Desenvolvimento Científico e Tecnológico-CNPq pelo apoio financeiro na concessão do Doutorado Sanduíche na The University of Western Australia (Processo nº 201393/94-8) sem o qual esse trabalho não teria sido possível.

Ao orientador Prof. Dr. Léo A. Hartmann pelo apoio, sugestões, críticas, e por ter me incentivado a redigir a tese na modalidade integração de artigos científicos.

Aos colegas do Departamento de Mineralogia e Petrologia, do Instituto de Geociências e da Reitoria da UFGRS pelas facilidades de tempo concedidas e pelo apoio ao afastamento do país para o desenvolvimento do Doutorado Sanduíche.

Ao Prof. David I. Groves pela auxílio no planejamento do trabalho desenvolvido na The University of Western Australia - UWA e pelas críticas, discussões e sugestões durante a redação dos artigos científicos.

Ao Prof. Dr. Neal J. McNaughton pela orientação e apoio durante todo o período de trabalho na The University of Western Australia, e em especial pela iniciação no equipamento SHRIMP e na sistemática Pb/Pb.

Ao Prof. Dr. Ian R. Fletcher pela orientação no treinamento para operação do equipamento SHRIMP e tratamento dos dados isotópicos obtidos.

Ao Prof. Dr. Brendon Griffin do Centre for Microscopy and Microanalyses da UWA pela iniciação no manuseio do Microscópio Eletrônico de Varredura.

Ao colega Dr. Jayme Leite pelo oportunidade de acompannhar as seções de treinamento no equipamento SHRIMP na Austrália e pelo auxílio na coleta de amostras.

À laboratorista Marion Dahl da UWA pelo apoio nos procedimentos analíticos para SHRIMP e isótopos radiogênicos.

Ao Prof. Dr. Paul Potter pelo incentivo e revisão dos manuscritos em língua inglesa.

Aos geólogos da Companhia Brasileira do Cobre (CBC): José L. Reischl e Nilson T. Dorneles pelo apoio no acesso a relatórios, amostras de minério e testemunhos de sondagem dos depósitos e prospectos da região de Caçapava do Sul, e pelas críticas e discussões; Luís L. Forgiarini pelo auxílio nos trabalhos de coleta de amostras na mina subterrânea e a céu aberto dos depósitos do Camaquã; Carlos M. Iglesias pelas discussões e apoio nos trabalhos de campo nos depósitos de Santa Bárbara, Faxinal, Bloco do Butiá e Cerro Rico.

Aos demais membros da equipe de prospecção e pesquisa da CBC pelo apoio nos trabalhos de campo e descrição de testemunhos de sondagem.

Ao geólogo Maurício Ribeiro pelo incentivo e apoio incondicionais ao desenvolvimento dessa tese.

À Profª Dra. Tamar Gallembeck (IG-UNESP - Rio Caro, SP) pelo apoio na preparação de amostras para análise de zircão.

Ao M.Sc. Víter M. Pinto pelo auxílio nos trabalhos de campo e na coleta de amostras para separação de zircão.

Aos geólogos Edu L. dos Santos e Carlos Maciel Filho, ambos do DNPM, pelo apoio ao acesso a mapas e relatórios sobre a geologia e metalogenia da região de Caçapava do Sul.

Ao geólogo João Castro (Laboratório de Polimento-IG-UFRGS) pelo apoio na confecção das lâminas delgadas e secções polidas e ao funcionário Renato (Difratometria de Raios X - CPGq-IG-UFRGS) pelo apoio na preparação de amostras.

I - INTRODUÇÃO

OBJETIVOS

O objetivo desta tese é demonstrar a origem dos depósitos de metais-base e Au do Bloco São Gabriel, localizados no setor oeste do Escudo Sul-riograndense. Os trabalhos enfocaram especificamente os depósitos de metais-base do sistema Camaquã-Santa Maria e mineralizações hospedados pela Formação Passo Feio na região de Caçapava do Sul (Andradas, Santa Bárbara, Faxinal, Coronel Linhares e Cioccari), além da jazida de Au da Bossoroca na região de São Sepé. Adicionalmente foram realizadas correlações com os depósitos do Bloco do Butiá (Au) e Cerro Rico (Cu-Au) da região de Lavras do Sul. A apresentação do problema, os resultados e as conclusões estão divididos em quatro capítulos enfocando cada uma das três áreas.

Os depósitos do sistema Camaquã-Santa Maria e Bossoroca foram os mais estudados nos trabalhos anteriores enquando que as mineralizações na Formação Passo Feio possuem menos informações disponíveis. As correlações anteriores entre os depósitos, em escala regional, basearam-se em observações de campo, petrográficas e de modo limitado, utilizando-se de imagens de satélite. Assim, as hipóteses genéticas propostas anteriormente careciam de parâmetros que permitissem a comparação entre os diferentes depósitos e a formulação de modelos integrados com maior precisão.

A determinação de idades U/Pb em zircão pelo SHRIMP - "Sensitive High Resolution Ion Micro Probe" (Microssonda Iônica de Alta Resolução) das rochas regionais combinado com determinações de isótopos de Pb dos minérios possibilitou estimar as idades dos depósitos estudados nas três áreas. Assim, tornou-se possível formular pela primeira vez, correlações baseadas nas idades dos diferentes depósitos, na assinatura isotópica de cada um e também das rochas regionais. A combinação destes dados permitiu situar temporalmente os depósitos estudados em relação as rochas encaixantes e regionais além de identificar o ciclo geotectônico em que foram gerados. As informações dos isótopos traçadores de proveniência (Pb, Nd e Sr) demonstram o envolvimento da crosta continental antiga (embasamento) e da crosta juvenil Brasiliana como regiões fonte para os depósitos de metais base e de Au,

respectivamente. As novas informações, detalhadas nos Capítulos II, III e IV, combinadas com aquelas extraídas dos trabalhos anteriores permitem finalmente o enquadramento dos depósitos estudados na classificação moderna dos depósitos hidrotermais.

METODOLOGIA

Para atingir os objetivos e os resultados mencionados utilizou-se a combinação de diferentes metodologias envolvendo: (a) revisão dos mapas geológicos nas escalas 1:250.000 e 1:50.000 da região de Caçapava do Sul e São Sepé; (b) mapeamento geológico complementar e revisão de mapas existentes nas escala 1:25.000 e 1:10.000 junto aos depósitos estudados, e coleta de amostras para análises utilizando os materiais convencionais de geólogo de campo; (c) petrografia das amostras estudadas envolvendo identificação dos minerais transparentes e opacos e texturas relacionadas através do uso de lupa binocular estereomicroscópica e microscópio petrográfico binocular; (d) geocronologia absoluta pelo método U/Pb em zircão através do SHRIMP; (e) determinação da composição isotópica do Pb em sulfetos, feldspatos e rocha total; (f) determinação da composição isotópica do S em sulfetos; (g) determinação da composição isotópica do Sr em baritas. Os três primeiros itens foram desenvolvidos no Brasil e os últimos quatro foram desenvolvidos na Austrália durante o Programa de Doutorado Sanduíche, realizado na The University of Western Australia, Perth, no período de junho/1995 a fevereiro/1997 com o apoio do CNPq.

Geocronologia SHRIMP

O SHRIMP é uma microssonda iônica de alta resolução de massa. Este equipamento é também denominado de "Microssonda Longa" pois possui grande raio de curvatura do espectrômetro de massa acoplado, de modo a permitir a separação de massas de elementos de peso atômico muito semelhantes. Embora possa ser utilizada para analisar virtualmente todos os elementos da tabela periódica de materiais naturais e artificiais, a sua aplicação mais importante em geologia é na geocronológica U/Pb do zircão. Além do zircão, outros minerais tais como titanita, xenotímio, badeleíta, apatita e alanita também podem ser

datados com precisão pelo métoto U/Pb através do SHRIMP, desde que possuam teores de urânio adequados. As principais vantagens do uso do SHRIMP para datação de zircão e outos minerais são: (1) a sua natureza não destrutiva, permitindo a observação dos locais analisados após a efetuação dos testes, possibilitando a repetição de análises no mesmo cristal; (2) a pequena área analisada com cerca de 20-30μm de diâmetro máximo permite, em grãos de tamanho adequado, a datação de porções diferentes do mesmo cristal; (3) a ausência de manipulações com reagentes químicos para dissolução dos minerais o que exigiria reagentes puríssimos e laboratórios superlimpos, e (4) a rapidez relativa das análises efetuando-se em média 30-40 análises por dia.

PREPARAÇÃO DAS AMOSTRAS

As amostras frescas coletadas durante os trabalhos de campo consistiram de cerca de 5 à 10 kg para os granitóides e cerca de 30 à 40 kg para as rochas metamórficas. O material coletado foi incialmente quebrado em peças menores com o auxílio de marretas e martelos. As peças selecionadas foram britadas no britador de mandíbulas e depois moídas em moinho de anel; o material moído foi passado numa peneira de nylon de malha 80. A porção que passou na peneira de malha 80 foi lavada em água de torneira, decantando-se a fração argilosa. A amostra resultante, foi seca e então passada no líquido Bromofórmio para separação dos minerais pesados. Os minerais magnéticos foram inicialmente separados com ímã de mão e posteriormente com o auxílio do separador magnético isodinâmico Frantz. A fração não magnética foi processada com di-iodo metano com o auxílio de uma centrífuga. Os zircões foram separados manualmente com o auxílio de uma lupa binocular e estilete de ponta fina. Cerca de 80 a 100 grãos de zircão foram finalmente montados, com seu eixo maior paralelo à superfície, sobre um disco de epoxy de 1 polegada de diâmetro, junto com fragmentos do zircão do padrão CZ3 que possui idade de 564 Ma (Pidgeon et. al., 1994). A secção foi polida de modo a desgastar até aproximadamente metade do grão deixando exposto para análise, idealmente, a sua outra metade. Em seguida, todos os grãos foram fotografados em luz transmitida e refletida para elaborar um mapa de localização dos grãos para a análise posterior. As amostras do bordo e do núcleo do Granito Lavras, dos dois fácies do Granito São Sepé e da

Formação Passo Feio (CERR e SBG) foram processadas preliminarmente (até a fase da separação magnética) no Laboratório de Separação de Minerais da UNESP, Rio Claro-SP. Os demais procedimentos foram todos realizados nos laboratórios da UWA, Perth, Austrália.

Adicionalmente, obteve-se imagens de elétrons retro-espalhados (back-scattered - BSE) e de cátodo-luminescência (cathodoluminescence - CL) dos grãos individualmente, através do uso do microscópio eletrônico de varredura (scanning electron microscope - SEM), de modo a permitir o estudo da estrutura interna dos zircões e conseqüentemente a seleção de áreas dentro do grão a serem analisadas. As imagens de microscópio eletrônico foram obtidas no equipamento SEM-JEOL do Centre for Microscopy and Microanalysis da University of Western Australia. A secção foi finalmente limpa, seca e coberta com uma película de ouro puro (99,99%) objetivando fornecer condutividade para a amostra.

CONDIÇÕES INSTRUMENTAIS DO SHRIMP

O equipamento utilizado neste trabalho para obtenção dos dados geocronólogicos é o SHRIMP II, localizado na Curtin University, Perth, Australia, o qual utiliza procedimentos analíticos para o zircão, similares ao do equipamento SHRIMP I da Research School of Earth Sciences, Canberra, Australia. Tais procedimentos analíticos e condições intrumentais para o zircão foram modelados por Compston et al. (1984) e Williams & Claesson (1987).

As condições de operação envolvem a focalização de um feixe de íons primário de O^{-2} de 1,6-3,0 nA de modo a extrair um pequeno volume da amostra, gerando um sulco de forma elíptica de aproximadamente 25 X 20 μm no zircão analisado. Antes da análise, o feixe de íon primário é alargado e acionado por cerca de 2-5 minutos, sobre uma área maior do que a área a ser analisada, visando remover as impurezas de Pb eventualmente existentes na superfície da amostra. Os dados gerados em cada ciclo de análise nas amostras de zircão e no padrão, constituem nove leituras cada. As espécies analisadas em cada leitura e o tempo de contagem em segundos (entre parênteses), na ordem de obtenção são: Zr_2O (2 s), Pb^{204} (10 s), "Back-ground", Pb^{206} (10 s), Pb^{207} (30 s), Pb^{208} (10 s), U^{238} (5 s), $Th^{232}O^{16}$ (5 s), $U^{238}O^{16}$ (2 s). A análise final é o resultado da obtenção destes dados em sete ciclos consecutivos e

demanda em média 17 minutos. O tempo de contagem para o Pb^{207} em amostras do Proterozóico superior e Fanerozóico é de 30 s e para as amostras mais antigas é de 40 s. Os demais detalhes de procedimentos analíticos e de calibração são similares aos descritos em Smith et al. (1998).

OBTENÇÃO E TRATAMENTO DOS DADOS SHRIMP

Durante uma sessão completa de 24 horas são realizadas entre 30 a 40 análises da amostra e aproximadamente 12 a 18 análises do padrão. A leitura do padrão é feita no intervalo entre três ou quatro determinações da amostra para vereficar a reprodutibilidade dos resultados e calcular as idades dos zircões da amostra em relação ao padrão.

Os dados obtidos foram corrigidos pelo Pb comum através do método do Pb^{204} (Compston et al.,1984). As correções de Pb comum das amostras foram calculadas a partir do Pb^{204} medido nos zircões e pela composição isotópica do Pb de Broken Hill. Os dados U/Pb finais baseiam-se nos resultados obtidos no padrão CZ3 e nas observações empíricas da correlação entre ln ($*Pb^{206}/U^{238}$) e ln (UO/U) com inclinação de 2,0. Para tais correções utilizam-se três programas (Prawn, Wallead e Plonk) desenvolvidos especificamente para redução dos dados SHRIMP e compatíveis com a plataforma Macintosh. O programa Prawn calcula a média aritmética das razões *Pb/U, UO/U e Zr/U do padrão, e verefica a probabilidade de que cada uma das sete medidas das espécies isotópicas seja incluída na reta de regressão obtida nas análises. As análises muito distantes da reta são eliminadas dos cálculos. As razões obtidas são utilizadas no programa Walled que calcula o valor do erro, em percentagem, obtido no standard, isto é, a reprodutibilidade do padrão, representando a precisão das análises (1 sigma). Todos os valores obtidos nas amostras de zircões são ajustados a esse erro e geram as tabelas de dados finais. Os dados resultantes da operação anterior são utilizados no programa Plonk que constrói o diagrama binário de Wetherill (Pb^{206}/U^{238} X Pb^{207}/U^{235}), além de fornecer as seguintes informações: a) as idades médias Pb^{206}/U^{238}, Pb^{207}/U^{235} e Pb^{207}/Pb^{206} das populações selecionadas, corrigidas pelo Pb comum, com os erros respectivos; b) o parâmetro estatístico $\chi 2$ que identifica o número de populações da amostra e que deve situar-se em

torno de valores menores ou igual a 1 para uma dada população; c) os valores das razões Pb^{206}/U^{238}, Pb^{207}/U^{235}, Pb^{207}/Pb^{206} e seus respectivos erros. No diagrama de Wetherill da Figura 1 pode-se observar a posição do polígono de seis lados, representativo de uma análise das amostras de zircão individual, que expressam as dimensões dos erros medidos para as razões Pb^{206}/U^{238}, Pb^{207}/U^{235} e Pb^{207}/Pb^{206}. Os erros nas razões isotópicas medidas são proporcionais a distância entre os segmentos de reta paralelos que formam os polígonos. A concordância das análises é tanto maior quanto mais próximo, o centro geométrico dos polígonos, estiverem da curva concórdia.

Os dados finais obtidos envolvem as idades Pb^{206}/U^{238}, Pb^{207}/U^{235} e Pb^{207}/Pb^{206}, além dos teores de U e Th em ppm. Os valores de idades utilizados são os das populações que apresentam maior concordância e menor erro. Como regra geral, utilizam-se idades Pb^{206}/U^{238} para rochas do Proterozóico superior e Fanerozóico, e Pb^{207}/Pb^{206} para as amostras mais antigas do que Proterózoico médio.

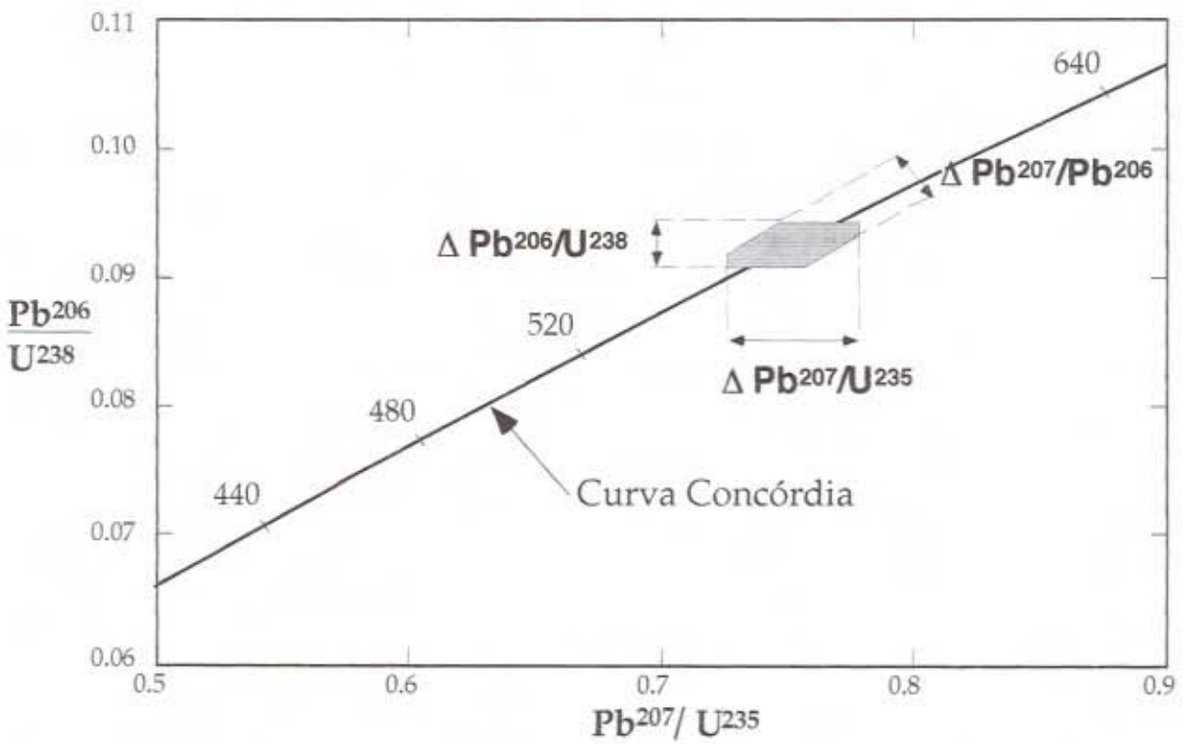

Fig. 1 Diagrama de Wetherill mostrando a localização geométrica de uma análise SHRIMP de um grão de zircão com idade concordante. As dimensões finais do polígono de seis lados são proporcionais ao erro da análise, representados esquematicamente na ilustração pelos valores de Δ (Pb/U e Pb/Pb). No exemplo a idade mais imprecisa (maior erro) é a Pb^{207}/U^{235}.

Composição isotópica do chumbo

Na natureza existem cerca de 32 isótopos de Pb conhecidos mas apenas quatro deles são importantes e possuem propriedades úteis e de aplicação na geologia; destes quatro, três são radiogênicos e produzidos pelo decaimento radioativo do Urânio (U^{238} e U^{235}) e Thório (Th^{232}) conforme observa-se na Tabela 1 (Faure, 1986; Bowen, 1988):

Tabela 1: Isótopos de U e Th radioativos e os diferentes tipos de Pb radiogênico produzidos em função do decaimento radioativo relacionados a meia-vida de cada sistema. O Pb^{204} é um isótopo estável e foi produzido durante a formação da terra.

Isótopos	Meia-vida
U^{238} ----------Pb^{206} ----------	$4,5 \times 10^9$ anos
U^{235} ----------Pb^{207}----------	$0,71 \times 10^9$ anos
Th^{232} ---------Pb^{208}----------	14×10^9 anos
Sem pai------- Pb^{204}	

Os parâmetros e equações utilizados no estudo dos isótopos de Pb são aqueles referidos em Faure (1986) e Dickin (1995) e compreendem: (a) constantes de decaimento; (b) razões isotópicas primitivas referida ao Pb contido na troilita (FeS) do Meteorito de Ferro do Cânion Diablo; (c) equações para o crescimento isotópico do Pb; (d) abundâncias relativas dos quatro isótopos e seu crescimento ao longo do tempo e (e) razões isotópicas: μ (U^{238}/Pb^{204}), ω (U^{235}/Pb^{204}), κ (Th^{232}/Pb^{204}) para diferentes modelos de crescimento isotópico.

O Pb possui uma composição isotópica bastante variável e essa propriedade é utilizada para obter informações extremamente valiosas sobre a sua fonte. O fato dos elementos radioativos (U e Th) observados na Tabela 1, decaírem para os três isótopos de Pb através de diferentes meia-vida possibilita a obtenção de três parâmetros distintos a partir do mesmo sistema. As composições isotópicas do Pb das rochas e minerais são resultantes das razões isotópicas iniciais do sistema, dos diferentes conteúdos de U e Th representados pelas razões U^{238}/Pb^{204}, U^{235}/Pb^{204} e Th^{232}/Pb^{204} e do tempo transcorrido desde o momento em que o sistema radioativo iniciou o decaimento. Tais razões combinadas com o modelamento apropriado e com a determinação da idade do

sistema, fornecem informações precisas sobre as razões U/Pb e Th/Pb das regiões fontes. Assim, o Pb é o único metal com assinatura isotópica adequada para identificar as rochas fontes dos metais em solução.

O estudo dos isótopos de Pb dos minérios e da ganga fornecem informações importantes a respeito da gênese dos depósitos de metais através do estabelecimento da fonte destes elementos. As galenas e o feldspato potássico são os melhores minerais para estimar a razão inicial do Pb de sistemas magmáticos e dos minérios, porque esses minerais possuem baixas razões U/Pb e idealmente não mudam sua composição isotópica com o tempo.

Os dados de isótopos de Pb são apresentados em diagramas binários Pb^{207} X Pb^{206} e Pb^{208} X Pb^{206} e comparados com curvas modelo de crescimento do Pb. As razões iniciais dos minerais de minério bem como dos sistemas magmáticos e/ou metamórficos em estudo são locados nestes diagramas, estabelecendo-se seus campos de variação e as superposições pertinentes.

PREPARAÇÃO E ANÁLISE DAS AMOSTRAS

As amostras frescas coletadas durante os trabalhos de campo consistiram de cerca de 2 a 3 kg para os granitóides e andesitos e cerca de 5 kg para as rochas metamórficas. O material coletado foi incialmente quebrado em peças menores com o auxílio de marretas e martelos. As peças selecionadas foram britadas no britador de mandíbulas e quarteadas em duas frações. A fração destinada a análise de rocha total foi moída num moinho de ágata para evitar efeitos de contaminação produzindo cerca de 100 gramas de pó. A fração destinada a separação de feldspatos foi moída em moinho de anel de tungstênio; o material moído foi em seguida passado numa peneira de nylon de malha 80. A porção que passou na peneira de malha 80 foi lavada em água de torneira, decantando-se a fração argilosa. A amostra resultante foi seca e então passada no líquido Bromofórmio para separação dos minerais leves. A fração leve não magnética foi processada com Bromofórmio e acetona de modo a produzir um líquido com densidade menor que o quartzo. A densidade ideal do líquido é atingida quando o quartzo do padrão afunda nesta solução e os feldspatos flotam. O grau de pureza do concentrado de feldspatos é checado com o auxílio de um microscópio

binocular e líquidos com índices de refração conhecidos. Cerca de 100 miligramas de concentrado de feldspatos são utilizados para análise isotópica.

As amostras do minério contendo sulfetos e/ou sulfatos foram quebradas manualmente num moinho de anel de tungstênio de modo a produzir fragmentos com diâmetro entre 0.1 a 2 mm aproximadamente. A amostra foi lavada em água de torneira decantando-se a fração argilosa. A amostra resultante foi seca e quarteada. Os sulfetos puros com baixo teor de Pb foram separados manualmente com o auxílio de um estilete e uma lupa estereomicroscópica até atingir cerca de 500 miligramas de concentrado puro. Cerca de 100 miligramas de concentrado de sulfetos foram pesados para posterior análise de isótopos de Pb. A separação da galena foi relativamente fácil pois um fragmento de cerca de 1 mm de diâmetro já é suficiente para a análise isotópica do Pb.

O Pb dos concentrados de feldspatos e de sulfetos além das amostras de rocha total foram extraídos através da cromatografia de troca de íons usando HBr no Laboratório livre de Pb da University of Western Australia. Os demais procedimentos químicos seguiram aqueles descritos em Ho et al. (1994). As amostras quimicamente preparadas foram analisadas no Espectrômetro de Massa VG354 na Curtin University of Technology, Perth, Western Australia. Os erros analíticos situam-se em torno de 0,15% para cada isótopo.

Composição isotópica do enxofre

Existem quatro isótopos de enxofre na natureza distribuídos da seguinte maneira: S^{32} = 95,02%; S^{33} = 0.75%; S^{34} = 4,21% e S^{36} = 0 .02%; a razão entre os dois isotópos mais abundantes S^{34}/S^{32} é utilizada na geoquímica isotópica e expressa em partes per mil relativamente ao padrão de referência da troilita (FeS) do Meteorito de Cânion Diablo (CDT) da seguinte forma (Faure, 1986; Hoefs, 1997):

$$\partial^{34}S\ ‰ = [S^{34}/S^{32}\ (\text{amostra}) - S^{34}/S^{32}\ (\text{padrão}) / S^{34}/S^{32}\ (\text{padrão})] \times 1000$$

A composição isotópica do enxofre dos sulfetos e sulfatos são utilizados para determinar a fonte do S e também como paleotermômetro; informações extremamente importantes para a interpretação da origem dos depósitos minerais a base de sulfetos (Rye

& Ohmoto, 1974; Ohmoto & Rye, 1979). Existem no planeta, três grandes reservatórios de enxofre com valores distintos de $\partial^{34}S$: (1) enxofre derivado do manto com valores variando entre -3 to +3‰ CDT; (2) enxofre da água do mar onde os valores são positivos, variam com o tempo e estão hoje ao redor de +20‰ CDT; e (3) enxofre sedimentar (reduzido) com valores variáveis e bastante negativos (Claypool et al., 1980; Chaussidon et al., 1990; Ohmoto et al. 1990).

A preparação das amostras e a separação dos sulfetos e sulfatos para análise seguiram os mesmos procedimentos descritos anteriormente para o método Pb/Pb. Cerca de 20 miligramas de sulfeto foram pesados e encaminhados para análise. As amostras de sulfetos e sulfatos foram transformadas em gás SO_2 e as análises isotópicas foram realizadas no Laboratório de Isótopos Estáveis da The Australia National University (Canberra, Australia). O erro analítico situa-se em torno de 0.10‰. Os dados de isótopos de enxofre são expressos em $\partial^{34}S$ ‰ e apresentados em histogramas de freqüência.

Composição isotópica do estrôncio

O método Rb/Sr e a sistemática Sr^{87}/Sr^{86} utilizadas neste trabalho estão baseados em Faure (1986) e Dickin (1995). A razão inicial do Sr é utilizada para traçar a fonte das mineralizações portadoras de minerais com baixa razão Rb/Sr. A razão inicial de um sistema formador de minério pode ser obtido por dois caminhos: pela intersecção de uma isócrona mineral ou rocha total com o eixo y ou alternativamente pela medida direta da razão isotópica num mineral que contenha teores muito baixos do isótopo radioativo pai. A barita além da sheelita, turmalina e estroncionita, entre outros minerais, possuem baixas razões Rb/Sr sendo minerais adequados para a determinação da razão inicial do Sr do fluido mineralizador (Kerrich, 1991).

A preparação das amostras e a separação das baritas para análise seguiram os mesmos procedimentos descritos anteriormente para o método Pb/Pb. O estrôncio foi separado das baritas no Labortório livre de Pb da University of Western Australia utilizando uma resina de Eichrom especial. Sua composição isotópica foi medida no Espectrômetro de Massa VG354 da Curtin University of Technology, Perth, Western Australia. Os valores do erro analítico para as razões medidas situam-se em torno de ±0,00010.

REVISÃO SOBRE OS DEPÓSITOS MINERAIS HIDROTERMAIS

Depósito mineral é uma concentração mineral localizadamente restrita (anômala) na crosta da terra, gerado por qualquer processo geológico em condições adequadas. Se a concentração mineral contém substâncias economicamente importantes e a concentração é rica o suficiente para garantir a sua mineração, tal depósito mineral passa a ser chamado de depósito de minério (Skinner, 1997). De acordo com o autor, os processos que produzem os depósitos de minério ricos são os mesmos que produzem os depósitos minerais não-econômicos.

Os depósitos minerais hidrotermais, ocorrem em ambientes geológicos diversificados e possuem grandes variações mineralógicas sendo em conseqüência originados por processos geológicos complexos. A conexão existente entre eles é a de que todos são originados a partir de fluidos aquosos quentes que percorreram um determinado caminho no interior da crosta e depositaram uma massa de minerais a partir da solução original mais ou menos modificada (Skinner, 1997). Outra feição comum dos depósitos hidrotermais, salientada pelo autor, é o limitado campo de minerais que eles concentram, notadamente sulfetos, que ocorrem com grande freqüência em áreas diversas, demonstrando uma consistência química entre si. Tais constatações, e o fato dos depósitos hidrotermais ocorrerem com grande freqüência em locais particulares da crosta possibilitou o seu agrupamento em famílias e a propostas de classificações em tipos distintos.

Classificação dos depósitos minerais hidrotermais

A tipologia dos depósitos minerais metálicos envolve critérios descritivos e genéticos com diversas classificações propostas por diferentes autores de modo que uma revisão histórica deste assunto foge ao escopo deste enfoque. Para comparar as características das jazidas de metais-base estudadas neste trabalho, utiliza-se as classificações modernas propostas para depósitos minerais associados a processos hidrotermais magmáticos (Hedenquist & Lowenstern,1994; Sillitoe, 1996). Os depósitos de Au constituídos por filões de quartzo mineralizado e conhecidos tradicionalmente como depósitos mesotermais, ligados ou não ao magmatismo, são classificados de

acordo com a proposição recente de Groves et al. (1998). A combinação e unificação dessas classificações, contendo os principais parâmetros geológicos e físico-químicos de cada tipo de depósito são mostradas na Tabela 2, e ilustradas nas Figuras 2 e 3, sendo descritas brevemente a seguir.

DEPÓSITOS DE PÓRFIROS

As principais características destes depósitos, baseadas nos trabalhos de Sillitoe (1996) e Hedenquist (1997), estão sumarizadas abaixo.

Os depósitos pórfiros, também conhecidos como Cobre nos Pórfiros ou Cu-Au-Pórfiro pela comum associação de rochas intrusivas com textura porfirítica e mineralizações de cobre, são constituídos principalmente por Cu, Mo e/ou Au; Mo, W ou Sn. Os depósitos de Cu-Mo e/ou Au estão localizados no topo dos plútons cilíndricos com dimensões desde aproximadamente 100 metros até cerca de vários quilômetros de diâmetro. Esses depósitos consistem tipicamente de sulfetos disseminados e em vênulas localizados dentro e adjacente a intrusões porfiríticas de composição ácida à intermediária, em profundidades entre 2-5 Km. Os "stocks" são multi-intrusivos com o minério de alto teor estando concentrado nas intrusões porfiríticas mais antigas, e em alguns depósitos, também nas rochas encaixantes. Os sistemas hidrotermais que formam estes depósitos são inicialmente muito quentes (500-600 °C), e dominados por líquidos hipersalinos coexistente com vapor de baixa densidade.

Considerável parte dos metais dos pórfiros ocorrem em vênulas de sulfetos ±quartzo em stockworks multi-direcionais que acompanham a alteração K-silicática representada pela biotita pós-magmática, e K-feldspato da porção central do pórfiro. As associações minerais de alteração são formadas à medida que os fluidos magmáticos reativos portadores de metais movem-se para fora da intrusão, resfriam e reagem com a rocha encaixante. A configuração final da zonação consiste numa zona K-silicática na porção central do plúton, dando lugar a uma zona intermediária de quartzo+clorita+albita e finalmente, na porção mais externa, a zona da sericita (sericita+quartzo+pirita). A alteração sericítica comumente superpõe-se à zona de alteração K-silicática, em muitos casos, removendo parcialmente ou completamente

os metais. As rochas encaixantes longe da intrusão podem alterar-se para epidoto+clorita+albita (zona propilítica).

Os depósitos de brecha magmática compreendem "pipes" que desenvolvem-se no interior das intrusões graníticas ou nas rochas encaixantes das proximidades; os minerais de minério cimentam os clastos das brechas ou impregnam a sua matriz constituída de fragmentos diminutos (Sillitoe, 1996). Embora existam depósitos de brecha magmática isolados, a grande maioria ocorre associado a depósitos de pórfiros e por isso são considerados aqui em conjunto com estes últimos.

DEPÓSITOS DE ESCARNITOS

Os depósitos de escarnitos originam-se através da transformação de rochas carbonáticas (principalmente) em assembléias de silicatos cálcicos ou magnesianos e minerais portadores de metais ao longo do contato ou próximos a intrusões graníticas. As intrusões graníticas relacionadas podem constituir depósitos pórfiros ou serem desprovidas de mineralização. Os escarnitos magnesianos formam associações mineralógicas à base de talco, tremolita, antigorita enquanto que os escarnitos cálcicos produzem granada andraditica, diopsídio, wolastonita e epidoto, entre outros minerais (Meinert et al., 1992; Lu et al, 1992). As assembléias minerais tardias depositadas em estágios retrógrados introduzem a maioria dos metais em conjunto com associações mineralogicas hidratadas tais como, actinolita, biotita, clorita, talco, carbonatos e quartzo (Einaudi et al., 1981). A localização dos depósitos de escarnito depende da existência de litologias favoráveis e falhamentos associados, possuindo em geral a forma "stratabound" ou controlada por fraturas e veios (Sillitoe, 1996).

Os depósitos de substituição de carbonatos situam-se em locais mais distantes dos "fronts" de escarnitos e são gerados pela interação dos fluidos magmáticos diluídos com as rochas carbonáticas, depositando sulfetos maciços ou quase maciços (Sillitoe, 1996). Tais depósitos podem ocorrer isoladamente ou associados a escarnitos e são considerados, para propósito deste trabalho, como uma variedade de depósito de escarnito.

Os graisens contém Sn, W e em alguns casos Mo, Bi ou Be acompanhados por metais-base, ocorrendo na cúpula das intrusões

graníticas e nas rochas encaixantes próximas (Sillitoe, 1996); os graisens mostram transições para depósitos de pórfiros, escarnitos e de substituição de carbonato, e embora constituam depósitos importantes são tratados para efeito de simplificação em conjunto com os escarnitos.

DEPÓSITOS DE VEIOS ASSOCIADOS A PLUTÕES

Os veios são normalmente controlados por falhas de alto ângulo que cortam as intrusões graníticas ou as rochas encaixantes. Os veios mais possantes extendem-se por vários quilômetros de extensão e podem atingir até cerca de um km de profundidade; historicamente, os depósitos de veios de alto teor foram a fonte mais importante de metais, como por exemplo o cobre no norte do Chile e Sn em Cornwall, Inglaterra (Sillitoe, 1996).

DEPÓSITOS EPITERMAIS

Depósito epitermal refere-se à uma classe de jazidas de minério hidrotermais formados a temperaturas relativamente baixas e profundidades rasas (T< 300°C; da superficie até 2 Km) (Hedenquist, 1997). De acordo com o autor, tais depósitos podem ser divididos em dois tipos principais (membros extremos) em função da mineralogia de alteração presente, a qual é conseqüência da composição química distinta dos fluidos envolvidos (Tabela 2 e Figura 2): (a) o tipo alta sulfetação, assim denominado pela presença de sulfetos em estado de alta sulfetação (enargita e luzonita), forma-se a partir de fluidos ácidos e oxidados, tendo como analogia moderna as fontes (nascentes) ácidas próximas a vulcões; estes depósitos formam-se próximos as fontes magmáticas de calor e geralmente estão espacialmente associados a Cu-Au-Pórfiros; (b) o tipo baixa sulfetação é o depósito epitermal clássico (adulária-sericita), o qual contém pirita, esfalerita e calcopirita, minerais considerados como de baixo estado de sulfetação (Barton & Skinner, 1979), ocorrendo numa posição distal em relação a fonte de calor. Esses depósitos originam-se a partir de fluidos reduzidos com pH quase neutro, similar aos sistemas geotermais.

DEPÓSITOS DE SULFETOS MAÇICOS

Os depósitos de sulfetos maciços, também denominados depósitos de sulfetos maciços vulcânico-exalativo, constituem acumulações predominantemente estratiformes de sulfetos que formam-se sobre ou imediatamente abaixo do assoalho oceânico pela precipitação de fluidos hidrotermais (Sangster, 1998). Esses depósitos ocorrem tipicamente em terrenos geológicos caracterizados pela presença de rochas vulcânicas e sedimentos derivados.

A maioria dos depósitos possuem um complexo alimentador similar a um "stockwork" no "footwall" (lapa) referido como depósito proximal devido a sua proximidade com os cones exalativos; a porção estratiforme do depósito contém > 60% de sulfetos; os sulfetos de ferro são as espécies dominantes, ocorrendo subordinadamente a esfalerita, calcopirita e a galena, e em alguns casos barita; a Ag, Au e Cd são os produtos subordinados mais comuns (Lyndon,1984; Sangster, 1998).

DEPÓSITOS OROGÊNICOS

O termo depósito orogênico foi proposto por Groves et al. (1998) para substituir a classe denominada depósito mesotermal, constituída por mineralizações de Au em veios de quartzo, hospedados por rochas metamórficas regionais deformadas. Tais depósitos ocorrem em rochas metamórficas de todos os graus, associados a orógenos acrecionais e colisionais de idades variáveis desde o Arqueano até o Terciário (Groves, 1993; Kerrich & Cassidy, 1994; Groves et al., 1998). De acordo com a profundidade de formação, os últimos autores ainda subdividem os depósitos orogênicos em: epizonais (< 6 Km), mesozonais (6-12 Km) e hipozonais (>12 Km).

Os depósitos orogênicos possuem forte controle estrutural, em geral associados a falha de grande escala, e caracterizam-se por conterem Au>Ag e As ±Te ±Sb ±B ±W associados, com baixos teores de Cu-Pb-Zn; a deposição ocorre a partir de soluções com baixa salinidade, com pH quase neutro e composição representado pelo sistema H2O-CO2 ±CH4 (Groves, 1996; Groves et al., 1998).

Origem dos depósitos minerais hidrotermais

O interesse pela origem dos metais constituintes dos depósitos minerais remonta ao século XVI, onde Agrícola propõe que a água da chuva aquecida lixiviava os metais das rochas e os transportava para o sítio de deposição do minério. Antagonicamente, Descartes propôs no século subseqüênte que o vapor que escapava do interior da terra durante a cristalização e resfriamento das rochas era o responsável pelo preenchimento de fraturas com minério (Hedenquist, 1997). Estava iniciado então a controvérsia e os debates, muitos dos quais duram até hoje, entre os Netunistas e Plutonistas. Um dos avanços notáveis nos dias atuais é o quase consenso dos geólogos envolvidos com estes assuntos, de que muitos depósitos minerais se formaram na realidade, pela mistura de fluídos de fontes endógenas e supergênicas. Tal formulação certamente deixaria perplexo os antecessores Netunistas e Plutonistas.

O entendimento global da origem de um depósito mineral hidrotermal entretanto, não é tão simples, e envolve idealmente além do conhecimento dos aspectos geológico-estruturais dos depósitos e da região em foco, os seguintes itens: (a) fontes dos fluídos (solventes); (b) fonte dos metais (solutos); (c) fontes de calor (energia para movimentar as soluções) e (d) mecanismos de transporte e deposição das soluções (causas da precipitação do minério), o qual envolve estudos das paragêneses mineralógicas dos minérios e da ganga e inclusões fluidas (Skinner, 1997).

FONTES DE CALOR

As fontes de calor são em última análise, as principais responsáveis que fazem as soluções de minério fluirem ao longo de canais gerados pela permeabilidade das rochas. As observações e medidas diretas em sistemas geotermais ativos associados à atividade vulcânica, tem permitido o esclarecimento da origem do calor e de diversos processos formadores de minério, e sua comparação e aplicação a depósitos minerais antigos (Hedenquist, 1997). Os granitóides intrusivos e corpos subvulcânicos relacionados constituem as principais fontes de calor para as mineralizações hidrotermais (Hedenquist & Lowenstern, 1994; Sillitoe, 1996 entre outros). As várias

fontes de calor magmáticas conhecidas ou inferidas, e geneticamente ou espacialmente associadas aos diferentes tipos de depósitos hidrotermais estão ilustradas na Tabela 2 e nas Figuras 2 e 3. Grande parte dos depósitos hidrotermais no entanto, não estão espacialmente associados aos corpos magmáticos geradores de calor como em alguns depósitos epitermais. Assim, a determinação de tais fontes necessita de estudos geotermométricos (paragênese mineralógica, inclusões fluidas, isótopos) do minério-ganga, do estabelecimento da idade dos depósitos e das rochas fontes potenciais além de isótopos traçadores.

Os depósitos minerais hidrotermais são feições pequenas, envolvendo alguns quilômetros cúbicos da crosta, quando comparadas com as grandes feições geológicas produzidas por processos geológicos de escala terrestre (Skinner, 1997). No entanto, os depósitos hidrotermais não são acidentes geológicos aleatórios e desprovidos de conexão com os processos geológicos formadores da crosta. Assim, a ocorrência de um depósito hidrotermal num terreno geológico particular possui sua origem ligada a determinado evento geológico específico ocorrido na área e que produziu uma certa quantidade de calor, suficiente para fazer as soluções de minério fluirem. Desta forma, torna-se importante determinar a cronologia de eventos magmáticos e tectono-metamórficos da região em estudo e se possível, estabelecer uma coluna estratigráfica de qualidade. Isto possibilita o estabelecimento de correlações entre o(s) evento(s) formadore(s) do depósito de minério com a seqüência de eventos geológios da área. Deste modo é possível determinar se os depósitos minerais em estudo são sin-deposicionais, epigenéticos ou singenéticos. Conseqüentemente torna-se de especial prioridade a obtenção de idades geocronológicas em tais terrenos, especialmente nas áreas Pré-cambrianas. Por esta razão, utilizou-se nessa tese a geocronologia U/Pb em zircão via SHRIMP, atualmente a metodologia mais precisa para datação de rochas Pré-Cambrianas, combinado com a sistemática de isotópos de Pb das rochas e do minério. Os corpos graníticos mais importantes da região (Granito Lavras, Granito Caçapava e Granito São Sepé) foram datados com precisão e tiveram estabelecida a sua assinatura isotópica do Pb. Mais adiante, estabeleceu-se as correlações pertinentes entre estes resultados e os dados da assinatura isotópica do Pb e S dos depósitos minerais. A discussão pormenorizada e as conclusões estão nos capítulos II,III e IV.

FONTE DAS SOLUÇÕES (SOLVENTES)

A expressão "a água é o principal solvente da natureza", aplica-se inteiramente aos depósitos minerais hidrotermais. As soluções hidrotermais são constituídas basicamente por H_2O contendo quantidades subordinadas de outros voláteis tais como CO_2, SO_2, Cl, F etc., além de outros sais e metais dissolvidos (Hedenquist, 1997, Skinner, 1997). As características físico-químicas destas soluções podem ser determinadas pelo estudo de inclusões fluidas em minerais transparentes como, quartzo, calcita, fluorita, esfalerita entre outros. Os estudos de diversos depósitos minerais antigos e sistemas geotermais ativos mostram que tais soluções apresentam composição e salinidade variáveis (Skinner et al. 1997, Hedenquist, 1997). Evidentemente nem todas as soluções hidrotermais que fluem ao longo da crosta formam depósitos minerais. Para que isto aconteça é necessário a ocorrência de uma combinação de fatores envolvendo a extração dos metais, o seu transporte e canalização junto com mudanças físico-químicas capazes de produzir a precipitação do minério dissolvido (Skinner, 1997).

Para se determinar a fonte dos solventes dos fluidos dos depósitos minerais utiliza-se a sistemática dos isotópos estáveis nos principais elementos constituintes das soluções: O, H, S e C. Os isótopos de O e H são utilizados para determinar a fonte da H_2O das soluções hidrotermais; os isótopos de carbono extraídos dos carbonatos da ganga são utilizados para inferir a fonte do C enquanto que os isótopos de S determinam a fonte do enxofre dos sulfetos dos depósitos minerais.

Baseado em estudos de isótopos de O e H, identificou-se quatro fontes principais para a água hidrotermal: (a) água da superfície (incluindo água dos rios, dos mares, dos lagos, da chuva e superficial do subsolo); (b) água cognata do subsolo; (c) água metamórfica e (d) água magmática (Skinner, 1997). Muitos depósitos hidrotermais no entanto, foram gerados a partir da deposição de soluções que continham água de duas ou mais fontes.

Os isótopos de O, H e C discutidos neste trabalho referem-se aos resultados obtidos por Koppe (1990) no depósito de Au da Bossoroca em sua tese de doutorado. Tais resultados combinados com os dados geocronologicos SHRIMP e de isótopos de Pb são utilizados como referencial para a discussão sobre a origem do Depósito de Au da Bossoroca, conforme Capítulo II.

Isótopos de enxofre

Os estudos de isótopos de enxofre de sistemas hidrotermais são utilizados para: (a) determinar a origem do enxofre contido nos corpos de minério a base de sulfeto ou sulfato; (b) estabelecer a temperatura de formação dos sulfetos/sulfatos e dos fluidos mineralizadores; (c) determinar o grau de equilíbrio alçancado e (d) inferir a razão água/rocha e os mecanismos de deposição do minério (Rye & Ohmoto, 1974; Ohmoto & Rye, 1979; Rollinson, 1993).

Os depósitos minerais hidrotermais apresentam grandes variações nos valores de ∂^{34}‰ (CDT) onde a maioria deles situa-se entre +50 e -50 ‰ (Ohmoto and Rye, 1979). Alguns depósitos hidrotermais apresentam variações pequenas como é o caso dos Cu Pórfiros indicando uma origem única para o enxofre, enquanto outros mostram grandes variações composicionais de isótopos de S indicando uma provável origem múltipla, como no caso dos depósitos do tipo Mississipi Valley (Rollinson, 1993).

O fracionamento isotópico do S^{32} e S^{34} pode modificar os valores de ∂^{34}‰ (CDT) do fluido mineralizador. Assim, a interpretação completa dos dados obtidos nas análises isotópicas dos sulfetos e sulfatos deve levar em consideração as condições físico-químicas de deposição do fluido como temperatura, pH e fugacidade de oxigênio entre outras variáveis (Rye & Ohmoto, 1974). Em temperaturas ≥ 400° C as espécies dominantes numa solução hidrotermal são H_2S e SO_2 e a composição isotópica do fluido é resultante do somatório do $\partial^{34}S$ destas espécies; abaixo de 350 °C as espécies dominantes no fluido são SO_4 e H_2S (Ohmoto & Rye, 1979). Diagramas construidos por esses autores, relacionando a atividade de oxigênio e pH destes sistemas hidrotermais mostram que sulfetos formados em equilíbrio com a magnetita terão valores de $\partial^{34}S$ menores que o dos fluidos. Em condições de pH e atividade de oxigênio baixos, os fluidos e os sulfetos analisados apresentarão valores de $\partial^{34}S$ iguais.

As principais fontes de enxofre estabelecidas para os depósitos hidrotermais baseado no sumário elaborado por Rollinson (1993) são: (1) O S de origem magmática é representado pelos depósitos de Cu-Au Pórfiros. Os valores de $\partial^{34}S$ medidos nestes depósitos variam entre -3 e +1‰ sendo portanto similares aos valores do manto. As temperaturas de deposição situam-se entre 450-650°C e os sulfetos ocorrem em equilíbrio. (2) Redução inorgânica do sulfato da água do mar a altas

temperaturas. Este tipo de mecanismo é o responsável pela formação de depósitos de sulfeto maciço ao longo das cristas oceânicas. Neste modelo a água fria do mar sulfatada é aquecida nas vizinhanças da câmara magmática levando a precipitação de alguma anidrita enquanto que o restante do enxofre é reduzido pela reação com o basalto. O fluido quente junto com os sulfetos é expelido de volta para mar a temperaturas de cerca de 350°C. Ao misturar-se com a água do mar os minerais são precipitados ao longo do assoalho oceânico como sulfetos sedimentares finos enquanto que nos canais hidrotermais a precipitação dos sulfetos leva a formação de chaminés de até 1 metro de altura. Os depósitos tipo Kuroko (Japão) formados por este mecanismo possuem sulfatos com valores de $\partial^{34}S$ entre +21,5 e +28,5‰ muito próximos daqueles da água do mar contemporânea. (3) Redução inorgânica do sulfato a baixas temperaturas. Os depósitos de cobre em camadas vermelhas da bacia de Cheshire (Inglaterra) associados a evaporitos ilustram este tipo de fonte para o enxofre. Os sulfetos deste depósito mostram valores de $\partial^{34}S$ entre -1,8 a 16,2 ‰ e a barita associada +13,8 a +19,3‰. Os valores encontrados nas baritas são muito próximos aos dos sulfatos dos evaporitos presentes nas seqüências sobrepostas. Os sulfetos e a barita do depósito foram formadas a partir de soluções derivadas dos evaporitos em temperaturas provavelmente acima daquelas em que as bactérias redutoras existem. (4) Redução bacteriológica dos sulfatos a baixas temperaturas. A jazida de Rammelsberg na Alemanha conhecida como um depósito de sulfeto maciço hospedado por rochas sedimentares contém várias proporções de clastos de pirita e calcopirita. Os valores de $\partial^{34}S$ medidos nos clastos de pirita caem em três grupos distintos (+12 a +16‰; +3 a -3‰ e -10 a -17‰). Os grupos com baixos valores são explicados pela redução bacteriogênica da água do mar com fracionamento de cerca 45 ±20‰. Os valores mais elevados são provavelmente de origem hidrotermal e os dois grupos de clastos foram misturados durante a sedimentação.

Os sulfetos dos depósitos do sistema Camaquã-Santa Maria possuem valores de $\partial^{34}S$ (CDT) bastante consistentes e próximos a 0 ‰, já demonstrados por Bettencourt (1976) e confirmados neste trabalho (ver Capítulo III). As condições de pH ácido das soluções mineralizadoras do sistema hidrotermal Camaquã-Santa Maria permitem inferir que os valores de $\partial^{34}S$ medidos nos sulfetos representam aproximadamente aqueles do fluido, sendo portanto de origem magmática.

Os depósitos hidrotermais epigenéticos de metais-base da Formação Passo Feio apresentam valores de $\partial^{34}S$ para os sulfetos, variáveis entre -15‰ a +11‰, indicando que mais de uma fonte pode estar envolvida na origem deste enxofre. A associação espacial e genética do Granito Caçapava com tais depósitos, entre outros parâmetros, favorece uma origem mista, magmática-sedimentar para esses sulfetos (ver Capítulo IV).

FONTE DOS METAIS

Os solutos carregados pelos fluidos mineralizadores e pelos magmas incluem os elementos Pb, Sr e Nd, os quais são traçadores isotópicos da região fonte destes elementos. A determinação destes isótopos nas associações de minérios/ganga e rochas regionais, combinados com estudos geocronólogicos e de isótopos estáveis fornecem informações valiosíssimas sobre a gênese dos depósitos minerais.

Isótopos de chumbo

Os isótopos de Pb são aplicados ao estudo da proveniência de rochas ígneas e dos metais contidos nos depósitos de minério além de auxiliar na detecção de fontes poluidoras (Faure, 1986). Convém salientar que um depósito de minério é freqüentemente uma ocorrência localizada de certos tipos de minerais, economicamente importantes, produzidos por processos petrogenéticos que afetaram um grande volume de rochas da crosta terrestre. Assim, a interpretação de sua origem está ligada ao ambiente geológico que contribuiu para a sua formação. A sistemática dos isótopos de Pb tem sido utilizadas extensivamente por diversos autores (Doe and Stacey 1974; Doe and Zartmann, 1979; McNaughton and Bickle,1987; Ho et al., 1994; Carr and Dean, 1995; McNaughton and Groves, 1996).

A obtenção de idades modelo em minerais portadores de Pb implica que todo o Pb contido no mineral estudado tenha sido separado do U e Th de uma fonte com determinada razão U/Pb e que tal composição isotópica permaneça congelada, isto é, não mude com o tempo. Deste modo, a razão isotópica do Pb medida no mineral é aquela do momento de sua extração da fonte e depende basicamente do tempo e da razão U/Pb

da fonte. O tempo e a razão U/Pb são calculados de acordo com o modelo de curva de crescimento adotada, baseados nos valores da composição isotópica do Pb medido. O modelamento é realizado através da construção de curvas de crescimento do Pb para razões U/Pb estimadas. As idades podem ser obtidas pela locação das amostras nestes diagramas ou através de cálculos, aplicando-se as equações desenvolvidas, com o auxílio de tabelas (Faure, 1986).

Os minerais mais adequados para obtenção de idades modelo são aqueles portadores do Pb comum (Pb que ocorre em minerais que possuem baixíssimas razões U/Pb e Th/Pb de modo que sua composição isotópica não muda consideravelmente com o tempo); tais minerais incluem a galena (PbS), cerusita ($PbCO_3$), anglesita ($PbSO_4$) e K-feldspato (Faure, 1986). O K-feldspato possui Pb comum em quantidades-traços relativamente elevadas quando comparado com os teores de U e Th baixíssimos, pois permite a substituição do Pb^{+2} pelo K^+ (Bowen, 1988).

Idades modelo para galenas

1) Modelo de Estágio Simples. Este modelo também conhecido como Holmes & Houtermans foi desenvolvido independentemente pelos dois autores em 1946 e assume que todo o Pb comum na amostra analisada resulta da mistura do Pb primitivo (meteorítico) com o Pb radiogênico (resultante da desintegração radioativa do U e Th) numa região fonte isolada (sistema fechado) com valores específicos de μ (Faure, 1986). A idade resultante da amostra é a do tempo transcorrido desde quando o Pb foi removido de sua região fonte e depositado na crosta como galena. A premissa é a de que o Pb possui uma história de crescimento de sua razão isotópica numa região fonte com μ, ω e κ constantes desde o início da formação da terra (4,57 Ga) até o tempo da mineralização (estágio simples), tendo sido removido desta fonte num evento único sem alterações posteriores. Galenas extraídas de fontes distintas durante um mesmo evento geológico geram isócronas em diagramas Pb^{207} X Pb^{206}, onde a inclinação da reta fornece a idade do evento geológico (Faure, 1986).

2) Modelo de dois estágios. A presença de excesso de Pb radiogênico em diversos depósitos minerais (Pb anômalo) é uma indicação de que a razão U/Pb da área fonte dos minérios de Pb aumentou episodicamente ou continuamente com o tempo. Os novos

modelos de evolução isotópica foram criados para acomodar dados de Pb provenientes de depósitos de minério concordantes e que não serviam nas curvas de estágio simples. Observou-se que o Pb dos depósitos mais jovens (Pós-Arqueano) eram os mais discordantes das curvas propostas.

Assim, Stacey & Kramers (1975) desenvolveram um modelo em dois estágios (episódico) onde a evolução do Pb inicia com razões isotópicas primordiais a 4,57 Ga. Posteriormente, há cerca de 3,7 Ga atrás, a razão U/Pb do reservatório (área fonte) modificou através da diferenciação geoquímica e permaneceu constante até o presente. Os valores utilizados para construir a curva de evolução isotópica do Pb em dois estágios foram derivados de: a) composição isotópica média de rochas sedimentares e vulcânicas depositadas em oceanos; (b) isócronas Pb/Pb de rochas graníticas antigas que intersectam-se num determinado ponto, o qual presumidamente representa a média do Pb crustal; (c) composição isotópica do Pb de 13 depósitos de minério concordantes.

A idade modelo do Pb em 2 estágios para o sistema Camaquã-Santa Maria, mais especificamente para as galenas do depósito Santa Maria é de 1,06 Ga e μ= 9,7. Esta idade é mais antiga que a das encaixantes da mineralização (Grupo Bom Jardim) e maior que a do valor obtido pelo modelo de estágio simples (647 Ma). Conseqüentemente o μ obtido também é maior. Isto indica que a área fonte possuia uma razão U/Pb mais baixa que a calculada. Utilizando-se a idade de 594 Ma para o evento mineralizador (magmatismo Lavras-Hilário), verefica-se que o valor da razão U/Pb calculada (modelo 2 estágios) para a área fonte, baixa dramaticamente situando-se em torno de 8,5. Tais valores são tipicamente encontrados na crosta continental empobrecida na razão U/Pb (crosta inferior ou média). A incerteza no valor calculado provém da dificuldade em estimar as épocas e o número de eventos que contribuiram para empobrecer a crosta continental do Escudo Sul-riograndense na razão U/Pb, antes do episódio mineralizador. Apesar destas incertezas é lícito afirmar que a área fonte da mineralização do sistema Camaquã-Santa Maria era empobrecida na razão U/Pb, pois o Pb teve um crescimento retardado ao longo das curvas Stacey & Kramers ou mesmo na de Holmes-Houtermanns. Tal fonte é compatível com a crosta continental antiga ,isto é, o embasamento antigo do Escudo Sul-riograndense (ver capítulo 2).

3) Modelos de estágios múltiplos. Cummings & Richards (1975) desenvolveram um modelo de evolução isotópica do Pb com modificações

contínuas da razão U/Pb. Tal modelo mostrou-se mais consistente com os dados de isótopos de Pb das galenas dos depósitos concordantes conhecidos naquela época.

Doe & Zartmann (1979, 1981) propuseram o modelo de estágios múltiplos a partir da construção de curvas evolutivas com trajetórias particulares para cada tipo de ambiente geológico (área fonte) com evolução episódica em 11 estágios de orogênese (reciclagem) a cada 400 Ma. Os valores da razão U/Pb e Th/U modificam a cada estágio de acordo com a quantidade de reciclagem de cada área fonte, isto é, do grau de envolvimento do ambiente geológico particular na orogênese. A transferência de matéria entre o manto e os diversos reservatórios da crosta é bidirecional e ocorre a partir dos processos da tectônica de placas derivando daí o nome do modelo Plumbotectonics. Eles consideraram três áreas fontes principais: (a) manto; (b) crosta superior; (c) crosta inferior. Essas três áreas fontes são recicladas e misturadas durante os processos de orogênese originando segmentos com razões U/Pb e Th/U diferenciadas, gerando um quarto reservatório de vida mais curta, denominado orógeno e representado no diagrama do Pb pela curva de crescimento de Stacey & Kramers (1975).

Assume-se que a crosta continental começou a ser gerada há 4.0 Ga atrás a partir da diferenciação do manto. A orogênese seguinte (3,6 Ga) envolve uma porção do manto e da crosta continental previamente formada. A crosta superior aumenta a razão U/Pb com o tempo, produzindo composições isotópicas radiogênicas. Exemplo disso são os depósitos de minério do tipo Mississipi Valley. A crosta inferior é representada freqüentemente por piroxênio granulitos ou outros tipos de rochas metamórficas de alto grau que possuem conteúdos de U baixíssimos (0,1 - 1,0 ppm) e razões U/Pb entre 0,5 e 5 (Zartmann & Doe, 1981). Portanto, a crosta inferior é empobrecida em U e produzirá curvas de crescimento retardado para o Pb (Pb primitivo) enquanto que a crosta superior é enriquecida em U apresentando curvas de crescimento acelerada (Pb radiogênico).

A composição isotópica das galenas dos depósitos minerais foram inicialmente utilizadas para estimar as idades da mineralização com referência a curvas modelo de crescimento do Pb. Em eras Pós-Arqueanas esta aproximação raramente é satisfeita devido a complexidade dos reservatórios crustais e do manto litosférico e astenosférico (Kerrich, 1991). Mais recentemente, os isótopos de Pb tem sido utilizados para avaliar as fontes de Pb e metais associados,

identificar distúrbios pós-mineralização e para definir províncias do embasamento (Doe & Zartmann, 1979). No Mesozóico e Cenozóico por exemplo, as assinaturas isotópicas dos depósitos minerais e das rochas ígneas são características para os diferentes ambientes geotectônicos possuindo uma ótima correlação com as áreas fontes sendo ainda possível obter idades modelo para as mineralizações (Doe & Zartmann, 1979; Zartmann & Doe, 1981). No caso do sistema Camaquã-Santa Maria e mesmo para os depósitos epigenéticos hidrotermais da Formação Passo Feio, o Pb das mineralizações mostra um crescimento retardado (ver Capítulos II e III).

Os sulfetos com baixo teor de Pb (pirita, calcopirita, bornita, calcosina entre outros) por sua vez, podem dar informações a respeito da composição isotópica da razão inicial do sistema, desde que a idade da mineralização seja conhecida. As adições de Pb radiogênico podem ser relacionados a uma isócrona, a qual inclui a composição isotópica inicial do sistema (Gulson et al., 1983; Ho et al., 1994; Bierlein and McNaughton, 1998). As razões isotópicas iniciais dos sistemas mineralizados que possuem apenas sulfetos com baixo teor de Pb são estimadas e comparadas com a assinatura isotópica das rochas regionais e com as diferentes curvas de crescimento modeladas.

O estágio atual de conhecimento indica uma tendência de construirem-se curvas de crescimento particulares para cada segmento crustal nos diferentes continentes, na tentativa de modelar o crescimento do Pb para os reservatórios respectivos. Tais modelamentos tem sido aplicados com sucesso para os terrenos geológicos do Mesozóico e Cenozóico (Doe & Zarmann,1979) para os terrenos Paleozóicos do Leste da Austrália (Carr and Dean, 1995) e também para o Arqueano (McNaughton, 1987). Resta ainda elaborar curvas modelo de crescimento do Pb apropriadas para os terrenos do Proterozóico nos diversos continentes.

Isótopos de estrôncio

As razões isotópicas de estrôncio das baritas são utilizadas como ferramenta para determinar a fonte dos fluidos mineralizadores porque essas possuem baixas concentrações de Rb (Lange *et al.*, 1983; Barbieri *et al.*, 1987; Canals and Cardelach, 1993; Galindo *et al.*, 1994). Assim, compara-se as razões isotópicas iniciais de Sr das baritas com a das

rochas regionais para estabelecer o provável reservatório de estrôncio do fluido mineralizador.

DISCUSSÃO E CONCLUSÕES

Este trabalho defende a tese de que os depósitos de metais-base (Camaquã, Santa Maria e na Formação Passo Feio), e Au (Bossoroca) mais importantes do Rio Grande do Sul foram gerados durante o Ciclo Brasiliano ao longo de três eventos distintos, relacionados ao magmatismo e metamorfismo contemporâneos (700, 594 e 562 Ma); os metais foram derivados de fontes relacionadas à crosta juvenil e ao embasamento antigo.

O depósito mais antigo, representado pela jazida de Au da Bossoroca é classificado como um depósito orogênico epizonal, e foi gerado há 700 Ma, contemporaneamente ao metamorfismo regional de baixa pressão e ao magmatismo TTG do Complexo Cambaí durante o início do Ciclo Brasiliano (conforme Capítulo II). Os depósitos de metais-base do sistema Camaquã-Santa Maria são hidrotermais magmáticos distantes, provavelmente ligados à intrusão Cu-Au Pórfiro, e foram gerados há cerca de 594 Ma durante o magmatismo pós-colisional Lavras-Hilário relacionado ao final da Orogenêse Dom Feliciano (ver Capítulo III). As mineralizações de Cu (Au) e Pb hospedados pela Formação Passo Feio são hidrotermais epigenéticas e foram gerados há 562 Ma durante a intrusão do Granito Caçapava (ver Capítulo IV).

A fonte dominante dos metais para os depósitos de Camaquã-Santa Maria é o embasamento antigo com contribuição das rochas da Formação Arroio dos Nobres. O enxofre dos sulfetos desses depósitos é de origem dominantemente magmática. Os metais dos depósitos hidrotermais epigenéticos da Formação Passo Feio foram também derivados do embasamento antigo, com contribuição importante das rochas meta-vulcanosedimentares da Formação Passo Feio, contendo componentes pré-Brasilianos e Brasilianos. O enxofre dessas mineralizações possui origem mista — sedimentar e magmática. A fonte do Pb determinada para o depósito de Au da Bossoroca é de origem profunda e corresponde a mesma fonte do magma de arco juvenil gerador das rochas vulcânicas da Formação Campestre.

A hipótese de que a área de proveniência dos sulfetos (clásticos) para os depósitos do sistema Camaquã-Santa Maria fosse os depósitos epigenéticos de metais-base da Formação Passo Feio deve ser reformulada. As estimativas de idade para a deposição dos minérios indica que o sistema Camaquã-Santa Maria é mais antigo que os depósitos epigenéticos da Formação Passo Feio e conseqüentemente, estes últimos não poderiam servir como área fonte para os primeiros.

Os depósitos de metais-base estudados, juntamente com os depósitos do Bloco do Butiá (Au) e Cerro Rico (Cu, Au) da região de Lavras do Sul estão em última análise, relacionados geneticamente ao magmatismo pós-colisional da Orogênese Dom Feliciano (600-550 Ma) do final do Ciclo Brasiliano.

Vários depósitos de Au de pequeno porte do tipo orogênico epizonal ocorrem ao longo do Arco Vulcânico da Bossoroca (por exemplo: Bossoroca, Cerrito do Ouro, Guardinha entre outros). Considerando que os fluidos mineralizadores deste tipo de depósito são de origem profunda e os principais controles para a mineralização do Depósito de Au da Bossoroca são os falhamentos de direção NE, deve-se priorizar a exploração nas rochas encaixantes com maior competência e com reatividade adequadas. Deste modo, os falhamentos de direção NE ao longo do Arco Vulcânico da Bossoroca localizados sobre rochas de alta competência e/ou próximo aos contatos com outras seqüências são os alvos potenciais para o Au no Bloco São Gabriel.

Os depósitos epigenéticos hidrotermais conhecidos da Formação Passo Feio apresentam potencial econômico relativamente menor. A origem destes depósitos está relacionada à remobilização e/ou assimilação de sulfetos pré-existentes de rochas meta-vulcanosedimentares da Formação Passo Feio durante a intrusão sin-tectônica do Granito Caçapava. A ocorrência do metamorfismo regional há 700 Ma, anteriormente a intrusão do Granito diminuiu relativamente a porosidade, permeabilidade e a quantidade de água disponível presente nos poros das rochas pré-metamórficas da Formação Passo Feio. Em conseqüência, as condições de lixiviação de metais e circulação do fluido hidrotermal durante a intrusão do granito foram limitadas. A descoberta de um depósito apreciável na Formação Passo Feio necessitaria da localização de halos de alteração provenientes de um sistema hidrotermal de proporções consideráveis que lixiviasse os metais e canalizasse os fluidos em circulação e os depositasse em zonas de baixa pressão sobre rochas reativas. Tal situação geológica

envolve a identificação de estruturas de baixa pressão (fraturas de alívio de direção NW e relacionadas), rochas reativas favoráveis a deposição, além da proximidade com a cúpula da intrusão. O prospecto Cioccari reúne as duas primeiras condições, faltando no entanto a comprovação do terceiro parâmetro.

As jazidas mais importantes (Camaquã-Santa Maria) possuem controle estrutural segundo direções E-W à NW. Esses depósitos e aqueles do Bloco do Butiá e Cerro Rico situados a oeste, juntamente com o prospecto descoberto recentemente na região de Amaral Ferrador (Pb, Ag), a leste, alinham-se segundo a direção E-W, paralelamente ao Rio Camaquã. Tal configuração geológica indica que estes depósitos estão controlados estruturalmente segundo a direção E-W e geneticamente relacionados. Visualisa-se também uma zonação grosseira dos metais com predomínio de Au no lado oeste (Bloco São Gabriel) e dos metais básicos, principalmente o Cu, na região central e finalmente o Pb no extremo leste, já no domínio do Batólito Pelotas, onde dominam os depósitos de Sn e W.

As conseqüências dos resultados e interpretações dessa tese são referências para a exploração de metais-base e Au no Escudo Sul-riograndense. Os controles estruturais e a conexão dos depósitos com o magmatismo pós-colisional requer a formulação de parâmetros novos e alternativos para a exploração mineral no Escudo Sul-riograndense tais como: (1) As fraturas regionais antigas de direção E-W a NW e sua intersecção são os sítios estruturais potenciais para a mineralização de metais-base. Estas direções foram canalizadoras dos fluidos hidrotermais há cerca de 594 Ma e em conseqüencia devem ser retomadas para pesquisa de metais no Escudo Sul-riograndense. Tais estruturas podem representar zonas de fraqueza antigas (Paleoproterozóico?) na litosfera e são sub-paralelas ao Lineamento de Ibaré, o qual forma o limite (zona de sutura?) entre o Bloco Taquarembó (terreno granulítico Paleoproterozóico) e o Bloco São Gabriel (terreno juvenil Brasiliano). Vários diques de diabásio de direção E-W a NW, controlados por estas estruturas, ocorrem ao longo da Bacia do Camaquã e podem ser utilizados como alvos estruturais. (2) Litologias com alta porosidade original (conglomerados e arenitos), ou rochas altamente reativas aos processos de substituição (margas e carbonatos) são as rochas encaixantes preferenciais para a mineralização. A fração sedimentar clástica do Grupo Bom Jardim e as rochas carbonáticas da Formação Passo Feio cortadas por fraturas NW e E-W são os alvos

potenciais. (3) As rochas do embasamento, principalmente as rochas máficas da Formação Passo Feio e as sequências sedimentares da Formação Arroio dos Nobres são fontes potenciais para os metais base. As assinaturas isotópicas dos sulfetos do sistema Camaquã-Santa Maria e os depósitos na Formação Passo Feio foram derivados de um embasamento crustal empobrecido em U/Pb e são compatíveis com o Pb dos arenitos da Formação Arroio dos Nobres e das rochas metassedimentares da Formação Passo Feio, respectivamente. (4) O plutonismo pós-colisional da Orogenêse Dom Feliciano é o mais provável candidato para as fontes de calor, enxofre e metais-base. As idades de 594 Ma estimadas para os depósitos do sistema Camaquã-Santa Maria e de 562 Ma para os depósitos epigenéticos da Formação Passo Feio, indicam que o final da Orogênese Dom Feliciano é o período mais provável para a geração de depósitos de metais-base no Escudo Sul-riograndense. (5) A geofísica (por ex. gravimetria) e os estudos de alteração são essenciais para detectar corpos intrusivos em profundidade, os quais podem ter potencial para depósitos do estilo Cu-Au-Pórfiro.

Fica assim demonstrada a tese de que os depósitos hidrotermais de metais-base e Au do Bloco São Gabriel foram gerados durante o Ciclo Brasiliano em três períodos distintos: 700, 594 e 562 Ma. O Au é orogênico epizonal e proveniente de uma fonte profunda, derivada da crosta juvenil há cerca de 700 Ma, durante o metamorfismo regional dinamotermal e magmatismo TTG da região do arco vulcânico. Os depósitos de metais-base são hidrotermais epigenéticos e ligados ao plutonismo pós-colisional da Orogênese Dom Feliciano e foram derivados do embasamento crustal antigo, empobrecido na razão U/Pb. As fraturas de direção E-W e NW foram os controles estruturais fundamentais na geração dos depósitos de metais-base de maior expressão.

BIBLIOGRAFIA

Barton, P.B. Jr & Skinner, B.J. 1979. Sulfide mineral stabilities. In: Barnes, H.L. editor. *Geochemistry of hydrothermal ore deposits*. Wiley, New York, USA, p. 278-403.

Barbieri, M.; Bellanca, A.; Neri, R. & Tolomeo, L. 1987. Use of strontium isotopes to determine the sources of hydrothermal fluorite and barite from northwestern Sicily (Italy). *Chemical Geology*, 66: 273-278.

Bierlein, F.P. & McNaughton, N.J. 1998. Pb isotope fingerprinting of mesothermal gold deposits from central Victoria, Australia: implications for ore genesis. *Mineralium Deposita*, 33: 633-638.

Bettencourt, J.S. (1976) Mineralogie, inclusions fluides et isotopes stables d'oxygene et de soufre de la mine de cuivre de Camaquã - RS (une ètude preliminaire). In: Congresso Brasileiro de Geologia, 29, Ouro Preto, MG. *Anais*, SBG: 2, 409-423.

Bowen, R. 1988. *Isotopes in the Earth Sciences*. Cambridge: Elsevier. 647p.

Canals, A. & Cardelach, E. 1993. Strontium and sulphur isotope geochemistry of the low temperature barite-fluorite veins of the Catalonian Coastal Ranges (NE Spain): a fluid mixing model and age constraints. *Chemical Geology*,104: 269-280.

Carr, G.R.; Dean, J.A.; Suppel, D.H. & Heithersay, P.S. 1995. Precise lead isotope fingerprinting of hydrothermal activity associated with Ordovician to Carboniferous metallogenic events in Lachlan Fold Belts of New South Wales. *Economic Geology,* 90: 1467-1505.

Chaudisson, M. and Lorand, J.P. 1990. Sulphur isotope composition of orogenic spinel lherzolite massifs from Ariege (N.E. Pyrinees, France): An ion microprobe study. *Geochimica Cosmochimica Acta.*, 54: 2835-2846.

Claypool, G.E, Holster, W.T., Kaplan, I.R., Sakai, H. & Zak, I. 1980. The age curves of sulfur and oxygen isotopes in marine sulfate and their mutual interpretation. *Chemical Geology*, 28:199-260.

Compston, W.; Williams, I.S. & Meyer, C. 1984. U-Pb geochronology of zircons from Lunar breccia 73217 using a sensitive high-mass resolution ion microprobe. *Journal of Geophysic Research*, 89, Suppl.: B525-B534.

Cummings, G.L. & Richards, J.R. 1975. Ore lead isotope ratios in a continuously changing earth. *Earth and Planetary Science Letters,* 28:155-171.

Doe, B.R. & Stacey, J.S. 1974. The application of Pb isotopes to the problems of ore genesis and ore prospect evaluation. A review. *Economic Geology*, 69: 757-776.

Doe, B.R & Zartmann, R.E. 1979. Plumbotectonics: The Phanerozoic. In: Barnes, H.L. (ed.) *Geochemistry of hydrothermal ore deposits.* , Wiley, New York, USA, p. 22-70.

Dickin, A. P. 1995. *Radiogenic isotope geology*, University Press, Cambridge, 490 p.

Einaudi, M.T.; Meinert, L.D.; Newberry, R.J. 1981. Skarn deposits: In:. Skinner, B.J. editor. *Economic Geology Senventy Fifth Anniversary Volume:1905-1980*, Lancaster Press, p.317-391.

Faure, G. 1986. *Principles of Isotope Geology.* 2nd edition, Wiley, New York, 589 p.

Galindo, C.; Tornos, F.; Darbyshire, D.P.F. & Casquet, C. 1994. The age and origin of the barite-fluorite (Pb-Zn) veins of the Sierra del Guadarrama (Spanish Central System, Spain): a radiogenic (Nd, Sr) and stable isotope study. *Chemical Geology*,112: 351-364.

Groves, D.I 1993. The crustal continuum model for late-Archean lode-gold deposits of Yilgarn Block, Western Australia. *Mineralium Deposita*, 28: 366-374.

Groves, D.I. 1996. Geological concepts in the exploration for large to giant late-orogenic (mesothermal) gold deposits — the Archean greenstone experience. In: *Mesothermal Gold Deposits — A Global Overview.* Geology Department (Key Centre) & University Extension, University of Western Australia Publication, 27: 114-117.

Groves, D.I.; Goldfarb, R.J.; Gebre-Mariam, M.; Hagemann, S.G.; & Robert, F. 1998. Orogenic gold deposits: A proposed classification in the context of their crustal distribution and relationship to other gold deposit types. *Ore Geology Reviews* , 13: 7-27.

Gulson, B.L., Perkins, W.G. & Mizon, K.J. 1983. Lead isotope studies bearing on the genesis of copper ore bodies at Mount Isa, Queensland. *Economic Geology* , 78:1466-1504.

Hedenquist, J.W. 1997. *Epithermal gold deposits: styles, characteristics and exploration.* Centre for Strategic Mineral Deposits - Department of Geology & University of Western Australia, A Short Course, 139p.

Hedenquist, J.W. & Lowenstern, J.B. 1994. The role of magmas in the formation of hydrothermal ore deposits. *Nature*, 370: 519-527.

Ho, S.E.; McNaughton, N.J. & Groves, D.I. 1994. Criteria for determining initial lead isotopic compositions of pyrite in Archaean lode-gold deposits: A case study at Victory, Kambalda, Western Australia. *Chemical Geology*, 111: 57-84.

Hoefs, J. 1997. *Stable isotope geochemistry.* 4rd edition, Springer -Verlag, Berlin, 201p.

Kerrich, R. 1991. Radiogenic isotope systems applied to mineral deposits. In: Heamann, L. & Ludden, J.N. (ed.) *Applications of radiogenic isotope systems to problems in geology*. Short Course Handbook, Toronto, Canadá, 19 (11): 365-498.

Kerrich, R. & Cassidy, K.F. 1994. Temporal relationships of lode gold mineralization to accretion, magmatism, metamorphism and deformation — Archean to present — A Review. *Ore Geology Review*. 9: 263-210.

Koppe JC (1990). *Metalogênese do Ouro da Mina da Bossoroca, São Sepé, RS.* Curso de Pós-Graduacao em Geociências, Universidade Federal do Rio Grande do Sul, Porto Alegre. Tese de Doutorado, 289p.

Lange, S.; Choudhuri, S. & Clares, N. 1983. Strontium isotope evidence for the origin of barites and sulphides from the Mississippi Valley-type ore deposits in southeast Missouri. *Economic Geology* , 78: 1255-1261.

Lu, C.; Reed; M.H. & Misra, K.C. 1992. Zinc-lead skarn mineralization at Tin Creek, Alaska: Fluid inclusion and skarn-forming reactions. *Geochimica et Cosmochimica Acta*, 56: 109-119.

Lyndon, J.W. 1984. Volcanogenic massive sulphide deposits. Part 1: A descriptive model. *Geoscience Canadá* 11: 195-202.

McNaughton, N.J 1987. Lead-isotope systematics for Archaean sulphide studies. In: Ho, S. E. & Groves, D.I. editors. *Recent advances in uderstanding Precambrian gold deposits.* Perth: University of Western Australia Publication, 11: 181-188.

McNaughton, N.J. & Bickle, M.J. 1987. K-feldspar Pb-Pb isotope systematics of post-kinematic granitoid intrusions of the Diemals area, central Yilgarn Block, Western Australia: *Chemical Geology*, 66: 193-208.

McNaughton, N.J & Groves, D.I. 1996. A review of Pb-isotope constraints on the genesis of lode-gold deposits in the Yilgarn Craton, Western Australia. *Journal of the Royal Society of Western Australia,* 79:123-129.

Meinert, L.D. 1992. Skarns and skarn deposits. *Geoscience Canadá*, 19: 145-162.

Ohmoto, H., Kaiser, C.J. & Geer, K.A. 1990. Systematics of sulphur isotopes in recent marine sediments and ancient sediment-hosted basemetal deposits. In: Herbert, H. K. & Ho, S. E. editors. *Stable*

Isotopes and Fluid Processes in Mineralization, Perth: University of Western Australia Publication, 23, 70-120.

Ohmoto, H. & Rye, R.O. 1979. Isotopes of sulfur and carbon. In: Barnes, H.L. editor. *Geochemistry of hydrothermal ore deposits.* Wiley, New York, USA, p. 509-567.

Pidgeon, R.T.; Furfaro, D.; Kennedy, A.K.; Nemchin, A.A. & van Bronswjk, W. 1994. Calibration of zircon standards for the Curtin SHRIMP II In: *Abstracts of the Eight International Conference on Geochronology, Cosmochronology and Isotope Geology*, Berkeley, USA. U.S. Geological Survey Circular, 1107, p.251.

Rollinson, H. R. 1993. *Using geochimical data: evaluation, presentation and interpretation.* Longmann, Singapure, 352p.

Rye, R.O & Ohmoto, H. 1974. Sulfur and carbon isotopes and ore genesis. A review. *Economic Geology,* 68: 826-842

Sangster, D.F. 1998. Volcanic-exhalative massive sulphide deposits. *Workshop: Depósitos Minerais Brasileiros de Metais-Base.* CPGG-UFBA/ADIMB-SBG. Salvador - BA, Brasil, p. 9-11.

Sillitoe, R. H. 1996. Granites and metal deposits. *Episodes*, 19 (4): 126-133.

Skinner, B. J. 1997. Hydrothermal Mineral Deposits: What We Do and What we Don't Know. In: Barnes, H.L. *Geochemistry of Hydrotermal Ore Deposits*, 3rd Edition, p.1-29.

Smith, J.B.; Barley, M.E.; Groves, D.I.; Krapez, B.; McNaughton, N.J.; Bickle M.J. & Chapman, H.J. 1998. The Scholl Shear Zone, West Pilbara; evidence for a domain boundary structure from the integrated tectonostratigraphic analyses, SHRIMP U-Pb dating and isotopic and geochemical data of granitoids. *Precambrian Research,* 88: 143-171.

Stacey, J.S. & Kramers, J.D. 1975. Approximation of terrestrial lead isotope evolution by a two stage model. *Earth Planetary Science Letters,* 26: 207-221.

Williams, I.S. & Claesson, S. 1987. Isotopic evidence for the Precambrian provenance and Caledonian metamorphism of high grade paragneisses from the Seve Nappes, Scandinavian Caledonides, II. Ion microprobe zircon U-Th-Pb. *Contribution to Mineralolgy and Petrology*, 97: 205-217.

Zartmann, R.E. & Doe, B.R. 1981. Plumbotectonics - The model. *Tectonophysics*, 75: 135-162

Tabela 2 Classificação unificada dos depósitos minerais hidrotermais (modificado de Hendequist & Lowenstern 1994; Sillitoe, 1996 e Groves et al. 1998). Salinidade (cloretos de Na e K) dos fluidos: hipersalino (> 50 %peso), moderado (10-20%peso), baixa(< 5% peso),

Tipos de depósitos	Relação com a fonte de calor magmática	Temperatuta/ Profundidade	Fluido	Metais associados	Exemplos
Pórfiros	Adjacente ou hospedado pela intrusão	> 600 °C 2-5 Km	hipersalino e vapor imiscível	Cu ±Mo ±Au, Mo,W ou Sn	El Teniente (Chile) Bingham (USA) Cadia Hill (Austrália) Endako (Canadá)
Escarnitos	Adjacente a intrusões em rochas carbonáticas	400-600 °C 1-5 Km	salino a moderadamente salino	Fe, Cu, Sn, W, Mo, Au, Ag, Pb-Zn	Marcona (Peru) Kamioka (Japan)
Veios relacionados a plutões	Fraturas no interior e próximas a intrusão	300-450 °C Variável	baixa salinidade a moderadamente salino	Cu, Au Sn, W, Mo ±Pb-Zn	Panasqueira (Portugal) San Rafael (Peru)
Epitermal (alta sulfteção)	Acima de intrusões genéticamente relacionadas	<300 °C próximo a superficie até >1,5 Km	salinidade moderada a baixa, condensado inicialmente ácido	Au-Cu Ag-Pb	El Indio (Chile) Rodalquilar (Espanha) Peak Hill (Australia) Summitville (USA) Lepanto (Filipinas)
Epitermal (baixa sulfetação)	Distante (?) da fonte de calor magmática	150-300 °C proximo a superficie até 1 - 2 Km	salinidade muito baixa, rico em gás, pH neutro	Au (Ag, Pb-Zn)	McLughlin (USA) Hishikari (Japan)
	Distante (?) da fonte de calor magmatica	150-300 °C proximo a superficie até 1 - 2 Km	Salinidade moderada	Ag-Pb-Zn (Au)	Kelian (Indonesia) Fresnillo (Mexico) Comstock (USA)
Sulfeto maciço vulcanogênico	Próximo a domos extrusivos	< 300 °C no fundo oceânico ou proximidades	Salinidade próxima da água do mar, rico em gás	Zn-Pb-Ag (Cu ou Au)	Kuroko (Japão) Bousquet (Canadá) Palmeirópolis (Brasil)
Orogênico epizonal	Distante da fonte de calor	150-300 °C < 6 Km	Baixa salinidade, pH quase neutro	Au	Wiluna (Austrália) Racetrack (Austrália
Orogênico mesozonal	Próximo (?) da fonte de calor	300-475 °C 6-12 Km	Baixa salinidade pH quase neutro	Au	Mt Charlotte (Austrália) Golden Mile (Austrália) Timmins (Canadá)
Orogênico hipozonal	Muito próximo (?) da fonte de calor	> 475 °C > 12 Km	Baixa salinidade pH quase neutro	Au	Marvel Loch (Austrália Griffins Find (Austrália)

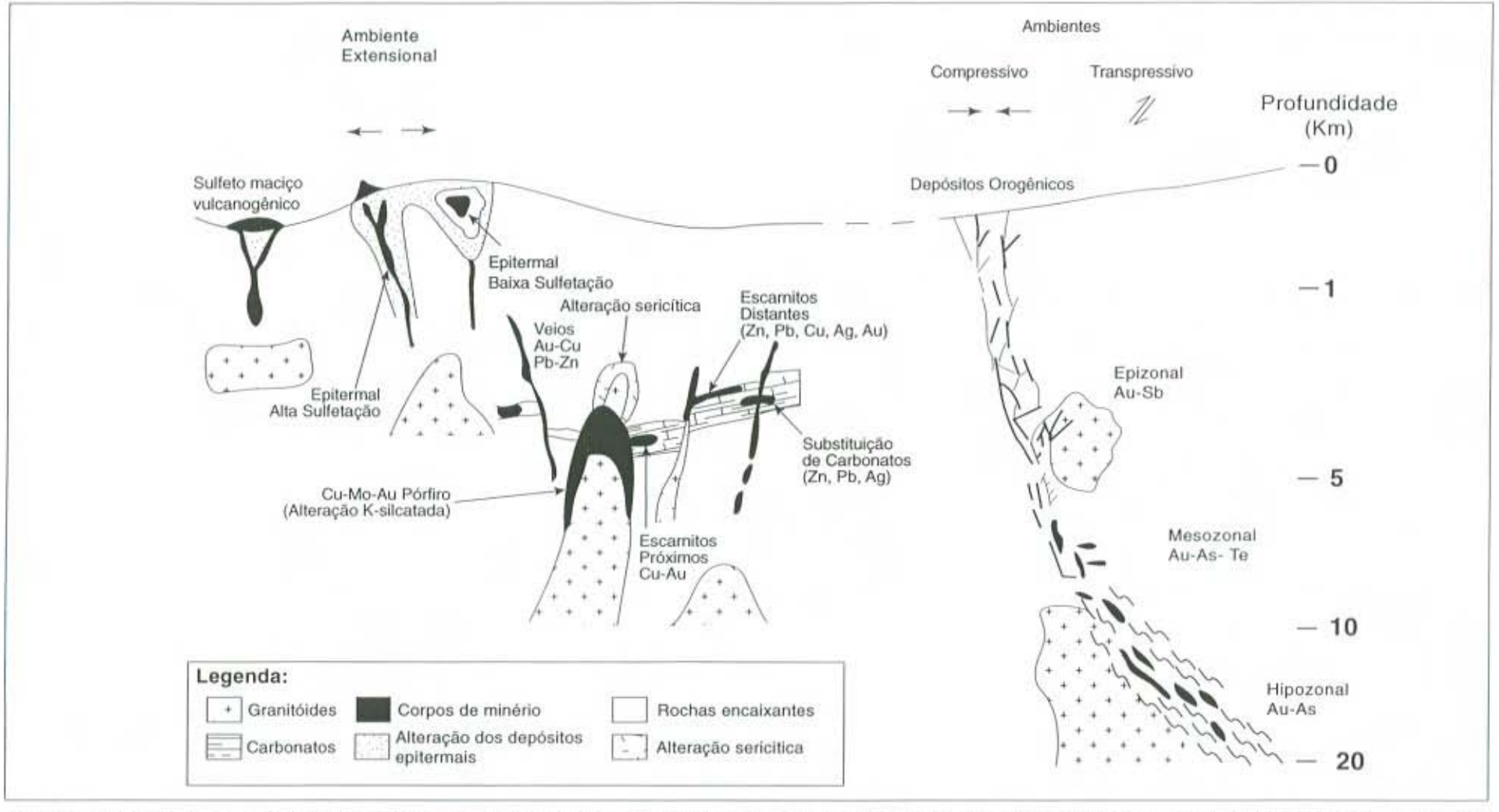

Fig. 2 - Distribuição dos depósitos hidrotermais de metais base e Au ao longo da crosta e ambientes estruturais em relação a uma margem de placa continental (modificado de Groves et al., 1998).

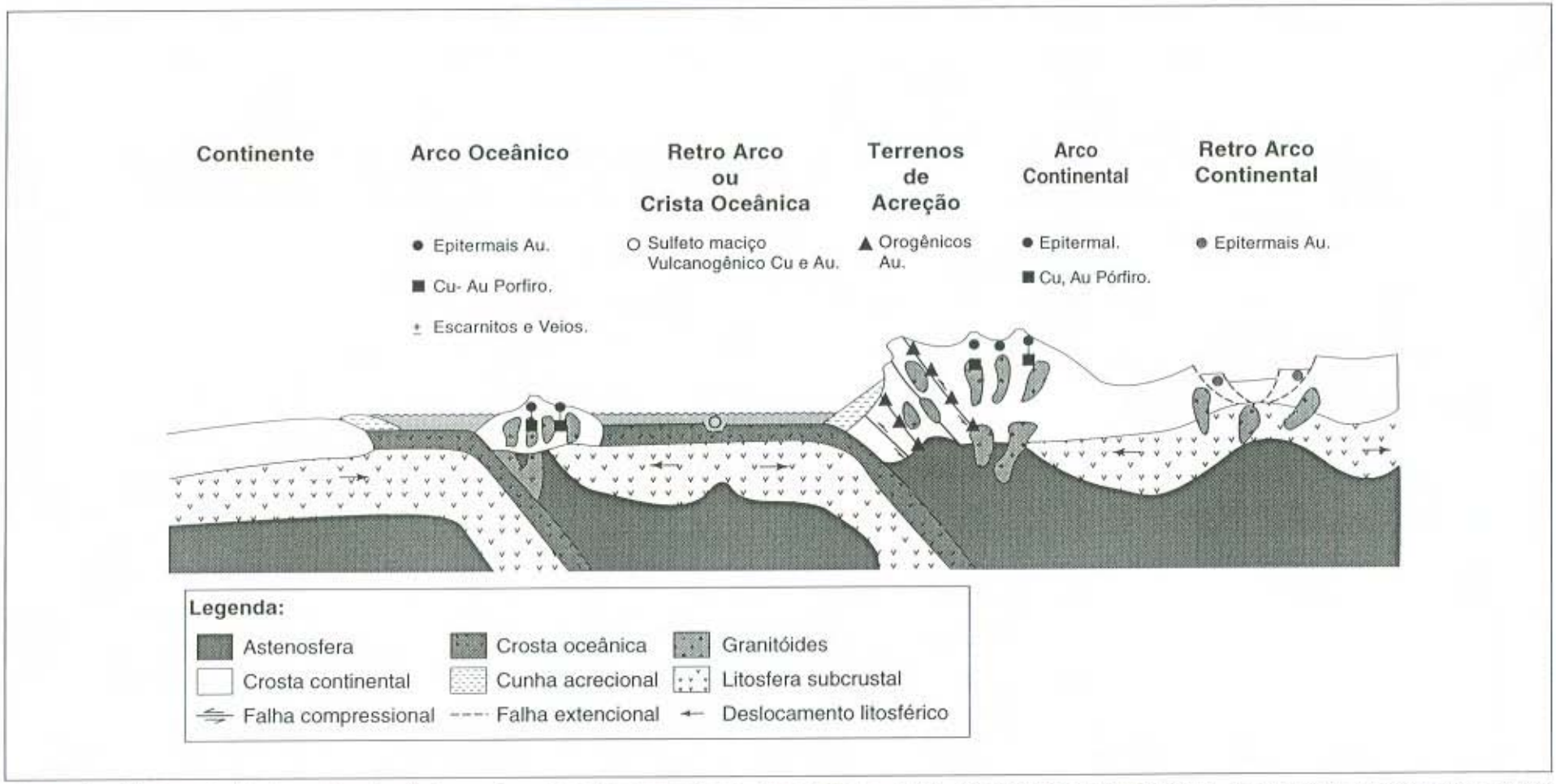

Fig. 3 - Ambientes tectônicos dos depósitos minerais hidrotermais de metais base e Au. Os depósitos de pórfiros, epitermais, escarnitos e veios associados a plutões são formados em profundidade $\leq$ 5 Km em arcos continentais e oceânicos, e em regimes compressivos e extensionais. Os depósitos de Au orogênicos são gerados em regiões compressivas e transpressivas em cinturões deformados, adjacentes a arcos magmáticos continentais (modificado de Groves et al.,1998).

CAPÍTULO II

GOLD IN THE NEOPROTEROZOIC JUVENILE BOSSOROCA VOLCANIC ARC OF SOUTHERNMOST BRAZIL: ISOTOPIC CONSTRAINTS ON TIMING AND SOURCES

Remus, M.V.D.[1]; McNaughton, N.J.[2]; Hartmann, L.A.[1]; Koppe, J.C.[1]; Fletcher, I.R.[2]; Groves, D.I.[2]; Pinto, V.M.[1]

[1] Instituto de Geociências, Universidade Federal do Rio Grande do Sul, Av. Bento Gonçalves, 9500; 91501-970, Porto Alegre, RS, Brazil

[2] Centre for Strategic Mineral Deposits, University of Western Australia, Nedlands, 6907, WA, Australia.

Submetido ao Journal of South American Earth Sciences

Abstract

The Neoproterozoic Bossoroca juvenile Volcanic Arc of southernmost Brazil contains arc-related gold deposits. The Bossoroca gold deposit consists of veins and stockworks of quartz-gold ores with minor pyrite, chalcopyrite, galena and tellurides. Carbonate, chlorite, sericite and tourmaline are the main gangue minerals. The ore shoots are contained in calc-alkaline pyroclastic andesites and dacites with minor basalts and epiclastic rocks of the Campestre Formation. SHRIMP U/Pb investigations of zircon show that the island-arc volcanogenic sequence was formed ca. 757 m.y. ago in the early Brasiliano Cycle and metamorphosed into transitional greenschist/amphibolite facies of low-pressure regional metamorphism at ca. 700 Ma. Nearby, the post-tectonic São Sepé Granite was intruded into the volcanic arc at ca. 550 Ma. The mineralizing fluids have been related either to metamorphism or to solutions derived from post-tectonic intrusive granites. Lead isotopic analyses, carried out on galena from the gold ore, on feldspar and total rock from the associated volcanic pile, and also on feldspar and total rock from the São Sepé Granite, indicate that gold mineralisation is related to the volcanogenic rocks, and that the deposit should be considered to be of an epizonal orogenic type.

Resumo

O Arco Vulcânico Juvenil da Bossoroca de idade Neoproterozóica possui depósitos de ouro relacionados a arco. O depósito de ouro da Bossoroca consiste de veios e "stock-works" de quartzo com pirita, calcopirita, galena e teluretos subordinados. Os principais minerais da ganga são carbonato, clorita, sericita e turmalina. Os filões de minério estão encaixados numa sequência piroclástica dacítica a andesítica calcico-alcalina com basaltos e rochas epiclásticas subordinadas. Investigações em zircões pelo método U/Pb via SHRIMP mostram que a sequência vulcanogênica do arco de ilhas foi gerada há 757 Ma durante o início do Ciclo Brasiliano e metamorfisada na transição do fácies xisto verde/anfibolito do metamorfismo regional de baixa pressão há cerca de 700 Ma. O Granito São Sepé, pós-tectônico, intrudiu no arco há cerca de 550 Ma. Os fluidos mineralizadores têm sido relacionados ao

metamorfismo ou a soluções derivadas dos granitos intrusivos pós-tectônicos. Análises isotópicas de Pb de galenas provenientes do minério aurífero, de feldspatos e rocha total da sequência vulcânica associada e também em feldspatos e rocha total do Granito São Sepé indicam que a mineralização aurífera está relacionada às rochas vulcanogênicas e que o depósito de ouro deve ser considerado como do tipo epizonal orogênico.

INTRODUCTION

Several small, epigenetic, quartz lode-gold deposits occur in the Neoproterozoic juvenile volcanic arc in the Precambrian shield of Rio Grande do Sul State in southernmost Brazil (Koppe, 1990; Babinski et al., 1996). The majority are enclosed in Precambrian metavolcanosedimentary sequences of low- to medium-metamorphic grade of the Vacacaí Group. Others are associated with granites and volcanic rocks formed at the end of the Precambrian to Early Paleozoic. The main deposit in the region is the Bossoroca lode-gold deposit, which has been mined for nearly seventy years. The ore occurs within quartz veins hosted by volcanic rocks of transitional low- to medium-metamorphic grade of the juvenile volcanic arc. This is a small deposit which contains a total of one ton of gold with average contents of about 15 g/ton (Koppe 1990). The mineralisation could either be related to the regional metamorphism or to the intrusion of the nearby post-tectonic São Sepé Granite, or to a related intrusion at depth. The deposit and associated rocks were investigated in order to establish some constraints on timing and metal sources of the ore-forming event, using techniques such as sensitive high-resolution ion microprobe (SHRIMP) U/Pb isotopic determinations on zircon (129 zircon grains), Pb isotope analyses on sulfides, feldspars and whole rocks (13 samples). O and C stable isotope analyses of guangue carbonates (8 samples) were essential for constraining the source of ore fluids.

GEOLOGICAL SETTING

The Precambrian shield of Rio Grande do Sul State is part of the southernmost extension of the Mantiqueira Province (Hasui et al., 1975) and has four major segments (Jost & Hartmann, 1984; Soliani Jr, 1986; Fragoso Cesar et al., 1986; Babinski et al., 1996) as shown in Figure 1. To the east, the 600 Ma-old Pelotas Batholith, derived from crustal reworking of ca. 2.0 Ga-old tonalite-granodiorite and metasedimentary gneisses, is juxtaposed against the 780 Ma-old Porongos schist belt to the west. The schist belt is composed of supracrustal sequences interleaved with ca 2.0 Ga-old basement gneisses. The western part of the shield contains the Taquarembó Block in the south and the São Gabriel Block in the north.

The Bossoroca lode-gold deposit occurs in the São Gabriel Block, near 30°S, 54°W. This block contains two major units (Fig. 2). One is the juvenile Neoproterozoic (Babinski et al., 1996) calc-alkaline volcano-plutonic island-arc association, named the Cambaí Complex for the plutonic rocks and the Vacacaí Group for the volcanic/sedimentary sequence. The other unit in this block is a late to post-tectonic volcano-plutono-sedimentary association named the Seival Association by Chemale Jr. et al. (1995), which occurs outside of the area represented in Figure 2. Known ages are ca. 753 Ma by Machado et al. (1990) for the Vacacaí Group (Campestre Formation) and ca. 704 Ma by Babinski et al. (1996) for the Cambaí Complex gneisses, both using conventional zircon U/Pb geochronology. The Seival Association straddles the Precambrian/Cambrian boundary (Gresse et al., 1996).

The local andesitic rocks are mostly of pyroclastic origin and have chemical compositions rather similar to those of modern arcs. The rocks are calc alkaline, low-K and low-Nb (Koppe & Hartmann, 1988), have a positive ε_{Nd} at 750 Ma and model ages (T_{DM}) younger than 900 Ma (Babinski et al., 1996). These seem to define an old (Neoproterozoic) fragmented, subduction-related arc, which is here informally termed the Bossoroca Volcanic Arc.

The gold mineralisation occurs in the Campestre Formation, which is made up of interlayered intermediate to acid flows (rare), coarse to fine-grained tuffs (abundant), lapilli tuffs, crystal tuffs, conglomerates, sandstones, pelites and minor chert and iron formation. Intermediate to acid compositions predominate, but some basaltic rocks

also occur. The magmatism is typically low-K calc-alkaline (Koppe and Hartmann, 1988).

The Cerro do Ouro Formation occurs on the western side of the Campestre Formation (Fig. 2), and contains abundant serpentinite and magnesian schist bodies interleaved with basalts, iron formations and cherts. It may be an ophiolite (Wildner 1990), but the abundance of mafic-ultramafic volcanic rocks and the komatiitic geochemical affinity of this and regional related ultramafic units (Zarpelon 1986, Remus 1990, Koppe 1990, Remus et al. 1993) is more typical of a Paleoproterozoic greenstone belt (sensu Condie, 1997) which comprises remnants blocks in the Neoproterozoic juvenile volcanic arc.

The overall structure of the rocks trends NE and dips 50° to the NW, and was probably formed by the thrusting component of a transpressive system. According to field observations, the Cambaí Complex gneisses were thrust over the Cerro do Ouro Formation, and both thrusted over the Campestre Formation. A regional metamorphic event is associated with the thrusting and varies from greenschist to middle amphibolite facies, with lower grade in the eastern part and higher grade in the western part of the area (Fig. 2). The structural evidence for thrusting is better developed in the Palma region, to the south of the mapped area. The Campestre Formation is typically altered to greenschist metamorphic grade, but in the Bossoroca deposit, the metamorphic grade reaches the transition to the amphibolite facies, with formation of hornblende in mafic schists as determined by electron microprobe analyses (Koppe, 1990). Deformation of the volcanic sequence was not very intense. The S1 schistosity or slaty cleavage, and the brittle S2 fracturing, overprinted, but did not obliterate, the sedimentary and volcanic characteristics of the rock pile. In low strain domains, the original fabrics of pyroclastic and epiclastic protoliths are very well preserved. The S1 foliation trends to the NE and dips to the NW. Local transposition of foliation is associated with the main D1 progressive deformation episode. Brittle-ductile transcurrent shear zones concordant with the schistosity formed late in the D1 episode.

Low-pressure type, regional dynamothermal metamorphism in mafic/ intermediate rocks of the Campestre Formation produced quartz + chlorite + white mica + albite + epidote + calcite asemblages in lower grade and quartz + albite + biotite + hornblende in higher grade rocks. In

metapelites, the paragenesis is: quartz + muscovite + chlorite + andalusite and quartz + muscovite + biotite + albite (Zarpelon 1986, Wildner 1990, Koppe 1990).

In the Bossoroca deposit, gold occurs as free gold and Au-pyrite inclusions in quartz veins of variable thicknesses. The quartz veins reach up to 1 m in thickness, but are normally around 0.3 m thick, while, in the nearby Cerrito do Ouro deposit, the quartz veins are up to 3 m thick. Veining is subparallel to the S1 schistosity, but it locally crosscuts the foliation at low angle. Veins are deformed by the D1 episode. These relationships suggest that quartz vein-related mineralization in the area was late to syn the D1 episode. Some late quartz veins and veinlets are oblique, or perpendicular, to S1, suggesting a later generation of extensional fracturing. The gold occurs between crystals of quartz, calcite and sulfide and subordinately as inclusions or as part of the pyrite structure. Free gold is also present in many small quartz veinlets over the entire area of the volcanic arc.

The São Sepé and two other related granite plutons are intrusive into the volcano-sedimentary arc (Fig. 2), and produce metamorphic contact aureoles superimposed on low-grade regional metamorphism. Metapelites close to the São Sepé Granite contact are transformed into andalusite + staurolite + biotite + plagioclase + quartz (+ cordierite + almandine garnet) hornfels.

METHODOLOGY

Geological field mapping was carried out over the entire volcanic arc at the 1:50,000 scale but a more detailed 1:5,000 survey was performed on the area close to the mine (Fig. 2). The mine itself was surveyed at the 1:500 scale in several levels as stripping progressed (Koppe 1990). Structural controls were established and rock and ore samples collected for laboratory studies.

Approximately five hundred thin sections of the entire volcanic arc were studied, followed by rock geochemistry and electron microprobe analyses of minerals (Koppe and Hartmann, 1988; Koppe, 1990). For the present investigation, rock samples were collected from the mine pit and from the São Sepé Granite. Samples weighing one kilogram were collected for Pb isotopic studies, and about forty

kilograms of a dacitic crystal tuff from the mine pit were collected for zircon studies, because the rock is poor in this mineral. Only five kilograms of granite were necessary for zircon separation. Feldspars were separated from the dacite and granites by conventional magnetic and heavy liquid procedures. Ore sulfides were collected in the mine pit for sulfide Pb-isotope studies; individual sulfides were separated by hand picking.

Zircon geochronology was undertaken in one sample to determine the age of the host dacite rock from the Campestre Formation. SHRIMP investigations of zircons were undertaken at Curtin University and follow the procedures of Compston et al. (1984) and Smith et al. (1998). Scanning electron microscope images of grains to be analysed were obtained using backscattered electron (BSE) and cathodoluminescence (CL) modes at the Centre for Microscopy and Microanalysis, University of Western Australia. The dacite contained few zircons: only twenty nine crystals were obtained and analysed from forty kilograms of rock.

Rock samples for isotopic analysis were crushed and milled in an agate mortar to minimise any contamination. Lead was extracted by ion exchange chromatography at the Lead-free Laboratory, University of Western Australia, and the isotopic measurements were made on a VG354 multicollector mass spectrometer housed at Curtin University.

SHRIMP ZIRCON U/Pb STUDIES

The wall-rock dacite from the open pit contains three morphological zircon types. The largest population is made up of small short prismatic, colourless, angular, commonly broken crystals. BSE/CL images (Fig. 3) reveal an internal igneous texture of oscillatory and sector zoning, most visible in the CL images. Oscilatory zoning is common in this population (Fig. 3A, 3A1). Sixteen analyses on fifteen crystals of this type (Table 1) are analytically indistinguishable from each other and show a $^{206}Pb/^{238}U$ age of 757±17 Ma (Fig 4). The U and Th contents of the zircons are low (Table 1, Fig. 5), and Th/U ratios vary from 0.2 to 0.5, which are typical of igneous zircons. The age of ca. 757 Ma is considered to be the magmatic age of the volcanic rock, and it is in agreement with the conventional U/Pb zircon age determination of 753±2 Ma obtained by Machado et al. (1990) for a rhyolite from the

Campestre Formation (Fig. 2). A few crystals yield the same age (ca. 757 Ma) on cores and rims (e.g. Fig. 3A), corresponding to the magmatic age. A special problem is encountered in four spots which yield ages around 800 Ma; these could be within analytical error of the 757 Ma-event or else be inherited cores. In crystal 31 (Table 1), the core is 816 Ma-old and the rim 788 Ma-old. This means that the core contains inherited lead, although there are no special textural features on BSE/CL images. As a consequence, spots 31-2, 30-1, 15-1 and 33-1 are not included in calculation of the average magmatic age.

Two zircon crystals display external forms similar to the first group, but the internal structure shows a core which is discordant to, and partly overgrows, the euhedral internal zoning (Fig. 3C, 3C1). An equivalent textural relationship of younger cores was recognized by Gebauer (1996, p. 312); this is also similar to the internal growth textures formed by fracture sealing, as described by Hartmann et al. (1997). The $^{206}Pb/^{238}U$ age of this zircon growth is 699±15 Ma, which coincides with the conventional U/Pb zircon age determination of 704±13 Ma on a syn-tectonic diorite from the nearby Cambaí Complex (Babinski et al. 1996). This ca. 700 Ma age is considered to be the age of the M1 metamorphic event affecting the Bossoroca Arc.

One inherited crystal was identified; it is clear and shows no internal zoning; the rounding probably indicates sedimentary recycling (Fig. 3D). The $^{206}Pb/^{238}U$ age obtained is 1023±22 Ma and agrees very well with previous conventional U/Pb dating of inherited zircon from a nearby rhyolite by Machado et al. (1990).

Four spot analyses have high common lead (Table 1) and have the same textural features as the magmatic population. Another group, which gives ages younger than the metamorphic event, is interpreted as a lead-loss group. These zircons lost lead, possibly due to incipient metamictization in higher U (about 900 ppm) spots and to solutions migrating through fractures.

The São Sepé Granite has two main textural facies, as characterized by field mapping, petrography and geochemistry (Sartori and Ruegg, 1978; Gastal et al., 1995). Zircons from two samples of the different granite facies were studied using the SHRIMP. The preliminary zircon date from this and another granite plutons of the São Gabriel Block were previously presented by Remus et al. (1997).

The monzogranite facies located in the northern part of pluton has a single zircon population with a $^{206}Pb/^{238}U$ age of 558±8 Ma (Fig. 7 and Table 2). The magmatic zircon population is made up of yellowish to colourless euhedral prismatic and short prismatic crystals with {100} and {010} symmetric well-developed faces. BSE and CL images reveal an internal texture of massive, complex or oscillatory zoned cores and oscillatory zoned rims (Figs 6A and 6B), which contain inclusions of very small long prismatic black and colorless minerals. The age of cores and rims of analysed zircons are analytically indistinguishable (Fig. 6A). The younger grains show the same texture as the main magmatic population. These zircons lost lead due to modern weathering or contain high common lead (Fig. 7).

The sample from the microgranite facies was collected from a quarry at the SE edge of the pluton, and has only one distinctive magmatic zircon population. It is represented by colorless and yellowish grains of prismatic and short prismatic zircons with symmetrical and asymmetrical {101} and {110} pyramid faces, and has a $^{206}Pb/^{238}U$ age of 550±6 Ma (Fig. 8 and Table 3) which is interpreted as the magmatic age of this granite border facies. BSE and CL images show an internal texture of massive or oscillatory and, rarely, complexly zoned cores. Oscillatory zoning is visible especially in the rims of grains (Figs 6C, 6D). The discordant Th-U-Pb zircon group and high common Pb group (Fig. 8) have the same morphologic characteristics as the magmatic population. A value of εNd of -10 for the microgranite facies, and a model age (T_{DM}) of 2.3 Ga, indicate its derivation from ancient crustal rocks (Remus et al. 1997). Older zircon xenocrysts are absent in this granite, and this may be due to the high temperature of the magma, which is likely to have caused complete dissolution of older zircons derived from the basement rocks and granite source region. This evidence, and Pb and Nd isotopic data, indicate an old crustal source origin (possibly granulites) for the granite which is compared to a A-type granites and agrees well with previous geochemical classification (Gastal et al. 1995).

FLUIDS

Fluid inclusion studies in quartz veins by Koppe (1990) indicate an average temperature of gold deposition of 247°C and a lithostatic pressure ranging from 500 to 1300 bars. The fluid composition is represented by the H_2O-CO_2 system with low salinity (about 1% NaCl equiv.) and average density of 0.82 g/cm^3. $\partial^{13}C$ values for gangue calcite are between -5.6 and -8.2‰ PDB (n = 8), whereas $\partial^{18}O$ values fall between +15 and +16.7‰ SMOW (n = 8). This indicates a homogeneous fluid and stable conditions of temperature and pressure during mineralisation. The data suggest that the ore fluid was a deeply derived fluid (Groves et al., 1992). Fluids probably ascended through regional shear zone structures and reached the registered transitional greenschist/amphibolite facies position in the upper crust (Koppe 1990).

LEAD ISOTOPES AND SOURCE OF MINERALIZATION

Lead isotopic analyses were performed on several minerals and rocks in order to assess the source of Pb in the mineralising system. Galenas from the main gold-quartz vein in the Bossoroca Mine pit were analysed. Analyses were also done on plagioclase and whole-rock samples from the wall-rock dacite, and also on K-feldspars from two facies of the São Sepé Granite. The feldspars were separated and analysed because their low U/Pb allowed the Pb isotope composition to better reflect the initial Pb in the granites (e.g. McNaughton and Bickle, 1987). The lead isotopic data are presented in Table 4, and shown on a common lead diagram in Figure 9. The plagioclase and two volcanic samples plot on a Pb-Pb isochron compatible with a ca. 750 Ma age of igneous crystallization, as determined by SHRIMP. The third sample plots off the isochron, probably because it is more altered and enriched in tourmaline (~2 wt%).

The galena data, which are considered the best estimates of the initial Pb composition in the ore system, are isotopically homogeneous and also plot on the ca. 750 Ma reference isochron. Although the galena-plagioclase-metadacite array of data could be interpreted as galena formation shortly after volcanism, the slope of the reference isochron

is relatively insensitive to age. The quartz vein-related mineralisation is considered to be late in the D1-M1 episode at ca. 700 Ma, based on field observations. This is the suggested age of deposition of gold in the Bossoroca Mine. The deposits in the area appear restricted to the interval 750-700 Ma. The Pb isotope data are compatible with the timing constraints. Further, the Pb in galenas from the Bossoroca deposit is also compatible with derivation solely from the host metadacites at ca. 700 Ma.

Lead isotopic data for K-feldspars from the border facies and core facies of the São Sepé granitic rocks are shown in Figure 9. The average of the least radiogenic Pb from K-feldspars from each facies of the granite is the best estimate for the initial Pb isotopic compositions of the magma. These compositions for the two facies are similar to each other, but distinctly more primitive than the galena data (Fig. 8). This large contrast in Pb isotopic composition is distinctive. Thus, a granite of similar isotopic characteristics and age to the São Sepé Granite could not have contributed with Pb to the mineralising fluid. Even a small contribution would have caused the galena data to fall below the 750 Ma reference isochron in Figure 9.

The Pb isotope data show that the ore fluids in the Bossoroca gold deposit were probably derived from the host terrain or the source rock of host terrane. The structural timing of mineralisation was late in the metamorphic cycle, and this deposit is considered to be an epizonal orogenic gold deposit in the sense of Groves et al. (1998). It is inferred that metals were mobilized by fluids ascending through the Campestre Formation volcanic pile. These ascending fluids scavenged lead and gold to deposit the metals in structurally controlled sites higher in the crust. Also, the metals could be derived from the same deep source region of volcanic rocks of Campestre Formation. The main source of fluids most probably was the deeper crust.

CONCLUSIONS

SHRIMP U/Pb dating of zircons from dacitic wall-rocks of the Campestre Formation, which host the Bossoroca lode-gold deposit, yields an age of 757±17 Ma for volcanism which formed this part of the juvenile island arc. The age of the peak of metamorphism for the

Campestre Formation is estimated to be ca. 700 Ma, based on SHRIMP age data on 757 Ma zircons which show textural re-equilibration. The structural timing of the ores is compatible with the younger age also being the age of mineralisation. Lead isotope evidence suggests that the Pb in the ore fluid was derived from the host Campestre Formation or its source region.

The São Sepé Granite intruded the volcanic arc at ca. 550 Ma and caused a marked metamorphic contact aureole on rocks of the Campestre Formation. However, the initial Pb composition of granite samples is markedly different from the initial Pb of the Bossoroca ore, showing that the granite, or a related magma at depth, could not be the source of the metals in the gold deposit.

This study indicates that metals concentrated in the Bossoroca lode-gold deposit were mobilized during regional dynamothermal metamorphism by deeply derived fluids that ascended through the volcano/sedimentary Campestre Formation, scavenged lead and gold, and later deposited the metals in structurally controlled sites at higher crustal levels. Also the metals could be derived from the same deep source region of volcanic rocks of Campestre Formation. The O-C stable isotope evidence is compatible with a deeply derived ore fluid.

Acknowledgments

This paper is part of a PhD study on the Copper Province of Rio Grande do Sul funded by CNPq - National Research Council of Brazil to the first author (Grant 201393/94-8). Zircon analyses were carried out on a Sensitive High Resolution Ion Micro-Probe mass spectrometer (SHRIMP II) operated by a consortium consisting of Curtin University of Technology, the Geological Survey of Western Australia and the University of Western Australia with the support of the Australian Research Council. Mrs Marion Dahl (UWA - Australia) is thanked for help with the analytical data. Dra. Tamar Galembeck (UNESP-SP) is thanked for the preliminary zircon sample preparation. Paul Potter reviewed the English version of the paper.

REFERENCES

Babinski, M., Chemale Jr., F., Hartmann, L.A., Van Schmus, W.R. and Silva. L.C. (1996) Juvenile accretion at 750-700 Ma in southern Brazil. *Geology*, 24 (5): 439-442.

Chemale Jr., F., Hartmann, L.A. and Silva, L.C. (1995) Stratigraphy and tectonism of Precambrian to Early Paleozoic units of southern Brazil and Uruguay. Excursion Guidebook, *Acta Geologica Leopoldensia*, 42 (XVIII): 5-117.

Compston, W., Williams, I.S. and Meyer, C. (1984) U-Pb geochronology of zircons from Lunar breccia 73217 using a sensitive high-mass resolution ion microprobe. *Jounal of Geophysical Research* 89 Suppl.: B525-B534.

Condie, K.C. (1997) *Plate Tectonics and Crustal Evolution*, 4th ed. Butterworth-Heinemann, Oxford, 282p.

Fragoso César, A.R.S., Figueiredo, M.C.H., Soliani Jr. E. and Faccini, U.F. (1986) O Batólito de Pelotas (Proterozóico Superior/Eo-Paleozóico) no Escudo do Rio Grande do Sul. In: *Congresso Brasileiro de Geologia, 34, Goiânia, Anais* 3, 167-191.

Gastal, M.C., Nardi, L.V.S. and Lafon, J.M. (1995) Classificação dos granitóides pertencentes a suite intrusiva Saibro (SIS), RS. In: *Simpósio Sul-Brasileiro de Geologia, 6, Porto Alegre, Resumos Expandidos*: 72-76.-

Gebauer, D. (1996) A P-T-t path for (ultra-?) high-pressure ultramafic/mafic rock-association and its felsic country-rocks based on SHRIMP-dating of magmatic and metamorphic zircon domains: Alpe Arami (Central Swiss Alps). *The American Geophysical Union, Geophysical Monograph*, 95, 307-329.

Gresse, P.G., Chemale Jr., F., Silva, L.C.; Walraven, F. and Hartmann, L.A. (1996) Late- to post-orogenic basins of the Pan-African-Brasiliano collision orogen in southern Africa and southern Brazil. *Basin Research*, 8, 157-171.

Groves, D.I., Barley, M.E., Barnicoat, A.C., Cassidy, K.F., Fare, R.J.; Hagemann, S.G., Ho, S.E., Hronsky, J.M.A., Mikucki, E.J., Mueller, A.G.; McNaughton, N.J., Perring, C.S., Ridley, J.R. and Vearcombe, J.R. (1992) Sub-greenschist to granulite-hosted Archaean lode-gold deposits of Yilgarn Craton: A depositional continuun from deep-sourced hydrothermal fluids in crustal scale plumbing systems. In: *The*

Archaen: Terrains, Processes and Metallogeny, eds. Glover, J.E and Ho, S.E., pp. 325-337, University of Western Australia Publication, 22, Perth, Australia.

Groves, D.I., Goldfarb, R.J., Gebre-Mariam, M., Hagemann, S.G. and Robert, F. (1998). Orogenic gold deposits: A proposed classification in the context of their crustal distribution and relationship to other gold deposit types. *Ore Geology Reviews*, 13, 7-27.

Hartmann, L.A., Takehara, L., Leite, J.A.D., McNaughton, N.J. and Vasconcellos, M.A.Z. (1997) Fracture sealing in zircon as evaluated by electron microprobe analyses and back-scattered electron imaging. *Chemical Geology*, 141, 67-72.

Hasui, Y.; Carneiro, C.D.R; Coimbra, A.M. (1975) The Ribeira Folded Belt. *Revista. Brasileira de Geociências*, 5(4), 257-266.

Jost, H. and Hartmann, L.A. (1984) Província Mantiqueira - Setor Meridional. In: *O Pré-Cambriano do Brasil*, eds. Almeida F.F.M. and Hasui, Y., pp. 345-367, Edgard Blücher, São Paulo, Brazil.

Koppe JC (1990) *Metalogênese do Ouro da Mina da Bossoroca, São Sepé, RS.* Unpublished Ph.D. Thesis, 289p. Universidade Federal do Rio Grande do Sul, Porto Alegre, Brazil.

Koppe, J.C. and Hartmann, L.A. (1988) Geochemistry of Bossoroca Greenstone Belt, southernmost Brazil. *Geochimica Brasiliense*. 2 (2), 167-174.

Machado, N., Koppe, J.C. and Hartmann, L.A. (1990) A late Proterozoic U-Pb age for the Bossoroca Belt, Rio Grande do Sul, Brasil. *Journal of South American Earth Sciences*, 3 (2/3), 87-90.

McNaughton, N.J. and Bickle, M.J. (1987) K-feldspar Pb-Pb isotope systematics of post-kinematic granitoid intrusions of the Diemals area, central Yilgarn Block, Western Australia: *Chemical Geology*, 66, 193-208.

Remus, M.V.D. (1990) *Geologia e geoquímica do Complexo Cambaizinho, São Gabriel- RS.* Unpublished M.Sc. Thesis, 267p. Universidade Federal do Rio Grande do Sul, Porto Alegre, Brazil.

Remus, M.V.D., Hartmann, L.A. and Formoso, M.L.L. (1993) Os padrões de Elementos Terras Raras (ETR) e a afinidade geoquímica komatiítica dos xistos magnesianos e rochas associadas do Complexo Cambaizinho, São Gabriel-RS. *Revista Brasileira de Geociências* 23 (4), 370-387.

Remus, M.V.D., McNaughton, N.J., Hartmann, L.A. and Fletcher, I.R. (1997) Zircon SHRIMP U/Pb dating and Nd isotope data of granitoids of the São Gabriel Block, southern Brazil: evidence for an Archaean/Paleoproterozoic basement. In: *International Symposium on Granites and Associated Mineralizations, 2,* Salvador, Brazil, Extended Abstracts, 271-272.

Smith, J.B., Barley, M.E., Groves, D.I., Krapez, B., McNaughton, N.J., Bickle M.J. and Chapman, H.J. (1998) The Scholl Shear Zone, West Pilbara; evidence for a domain boundary structure from the integrated tectonostratigraphic analyses, SHRIMP U-Pb dating and isotopic and geochemical data of granitoids. *Precambrian Research,* 88,143-171.

Soliani Jr, E. (1986) *Os dados geocronológicos do Escudo Sul-Riograndense e suas implicações de ordem geotectônica.* Unpublished Ph.D. Thesis, 239p. Universidade de São Paulo, São Paulo, Brazil.

Wildner, W. (1990) *Caracterização geológica e geoquímica das seqüências ultramáficas e vulcano-sedimentares da região da Bossoroca-RS.* Unpublished M.Sc Thesis, 170p. Universidade Federal do Rio Grande do Sul, Porto Alegre, Brazil.

Zarpelon P.R. (1986) *Geologia estrutural, estratigrafia e petrologia de uma parte do "greenstone-belt" Cerrito do Ouro, município de São Sepé-RS.* Unpublished M.Sc. Thesis, 215p. Universidade Federal do Rio Grande do Sul, Porto Alegre, Brazil.

Figure Captions

Fig. 1 Schematic geotectonic map showing the regional setting of the Bossoroca Gold Deposit in the Sul-Riograndense Shield (after Jost & Hartmann, 1984; Soliani Jr, 1986; Fragoso Cesar et al., 1986; Babinski et al.,1996).

Fig. 2 Geologic map of the Bossoroca Gold Deposit district (after Koppe & Hartmann, 1988).

Fig. 3 SEM images of sectioned zircons from dacitic metatuff of the Campestre Formation. On the left are the BSE (backscattered electron) images, whereas CL (cathodoluminescence) images of the same grain are shown on the right. Circles indicate areas of analyses; scale bar indicated. Zircons A and B (grains 6A.9 and 6A.20) show igneous textural zonation. Zircon C (grain 6A.22) shows textural replacement of the core region, which is younger than the igneous zonation. Zircon D (grain 6A.23) is older than the magmatic event and the rounding is suggestive of inherited sedimentary zircon.

Fig. 4 Concordia diagram of zircon populations from dacitic metatuff, the hostrock of the Bossoroca Gold Deposit. The main zircon population (unfilled pattern) defines the age of igneous crystallization. The oldest zircon grain is an inherited xenocryst (medium gray pattern) and the younger grains in the detail box (light gray pattern) are the zircon population affected by metamorphism at ca. 700 Ma. High common Pb and Pb-loss populations are discussed in the text.

Fig. 5 206Pb/238U age (Ma) versus U and Th (ppm) diagram showing the relatively low U and Th contents of zircons from the dacitic metatuff of the Campestre Formation (A). Th/U ratios of zircons from the dacitic metatuff showing typical ratios of igneous zircons. Th/U ratios of two metamorphic spots also shown (B).

Fig. 6 SEM images of sectioned zircons from the São Sepé Granite. The images on the left are BSE, whereas CL images of the same grains are shown on the right. Marks indicate areas of analysis; scale bar indicated. Zircons A and B (grains 15B.29 and 15B.19) are from the monzogranite central facies, zircons C and D (grains 15A.33 and 15A.22) are from the microgranite border facies.

Fig. 7 Concordia diagram of zircon populations from the monzogranite central facies of the São Sepé Granite pluton. The main zircon group (unfilled pattern) defines the magmatic age of the central facies of the pluton. The younger zircon populations refer to a high common Pb (stippled pattern) and to the zircons that lost Pb due to modern weathering (medium gray pattern).

Fig. 8 Concordia diagram of zircon populations from the microgranite border facies of the São Sepé Granite pluton. The main zircon group (unfilled pattern) defines the magmatic age of the border facies of the pluton. The younger zircons close to the magmatic population refer to a discordant Th-U-Pb group (gray pattern). The high common-Pb zircons are stippled.

Fig. 9 Common-lead isotope diagram showing the Campestre Formation (dacite) whole- rocks and plagioclase, and galenas from quartz gold veins of the Bossoroca Gold Deposit. K-feldspars from the border and central facies of the São Sepé Granite are also shown for comparison. The 750 Ma reference isochron for the Campestre Formation and the Stacey & Kramer (1975) growth curve are shown for reference.

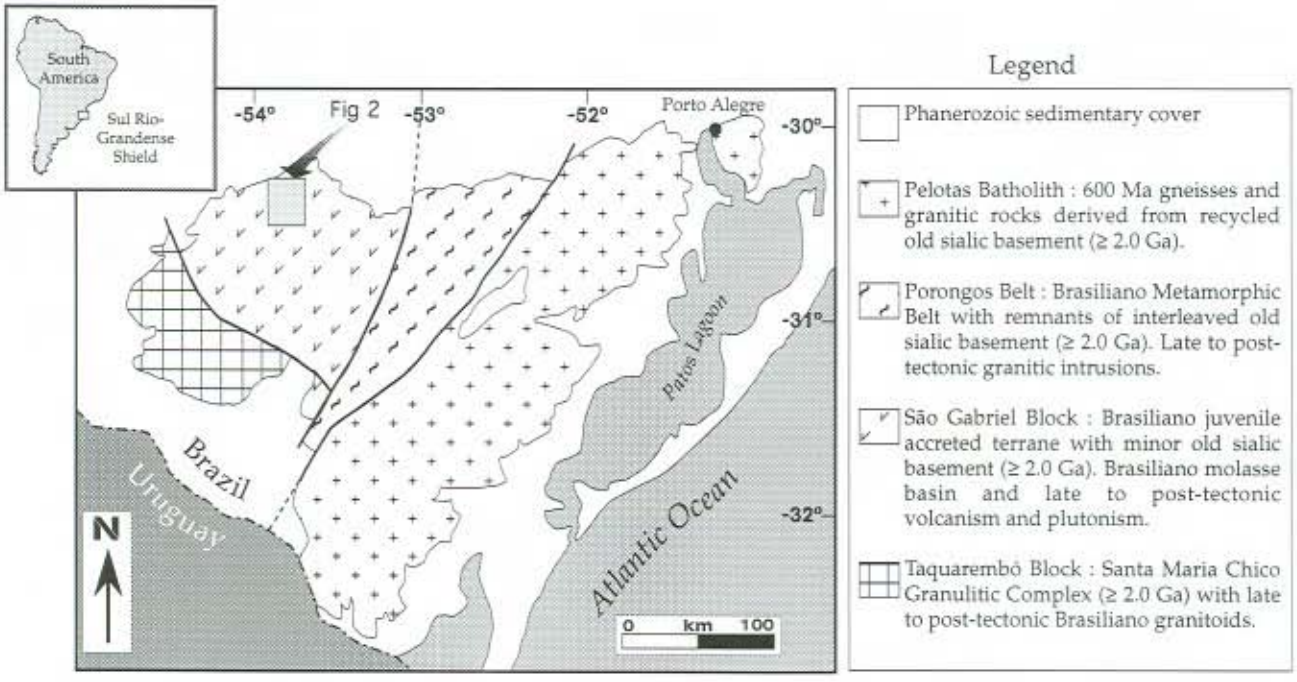
South America
Sul Rio-Grandense Shield
-54°
Fig 2
-53°
-52°
Porto Alegre
-30°
-31°
-32°
Patos Lagoon
Brazil
Uruguay
Atlantic Ocean
N
0 km 100
Legend
Phanerozoic sedimentary cover
Pelotas Batholith : 600 Ma gneisses and granitic rocks derived from recycled old sialic basement (≥ 2.0 Ga).
Porongos Belt : Brasiliano Metamorphic Belt with remnants of interleaved old sialic basement (≥ 2.0 Ga). Late to post-tectonic granitic intrusions.
São Gabriel Block : Brasiliano juvenile accreted terrane with minor old sialic basement (≥ 2.0 Ga). Brasiliano molasse basin and late to post-tectonic volcanism and plutonism.
Taquarembó Block : Santa Maria Chico Granulitic Complex (≥ 2.0 Ga) with late to post-tectonic Brasiliano granitoids.

Figura 1

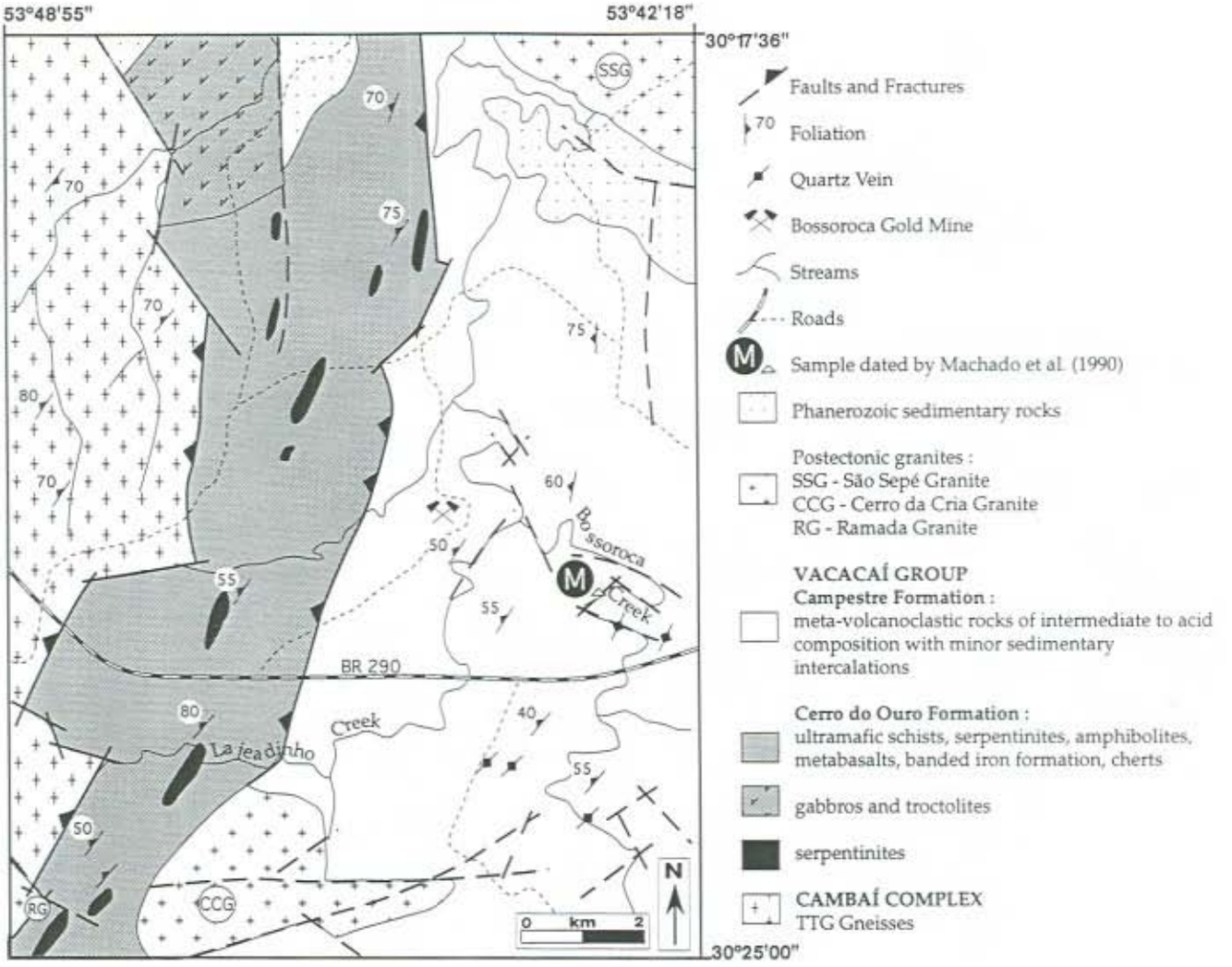
53°48'55"
53°42'18"
30°17'36"
30°25'00"
SSG
CCG
RG
BR 290
Bossoroca Creek
Lajeadinho Creek
70
75
80
60
50
55
40
0 km 2
N
Faults and Fractures
Foliation
Quartz Vein
Bossoroca Gold Mine
Streams
Roads
Sample dated by Machado et al. (1990)
Phanerozoic sedimentary rocks
Postectonic granites :
SSG - São Sepé Granite
CCG - Cerro da Cria Granite
RG - Ramada Granite
VACACAÍ GROUP
Campestre Formation :
meta-volcanoclastic rocks of intermediate to acid composition with minor sedimentary intercalations
Cerro do Ouro Formation :
ultramafic schists, serpentinites, amphibolites, metabasalts, banded iron formation, cherts
gabbros and troctolites
serpentinites
CAMBAÍ COMPLEX
TTG Gneisses

Figura 2

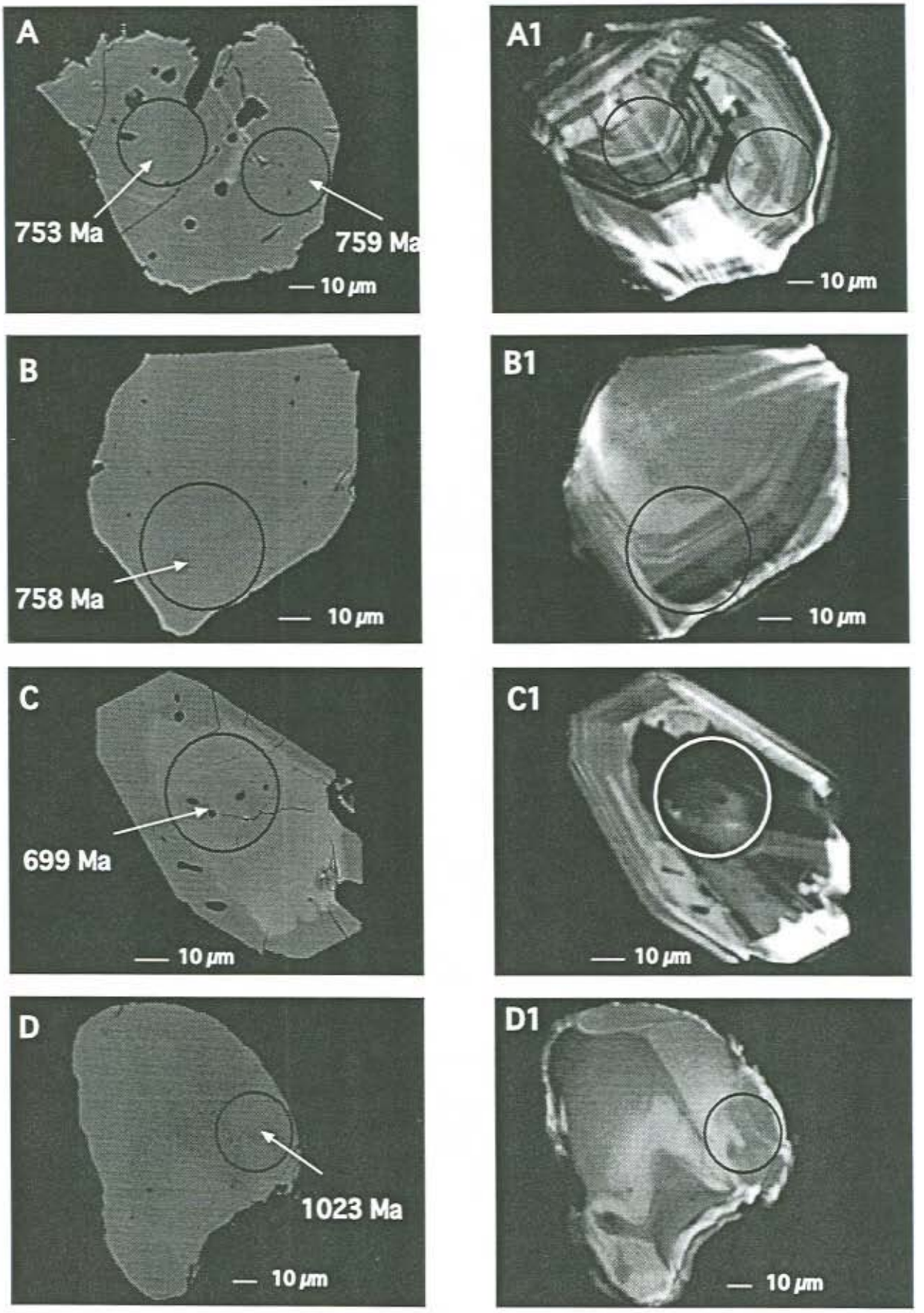
A
753 Ma
759 Ma
— 10 µm
A1
— 10 µm
B
758 Ma
— 10 µm
B1
— 10 µm
C
699 Ma
— 10 µm
C1
— 10 µm
D
1023 Ma
— 10 µm
D1
— 10 µm

Figura 3

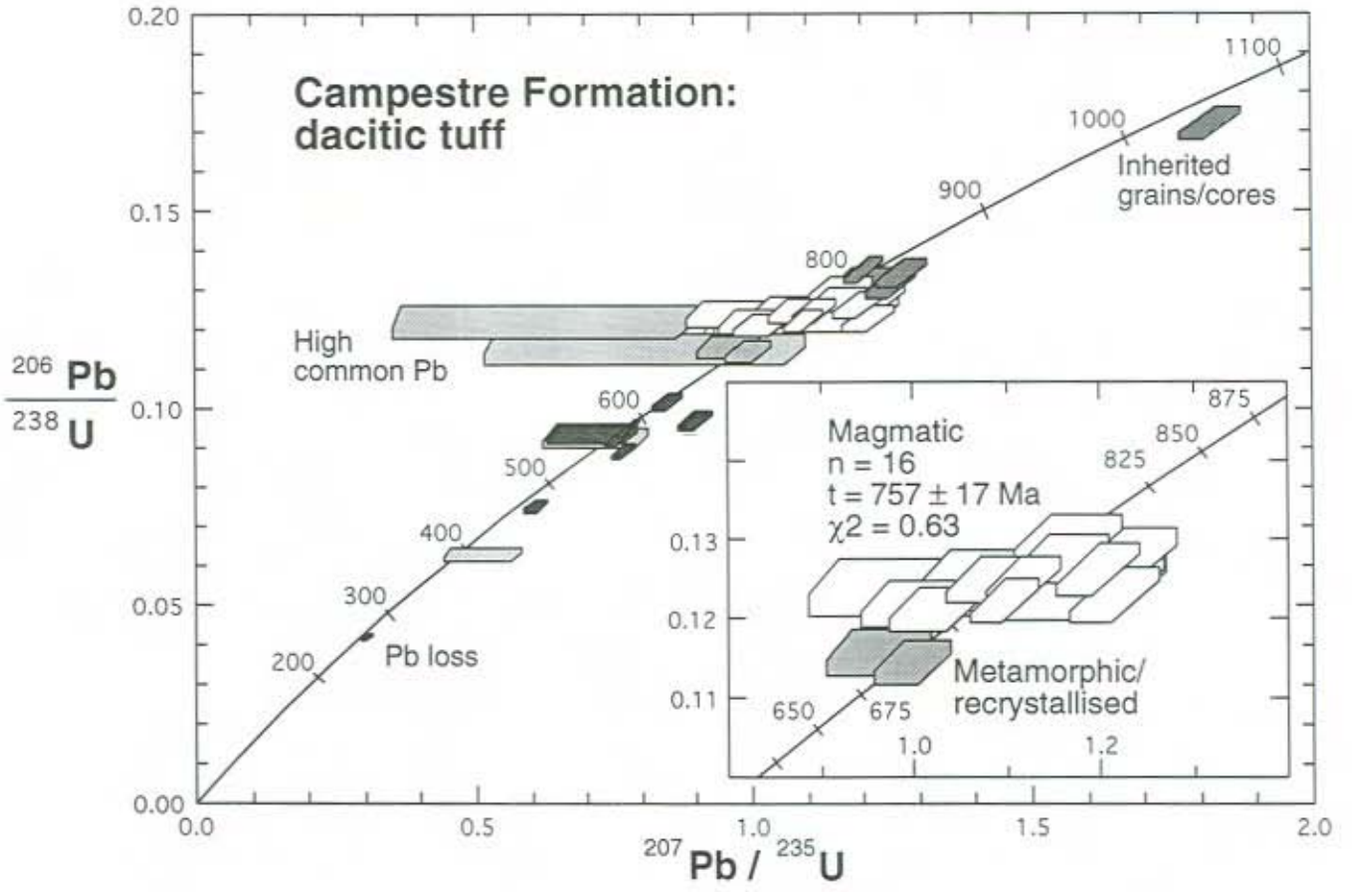
Campestre Formation:
dacitic tuff
Inherited
grains/cores
High
common Pb
Pb loss
Magmatic
n = 16
t = 757 ± 17 Ma
χ2 = 0.63
Metamorphic/
recrystallised
206 Pb / 238 U
207 Pb / 235 U
0.00
0.05
0.10
0.15
0.20
0.0
0.5
1.0
1.5
2.0
200
300
400
500
600
800
900
1000
1100
0.11
0.12
0.13
650
675
825
850
875
1.0
1.2

Figura 4

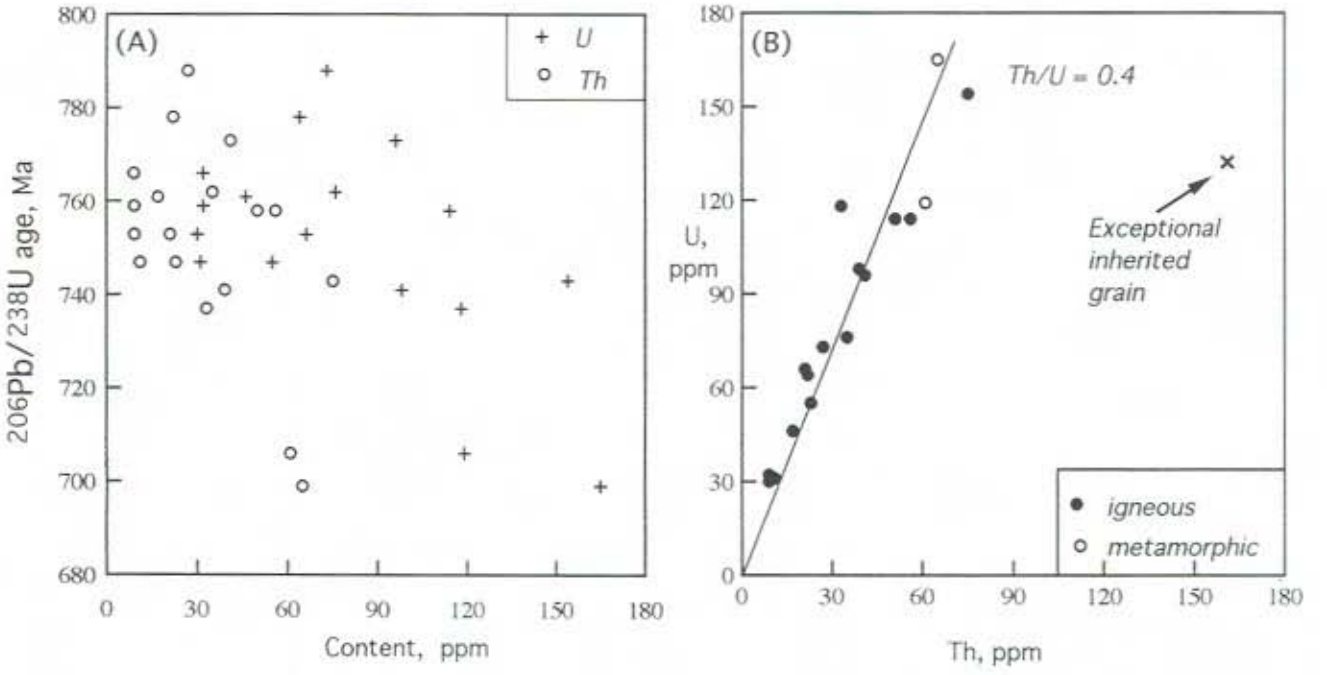
(A)
+ U
o Th
206Pb/238U age, Ma
Content, ppm
(B)
Th/U = 0.4
Exceptional inherited grain
igneous
metamorphic
U, ppm
Th, ppm

Figura 5

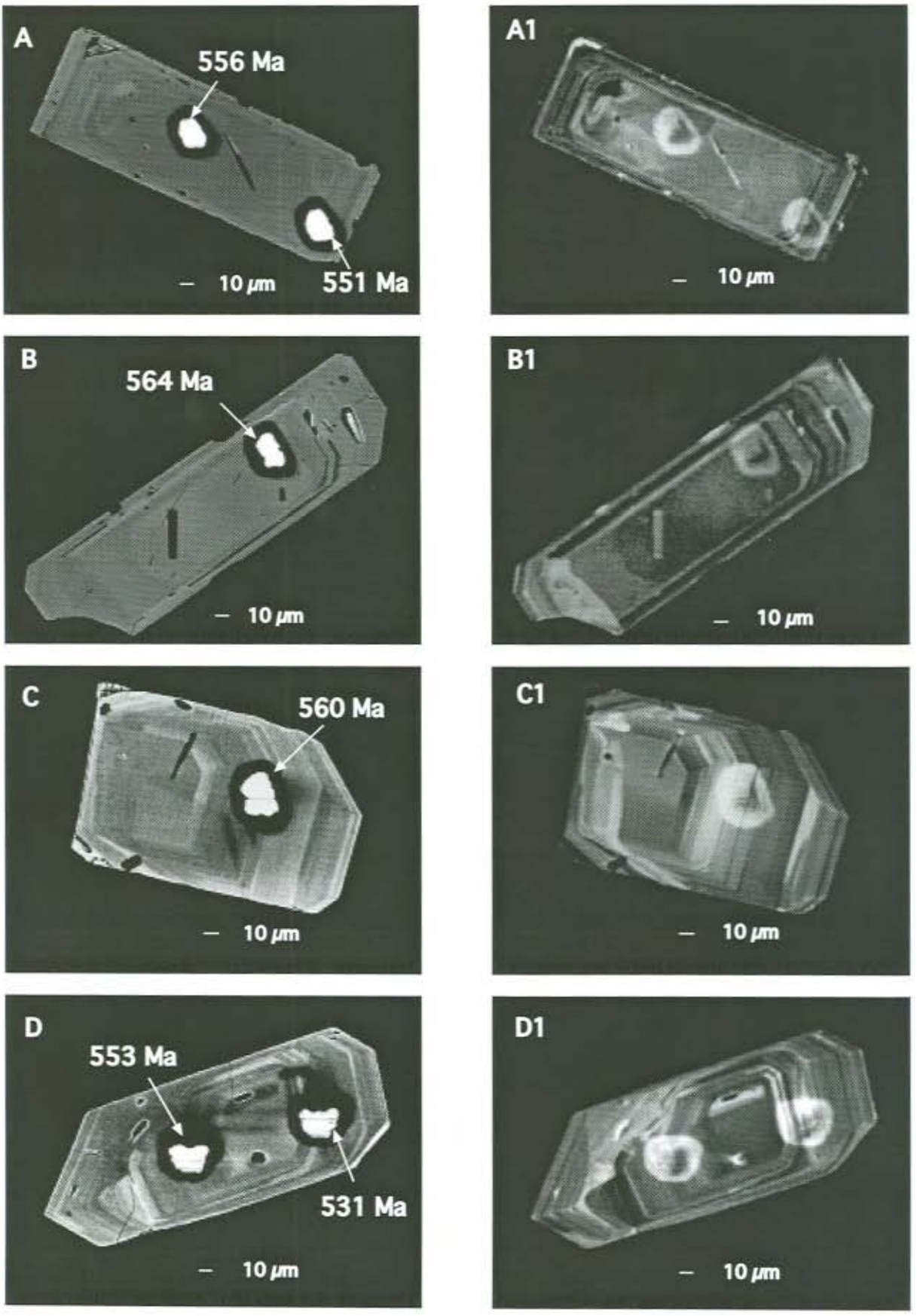
A
556 Ma
551 Ma
10 µm
A1
10 µm
B
564 Ma
10 µm
B1
10 µm
C
560 Ma
10 µm
C1
10 µm
D
553 Ma
531 Ma
10 µm
D1
10 µm

Figura 6

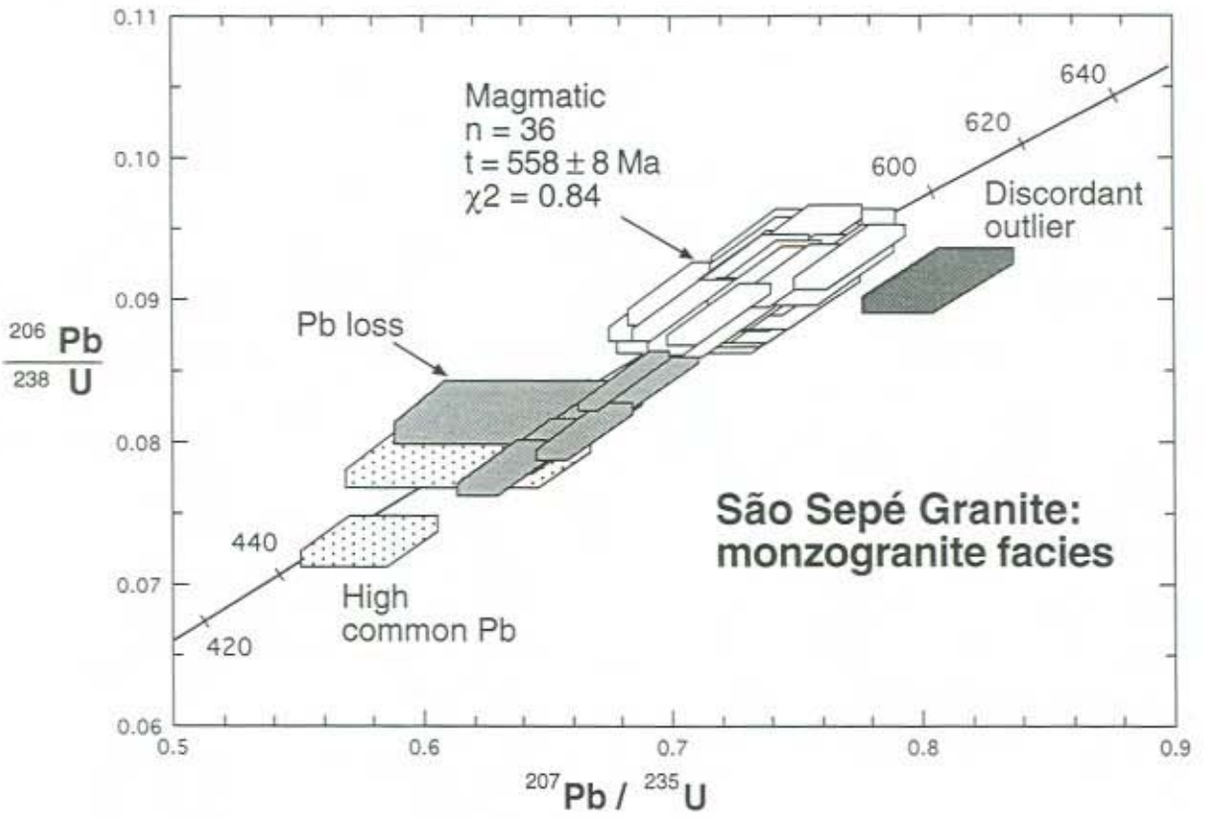
Magmatic
n = 36
t = 558 ± 8 Ma
χ2 = 0.84
Pb loss
High
common Pb
Discordant
outlier
São Sepé Granite:
monzogranite facies
640
620
600
440
420
0.11
0.10
0.09
0.08
0.07
0.06
0.5
0.6
0.7
0.8
0.9
206 Pb / 238 U
207 Pb / 235 U

Figura 7

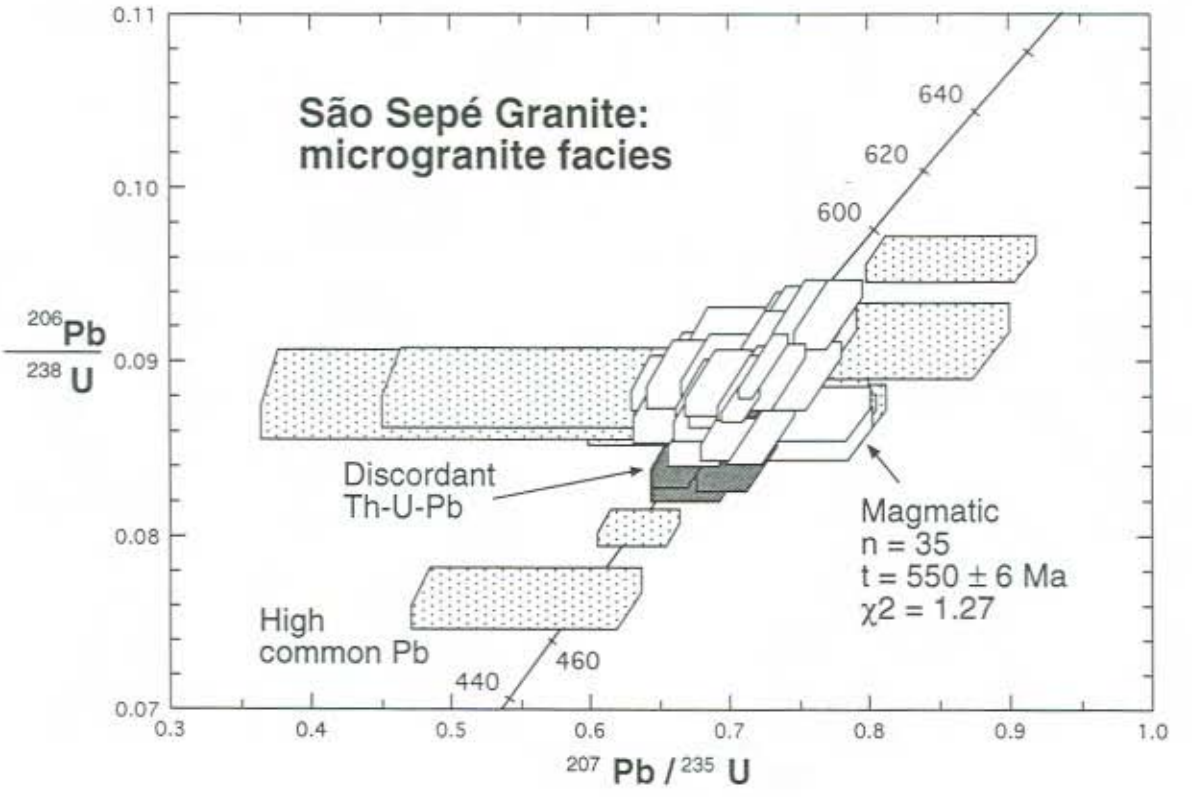
São Sepé Granite:
microgranite facies
640
620
600
Discordant
Th-U-Pb
Magmatic
n = 35
t = 550 ± 6 Ma
χ2 = 1.27
High
common Pb
460
440
0.11
0.10
0.09
0.08
0.07
0.3
0.4
0.5
0.6
0.7
0.8
0.9
1.0
206Pb / 238U
207Pb / 235U

Figura 8

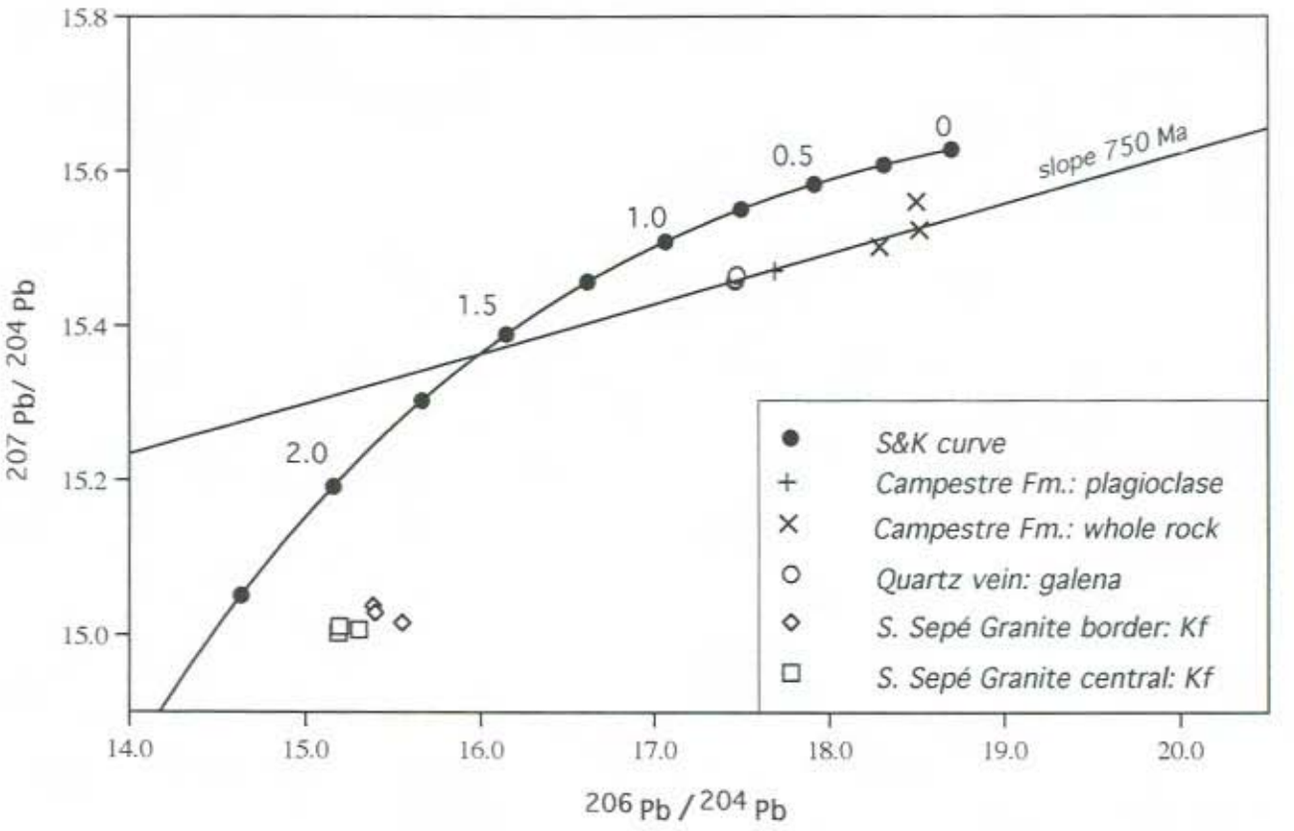
15.8
15.6
15.4
15.2
15.0
207 Pb/ 204 Pb
14.0
15.0
16.0
17.0
18.0
19.0
20.0
206 Pb / 204 Pb
0
0.5
1.0
1.5
2.0
slope 750 Ma
S&K curve
Campestre Fm.: plagioclase
Campestre Fm.: whole rock
Quartz vein: galena
S. Sepé Granite border: Kf
S. Sepé Granite central: Kf

Figura 9

Table Captions

Table 1. SHRIMP U/Pb data on zircons from dacitic metatuff of the Campestre Formation of the Vacacaí Group (sample MRB; SHRIMP mount nº 9656 A; errors = 1 sigma).

Table 2. SHRIMP U/Pb on zircons from the monzogranite central facies of the São Sepé Granite (sample BSS; SHRIMP mounts nº 9614 B and 9615 B; errors = 1 sigma).

Table 3 - SHRIMP U/Pb data on zircons from the microgranite border facies of the São Sepé Granite (sample ASS; SHRIMP mounts nº 9614 A and 9615 A; errors = 1 sigma).

Table 4. Lead isotope data from lode gold quartz of Bossoroca Deposit, Campestre Formation and São Sepé Granite border and central facies. A total analytical error is ± 0.15% to each Pb-isotope ratio.

Tabela 1

grain-spot	U (ppm)	Th (ppm)	Th U	4f206 (%)	207* 206*		208* 206*		206* 238		207* 235		208* 232		%conc.	207* 206* Age(Ma)		206* 238 Age(Ma)		7f206 (%)
Magmatic grains																				
6A.3-1	114	50	0.44	0.187	0.0649	± 16	0.1317	± 38	0.1248	± 30	1.117	± 40	0.0372	± 14	98	773	± 51	758	± 17	0.241
6A.4-1	76	35	0.46	0.568	0.0618	± 31	0.1336	± 74	0.1255	± 31	1.070	± 62	0.0367	± 22	114	667	± 107	762	± 17	0.226
6A.6-1	64	22	0.34	1.719	0.0676	± 43	0.1062	± 103	0.1283	± 32	1.195	± 86	0.0396	± 40	91	856	± 134	778	± 18	2.015
6A.7-1	32	9	0.29	0.000	0.0688	± 16	0.1040	± 32	0.1261	± 34	1.197	± 45	0.0461	± 20	86	893	± 48	766	± 19	0.494
6A.7-2	55	23	0.43	0.606	0.0684	± 31	0.1255	± 74	0.1228	± 32	1.157	± 64	0.0360	± 23	85	880	± 95	747	± 18	1.114
6A.8-1	98	39	0.40	1.168	0.0593	± 26	0.1021	± 62	0.1219	± 29	0.996	± 53	0.0313	± 21	129	576	± 96	741	± 17	0.602
6A.9-1	32	9	0.29	0.400	0.0679	± 53	0.0920	± 125	0.1250	± 35	1.171	± 101	0.0396	± 55	88	867	± 163	759	± 20	0.812
6A.9-2	66	21	0.33	0.358	0.0658	± 32	0.1027	± 75	0.1240	± 30	1.125	± 64	0.0389	± 30	94	800	± 101	753	± 17	0.534
6A.12-1	30	9	0.30	1.643	0.0600	± 76	0.0792	± 181	0.1239	± 35	1.024	± 137	0.0331	± 77	125	602	± 278	753	± 20	1.120
6A.13-1	46	17	0.37	0.622	0.0684	± 46	0.1132	± 108	0.1252	± 33	1.181	± 88	0.0388	± 39	86	880	± 139	761	± 19	1.080
6A.18-1	96	41	0.42	0.132	0.0659	± 23	0.1327	± 54	0.1275	± 30	1.159	± 51	0.0399	± 19	96	805	± 72	773	± 17	0.250
6A.20-1	114	56	0.49	0.254	0.0625	± 16	0.1441	± 40	0.1248	± 29	1.076	± 40	0.0367	± 14	110	691	± 56	758	± 17	0.012
6A.21-1	154	75	0.49	0.212	0.0652	± 14	0.1445	± 33	0.1222	± 29	1.098	± 37	0.0361	± 12	95	779	± 44	743	± 16	0.346
6A.24-1	31	11	0.36	0.000	0.0718	± 18	0.1112	± 37	0.1229	± 35	1.216	± 49	0.0384	± 18	76	979	± 51	747	± 20	0.920
6A.27-1	118	33	0.28	0.843	0.0612	± 23	0.0758	± 54	0.1211	± 29	1.022	± 48	0.0325	± 25	114	647	± 81	737	± 16	0.528
6A.31-1	73	27	0.37	0.352	0.0650	± 26	0.1153	± 60	0.1300	± 32	1.165	± 57	0.0406	± 24	102	776	± 83	788	± 18	0.308
Metamorphic/recrystallised grains																				
6A.11-1	119	61	0.51	0.473	0.0603	± 31	0.1451	± 75	0.1157	± 28	0.962	± 57	0.0327	± 19	115	615	± 111	706	± 16	0.159
6A.22-1	165	65	0.40	0.332	0.0633	± 19	0.1077	± 45	0.1144	± 27	0.999	± 40	0.0312	± 15	97	718	± 64	699	± 15	0.401
Inherited grains/cores																				
6A.15-1	54	20	0.36	0.232	0.0667	± 29	0.1145	± 69	0.1320	± 33	1.213	± 65	0.0418	± 28	97	827	± 92	799	± 19	0.338
6A.23-1	132	161	1.22	0.170	0.0771	± 13	0.3352	± 37	0.1719	± 40	1.828	± 55	0.0472	± 12	91	1124	± 33	1023	± 22	0.170
6A.30-1	42	15	0.36	0.000	0.0689	± 14	0.1167	± 30	0.1344	± 36	1.276	± 45	0.0431	± 17	91	896	± 42	813	± 20	0.327
6A.31-2	89	30	0.33	0.000	0.0650	± 9	0.1016	± 19	0.1350	± 33	1.209	± 36	0.0416	± 13	105	774	± 30	816	± 19	0.000
6A.33-1	40	15	0.38	0.000	0.0695	± 15	0.1272	± 33	0.1313	± 35	1.258	± 45	0.0437	± 17	87	914	± 43	795	± 20	0.467
High common Pb																				
6A.1-1	17	5	0.28	5.244	0.0373	± 162	0.0099	± 386	0.1220	± 44	0.628	± 276	0.0043	± 166	0	0	± 61	742	± 25	2.186
6A.8-2	44	14	0.32	22.985	0.0511	± 182	-0.0071	± 434	0.1151	± 37	0.811	± 293	0.0000		286	245	± 662	702	± 21	21.894
6A.14-2	49	50	1.02	2.210	0.0564	± 72	0.3047	± 181	0.0926	± 25	0.720	± 96	0.0276	± 18	122	468	± 286	571	± 15	1.893
6A.32-1	305	366	1.20	12.042	0.0592	± 78	0.2313	± 189	0.0628	± 15	0.513	± 70	0.0121	± 10	69	573	± 289	393	± 9	12.529
Pb-loss																				
6A.5-1	305	202	0.66	0.293	0.0590	± 14	0.2048	± 37	0.0751	± 17	0.611	± 22	0.0232	± 7	82	569	± 53	467	± 10	0.613
6A.10-1	605	28	0.05	0.251	0.0628	± 9	0.0153	± 19	0.0891	± 20	0.772	± 22	0.0297	± 38	78	703	± 31	550	± 12	0.767
6A.10-2	674	49	0.07	1.217	0.0607	± 11	0.0134	± 25	0.1016	± 23	0.851	± 26	0.0187	± 35	99	630	± 39	624	± 13	1.238
6A.14-1	43	33	0.77	1.011	0.0553	± 60	0.2275	± 151	0.0935	± 26	0.712	± 82	0.0275	± 20	136	423	± 245	576	± 15	0.539
6A.16-1	901	250	0.28	0.068	0.0595	± 4	0.0839	± 9	0.0951	± 21	0.780	± 19	0.0288	± 7	100	585	± 15	585	± 12	0.067
6A.25-1	495	339	0.68	0.001	0.0522	± 12	0.2092	± 32	0.0420	± 10	0.303	± 10	0.0129	± 4	90	295	± 50	265	± 6	0.081
6A.28-1	123	39	0.32	0.000	0.0675	± 14	0.1006	± 29	0.0968	± 24	0.901	± 31	0.0306	± 12	70	853	± 44	596	± 14	0.928
6A.29-1	966	311	0.32	0.633	0.0597	± 7	0.0964	± 16	0.0922	± 21	0.759	± 20	0.0276	± 8	96	593	± 25	569	± 12	0.711
CZ3 (n = 10)																				
mean (wtd.)	550	30.2	0.06	0.046	0.0589		0.0172		0.0913		0.74		0.0283		102	563		564		
1s (wtd.)	20	1.5	0.00	0.041	0.0007		0.0007		0.0021		0.02		0.0018		4	25		12		
chi^2					1.6400		1.49		1.02		1.17		1.97			1.68		0.99		

SHRIMP analysis date 6/10/96.

Precisions are 1s in the last digits listed.

Pb isotopic values and dates are corrected for common Pb, calculated using a Pb composition from the Cumming and Richards (1975) model at 760 Ma and the measured Pb-204.

4f206 = Proportion of Pb-206 calculated to be common Pb; %conc. = Concordance, as 100t[206*/238]/t[207*/206*].

Tabela 2

grain-spot	U (ppm)	Th (ppm)	Th U	4f206 (%)	207*/206*			208*/206*			206*/238			207*/235			208*/232			%conc.	207*/206* Age(Ma)			206*/238 Age(Ma)			7f206 (%)
Magmatic grains																											
14B.1-1	228	134	0.59	0.000	0.0582	±	12	0.1824	±	23	0.0896	±	14	0.719	±	20	0.0277	±	6	103	537	±	45	553	±	8	0.000
14B.2-1	335	171	0.51	0.059	0.0586	±	12	0.1578	±	25	0.0915	±	14	0.740	±	20	0.0283	±	6	102	554	±	46	565	±	8	0.023
14B.2-2	128	39	0.31	0.411	0.0590	±	26	0.0873	±	52	0.0878	±	15	0.714	±	35	0.0251	±	16	96	567	±	97	542	±	9	0.494
14B.3-1	277	209	0.75	0.209	0.0574	±	18	0.2294	±	41	0.0885	±	14	0.701	±	26	0.0269	±	6	108	509	±	69	547	±	8	0.086
14B.4-1	249	147	0.59	0.178	0.0599	±	18	0.1770	±	38	0.0883	±	14	0.729	±	26	0.0265	±	7	91	599	±	65	546	±	8	0.357
14B.5-1	227	273	1.20	0.265	0.0596	±	21	0.3699	±	54	0.0898	±	14	0.738	±	30	0.0277	±	6	94	589	±	77	555	±	8	0.379
15B.1-1	341	227	0.67	0.481	0.0591	±	13	0.2052	±	30	0.0904	±	22	0.737	±	26	0.0279	±	8	97	572	±	49	558	±	13	0.528
15B.4-1	1009	491	0.49	0.547	0.0593	±	8	0.1586	±	17	0.0916	±	22	0.749	±	22	0.0299	±	8	98	577	±	29	565	±	13	0.584
15B.6-1	177	73	0.42	0.714	0.0582	±	23	0.1329	±	50	0.0940	±	24	0.754	±	37	0.0300	±	14	108	538	±	86	579	±	14	0.578
15B.7-1	365	159	0.43	0.160	0.0577	±	12	0.1298	±	25	0.0926	±	23	0.737	±	25	0.0277	±	9	110	519	±	46	571	±	13	0.000
15B.8-1	192	180	0.94	0.226	0.0579	±	17	0.2850	±	42	0.0936	±	23	0.747	±	31	0.0285	±	8	109	527	±	65	577	±	14	0.064
15B.9-1	313	153	0.49	0.110	0.0579	±	14	0.1520	±	29	0.0894	±	22	0.714	±	26	0.0278	±	9	105	527	±	52	552	±	13	0.027
15B.10-1	467	299	0.64	0.040	0.0580	±	10	0.1998	±	21	0.0893	±	22	0.714	±	22	0.0278	±	7	104	530	±	36	551	±	13	0.000
15B.12-1	206	228	1.11	0.102	0.0593	±	17	0.3400	±	44	0.0929	±	23	0.759	±	31	0.0285	±	8	99	578	±	64	573	±	14	0.121
15B.13-1	405	225	0.56	0.041	0.0601	±	10	0.1738	±	19	0.0931	±	23	0.771	±	24	0.0292	±	8	94	607	±	34	574	±	13	0.154
15B.14-1	346	192	0.55	0.067	0.0582	±	10	0.1672	±	20	0.0919	±	23	0.738	±	23	0.0277	±	8	105	539	±	38	567	±	13	0.000
15B.15-1	273	124	0.46	0.000	0.0605	±	10	0.1425	±	15	0.0919	±	23	0.766	±	24	0.0288	±	8	91	621	±	35	567	±	13	0.182
15B.17-1	190	126	0.66	0.199	0.0573	±	18	0.1962	±	40	0.0904	±	23	0.714	±	30	0.0267	±	9	111	502	±	68	558	±	13	0.017
15B.18-1	399	154	0.39	0.057	0.0576	±	10	0.1173	±	20	0.0923	±	23	0.733	±	23	0.0280	±	8	110	515	±	39	569	±	13	0.000
15B.19-1	587	516	0.88	0.073	0.0585	±	8	0.2707	±	20	0.0915	±	22	0.738	±	22	0.0282	±	7	103	548	±	31	564	±	13	0.020
15B.20-1	319	177	0.55	0.136	0.0579	±	11	0.1691	±	23	0.0943	±	23	0.753	±	25	0.0288	±	8	111	525	±	42	581	±	14	0.000
15B.22-1	184	172	0.94	0.000	0.0581	±	11	0.2971	±	28	0.0938	±	23	0.751	±	25	0.0298	±	8	108	533	±	42	578	±	14	0.000
15B.24-1	388	214	0.55	0.153	0.0599	±	10	0.1721	±	21	0.0911	±	22	0.752	±	24	0.0283	±	8	94	599	±	37	562	±	13	0.276
15B.26-1	485	230	0.48	0.123	0.0575	±	10	0.1438	±	19	0.0893	±	22	0.707	±	22	0.0271	±	8	108	509	±	37	551	±	13	0.000
15B.28-1	378	273	0.72	0.000	0.0603	±	8	0.2158	±	16	0.0930	±	23	0.773	±	22	0.0278	±	7	94	613	±	28	573	±	13	0.133
15B.29-1	447	231	0.52	0.044	0.0594	±	10	0.1600	±	21	0.0901	±	22	0.738	±	23	0.0280	±	8	95	583	±	37	556	±	13	0.133
15B.29-2	243	89	0.37	0.015	0.0590	±	14	0.1159	±	28	0.0892	±	22	0.725	±	26	0.0282	±	10	97	566	±	52	551	±	13	0.065
15B.30-1	289	165	0.57	0.122	0.0581	±	12	0.1747	±	26	0.0913	±	22	0.731	±	25	0.0280	±	8	106	532	±	47	563	±	13	0.021
15B.31-1	387	223	0.58	0.409	0.0598	±	14	0.1761	±	30	0.0900	±	22	0.742	±	26	0.0276	±	8	93	596	±	49	556	±	13	0.542
15B.32-1	244	176	0.72	0.042	0.0604	±	13	0.2193	±	29	0.0901	±	22	0.751	±	26	0.0274	±	8	90	619	±	47	556	±	13	0.255
15B.33-1	413	230	0.56	0.030	0.0593	±	11	0.1748	±	23	0.0924	±	23	0.755	±	24	0.029	±	8	99	576	±	40	570	±	13	0.053
15B.34-1	629	295	0.47	0.055	0.0587	±	7	0.1453	±	13	0.0890	±	22	0.720	±	21	0.0276	±	7	99	555	±	26	550	±	13	0.074
15B.35-1	342	159	0.47	0.164	0.0584	±	12	0.1395	±	26	0.0901	±	22	0.726	±	25	0.027	±	8	102	545	±	46	556	±	13	0.126
15B.36-1	199	136	0.69	0.098	0.0597	±	19	0.2135	±	43	0.0889	±	22	0.732	±	31	0.0277	±	9	93	593	±	69	549	±	13	0.243
15B.37-1	306	201	0.66	0.000	0.0593	±	9	0.2024	±	18	0.0881	±	22	0.720	±	22	0.0271	±	7	94	578	±	34	544	±	13	0.112
15B.39-1	438	206	0.47	0.008	0.0585	±	9	0.1450	±	16	0.0883	±	22	0.713	±	22	0.0272	±	7	99	550	±	33	545	±	13	0.022
High common Pb																											
15B.25-1	506	434	0.86	2.712	0.0574	±	22	0.2133	±	51	0.0731	±	18	0.579	±	27	0.0182	±	6	90	508	±	82	455	±	11	2.874
15B.34-2	166	116	0.70	2.904	0.0570	±	41	0.1517	±	96	0.0787	±	20	0.618	±	49	0.0171	±	12	100	490	±	160	489	±	12	2.910
Pb loss																											
15B.2-1	1965	1077	0.55	0.340	0.0586	±	5	0.1620	±	11	0.0843	±	20	0.682	±	18	0.0249	±	6	94	554	±	19	522	±	12	0.444
15B.5-1	901	512	0.57	0.586	0.0598	±	9	0.1852	±	19	0.0808	±	20	0.666	±	20	0.0263	±	7	84	596	±	31	501	±	12	0.896
15B.16-1	648	259	0.40	0.528	0.0592	±	11	0.1332	±	24	0.0807	±	20	0.658	±	21	0.0269	±	8	87	574	±	40	500	±	12	0.768
15B.23-1	502	168	0.33	0.479	0.0590	±	11	0.0880	±	22	0.0798	±	19	0.649	±	21	0.0210	±	7	87	567	±	41	495	±	12	0.711
15B.24-2	89	47	0.53	0.384	0.0564	±	40	0.1674	±	92	0.0821	±	22	0.639	±	50	0.0261	±	16	108	470	±	158	509	±	13	0.262
15B.27-1	623	325	0.52	0.597	0.0589	±	11	0.1725	±	24	0.0782	±	19	0.635	±	21	0.0259	±	7	86	562	±	41	485	±	11	0.844
15B.38-1	564	274	0.49	0.407	0.0592	±	11	0.1540	±	24	0.0844	±	21	0.690	±	22	0.0268	±	8	91	575	±	41	523	±	12	0.580
Discordant outlier																											
15B.22-2	112	84	0.75	0.000	0.0641	±	15	0.2345	±	32	0.0914	±	23	0.808	±	30	0.0287	±	8	76	746	±	51	564	±	14	0.640
CZ3 (n = 17)																											
mean (wtd.)	550	30.1	0.06	0.055	0.0589			0.0169			0.0914			0.743			0.0283			99	565			564			0.074
1s (wtd.)	10	0.7	0.06	0.001	0.0007			0.0012			0.0020			0.018			0.0021			5	24			12			0.074
chi^2					0.62			0.92			0.09			0.92			1.02				0.63			0.92			

SHRIMP analysis dates 2/5/96 and 17/5/96.

Precisions are 1s in the last digits listed.

Pb isotopic values and dates are corrected for common Pb, calculated using a Pb composition from the Cumming and Richards (1975) model at 560 Ma and the measured Pb-204.

4f206 = Proportion of Pb-206 calculated to be common Pb; %conc. = Concordance, as 100t[206*/238]/t[207*/206*].

Tabela 3

grain-spot	U (ppm)	Th (ppm)	Th/U	4f206 (%)	207*/206*		208*/206*		206*/238		207*/235		208*/232		%conc.	207*/206* Age(Ma)		206*/238 Age(Ma)		7f206 (%)
Magmatic																				
14A.1-1	57	40	0.70	0.354	0.0613	± 53	0.2170	± 124	0.0870	± 16	0.736	± 67	0.0268	± 16	83	651	± 186	538	± 9	0.736
14A.4-1	55	48	0.87	0.293	0.0622	± 54	0.2464	± 127	0.0859	± 16	0.737	± 67	0.0244	± 14	78	683	± 185	531	± 9	0.807
14A.5-1	63	32	0.50	0.767	0.0567	± 50	0.1431	± 113	0.0888	± 16	0.694	± 64	0.0252	± 21	114	480	± 195	548	± 9	0.551
14A.6-1	122	54	0.45	0.000	0.0609	± 16	0.1435	± 26	0.0889	± 13	0.746	± 24	0.0286	± 7	86	636	± 57	549	± 7	0.295
14A.9-1	215	109	0.51	0.598	0.0585	± 21	0.1561	± 45	0.0901	± 12	0.726	± 29	0.0276	± 9	102	547	± 78	556	± 7	0.570
14A.10-1	633	360	0.57	0.059	0.0588	± 8	0.1754	± 16	0.0876	± 10	0.709	± 14	0.0270	± 4	97	558	± 30	541	± 6	0.115
14A.11-1	211	123	0.58	0.146	0.0586	± 16	0.1784	± 35	0.0931	± 12	0.753	± 24	0.0285	± 7	104	554	± 61	574	± 7	0.080
14A.12-1	108	86	0.79	0.130	0.0556	± 27	0.2438	± 64	0.0903	± 14	0.692	± 37	0.0278	± 9	128	437	± 109	557	± 8	0.000
14A.13-1	349	178	0.51	0.342	0.0568	± 15	0.1393	± 31	0.0882	± 11	0.691	± 21	0.0240	± 6	112	486	± 58	545	± 6	0.152
15A.6-1	338	369	1.09	0.392	0.0610	± 14	0.3234	± 34	0.0860	± 18	0.724	± 24	0.0254	± 6	83	641	± 48	532	± 11	0.758
15A.7-1	145	73	0.50	0.518	0.0549	± 24	0.1483	± 52	0.0893	± 20	0.676	± 34	0.0263	± 11	135	408	± 96	551	± 12	0.069
15A.8-1	178	97	0.55	0.093	0.0577	± 19	0.1654	± 41	0.0873	± 19	0.694	± 29	0.0263	± 9	104	518	± 72	539	± 11	0.025
15A.9-1	118	121	1.03	0.254	0.0592	± 25	0.3246	± 62	0.0910	± 20	0.743	± 37	0.0288	± 9	98	574	± 92	562	± 12	0.295
15A.9-2	125	53	0.42	0.387	0.0560	± 26	0.1226	± 56	0.0911	± 20	0.704	± 38	0.0264	± 14	124	453	± 102	562	± 12	0.041
15A.11-1	221	106	0.48	0.355	0.0568	± 18	0.1401	± 38	0.0882	± 19	0.691	± 28	0.0257	± 9	112	485	± 70	545	± 11	0.162
15A.12-1	861	393	0.46	0.004	0.0587	± 6	0.1391	± 11	0.0897	± 19	0.726	± 18	0.0273	± 6	100	554	± 23	554	± 11	0.006
15A.14-1	66	94	1.43	0.333	0.0571	± 42	0.4448	± 112	0.0874	± 21	0.688	± 55	0.0272	± 10	109	494	± 164	540	± 12	0.185
15A.15-1	163	84	0.52	0.000	0.0615	± 13	0.1605	± 22	0.0892	± 19	0.757	± 25	0.0277	± 7	84	658	± 46	551	± 11	0.365
15A.16-1	445	535	1.20	0.248	0.0585	± 10	0.3554	± 27	0.0885	± 19	0.714	± 21	0.0261	± 6	100	549	± 39	547	± 11	0.257
15A.17-1	178	65	0.37	0.100	0.0563	± 19	0.1085	± 39	0.0897	± 19	0.697	± 29	0.0266	± 11	119	465	± 74	554	± 12	0.000
15A.19-1	132	59	0.45	0.000	0.0584	± 15	0.1443	± 25	0.0893	± 20	0.719	± 26	0.0286	± 8	102	543	± 57	552	± 12	0.000
15A.22-1	161	108	0.67	0.315	0.0572	± 20	0.1998	± 45	0.0896	± 20	0.706	± 31	0.0268	± 9	111	497	± 78	553	± 12	0.134
15A.22-2	166	62	0.37	0.334	0.0578	± 19	0.1075	± 38	0.0859	± 19	0.685	± 29	0.0248	± 10	101	524	± 74	531	± 11	0.310
15A.26-1	258	534	2.07	0.125	0.0575	± 17	0.6430	± 56	0.0881	± 19	0.698	± 27	0.0273	± 6	107	510	± 65	544	± 11	0.016
15A.27-1	173	133	0.77	0.000	0.0604	± 13	0.2409	± 27	0.0927	± 20	0.772	± 25	0.0290	± 7	92	618	± 45	571	± 12	0.160
15A.28-1	238	113	0.48	0.235	0.0583	± 15	0.1404	± 31	0.0909	± 19	0.730	± 26	0.0268	± 8	104	539	± 57	561	± 12	0.164
15A.29-1	123	93	0.75	0.000	0.0594	± 15	0.2257	± 31	0.0926	± 21	0.758	± 27	0.0277	± 7	98	581	± 54	571	± 12	0.033
15A.30-1	373	261	0.70	0.000	0.0599	± 9	0.2159	± 18	0.0891	± 19	0.736	± 20	0.0274	± 6	91	601	± 31	550	± 11	0.171
15A.31-1	145	74	0.51	0.246	0.0600	± 26	0.1535	± 59	0.0912	± 20	0.754	± 39	0.0275	± 12	93	604	± 95	562	± 12	0.384
15A.32-1	184	117	0.64	0.000	0.0566	± 14	0.1966	± 27	0.0888	± 19	0.693	± 24	0.0274	± 7	115	477	± 54	548	± 11	0.000
15A.33-1	103	71	0.69	0.105	0.0582	± 30	0.2046	± 70	0.0907	± 21	0.729	± 43	0.0270	± 11	104	539	± 114	560	± 12	0.036
15A.34-1	181	76	0.42	0.000	0.0590	± 12	0.1284	± 18	0.0865	± 22	0.704	± 24	0.0263	± 8	94	569	± 44	535	± 13	0.111
15A.35-1	218	115	0.53	0.189	0.0571	± 17	0.1629	± 38	0.0876	± 22	0.690	± 29	0.0270	± 9	109	496	± 67	541	± 13	0.044
15A.36-1	290	162	0.56	0.034	0.0588	± 13	0.1719	± 27	0.0888	± 22	0.720	± 25	0.0274	± 8	98	560	± 48	548	± 13	0.072
15A.38-1	139	102	0.73	0.205	0.0589	± 22	0.2118	± 49	0.0917	± 23	0.745	± 35	0.0265	± 9	101	563	± 80	566	± 14	0.195
High common Pb																				
14A.3-1	180	238	1.32	0.566	0.0642	± 29	0.4005	± 73	0.0869	± 12	0.769	± 37	0.0264	± 6	72	747	± 94	537	± 7	1.295
14A.7-1	254	321	1.26	1.117	0.0573	± 25	0.3500	± 63	0.0805	± 10	0.636	± 30	0.0224	± 5	99	502	± 96	499	± 6	1.125
14A.8-1	232	50	0.22	1.454	0.0569	± 28	0.0705	± 62	0.0901	± 12	0.706	± 37	0.0293	± 26	114	487	± 109	556	± 7	1.233
14A.14-1	182	88	0.48	3.995	0.0651	± 44	0.1692	± 102	0.0958	± 13	0.860	± 61	0.0336	± 21	76	777	± 143	590	± 8	4.638
14A.16-1	55	48	0.88	2.601	0.0589	± 87	0.2736	± 210	0.0869	± 17	0.706	± 107	0.0270	± 22	95	563	± 326	537	± 10	2.684
15A.18-1	92	125	1.35	4.387	0.0646	± 67	0.2460	± 160	0.0912	± 22	0.811	± 89	0.0166	± 12	74	760	± 222	562	± 13	5.054
15A.21-1	126	220	1.74	7.947	0.0526	± 76	0.3010	± 184	0.0764	± 18	0.555	± 83	0.0132	± 9	152	313	± 300	475	± 11	7.503
15A.24-1	75	70	0.94	11.548	0.0480	± 109	0.2214	± 260	0.0885	± 23	0.586	± 135	0.0209	± 25	543	101	± 462	547	± 13	10.416
15A.25-1	165	251	1.52	43.049	0.0479	± 177	0.4796	± 434	0.0881	± 25	0.582	± 218	0.0278	± 26	564	96	± 699	544	± 15	42.319
Discordant U-Th-Pb																				
14A.2-1	531	303	0.57	0.265	0.0590	± 12	0.1368	± 25	0.0878	± 10	0.714	± 18	0.0210	± 5	96	566	± 44	542	± 6	0.343
15A.13-1	201	177	0.88	0.134	0.0607	± 20	0.1592	± 43	0.0843	± 18	0.706	± 29	0.0152	± 5	83	630	± 70	522	± 11	0.496
15A.20-1	332	154	0.46	0.465	0.0573	± 15	0.1095	± 32	0.0846	± 18	0.668	± 24	0.0200	± 7	104	502	± 58	524	± 11	0.396
15A.37-1	134	137	1.03	0.156	0.0587	± 26	0.1893	± 60	0.0842	± 21	0.681	± 37	0.0155	± 6	94	556	± 98	521	± 13	0.271
CZ3 (n = 36)																				
mean (wtd.)	550	30.2	0.06	0.059	0.0590		0.0167		0.0914		0.744		0.0278		100	567		564		0.080
1s (wtd.)	14	1	0.00	0.048	0.0007		0.0011		0.0017		0.017		0.0018		5	27		10		0.070
chi^2					0.77				0.91		0.83		1.97			0.77		0.98		

SHRIMP analysis dates 29/4/96, 2/5/96 and 17/5/96.
Precisions are 1s in the last digits listed.
Pb isotopic values and dates are corrected for common Pb, calculated using a Pb composition from the Cumming and Richards (1975) model at 560 Ma and the measured Pb-204.
4f206 = Proportion of Pb-206 calculated to be common Pb; %conc. = Concordance, as 100t[206*/238]/t[207*/206*].

Tabela 4

Sample number	Geologic unit	Lithologic unit	Sample type	206 Pb/ 204Pb	207Pb/ 204Pb	208Pb/ 204Pb
GA-1	Bossoroca lode	quartz vein	galena	17.465	15.458	37.112
GA-2	Bossoroca lode	quartz vein	galena	17.468	15.460	37.130
GA-0	Bossoroca lode	quartz vein	galena	17.476	15.465	37.126
EBL-3	Campestre Formation	dacitic metatuff	plagioclase	17.692	15.471	37.171
EB	Campestre Formation	dacitic metatuff	whole rock	18.502	15.560	37.802
EB2	Campestre Formation	dacitic metatuff	whole rock	18.292	15.502	37.438
EB3	Campestre Formation	dacitic metatuff	whole rock	18.518	15.524	37.675
ASS	S.Sepé Granite-border	microgranite	k-feldspar	15.397	15.029	35.860
A2	S.Sepé Granite-border	microgranite	k-feldspar	15.387	15.038	35.849
A3	S.Sepé Granite-border	microgranite	k-feldspar	15.552	15.016	35.842
BSS	S. Sepé Granite-central	monzogranite	k-feldspar	15.302	15.007	35.827
B1	S. Sepé Granite-central	monzogranite	k-feldspar	15.190	15.011	35.808
B2	S. Sepé Granite-central	monzogranite	k-feldspar	15.184	15.003	35.829

CAPÍTULO III

A DISTAL MAGMATIC-HYDROTHERMAL ORIGIN FOR THE CAMAQUÃ Cu (Au-Ag) AND SANTA MARIA Pb, Zn (Cu-Ag) DEPOSITS, SOUTHERN BRAZIL

Remus, M.V.D.[1]; Hartmann, L.A.[1]; McNaughton, N.J.[2]; Groves, D.I.[2] and Reischl, J.L[3]

[1]Centro de Estudos em Petrologia e Geoquímica, Instituto de Geociências, Universidade Federal do Rio Grande do Sul, Porto Alegre, RS, Brazil

[2]Centre for Strategic Mineral Deposits, University of Western Australia, Nedlands, 6907, WA, Australia

[3]Companhia Brasileira do Cobre, Porto Alegre, RS, Brasil

Submetido a Revista Gondwana Research

Abstract

The Camaquã Cu (Au, Ag) and Santa Maria Pb-Zn (Cu, Ag) deposits are the major discovered base-metal deposits hosted in sedimentary clastic sequences of the Neoproterozoic-age Camaquã Basin. The origin of the Camaquã-Santa Maria deposits has been the centre of dispute, with three alternative genetic hypotheses proposed: 1) a syngenetic model; 2) a diagenetic model; 3) a magmatic hydrothermal model. In detail, this mineralization has been related to sedimentary clastic-diagenetic processes, derivation from volcanic related processes, or evolution from a deep granitic magma body.

Reavaluation of previous data and new studies in the area yield the following conclusions:

(1) mineralization is fracture-controlled and magmatic-hydrothermal in origin rather than stratiform syngenetic or diagenetic;

(2) the temperature of deposition of the main ore minerals was 210 to 300°C;

(3) the $\partial^{34}S$ of sulphides from the mines of around 0‰ indicates an external magmatic-hydrothermal source of sulphur;

(4) lead isotope ratios of sulphides from the mines indicate that metals were derived from a largely crustal source with very primitive Pb at the end of the Brasiliano Cycle;

(5) the age of mineralization is 594 Ma, as constrained by U/Pb SHRIMP determinations on zircons of the Lavras Granite.

Thus, the Camaquã and Santa Maria deposits are interpreted to be of magmatic-hydrothermal origin with the metals derived from an old crustal basement source during the end of Dom Feliciano Collisional Orogeny, at 594 Ma, late in the Brasiliano Cycle.

The consequences of the interpretation above are critical for base-metal exploration in the Sul Riograndense Shield. Exploration methodologies used in the last decades followed mainly models based on a sedimentary hypothesis for the origin of the deposits. However, mineralization along fractures and near specific wall-rocks requires consideration of alternative exploration parameters such as: ancient E-W- and NW-trending regional fractures and their intersections which are potential structural sites for base-metal mineralization;

lithologies with high original porosity or rocks which are highly susceptible to replacement processes are the preferential wall-rock sites for mineralization; the post-collisional plutonism of the Dom Feliciano Orogeny is the most likely heat source, and also source of sulphur and base metals. Geophysics (e.g. gravity survey) and alteration studies are essential to determine the presence of intrusive bodies at depth which may have potential to host porphyry-style Cu-Au deposits.

Key words: magmatic-hydrothermal mineralization; Pb-S isotope geochemistry; SHRIMP U/Pb zircon age; base metal deposits; exploration guidelines

INTRODUCTION

This paper reviews the geology and isotope geochemistry of the large ore bodies of the Camaquã Cu (Au, Ag) and Santa Maria Pb-Zn (Cu, Ag) deposits, located near 30°50'S; 53°25'W in the central part of the Sul-Riograndense Shield, near Caçapava do Sul town, southern Brazil (Figs. 1 and 2). These represent the main known base-metal deposits of the shield hosted by the sedimentary sequences of the Neoproterozoic age Camaquã Basin. The host rocks to both deposits are arenites and conglomerates of the Arroio dos Nobres Formation of the Bom Jardim Group, interpreted as deposits related to the subaqueous portions of deltas (Paim et al; 1995). The Camaquã deposit consists of massive veins, stockworks and disseminated ores, with chalcopyrite, pyrite, bornite, chalcocite, gold, silver and hematite, whereas the Santa Maria deposit contains disseminations and massive veins of galena and sphalerite with minor pyrite, chalcopyrite, bornite, chalcocite and native silver. The Camaquã Mine was discovered in 1865, and was mined from the end of the last century until recently, whereas the Santa Maria deposit was located in 1978 but has not yet been mined.

The genesis of the Camaquã-Santa Maria deposits is controversial, with the main literature discussion considering three different hypothesis — syngenetic, diagenetic or magmatic-hydrothermal, involving different metals, fluids and heat sources (Bettencourt, 1972, 1976; Ribeiro, 1986; Badi and Gonzales, 1988; Beckel, 1990; Ribeiro, 1991; Veigel, 1992).

Several intrusive granitoids and related volcanic rocks in the Province were investigated by SHRIMP U/Pb in zircon and Pb isotopes

studies in whole-rocks and feldspars to assess them as mineralization source(s). The potential orthomagmatic sulfur and metal source(s) for mineralization in the province are magmatism related to the Lavras Granite, Hilario volcanics and Caçapava Granite plutonism.

The different hypotheses of ore genesis are tested using Pb and S isotopes, integrated with SHRIMP U/Pb ages in zircons, within the framework of previous investigations, and field mapping in the open pit and the surrounding region. The present data base includes SHRIMP U/Pb ages on zircons (69 analyses), combined with scanning electron microscope images of these grains using backscattered electron (BSE) and cathodoluminescence (CL) modes, 35 Pb isotopic determinations in minerals and whole rocks and 16 sulphur isotopic determinations on sulphide minerals. A genetic model which explains all these data is proposed.

REGIONAL GEOLOGY

The Camaquã Basin, containing the Camaquã Cu (Au-Ag) and Santa Maria Pb-Zn (Cu-Ag) base-metal deposits, was formed in the Neoproterozoic to Ordovician at the end of the Brasiliano Cycle. The volcano-sedimentary rocks in the basin were deposited in rifts in the Precambrian basement of Rio Grande do Sul State; this shield is the southernmost extension of the Mantiqueira Province (Hasui et al., 1975) and has four major segments (Jost and Hartmann, 1984; Soliani Jr., 1986; Fragoso Cesar et al., 1986; Babinski et al., 1996, Hartmann et al., 1998) as shown in Figure 1. These segments have been identified using particular petrotectonic associations, NE and NW lineaments and isotopic data. To the east, where it is in direct contact with the 780 Ma-old Porongos schist belt, the ca. 600 Ma-old Pelotas Batholith was derived from crustal reworking of ca. 2.0 Ga-old tonalite-granodiorite and metasedimentary gneisses (Mantovani et al.,1987; Babinski et al., 1997). The schist belt is composed of supracrustal sequences intercalated with ca 2.0 Ga-old basement gneisses. The westernmost part of the shield contains the Taquarembó Block in the south, an old granulite block, and the São Gabriel Block in the north, a juvenile terrain. The NE- and NW-trending structures, well defined by elongation

of the Porongos Belt and the Ibaré Lineament, were the main structural controls on deposition in the Camaquã Basin (Figs. 1 and 2).

The history of the Camaquã Basin started at the end of the Dom Feliciano Collisional Orogeny (630-600 Ma) and ended with the extensional basic volcanism of the Rodeio Velho Member at ca. 470 Ma (Hartmann et al., 1998). The modified stratigraphic column of the basin (Ribeiro et al. 1966; Paim et al., 1992; Gresse et al., 1996) is shown in Figure 3. The evolutionary history and classification of the basin have been evaluated in several papers and discussed by Paim et al. (1995) and Gresse et al. (1996). Current dispute is centred around whether it is a foreland or strike-slip related basin. The São Sepé, Lavras and Caçapava granite plutons which intruded the lowest part of basin have been dated by SHRIMP U/Pb in zircon (Remus et al.; 1998; Remus et al.,1999).

Deposition started in the basin with the Maricá Formation directly over the Vacacaí Group and Cambaí Complex Precambrian basement rocks. The Maricá Formation is made up of alluvial conglomerates and sandstones at its base and grades upwards into marine areno-pelitic arkosic rhythmites, interpreted as shallower marine sequences (Paim et al., 1995). Metamorphic transformations in the unit are of very low to low grade (regional burial) or related to the formation of slates along shear zones (Ribeiro, 1983).

The Bom Jardim Group depositional sequences started with volcanism of andesitic flows and intermediate pyroclastic rocks related to the Hilario Formation of shoshonitic geochemical affinity (Nardi and Lima, 1985), which are more abundant in the western part of the basin. To the east, closer to the Camaquã Mines, the stratigraphy is dominated by the Arroio dos Nobres Formation, consisting of alluvial fan conglomerates and sandstones followed by a thick sequence of delta-front rhythmites (Paim et al., 1995). SHRIMP U/Pb in zircon data yield an age of 594 ±5 Ma for the volcano-plutonic magmatic event of the Bom Jardim unit (see further).

The widespread presence of mud cracks, ripple marks and other shallow water structures in the Arroio dos Nobres unit indicate that the sequences of the Bom Jardim Group were frequently exposed to sub-aerial environments and consequently to oxidising conditions. A dominant continental depositional environment for the Bom Jardim unit is reinforced by boron geochemistry and geotectonic constraints on the

sequence (Altamirano, 1992; Oliveira, 1992). Mineral transformations in the sedimentary fraction are related to the anquizone (Altamirano, 1992). The hydrothermal or low grade conditions are particularly visible in the volcanogenic fraction of that unit, where albite, epidote, carbonate and chlorite form veinlets, or replace plagioclases and pyroxenes, and also occur in the very fine, in places, vitreous matrix of rocks (Ribeiro, 1986).

Syntectonic Caçapava Granite intrusion at ca. 560 Ma (Remus et al., 1999) was contemporaneous with the NE strike-slip and related fault system that deforms the Bom Jardim unit.

The Santa Bárbara depositional unit starts at the base with an alluvial conglomerate facies and ends with deltaic systems (Paim et al., 1992). The Acampamento Velho Formation comprises thick successions of pyroclastic (breccias, fall and ash acid tuffs) and lava flow rocks (rhyolites and trachytes). The geochemical affinity of the Acampamento Velho Formation is alkalic, and may be grouped with the Saibro Suite (Hartmann and Nardi, 1982; Nardi and Bonin,1991; Lima and Nardi, 1998). On the other hand, SHRIMP U/Pb zircon studies in the São Sepé Granite yield an age of ca. 550 Ma (Remus et al., 1998), probably coeval with Acampamento Velho Formation magmatism. This also defines the maximum age of the Santa Bárbara unit. This age agrees very well with the ca. 545 Ma Rb/Sr isochron from previous results on volcanic acid rocks of that unit (Almeida et al., 1996).

The end of Camaquã basin fill is marked by deposition of the Guaritas Formation which lies mostly horizontal over the Bom Jardim and Santa Bárbara units. The Guaritas unit started with rift-related basic to intermediate volcanism of the Rodeio Velho Member, intercalated with aeolian, lacustrine and alluvial deposits in the base, and finished with alluvial fans and deltaic depositional sequences in the top (Ribeiro et al., 1966; Paim et al., 1995).

METHODOLOGY

Geological field maps were revised over the entire copper province at the 1:250,000 scale but a more detailed 1:25,000 survey was performed on the area close to the mine. The mine itself was surveyed at the 1:500 scale in several levels as stripping progressed

(Bettencourt, 1972; Reischl, 1988; Teixeira and Gonzales, 1988). Structural controls were established, and rock and ore samples collected for laboratory studies. Approximately eighty thin sections and one hundred and fifty polished sections of ores were studied in the mine sites and from prospects, followed by rock geochemistry.

For this investigation, rock samples were collected from the mine pit and from the Lavras Granite, Hilário and Arroio dos Nobres Formations. Whole rock samples weighing one kilogram were collected for Pb isotopic studies, and about ten kilograms of a perthitic granite and granodiorite from Lavras Granite were collected for zircon studies. Feldspars were separated from the granites and andesites by conventional magnetic and heavy liquid procedures. Ore sulphides were collected in the open pit and underground mine and in the prospects for sulfide Pb-isotope studies. Individual sulfides of coarse samples were separated by hand picking and analytical procedures as outlined in Ho et al. (1994).

Zircon geochronology was undertaken on two samples of different granite facies to determine the age of the Lavras Granite. SHRIMP investigations of zircons were undertaken at Curtin University and follow the procedures of Compston et al. (1984) and Smith et al. (1998). Scanning electron microscope images of grains to be analysed were obtained using backscattered electron (BSE) and cathodoluminescence (CL) modes at the Centre for Microscopy and Microanalysis, University of Western Australia.

Rock samples for isotopic analysis were crushed and milled in an agate mortar to minimise any contamination. The concentration of U, Th and Pb (ppm) was determined in whole rocks of Lavras Granite, Hilario and Arroio dos Nobres Formations using inductively coupled-plasma-mass spectrometer (ICP-MS) available commercially through Genalyses Laboratory Services Pty. Ltd. (Perth, Australia). SiO_2 (wt %) was determined in whole rocks by the XRF method at Analabs Pty. Ltd. (Perth, Australia). Lead was extracted by ion exchange chromatography at the Lead-free Laboratory, University of Western Australia, and the isotopic measurements were made on a VG354 multicollector mass spectrometer housed at Curtin University.

GEOLOGY OF CAMAQUÃ-SANTA MARIA ORE DISTRICT

The Camaquã and Santa Maria Mines are 3 Km apart and occur along a structural high named the Bom Jardim Window (Figs 2 and 4). This is an elongated domal structure, with a N45°E-trending major axis, cut by a regional transcurrent N30°E fault (Camaquã Mine Fault). Older sedimentary beds of the Bom Jardim unit occur in the core, over an area of about 80 Km^2, whereas the younger red beds of the Guaritas unit occupy the flanks. The major N30°E-trending transcurrent faults belong to the Irapuá Fault System, and have been interpreted as ancient reactivated zones of weakness (Bettencourt and Damasceno, 1974), representing a deep-seated wrench-fault system formed during the Neoproterozoic Dom Feliciano Collisional Orogeny.

The host rocks of the ore deposits are conglomerates, sandstones and rhythmites of the Arroio dos Nobres Formation (Vargas and Mangueirão Members) of the Bom Jardim Group. The proposed stratigraphic column for the ore district is modified from Faccini et al. (1987) and shown in Figure 5. The Vargas Member in the mine area is subdivided into lower, middle and upper sandstones and lower and upper conglomerates.

Pre-mining ore reserves for the Camaquã deposits were 30.8 million tonnes averaging 1.06% Cu with Au and Ag as the main by-products in the hematite and sulphides (Teixeira and Gonzalez, 1978). The Camaquã Mines produced 5 tonnes of Au (0.20 g/ton) and 170 tonnes of Ag (8 g/ton). The geologic reserves of Santa Maria deposit are 33.4 million tonnes averaging 1.44% Pb and 1.06% Zn with Ag (12-15 g/ton) and Cu as the main by-products (Badi, 1987).

Previous K/Ar determinations on diagenetic clay minerals in arenites of the Arroio dos Nobres Formation yield ages between 535±16 Ma and 572±17 Ma (Bonhome and Ribeiro, 1983). Recent SHRIMP U/Pb in zircons studies yield a more precise age of 594±5 Ma for the volcano-plutonic magmatic event of the Bom Jardim unit (see further). Radiometric ages of copper mineralisation of the Camaquã Mine are poorly constrained. The K/Ar ages of clay minerals (illites) associated with the ores are between 457 and 474 ±11 Ma (Bonhome and Ribeiro, 1983), which are interpreted as a minimum age for this deposit. New K/Ar determinations in white micas from the sericitic alteration zone of the sulphide lodes of the Uruguay sector (level +180) of the Camaquã

Mines yield an age of 538 ±7 Ma (J.C. Biondi, 1998 personal communication), which is also interpreted as a minimum age for this deposit.

SHRIMP U/Pb ZIRCON AGES

Two samples of different petrographic facies of the Lavras Granite were collected close to Lavras do Sul town and studied by the U/Pb method using SHRIMP. The granodiorite facies of shoshonitic geochemical affinity (Nardi and Lima, 1985), located in the core of Lavras Granite pluton shows a single morphologic population. This population is composed of prismatic and short prismatic crystals with well developed {010} and {100} faces and symmetrical and assymetrical {101} and {031} less-developed pyramid faces. BSE and CL images of these zircons show a concentric or irregular zonation patterns in the rim regions, whereas cores are massive or have a less-developed zonation (Figs 6A-B, C-D and E-F). The majority of grains have many inclusions (Figs 6C-D). Thirty nine analyses were done in the core and rim region of twenty nine zircons, which have a spread in $^{206}Pb/^{238}U$ ages between 614 of 441 Ma (Fig. 7 and Table 1). The magmatic $^{206}Pb/^{238}U$ age of 594±5 Ma was obtained on thirty six analyses of that zircon population. Three spots present Pb-loss and are shown in the concordia diagram of Figure 7. The sample of the perthite granite facies of alkaline geochemical affinity, located in the margin of Lavras Granitic, was colleted in the northwestern part of the pluton and shows two distinct morphologic zircon groups with an indistinguishable age. One group is represented by prismatic and short prismatic crystals with well developed {100} and {010} faces. These zircons show distinctive massive cores, in places with irregular or complex zoned patterns. The rims are invariably concentrically zoned (Figs 6 G-H). The other group comprises prismatic and long prismatic crystals with very well developed {100} and {010} faces and irregular or complex zonation pattern (Figs 6 I-J). Thirty analyses, done in the core and rim region of twenty six zircons of both morphologic groups, have a spread in $^{206}Pb/^{238}U$ ages of 608 to 322 Ma (Fig. 8 and Table 2). The $^{206}Pb/^{238}U$ age of 594±4 Ma was obtained on the cores and rims of zircon from both groups, which are analytically indistinguisable, and it is interpreted as

the magmatic age of the perthite granite facies. Three zircon grains have lead-loss and are shown in the concordia diagram of Figure 8.

ORE GEOLOGY

The main sulphide ore lodes of the Camaquã deposits are enclosed in conglomerates and sandstones of the Vargas Member of the Arroio dos Nobres Formation, located in the upper and lower conglomerate and middle sandstone sequences (Figs 9 and 10). In the Santa Maria deposit, they are located in arenites (mainly) and conglomerates of the Vargas Member. Mining activities in the Camaquã Deposit were concentrated in the Uruguay and São Luiz Sectors about 1 Km apart (Fig. 10).

The coarse conglomerates of the Vargas Member have a framework of clasts, blocks and minor boulders of granitoids, acid and intermediate volcanic rocks, gneisses, mylonites, schists, phyllites, quartzites, quartz, feldspars and sedimentary intraclasts, while the matrix is of arenite of arkosic composition (Ribeiro et al., 1966; Veigel, 1992). Several stages of diagenetic processes have been described in the area (Bettencourt, 1972; Veigel, 1992). Intercalated sandstone sequences are texturally immature arkosic arenites.

The orientation of the mineralised fracture system has three maxima in the Camaquã Mines. In the São Luiz sector, it is N20°W, 81°NE, associated with breccia and cataclastic rocks and N70°W, 50°NE with breccia, while, in the Uruguay sector, it is N50°W, 70°SW with breccia (Bettencourt and Damasceno, 1974). These fracture sets could either be secondary fractures of a Riedel system linked to the NE-trending transcurrent Camaquã Mine Fault (Fig. 2) or to E-W to NW lateral ramps of a thrust system. The slickensides along the fault planes indicate ambiguous senses of movement. The alternative hypothesis for the origin of the mineralized fracture sets, is that this was linked to lateral ramps of a major thrust system which were generated by movements along an ancient E-W to NW (Paleoproterozoic?) fracture zone, subparalell to Ibaré Lineament (Fig. 2). The E-W lineament, close to the Camaquã River, along a trend including the Camaquã Deposits and Cerro Rico and Butiá Prospects (Fig. 2) have been previously recognized as an ancient large fracture zone

that controlled important precious- and base-metal mineralization in the Sul-Riograndense Shield (Offield et al., 1977).

The mineralogy, lode shapes, textures and parageneses of the Camaquã Mines have been described by several authors (Leinz and Almeida, 1941; Bettencourt, 1972, 1976; Teixeira and Gonzales, 1988; Reischl et al., 1988; Veigel and Dardenne, 1990; Ribeiro, 1991) as summarized below.

The Camaquã Mines consist of sulphide copper mineralisation of chalcopyrite, bornite and chalcocite, gold and silver. Chalcopyrite is the main ore mineral in the Camaquã Mines, and occurs in the massive major veins with minor pyrite or as irregular masses associated with hematite or quartz. It also occurs as euhedral crystals in open spaces, as anhedral isolated crystals, or as cement filling the intergranular space of arenites and conglomerates. Bornite is the second most abundant sulphide, occurring as massive veins and veinlets or associated with chalcopyrite and hematite. Locally, fine grained bornite is disseminated in arenites and conglomerates as the main rock cement. Chalcocite rarely forms massive veins and veinlets; it is mainly disseminated in arenites and conglomerates. Gold occur as inclusions in hematite or chalcopyrite veins, and Ag is associated with chalcocite and bornite. Pyrite occurs as isolated disseminated grains and irregular masses associated with chalcopyrite and other sulphides and does not contain gold. Barite is concentrated in veins, locally with minor chalcopyrite.

In the Uruguay Sector of the Camaquã Mines, the mineralized area is 600 m wide and up to 1 Km long and about 700 m deep; ore is composed of tens of subparallel lodes which reach individually up to 600 m in length and 2 m in width. In the São Luiz Sector, the mineralization is concentrated in a zone 20-110 m wide by 700 m long. At the deposit scale, ore bodies of both sectors of the Camaquã Mines have a conical form (Fig. 10). A roughly horizontal zonation of sulphides occurs along NW-trending fracture-hosted lodes where pyrite/chalcopyrite and hematite (and gold) occur in the SE and chalcocite and bornite in the NW sector. The vertical zonation is marked by a dominance of chalcopyrite and pyrite in the deeper parts of the Uruguay Sector. A similar mineral zonation in the São Luiz Sector shows an increase of chalcocite in a NW direction, while chalcopyrite

dominates in the SE part. This ore mineral zonation cross-cuts the stratigraphy.

The hydrothermal alteration in the wall rocks is marked by changing original colors of arenites and conglomerates from brown or pink to greenish colors. It is accompanied by chloritization, silicification, albitization, carbonation and sericitic alteration of the wall rocks. In the Uruguay Sector, chloritization and sericitization are the main alteration halos, whereas, in the São Luiz Sector, silicification and sericitization dominate.

The paragenesis and textures of ore minerals of the Santa Maria Deposit were investigated by Badi and Gonzalez (1988), Veigel and Dardenne (1990), Beckel et al. (1991), Ribeiro (1991), Veigel (1992) and Dorneles (1996), and are summarized below.

The Santa Maria ore bodies occur in three areas; 56% of the ore is concentrated in area 3 (Figs 4 and 9). It is a polymetallic deposit, with Pb> Zn> Cu, where Ag and Cd are the main by products. The Ag- and Cu-enriched ore zones are concentrated at the base of the conglomerate unit, while the Pb zone is near the contact between conglomerates and sandstones; Zn is sited in the sandstones of area 3.

Galena and sphalerite, the two main minerals of the deposit, are disseminated in arenites and conglomerates or as massive lodes crosscutting the stratigraphy. The massive lodes are concentrated in subvertical fractures oriented N10-30°W. Disseminated sphalerite is commonly black and becomes honey colored in veins. Sphalerite and galena intergrowths are the dominant texture in the ores; in places, galena surrounds sphalerite which, in turn, wraps galena. This shows that the two ore minerals grew simultaneously. Chalcopyrite occurs as intergrowths in sphalerites or is surrounded by bornite and chalcocite, showing the same trend of later Cu-bearing fluids as in the Camaquã Mines. Pyrite is more abundant outside of the mineralized zone and, where it occurs, the crystals are replaced by galena and sphalerite.

The Butiá Au-prospect is enclosed by the perthite-granite facies of the Lavras Granite, and consist of an set of E-W to NW vein system composed by pyrite, white mica, invisible gold with minor chalcopyrite, galena and carbonate (Kaul and Zir F°, 1974; Reischl, 1980; Nardi and Lima, 1988; Mexias et al., 1995). The Cerro Rico Prospect is enclosed by volcanic rocks of the Hilario Formation and consists of a set of quartz veins oriented to NW and composed of pyrite, chalcopyrite, invisible

gold and minor hematite and galena. Previous K/Ar determinations on white micas from the sericitic alteration zones of veins in the perthite-granite facies and in the granodiorite central facies of Lavras Granite yield ages between 602 ±13 Ma and 600 ±8 Ma, respectively (Soliani Jr., 1986).

Geothermometry

Heating experiments on fluid inclusions in quartz from the Camaquã Mines indicate that the first circulating fluids had a maximum homogenisation temperature of 222°C (n = 39) and the minimum pressure was around 20 atm, and the fluid composition of the system has a salinity between 7.1 to 14% NaCl equiv. and density of 0.95 to 1.10 g/cm^3 (Beckel, 1992). The fluid inclusions in barites indicate temperatures of 20-80°C, with salinity of 8 to 10% NaCl equiv. (Bettencourt, 1976)., which are related to the final stage of fracturing and circulation of fluids which is interpreted to correspond to mixing of hydrothermal solutions and meteoric water

Homogenisation temperature measurements in primary inclusions of sphalerites and carbonates from the Santa Maria Mine fall between 117 and 289°C, with a mean of 210°C, with salinity in the range of 2.3 to 17.7% NaCl equiv., while secondary fluid inclusions in quartz yield temperatures between 90 and 160°C, with a mean around 137°C (Lima et al., 1998).

Geothermometric calculations, based on S-isotopic fractionation between galena-sphalerite pairs (Ohmoto and Rye, 1979), yield a temperature of 280 to 301±20°C for deposition of massive vein sulphides in the Santa Maria Deposit (Remus et al., 1997a). These values agree approximately with those estimated using microprobe data from ore-related chlorites (268-315°C) in the matrix of arenites of the Santa Maria Deposit, and are slightly higher than fluid inclusions homogenisation temperatures from sphalerites and carbonates, with mean values around 210°C (Lima et al., 1998).

Sulphur isotopes

Sulphur isotope analyses were carried out on sulphide ore minerals from the Camaquã (pyrite, chalcopyrite and bornite) and Santa

Maria Mines (galena and sphalerite) to constrain the source of metals and sulphur. Pyrites from the Cerro Rico and Butiá Prospects were also analysed for comparison. The $\partial^{34}S$ results are very homogeneous in both deposits and prospects, with values in the range of -1.8 to +0.6‰ for the Camaquã Mine and -2.6 to +1.1‰ for the Santa Maria deposit and +1.7 to +2.2‰ for the Cerro Rico and Butiá Prospects, and are shown in Table 3. Previous results for both deposits (Bettencourt, 1976; Beckel et al., 1991) are very similar to these data, and all three data sets indicate a magmatic origin for the sulphur (Fig. 11a and b) (Ohmoto and Rye, 1979). Sulfur isotope values of pyrites from the prospects also indicate a magmatic origin for sulfur (Fig. 11 c). Low-temperature barites, formed later in the paragenetic sequence and collected from a distal part of the sulphide veins of the Camaquã deposit, have $\partial^{34}S$ in the range of +10.3 to +14.0‰ (Bettencourt, 1976), which may indicate mixing between marine water and the magmatic S source. Alternatively, they may indicate oxidation of the fluids due to falling temperature, by mixing of a hot rising solution with cold meteoric water, leading to precipitation of the final-stage mineral paragenesis (barite, hematite, quartz and minor sulphides) in the Camaquã Mines. The values of $\partial^{34}S$ of -2.6 to -7.1‰, in samples (n= 6) consisting of sphalerite + galena ± pyrite from the Santa Maria Deposit (Beckel et al., 1991; Garcia, 1997), indicate a minor contribution of sedimentary reduced-sulphur, possibly derived from the remobilization by magmatic fluids of framboidal diagenetic pyrites described by Veigel (1992).

Lead isotopes

Lead isotope data for the Lavras Granite (K-feldspar and whole rock) and pyrite from the Butiá Prospect, near the western border of the granite, are shown on a common lead diagram (Fig. 12 and Table 3). The granite and pyrite data plot on a straight line, compatible with the 594 Ma age for this granite as defined by SHRIMP U/Pb zircon geochronology. The sample from the perthite granite facies (K-feldspar and whole rock) plots off the isochron, probably because it is more altered and enriched in perthite. Also shown are data for trachy-andesitic volcanic rocks of the Hilario Formation (plagioclase and whole rock) and pyrite samples from the Cerro Rico Prospect within the Hilario Formation.

These samples also plot on the 594 Ma isochron for the Lavras Granite, and indicate that Pb in pyrites from this prospect was probably derived from the granite and/or volcanic rocks, and further suggest a genetic link between these rock types. A genetic link between the granite and volcanic rocks, both belonging to a shoshonitic magmatic association, had been previously suggested (Nardi and Lima, 1985) based on petrological data.

The least-radiogenic isotopic composition of the pyrite sample from the granite-volcanic rocks is shared by two samples of pyrite in volcanic rocks and an ore-related pyrite hosted by granite. The mean for these three analyses is considered to be the best estimate of the initial Pb in these samples. The initial Pb is very primitive compared to typical lithosphere, as estimated by Stacey and Kramers (1975) growth curve at 594 Ma.

The Pb isotope results for sulphides from the Camaquã and Santa Maria deposits are very consistent and form a linear array (Fig. 13 and Table 4). The array for the sulphides from the mines is subparallel to the 594 Ma reference isochron. This line also includes the composition of unaltered sedimentary rocks of the Arroio dos Nobres Formation and suggests that the Pb in the sedimentary rocks and sulphides have a similar source. Further, their subparallel nature suggests that mineralisation could have occurred at 594 Ma, thus being related to Bom Jardim shoshonitic plutonism. This age agrees very well with the ca. 600 Ma K/Ar age obtained on white micas from sericitic alteration zones on gold mineralization in the Lavras Granite (Soliani Jr., 1986).

THE ORIGIN OF THE ORES

This mineralization has been related to volcanic rocks (Leinz and Almeida, 1941; Ribeiro et al., 1966; Ribeiro, 1986; Lima et al., 1998), to a deep magmatic body (Melcher and Mau, 1960; Bettencourt, 1972, 1976; Beckel, 1990; Remus et al., 1997a), or to derivation from sedimentary clastic-diagenetic processes (Ribeiro et al. 1980; Badi, 1983; Badi and Gonzales, 1988; Teixeira and Gonzalez, 1988; Veigel and Dardene, 1990; Ribeiro, 1991; Garcia, 1997). One group of genetic hypotheses considers the deposits to be diagenetic, based on

observations of the stratiform control of part of the mineralization, and also on the fine grain size of ores in the structures.

Most of syngenetic/diagenetic base-metal sedimentary deposits around the world are hosted by low-energy, marine-sedimentary sequences (Ohmoto et al., 1990). In contrast, the sedimentary sequence hosting the Camaquã and Santa Maria Mines is high energy, continental delta-fan, and dominantly non-marine. These characteristics of the Bom Jardim Group argue against a sedimentary syngenetic-diagenetic origin for the mineralization. However, some sulphur contribution to the basin could be derived from sulphides in volcaniclastic fragments of host rocks and possibly from fumaroles related to volcanic events recorded in the Hilario Formation.

The depositional mechanism for the Camaquã and Santa Maria mineralization has not been studied in detail. Beckel (1992) argue that the metals, which were carried as chloride complexes, were deposited by abrupt lowering of temperature and pressure, triggered by hydraulic fracturing of the sedimentary pile. An alternative mechanism is the chemical reaction of mineralizing fluids with the host rocks. A possible depositional mechanism for the Camaquã deposits relates to hydrolysis reactions during hydrothermal alteration of wall rocks, during which the clay minerals were transformed into chlorites, and the feldspars in arenites and conglomerates were localy altered to white micas. A similar mechanism of ore deposition, in the Santa Maria deposit, could be the neutralization of an originally acid solution. In this model, the ore solution infiltrated the sedimentary sequences and encountered domains with a high concentration of carbonates (diagenetic cements); at this point, sulphide precipitated due to neutralization of the original acid solution. Evidence of this is the common association of carbonate veins with Pb-Zn-Cu mineralization (Badi, 1983; Badi & Gonzales, 1988), the high temperatures of carbonate deposition (Lima et al., 1998), and the textures of ore minerals, in which galena is surrounded by calcite which, in turn, is wrapped by sphalerite (Ribeiro, 1991).

The Pb isotope results for sulphides from the Camaquã-Santa Maria Mines indicate that the metals were derived from a largely crustal source with very primitive Pb at the end of the Brasiliano Cycle. Mineralization is related to a magmatic event at the end of Brasiliano magmatism, possibly the Lavras Granite plutonism or related buried bodies. However, Pb was derived largely from old basement and from

the sedimentary rocks of the Bom Jardim Group, when magmatic fluids ascended through the thick volcano-sedimentary package.

The overall evidence (structural control of mineralization, mineral zonation at the deposit scale and the isotopic results) indicates that the mineralization is magmatic hydrothermal/epithermal in origin. In support, in 1993, the geologists from Companhia Brasileira do Cobre identified a 3 m wide stockwork of chalcopyrite in a chloritic matrix, in the underground Uruguay Sector (-200 m level), which they considered to be a hydrothermal conduit for the generation of these deposits.

These data and interpretations are critical for base-metal exploration in the Sul-Riograndense Shield. Hence, mineralization is likely to be located along fractures and their intersections, in lithological traps, and, most significantly, in and above deep granitic bodies. The style of mineralization shows some similarities to granite-related epithermal veins and to Telfer-style deposits in Australia (e.g. Rowins et al., 1997). In either case, there are potential porphyry-Cu-Au style deposits in the environment. These represent potential bulk low-grade targets in the region.

CONCLUSIONS

Re-evaluation of previous data and new studies in the area yield the following conclusions:

(1) mineralization is fracture-controlled and distal magmatic-hydrothermal in origin rather than stratiform syngenetic or diagenetic;

(2) the temperature of deposition of the main ore minerals was 210 to 300°C;

(3) deposit-scale ore-mineral zonation crosscuts the stratigraphy;

(4) hydrothermal alteration of wall rocks is represented by chloritization, silicification, sericitization and carbonation;

(5) the $\partial^{34}S$ of sulphides from the mines of around 0‰ indicates an external magmatic-hydrothermal related source of sulphur;

(6) lead isotope results of sulphides from the mines indicate that the metals were derived from a largely crustal source with very primitive Pb at the end of the Brasiliano Cycle;

(7) the age of mineralization is interpreted to be ca. 594 Ma as constrained by U/Pb SHRIMP determinations on zircons of the Lavras Granite.

DISCUSSION

The hydrothermal origin of deposits, together with the total original metal reserves (300,000 tons of Cu, 350,000 tons of Zn, 500,000 tons of Pb, 200 tons of Ag and 5 tons of gold) along the mineralized zone of the Bom Jardim Window (about 12 Km^2) indicate a high mineral potential for the district (Ribeiro, 1991).

Exploration methodologies used in the last few decades followed mainly guidelines based on the hypothesis of a sedimentary origin for the mineralization. The exploration was directed to the discovery of extensive mineralized sedimentary horizons (beds) and not mineralized sites controlled by fractures and by the permeability of wall rock, as at the Camaquã and Santa Maria deposits. However, new parameters need be used for base-metal exploration in the Sul-Riograndense Shield based on this review: (1) Ancient E-W- and NW-trending regional fractures and their intersections are potential structural sites for base-metal mineralization. These structures could represent ancient (Paleoproterozoic?) weakness zones in the lithosphere and are subparallel to the Ibaré Lineament which forms the boundary between the Taquarembó Block (Paleoproterozoic granulitic terrain) and the São Gabriel Block (Brasiliano juvenile terrain). Several E-W to NW- trending diabase dikes, which are controled by such structures, occur along the Camaquã Basin and could be used as a structural targets. (2) Lithologies with high original porosity (conglomerates and arenites), or rocks which are highly reactive to replacement processes (carbonates), are the preferential wall-rock sites for mineralization. The sedimentary clastic fraction of the Bom Jardim Group and carbonate rocks of Passo Feio Formation cross-cut by NW to E-W fractures are potential targets, as shown by the structural control of the Camaquã-Santa Maria deposits and the Cioccari and Coronel Linhares prospects, respectively. (3) The basement rocks, namely Passo Feio Formation mafic rocks and Arroio dos Nobres sedimentary sequences, are potential sources of base metals. The lead-isotope signatures of sulphides from the Camaquã-

Santa Maria deposits, and from deposits in the Passo Feio Formation, are derived from a depleted crustal basement and are compatible with lead in arenites from the Arroio dos Nobres Formation and metasedimentary rocks of the Passo Feio Formation (4) The post-collisional plutonism of the Dom Feliciano Orogeny is the most likely candidate for the heat source, sulphur and base metals. The well-constrained age of 594 Ma for the Camaquã/Santa Maria deposits, and ca. 560 Ma for deposits in the Passo Feio Formation, indicate that the end of Dom Feliciano Collisional Orogeny is the most probable period for base-metal deposit generation in the Sul-Riograndense Shield (5) Geophysics (e.g. gravity survey) and alteration studies are essential to detect intrusive bodies at depth which may have potential for porphyry-style Cu-Au deposits.

Acknowledgments

This paper is part of the Ph.D. thesis of the first author on the Copper Province of Rio Grande do Sul. Funding by CNPq - National Research Council of Brazil (Grant 201393/94-8) is acknowledged. Luis L. Forgiarini and Nilson T. Dorneles (CBC, Brazil) are thanked for his help with the field work and Mrs. Marion Dahl (UWA-Australia) for help with the analytical procedures. Paul Potter reviewed the English version of the paper. Zircons were analysed on the SHRIMP II operated by a consortium consisting of Curtin University of Technology, the Geological Survey of Western Australia and the University of Western Australia, with the support of the Australian Research Council.

References

Almeida, D.P.M., Zerfass H. and Basei, M.A. (1996) Mineralogia, geoquímica e novas idades para o vulcanismo ácido da Bacia do Camaquã. In: Congresso. Brasileiro de Geologia, 39, Salvador. Anals, SBG, v. 2, pp. 19-21.

Altamirano Flores, J.A. (1992) O boro nos sedimentitos da Formação Arroio dos Nobres, Proterozóico Superior do Escudo Sul-Riograndense.

In: 1st Workshop sobre as bacias molássicas Brasilianas, São Leopoldo-RS. Resumos Expandidos, pp. 31-34.

Babinski, M., Chemale Jr F., Hartmann, L.A., Van Schmus W.R. and Silva L.C. (1996) Juvenile accretion at 750-700 Ma in southern Brazil. Geology, v.24, pp. 439-442.

Babinski, M., Chemale Jr F., Van Schmus, W.R., Hartmann, L.A. and Silva L.C. (1997) U-Pb and Sm-Nd geochronology of the Neoproterozoic granitic-gneissic Dom Feliciano Belt, southern Brazil. J. South Am. Earth Sc., v.10 (3-4), pp. 263-274.

Badi, W.S.R. (1983) Mineralização de chumbo e zinco em arenitos do distrito Camaquã-RS. Unpublished M.Sc. Thesis. Universidade Federal do Rio Grande do Sul, Porto Alegre, Brazil,137p.

Badi, W.S.R. (1987) Relatório final de pesquisa. Unpublished Report, CBC, Porto Alegre, Brazil. 120p.

Badi, W.S.R. and Gonzalez, A.P. (1988) Jazida de metais básicos de Santa Maria, Caçapava do Sul-RS. In: Schobbenhaus, C. and Silva Coelho, C.E. (Eds.) Principais Depósitos Minerais do Brasil. DNPM/CVRD, Rio de Janeiro, RJ, v. 3, pp. 157-170.

Beckel, J. (1990) Metalogenia del Cu, Pb y Zn en la cuenca de Camaquã durante El Ciclo Orogenico Brasiliano, Rio Grande do Sul (Brasil). Unpublished Ph.D. Thesis. Universidade de Salamanca, Salamanca, Spain, 274p.

Beckel, J. (1992) Características físico-químicas do fluído hidrotermal formador das mineralizações de cobre das Minas do Camaquã, RS. In: 1st Workshop sobre as bacias molássicas Brasilianas, São Leopoldo-RS. Resumos Expandidos, pp. 6-11.

Beckel, J., Arribas, A. and Almeida, D.P.M. (1991) Estudio isotopico del azufre de las Minas de Cu-Pb-Zn de Camaquã, Rio Grande do Sul, Brasil. In: Congresso Geológico Chileno, 6. Resumenes Expandidos, pp. 440-444.

Bettencourt, J.S. (1972) A Mina de cobre de Camaquã, Rio Grande do Sul. Unpublished Ph.D. Thesis. Universidade de São Paulo, São Paulo, Brazil,175p.

Bettencourt, J.S. (1976) Mineralogie, inclusions fluides et isotopes stables d'oxygene et de soufre de la mine de cuivre de Camaquã - RS (une ètude preliminaire). In: Congresso Brasileiro de Geologia, 29, Ouro Preto, MG. Anals, SBG, v. 2, 409-423

Bettencourt, J.S. and Damasceno, E.C. (1974) Análise tectônica e controles da mineralização no Distrito Cuprífero de Camaquã, RS. In: Congresso Brasileiro de Geologia, 28, Porto Alegre, RS. Anals, SBG, v.2, pp. 409-423.

Bonhome, M.G. and Ribeiro, M.J. (1983) Datações K-Ar das argilas associadas a mineralização de cobre da Mina do Camaquã e de suas encaixantes.: 1st Simpósio Sul-Brasileiro de Geologia, SBG, Porto Alegre. Atas v. 1, pp. 82-88.

Compston, W., Williams, I.S. and Meyer, C. (1984) U-Pb geochronology of zircons from Lunar breccia 73217 using a sensitive high-mass resolution ion microprobe. J. Geophys. Res., 89 Suppl.: B525-B534.

Dorneles, N.T. (1996) Jazida Santa Maria. Unpublished Report, CBC. Porto Alegre, Brazil,10 p.

Faccini, U.F, Paim, P.S.G. and Fragoso César, A.R.S. (1987) Análise faciológica das molassas Brasilianas na região das Minas do Camaquã. 3rd: Simpósio Sul-Brasileiro de Geologia, SBG, Curitiba, PR. Atas, v.1, pp. 75-91.

Fragoso César, A.R.S., Figueiredo M.C.H., Soliani Jr. E. and Faccini U.F. (1986) O Batólito de Pelotas (Proterozóico Superior/Eo-Paleozóico) no Escudo do Rio Grande do Sul. In: Congresso Brasileiro de Geologia, 34, Goiânia, GO. Anals, SBG, v.3, pp.167-191.

Garcia, A.J.V. (1997) Diagenetic and isotopic approach to study of ancient fluid flow within sedimentary ore deposits in tardi to post-orogenic molassic basin. In: South-American Symposium on Isotope Geology, Campos do Jordão, Brazil. Extended Abstracts, pp.121-122.

Gresse, P.G., Chemale Jr.F., Silva, L.C., Walraven, F. and Hartmann, L.A. (1996). Late-to post-orogenic basins of the Pan-African/Brasiliano collision orogen in southern Africa and southern Brazil. Basin Research, v. 8, pp. 157-171.

Hartmann, L.A. and Nardi, L.V.S. (1982) Os granitos Santo Afonso, Saibro e Vauthier da região do Arroio Santa Maria Chico, Dom Pedrito, RS - Geologia, petrografia e química de elementos maiores com interpretação geotectônica. Acta Geologica Leopoldensia, v.12, pp. 153-178.

Hartmann, L.A., Silva, L.C., Remus, M.V.D., Leite, J.A. and Philipp, R.P. (1998) Evolução geotectônica do Sul do Brasil e Uruguai entre 3,3 Ga e 470 Ma. In: Congreso Uruguayo de Geologia, 2, Punta Del Este, Actas pp. 277-284.

Hasui, Y., Carneiro, C.D.R. and Coimbra, A.M. (1975) The Ribeira Folded Belt. Revista Brasileira de Geociências, 5 (4), pp. 257-266.

Ho, S.E., McNaughton, N.J. and Groves, D.I. (1994) Criteria for determining initial lead isotopic compositions of pyrite in Archaean lode-gold deposits: A case study at Victory, Kambalda, Western Australia. Chem. Geol., 111, pp. 57-84.

Jost, H. and Hartmann, L.A. (1984) Província Mantiqueira - Setor meridional. In: Almeida, F.F.M. and Hasui, Y. (Coord.) O Pré-Cambriano do Brasil. Edgard Blücher, São Paulo, pp. 345-367.

Kaul, P.F.T. and Zir F°, A. (1974) Mineralizações auríferas de Lavras do Sul, RS: tipos, controle tectônico, aspectos genéticos e guias para localização de novos corpos mineralizados. In: Congresso Brasileiro de Geologia, 28, Porto Alegre, RS. Anals, SBG, v.6, pp. 115-130.

Leinz, V. and Almeida, S.C. (1941) Gênese da Jazida de cobre "Camaquan" Boletim DPM, Porto Alegre, RS, v. 88, 47p. In: Congresso Brasileiro de Geologia, 28, Porto Alegre, RS. Anals, SBG, v.6, pp.115-130.

Licht, O.A.B. (1978) A descoberta da jazida de Santa Maria, um caso histórico de prospecção geoquímica. In: Congresso Brasileiro de Geologia, 31, Balneário de Camboriú, SC. Anals, SBG, v.1, pp.141-153.

Lima, E.F. and Nardi, L.V.S. (1998) O vulcanismo shoshonítico e alcalino da Bacia do Camaquã: estado do Rio Grande do Sul-Brasil. In: Congresso Uruguayo de Geologia, 2, Punta Del Este, Actas, pp. 263-268.

Lima, L., Almeida, D.P.M., Collao, S. and Zerfass, H. (1998) El yacimento Santa Maria (Pb-Zn-Ag), del distrito minero de Camaquã, RS - Brasil: petrografia, paragenesis mineralogica y temperatura de formacion. In: Congresso Uruguayo de Geologia, 2, Punta Del Este. Actas, pp. 227-231.

Mantovani, M.S.M., Hawkesworth, C.J. and Basei, M.A.S. (1987) Nd and Pb isotope studies bearing on the crustal evolution of southeastern Brazil. Revista Brasileira de Geociências, v.17 (3), pp. 263-268.

Melcher, G.C. and Mau, H. (1960) Novas observações geológicas na região de Caçapava do Sul, RS. Anais Academia Brasileira de Ciencias, Rio de Janeiro, v.32 (1), pp. 43-50.

Nardi, L.V.S. and Bonin, B. (1991) Post-orogenic and non-orogenic alkaline granite associations: the Saibro Intrusive Suite, Southern Brazil. A case study. Chem. Geol., v. 92 (1/3), pp. 197-212.

Nardi, L.V.S. and Lima. E.F. (1985) A associação shoshonítica de Lavras do Sul, RS. Revista Brasileira de Geociências, v. 15 (2), pp. 139-146.

Nardi, L.V.S. and Lima. E.F. (1985) A associação shoshonítica de Lavras do Sul, RS. Revista Brasileira de Geociências, v. 15 (2), pp. 139-146.

Nardi, L.V.S. and Lima, E.F. (1988) Hidrotermalismo no Complexo Granítico Lavras e vulcânicas associadas, RS. Revista Brasileira de Geociências, v. 18 (3), pp. 369-375.

Offield, T.W., Abott, E.A., Gillespie, A.R. and Loguercio, S.O. (1977) Structure mapping on enhanced landsat images of southern Brazil: tectonic control of mineralization and speculation on metalogeny. Geophysics, v.42 (3), pp. 482-500.

Ohmoto, H., Kaiser, C.J. and Geer, K.A. (1990) Systematics of sulphur isotopes in recent marine sediments and ancient sediment-hosted basemetal deposits. In: Herbert, H. K. & Ho, S. E. (eds) Stable Isotopes and Fluid Processes in Mineralization. Geology Department and University Extension, The University of Western Australia Publication 23, pp. 70-120.

Ohmoto, H. and Rye, R.O. (1979) Isotopes of sulfur and carbon. In: Barnes, H.L. (ed.) Geochemistry of hydrothermal ore deposits. Wiley, New York, pp. 509-567.

Oliveira, J.M.M.T. (1982) Formação Arroio dos Nobres: depósitos marinhos ou continentais? In: 1st Workshop sobre as bacias molássicas Brasilianas, São Leopoldo - RS. Resumos Expandidos, pp.106-112.

Paim, P.S.G., Faccini, U.F., Netto, R.G. and Nowatzki, C.H. (1992) Estratigrafia de seqüências e sistemas deposicionais das Bacias do Camaquã e Santa Bárbara. Série Correlacion Geológica, Universidade Nacional de Tucuman, v. 9, pp. 41-45.

Paim, P.S.G., Lopes, R.C. and Chemale Jr., F. (1995) Aloestratigrafia, sistemas deposicionais e evolução paleogeográfica da Bacia do Camaquã - Vendiano Superior/Ordoviciano inferior. In: 6th Simpósio Sul-Brasileiro de Geologia, SBG, Porto Alegre. Boletim de Resumos Expandidos, pp. 39-50.

Reischl, J.L. (1980) Mineralizações auríferas associadas ao Complexo Granítico de Lavras do Sul-RS. In: Congresso Brasileiro de Geologia, 31, Camboriú. Anals, SBG, 3, pp. 1700-1712.

Reischl, J.L., Feldmann, E., Forgiarini, L.L., Dorneles, N.T., Ribeiro, M., Lima, P.P., Scola, J.C., Pavão, L.P. and Zonta, N.A. (1988) Projeto Ouro - Zona Piritas. Unpublished Report, CBC, Porto Alegre, 35p.

Remus, M.V.D., Hartmann, L.A., McNaughton, N.J., Groves, D.I. and Fletcher, I.R. (1999) The link between hydrothermal epigenetic copper mineralization and the Caçapava Granite of Brasiliano Cycle in Southern Brazil. J. South Am. Earth Sc. (submitted).

Remus, M.V.D., McNaughton, N.J., Hartmann, L.A. and Fletcher, I.R. 1997b. Zircon SHRIMP U/Pb dating and Nd isotope data of granitoids of the São Gabriel Block, southern Brazil: evidence for an Archaean/Paleoproterozoic basement. In: Second International Symposium on Granite and Associated. Mineralization, Salvador, BA-Brazil. Extended Abstracts, pp.271-272.

Remus, M.V.D., McNaughton, N.J., Hartmann, L.A., Groves, D.I. and Reischl, J.L. (1997a) Pb and S isotope signature of sulphides and constraints on timing and sources of Cu(Au) mineralisation at the Camaquã and Santa Maria Mines, Caçapava do Sul, southern Brazil. In: South-American Symposium on Isotope Geology, Campos do Jordão, Brazil. Extended Abstracts, pp, 253-255.

Remus, M.V.D., McNaughton, N.J., Hartmann, L.A., Koppe, J.C., Fletcher, I.R., Groves D.I. and Pinto, V.M. (1998) Gold in the Neoproterozoic juvenile Bossoroca Volcanic Arc of southernmost Brazil: isotopic constraints on timing and sources. J. South Am. Earth Sc. (submitted).

Ribeiro, M. (1983) Informes sobre a Formação Maricá. Inheringia, Sér. Geol., Porto Alegre, RS, v. 9, pp. 3-50.

Ribeiro, M. (1986) O metamorfismo dos campos termais do Escudo Sul-Riograndense. Iheringia, Série Geológica, v. 11, pp.15-28.

Ribeiro, M., Bocchi, P.R., Figueiredo Filho, P.M. and Tessari, R.I. (1966) Geologia da quadrícula de Caçapava do Sul, RS, Brasil. Boletim da Divisão de Geologia e Mineralogia, DPM-DNPM, v.127, 232p.

Ribeiro, M. and Carraro, C.C. (1971) Geotectonic map of the Caçapava do Sul region - RS. Instituto de Geociências, Universidade Federal do Rio Grande do Sul, Porto Alegre, RS.

Ribeiro, M.J. (1991) Sulfetos em sedimentos detríticos Cambrianos do Rio Grande do Sul, Brasil. Unpublished, Ph.D. Thesis. Universidade Federal do Rio Grande do Sul, Porto Alegre, Brazil, 416p.

Ribeiro, M.J., Badi, W.S.R., Gonzalez, A.M., Licht, O.A.B. and Teixeira, G. (1980) Jazida Santa Maria, chumbo e zinco no Grupo Bom Jardim-RS. In: Congresso. Brasileiro de Geologia, 31, Camboriú, SC. Anals, SBG, v. 3, pp.1725-1742.

Rowins, M.S, Groves, D.I., McNaughton, N.J., Palmer, M.R. and Eldridge, C.S. (1997) A reinterpretation of the role of granitoids in the genesis of Neoproterozoic gold mineralization in the Telfer Dome, Western Australia. Econ. Geol., v.92 (2), pp.133-160.

Santos, E.L., Ramgrab, G.E., Maciel, L.A and Mosmann, R. (1989) Mapa geológico do Estado do Rio Grande do Sul, escala 1: 1,000000 e parte do Escudo Sul-riograndense, escala 1: 600,000. DNPM-MME, Porto Alegre, Brazil.

Smith, J.B., Barley, M.E., Groves, D.I., Krapez, B., McNaughton, N.J., Bickle M.J., and Chapman, H.J. (1998) The Scholl Shear Zone, West Pilbara; evidence for a domain boundary structure from the integrated tectonostratigraphic analyses, SHRIMP U-Pb dating and isotopic and geochemical data of granitoids. Precamb. Res., v. 88, pp.143-171.

Soliani, Jr E. (1986) Os dados geocronológicos do Escudo Sul-Riograndense e suas implicações de ordem geotectônica. Unpublished Ph.D. Thesis, Universidade de São Paulo, São Paulo, Brazil, 239p.

Stacey, J.S. and Kramers, J.D. (1975) Approximation of terrestrial lead isotope evolution by a two stage model. Earth Plan. Sci. Let., v. 26, pp. 207-221.

Teixeira, G. and Gonzales, M.A. (1978) Projeto Expansão Camaquã - Reavaliação das Jazidas. Unpublished Report, CBC, Porto Alegre, 134p.

Teixeira, G. and Gonzales, M.A. (1988) Minas do Camaquã, município de Caçapava do Sul, RS. In: Schobbenhaus, C. and Silva Coelho, C.E. (Eds.) Principais Depósitos Minerais do Brasil, DNPM/CVRD, Rio de Janeiro, v. 3, pp. 33-41.

Veigel, R. (1992) Diagênese de rochas siliciclásticas: o exemplo do Membro Vargas, Eopaleozóico da Bacia do Camaquã-RS. Acta Geológica Leopoldensia, v. 35, pp. 27-154.

Veigel, R. and Dardenne, M.A. (1990) Paragênese e sucessão mineral nas diferentes etapas de evolução da mineralização Cu-Pb-Zn do Distrito Camaquã-RS. Revista Brasileira de Geociências, 20(1-4), pp. 55-67.

Figure Captions

Fig. 1 Schematic map showing the geotectonic segments of the Sul-Riograndense Shield (after Jost & Hartmann, 1984; Soliani Jr, 1986; Fragoso Cesar et al., 1986; Babinski et al.,1996).

Fig. 2 Geologic map of the São Gabriel Block showing the distribution of base-metal deposits and prospects (modified from Santos et al., 1989).

Fig. 3 Stratigraphic column for the Camaquã Basin which hosts the principal base-metal deposits of Rio Grande do Sul State (modified from Ribeiro et al. 1966, Paim et al, 1995; Gresse et al, 1996).

Fig. 4 Geologic map of the Camaquã-Santa Maria ore district showing the location of the Camaquã Mines (Uruguay and São Luiz Sectors) and Santa Maria deposits, including A1 and A2 (Areas 1 and 2 prospects of Pb, Zn, Cu) (modified from Ribeiro & Carraro, 1971; Badi & Gonzalez, 1988).

Fig. 5 Stratigraphic column of host rocks of the Camaquã-Santa Maria ore district (modified from Faccini et al., 1987).

Fig. 6 SEM images of sectioned zircons from the granodiorite and perthite granite facies of the Lavras Granite. On the left are the BSE (backscattered electron) images, whereas CL (cathodoluminescence) images of the same grain are shown on the right. Circles and marks indicate areas of analyses; scale bar is 10 μm. Zircons from images A-B; C-D; E-F (grains 617A.2, 616A.5 and 617A.1) are from the granodiorite central facies; zircons from images G-H and I-J (grains 616B.7 and

616B.12) are from the perthite-granite border facies. The $^{206}Pb/^{238}U$ ages of cores and rims of both zircon populations are analytically indistinguishable.

Fig. 7 Concordia diagram of zircon populations from the granodiorite central facies of the Lavras Granite pluton (sample LN4Z; SHRIMP mounts n° 9616A and 9617A; errors boxes = 1 sigma). The main zircon group (unfilled pattern) defines the magmatic age of the central facies of the pluton. The younger zircon population refers to zircons that have lost Pb due to modern weathering (stippled pattern).

Fig. 8 Concordia diagram of zircon populations from the perthite-granite border facies of the Lavras Granite pluton (sample LP4Z; SHRIMP mounts n° 9616B and 9617B; errors boxes = 1 sigma). The main zircon group (unfilled pattern) defines the magmatic age of the marginal facies of the pluton. The younger zircon population refer to zircons that have lost Pb due to modern weathering (stippled pattern).

Fig. 9 Generalised longitudinal section (P - P') of the Camaquã and Santa Maria deposits showing the distribution and structural control of mineralization. Area 3 is the site of the principal Pb-Zn mineralisation of the Santa Maria deposit (modified from Dorneles ,1996).

Fig.10 Schematic profile of the Uruguay and São Luiz Sectors of the Camaquã Cu (Au-Ag) deposits. The conical shape of mineralization is controlled by the NW-trending fracture system. Chlorite and sericite alteration halos in the host rocks are also shown (modified from Teixeira & Gonzalez, 1988).

Fig. 11 Sulphur isotopic composition on sulphides and sulphates from (a) Camaquã and (b) Santa Maria Mines, including previous (Bettencourt, 1976 ; Beckel et al., 1991) and new data, and on pyrites from Cerro Rico (Hilario Formation) and Butiá (Lavras Granite) prospects.

Fig. 12 Common Pb-isotopic diagram for feldspars, whole-rocks and pyrite ores hosted by the Lavras Granite and Hilario Formation volcanic rocks. A 594 Ma reference isochron for the Lavras Granite and the growth curve of Stacey & Kramer (1975) are shown for reference.

Fig. 13 Common lead-isotope diagram showing the lead isotope ratios for the sulphides from the Camaquã and Santa Maria deposits and arenites from the Arroio dos Nobres Formation and the initial ratio (IR) of pyrite of magmatic ores (mean; from Fig. 12). The 594 Ma reference isochron for the Lavras Granite and the Stacey & Kramer (1975) growth curve are shown for reference.

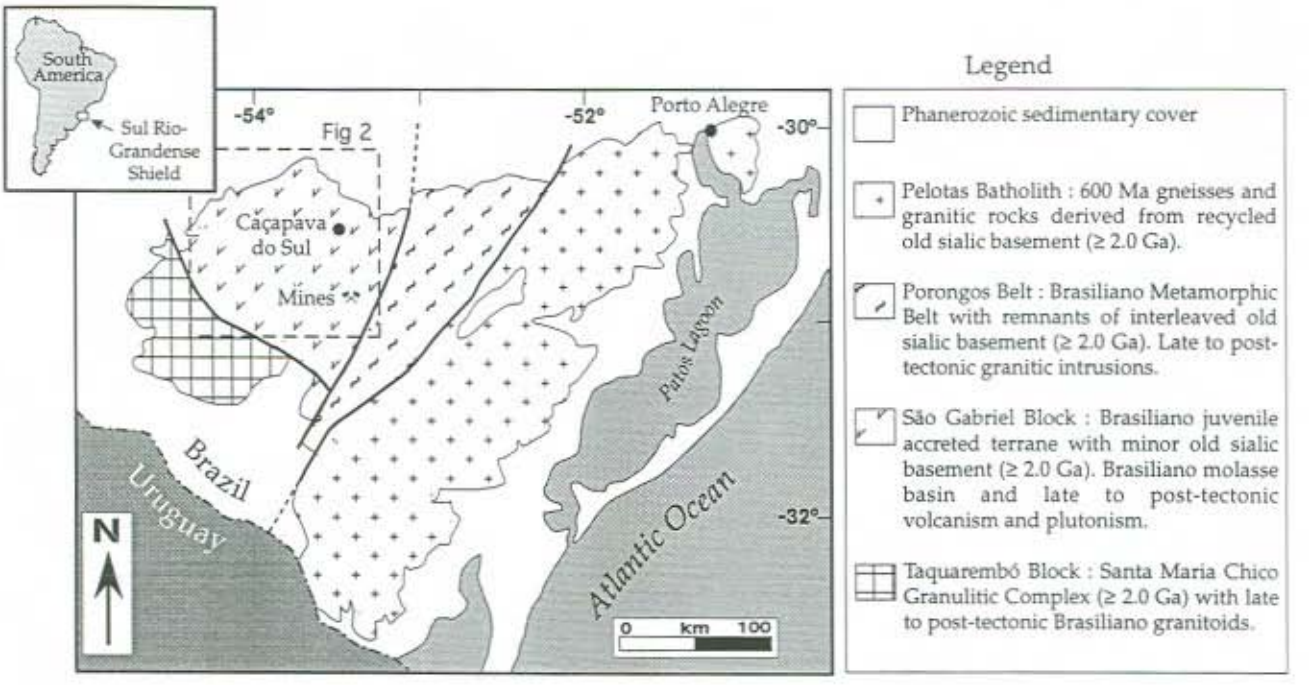
South America
Sul Rio-Grandense Shield
-54°
Fig 2
-52°
Porto Alegre
-30°
Caçapava do Sul
Minas
Patos Lagoon
Brazil
Uruguay
Atlantic Ocean
-32°
N
0 km 100
Legend
Phanerozoic sedimentary cover
Pelotas Batholith : 600 Ma gneisses and granitic rocks derived from recycled old sialic basement (≥ 2.0 Ga).
Porongos Belt : Brasiliano Metamorphic Belt with remnants of interleaved old sialic basement (≥ 2.0 Ga). Late to post-tectonic granitic intrusions.
São Gabriel Block : Brasiliano juvenile accreted terrane with minor old sialic basement (≥ 2.0 Ga). Brasiliano molasse basin and late to post-tectonic volcanism and plutonism.
Taquarembó Block : Santa Maria Chico Granulitic Complex (≥ 2.0 Ga) with late to post-tectonic Brasiliano granitoids.

Figura 1

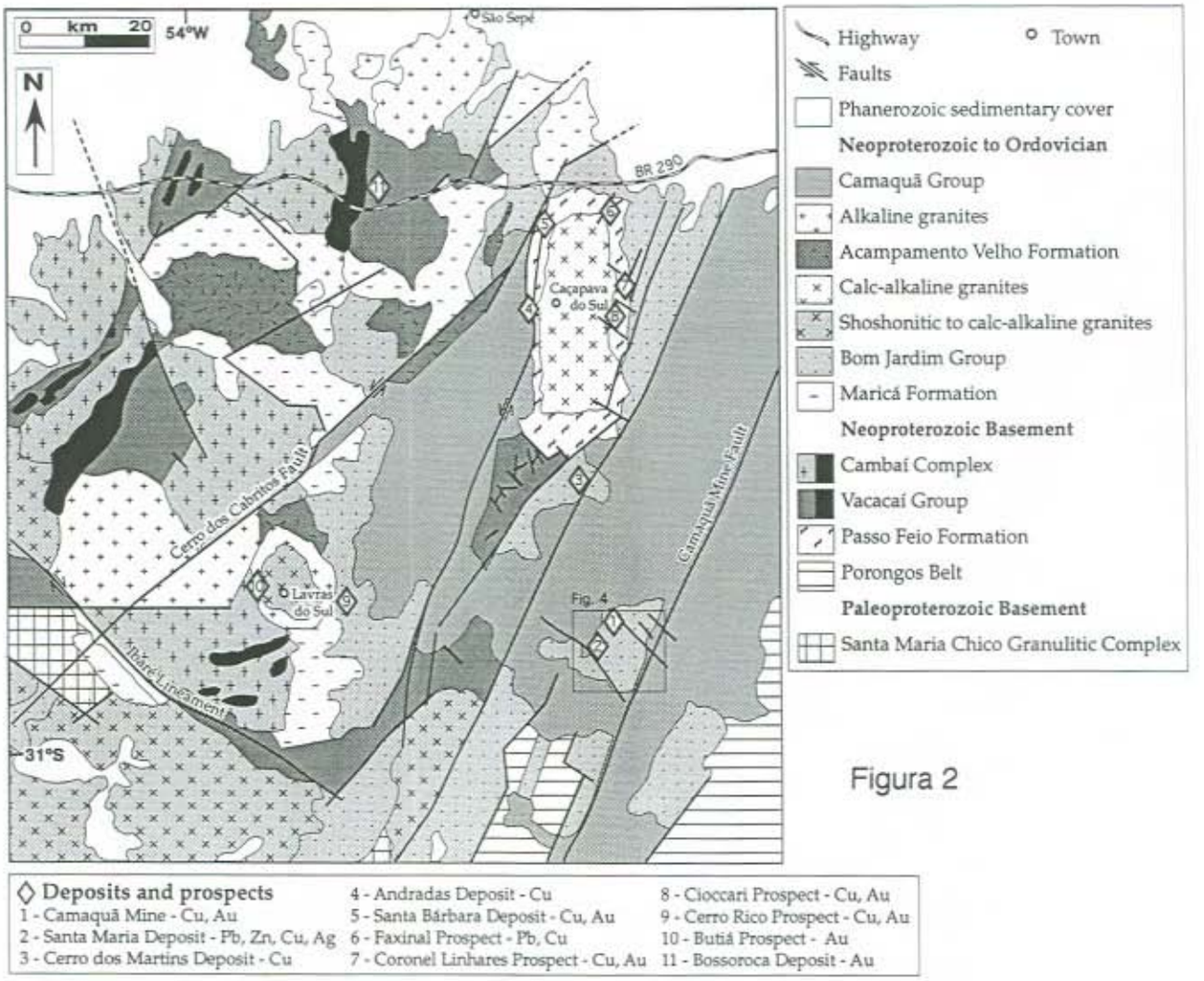

Figura 2

◇ **Deposits and prospects**

1 - Camaquã Mine - Cu, Au
2 - Santa Maria Deposit - Pb, Zn, Cu, Ag
3 - Cerro dos Martins Deposit - Cu
4 - Andradas Deposit - Cu
5 - Santa Bárbara Deposit - Cu, Au
6 - Faxinal Prospect - Pb, Cu
7 - Coronel Linhares Prospect - Cu, Au
8 - Cioccari Prospect - Cu, Au
9 - Cerro Rico Prospect - Cu, Au
10 - Butiá Prospect - Au
11 - Bossoroca Deposit - Au

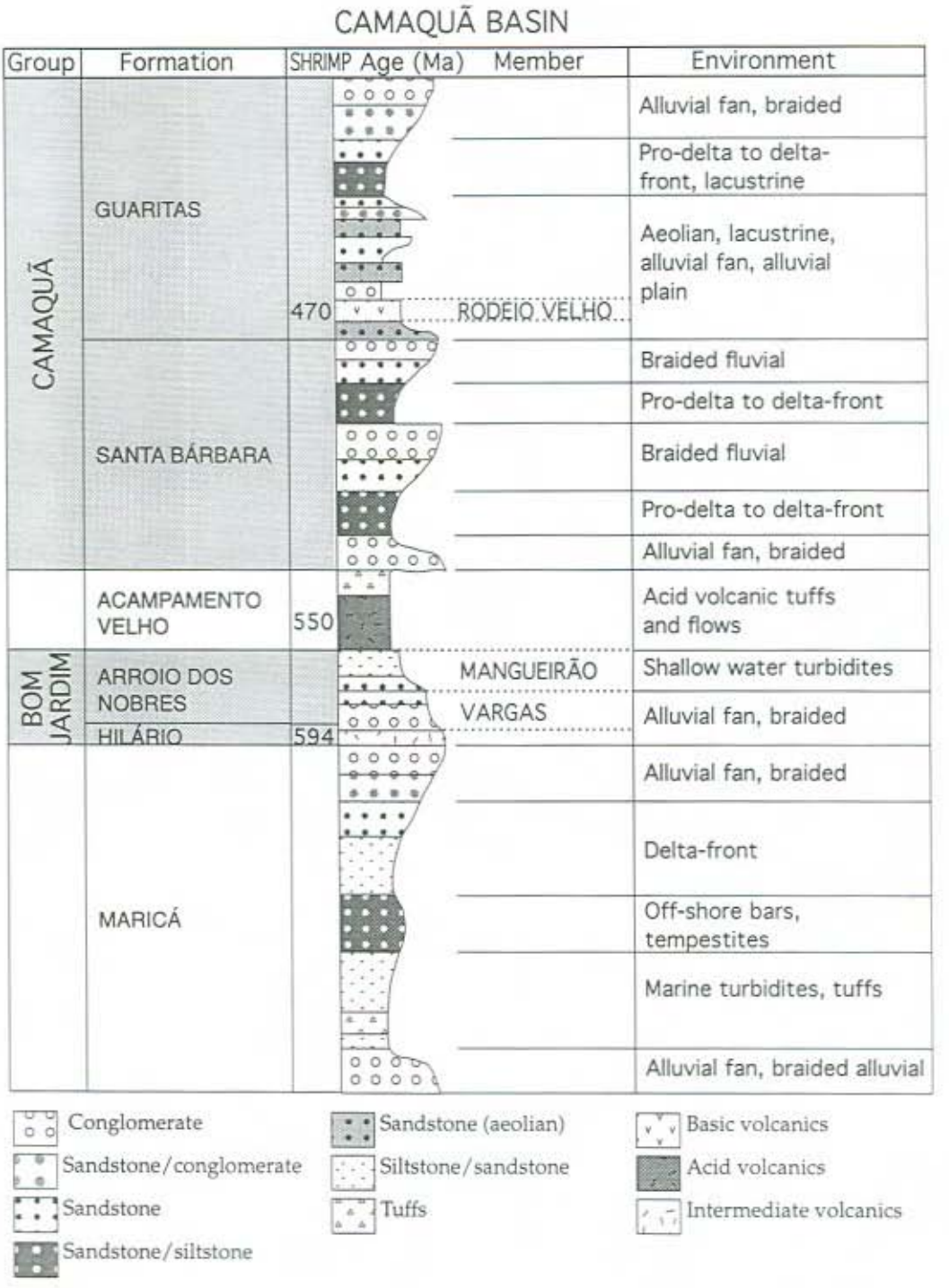
CAMAQUÃ BASIN
Group
Formation
SHRIMP Age (Ma)
Member
Environment
CAMAQUÃ
GUARITAS
SANTA BÁRBARA
ACAMPAMENTO VELHO
BOM JARDIM
ARROIO DOS NOBRES
HILÁRIO
MARICÁ
470
550
594
RODEIO VELHO
MANGUEIRÃO
VARGAS
Alluvial fan, braided
Pro-delta to delta-front, lacustrine
Aeolian, lacustrine, alluvial fan, alluvial plain
Braided fluvial
Pro-delta to delta-front
Braided fluvial
Pro-delta to delta-front
Alluvial fan, braided
Acid volcanic tuffs and flows
Shallow water turbidites
Alluvial fan, braided
Alluvial fan, braided
Delta-front
Off-shore bars, tempestites
Marine turbidites, tuffs
Alluvial fan, braided alluvial
Conglomerate
Sandstone/conglomerate
Sandstone
Sandstone/siltstone
Sandstone (aeolian)
Siltstone/sandstone
Tuffs
Basic volcanics
Acid volcanics
Intermediate volcanics

Figura 3

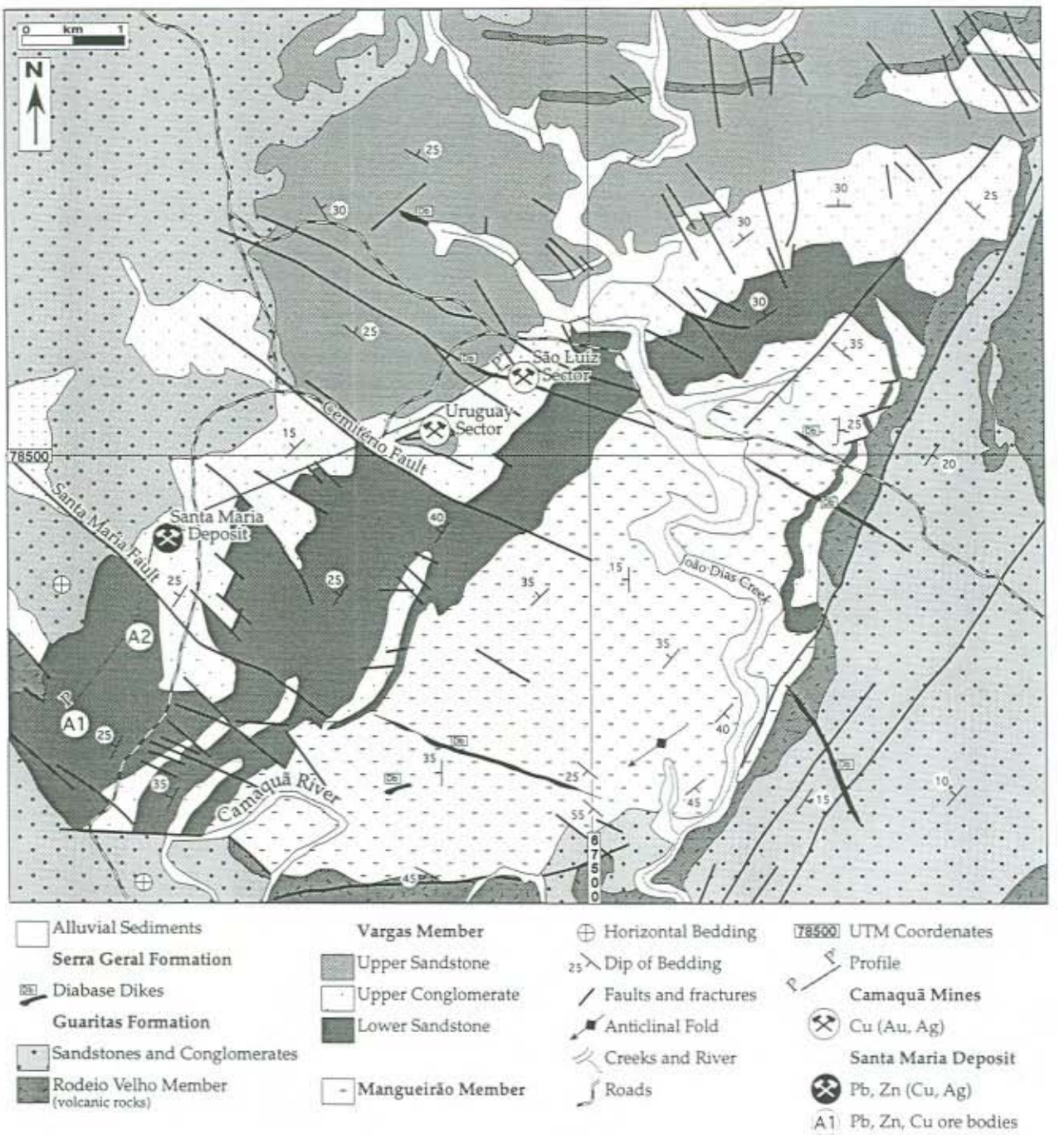
0 km 1
N
São Luiz Sector
Uruguay Sector
Cemitério Fault
Santa Maria Deposit
Santa Maria Fault
João Dias Creek
Camaquã River
A1
A2
78500
8750000
Alluvial Sediments
Serra Geral Formation
Diabase Dikes
Guaritas Formation
Sandstones and Conglomerates
Rodeio Velho Member
(volcanic rocks)
Vargas Member
Upper Sandstone
Upper Conglomerate
Lower Sandstone
Mangueirão Member
Horizontal Bedding
Dip of Bedding
Faults and fractures
Anticlinal Fold
Creeks and River
Roads
UTM Coordenates
Profile
Camaquã Mines
Cu (Au, Ag)
Santa Maria Deposit
Pb, Zn (Cu, Ag)
Pb, Zn, Cu ore bodies

Figura 4

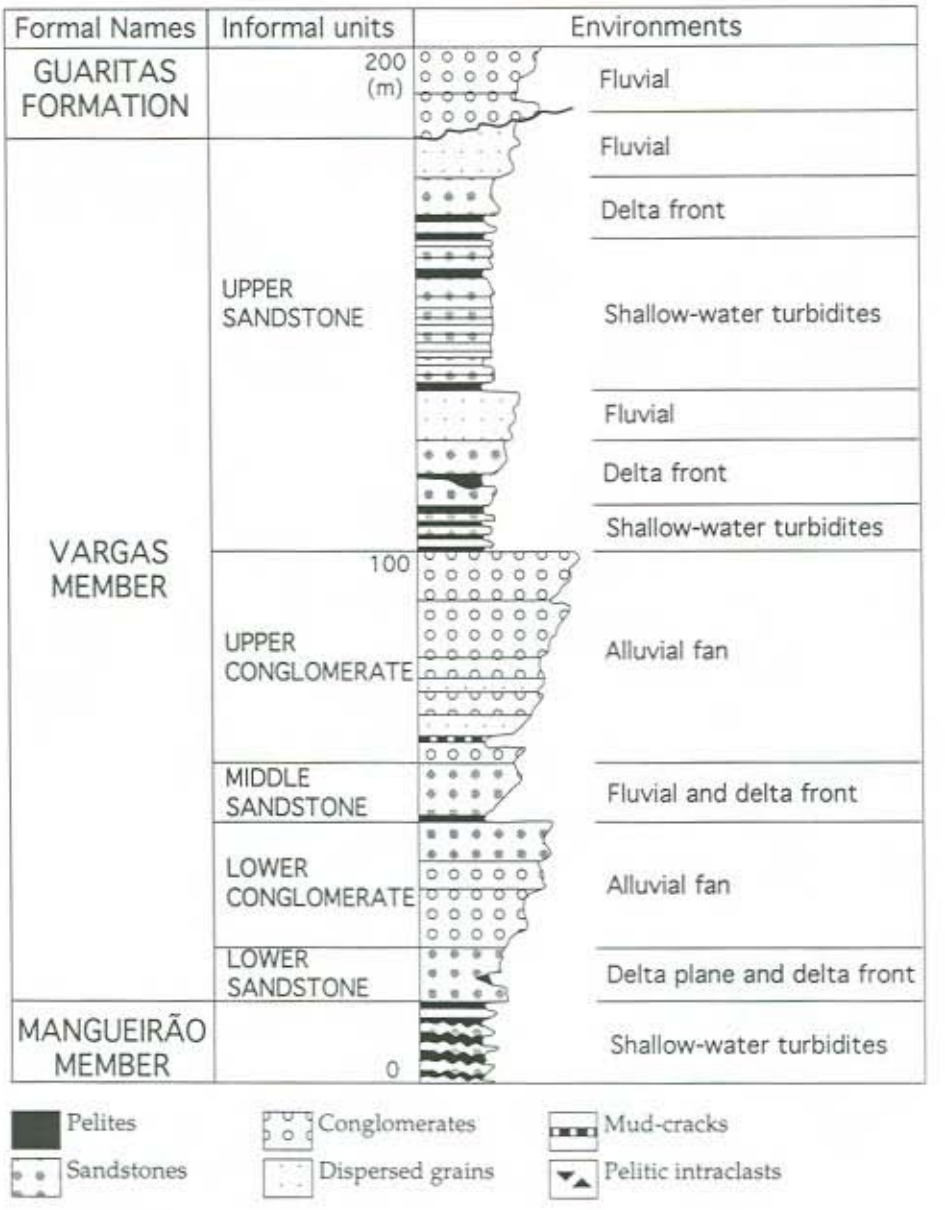
Formal Names
Informal units
Environments
GUARITAS FORMATION
200 (m)
Fluvial
VARGAS MEMBER
UPPER SANDSTONE
Fluvial
Delta front
Shallow-water turbidites
Fluvial
Delta front
Shallow-water turbidites
100
UPPER CONGLOMERATE
Alluvial fan
MIDDLE SANDSTONE
Fluvial and delta front
LOWER CONGLOMERATE
Alluvial fan
LOWER SANDSTONE
Delta plane and delta front
MANGUEIRÃO MEMBER
0
Shallow-water turbidites
Pelites
Conglomerates
Mud-cracks
Sandstones
Dispersed grains
Pelitic intraclasts

Figura 5

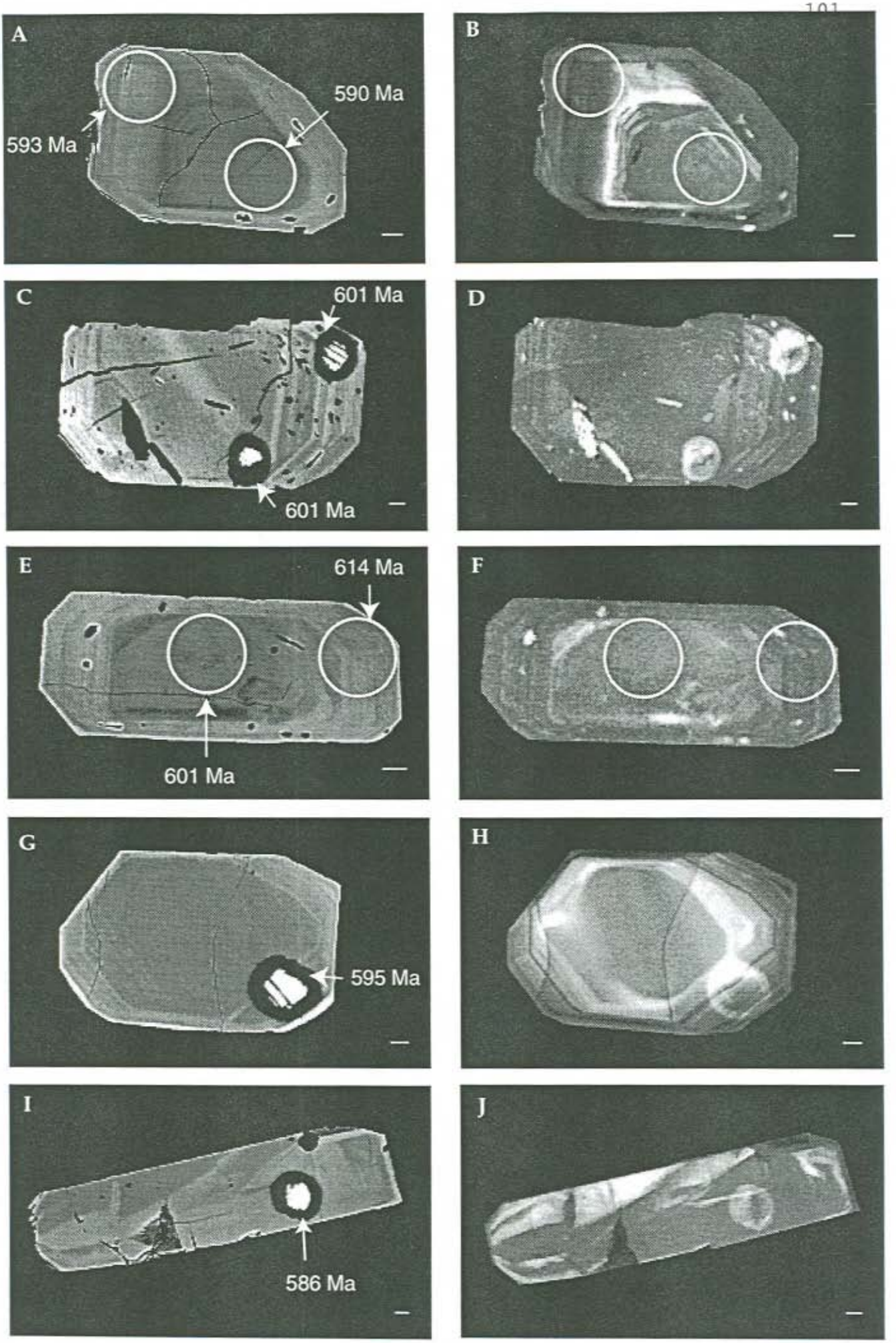
A
590 Ma
593 Ma
B
C
601 Ma
601 Ma
D
E
614 Ma
601 Ma
F
G
595 Ma
H
I
586 Ma
J

Figura 6

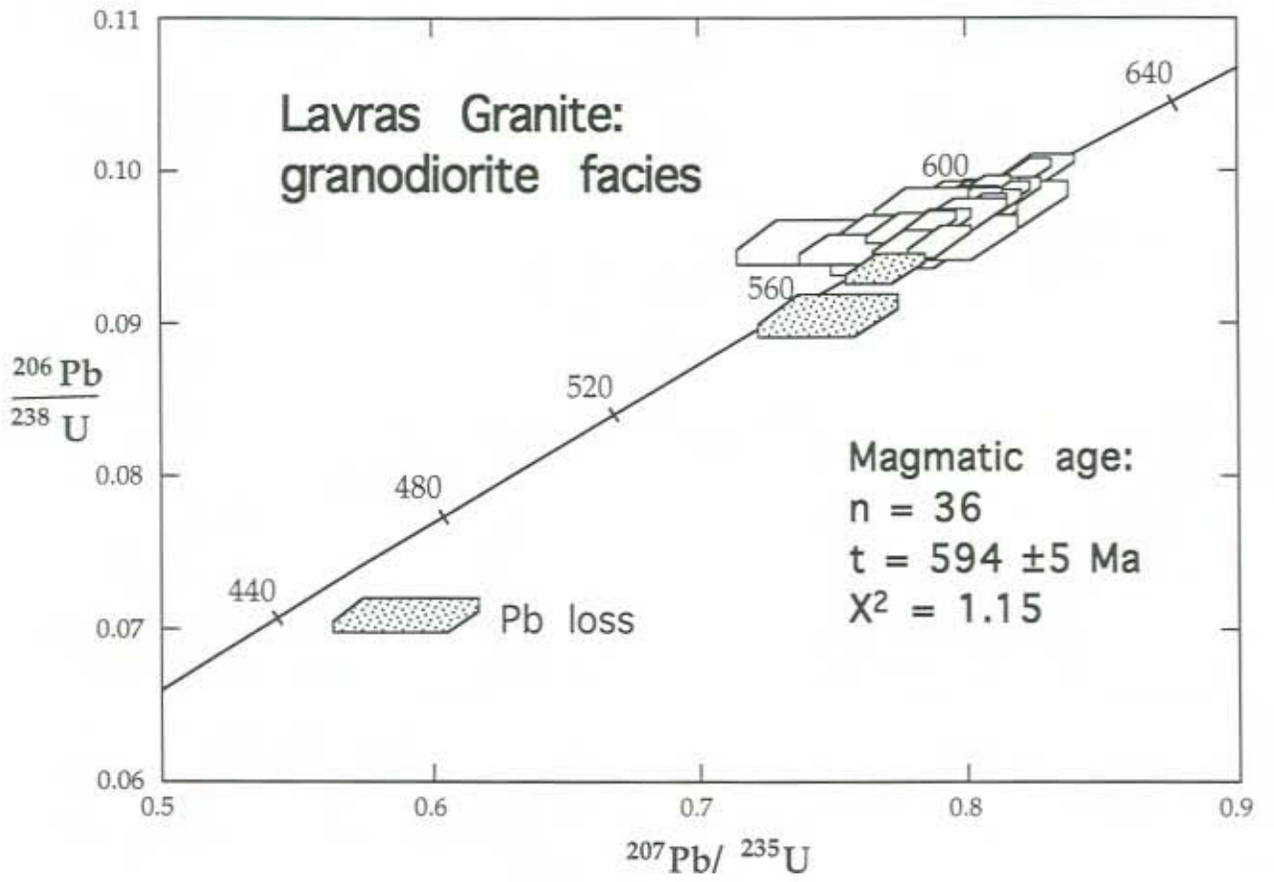
Lavras Granite:
granodiorite facies
Magmatic age:
n = 36
t = 594 ±5 Ma
X² = 1.15
Pb loss
640
600
560
520
480
440
0.11
0.10
0.09
0.08
0.07
0.06
0.5
0.6
0.7
0.8
0.9
206 Pb / 238 U
207 Pb/ 235 U

Figura 7

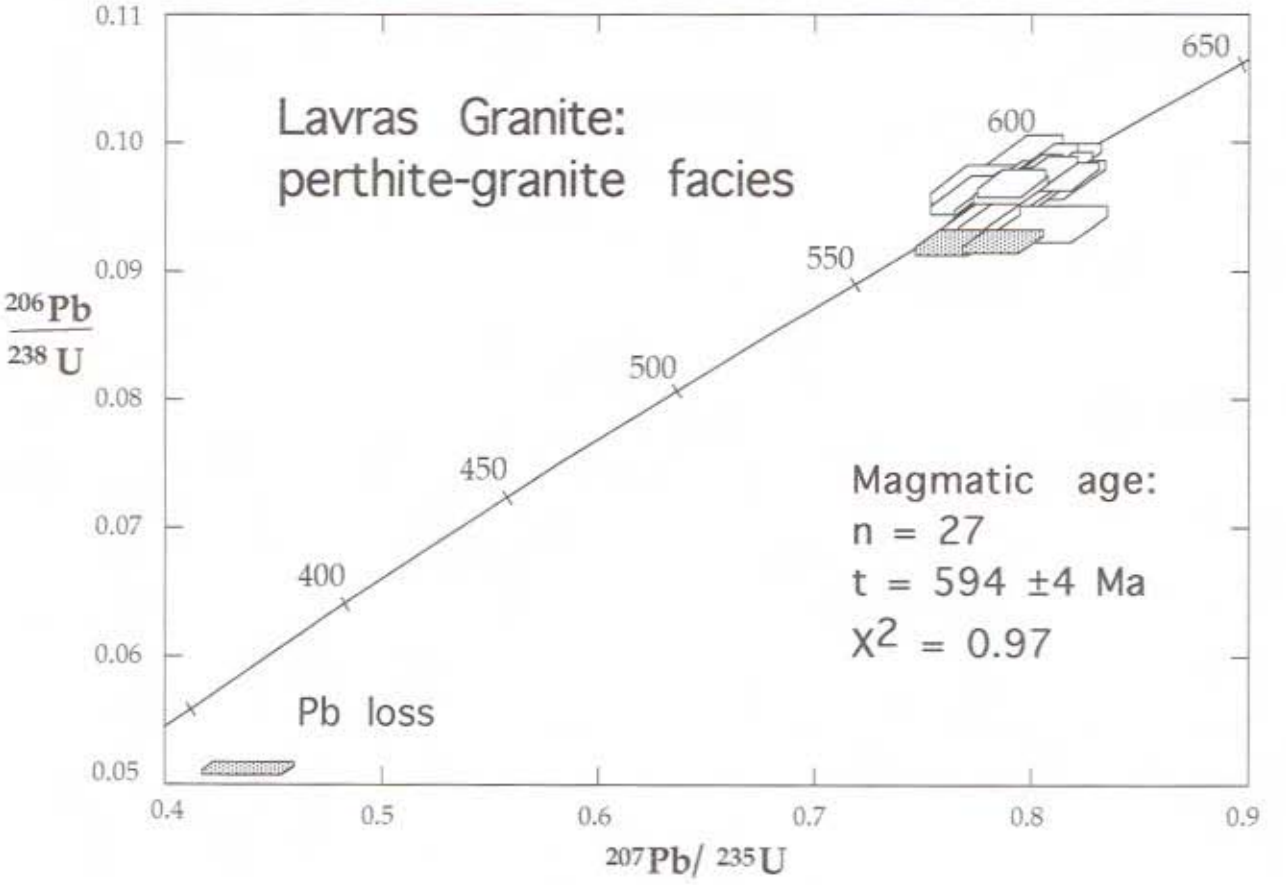
Lavras Granite:
perthite-granite facies
Magmatic age:
n = 27
t = 594 ±4 Ma
X2 = 0.97
Pb loss
650
600
550
500
450
400
0.11
0.10
0.09
0.08
0.07
0.06
0.05
0.4
0.5
0.6
0.7
0.8
0.9
206Pb/238U
207Pb/235U

Figura 8

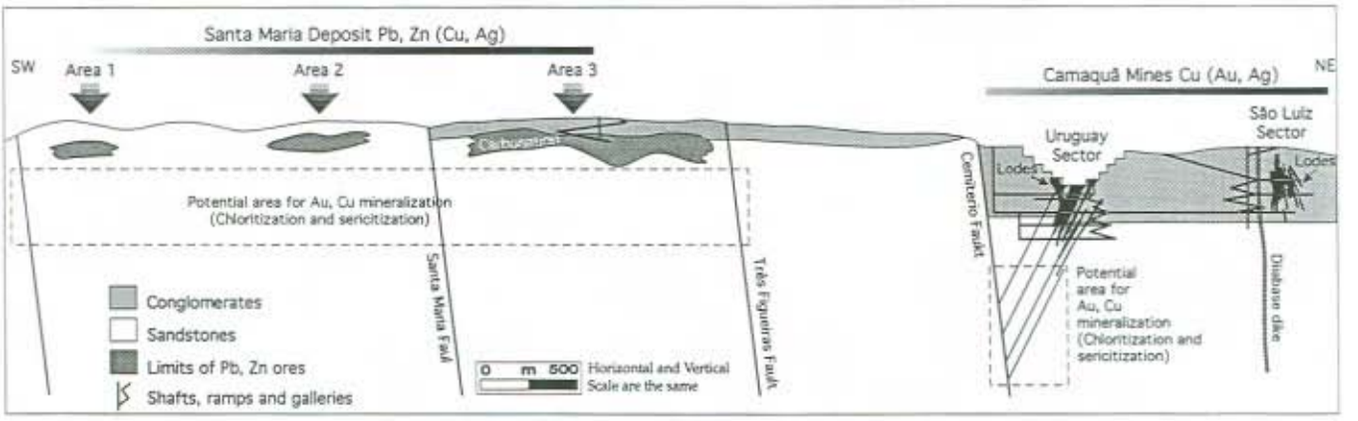
Santa Maria Deposit Pb, Zn (Cu, Ag)
SW
Area 1
Area 2
Area 3
Camaquã Mines Cu (Au, Ag)
NE
Uruguay Sector
São Luiz Sector
Lodes
Lodes
Cemiterio Fault
Potential area for Au, Cu mineralization (Chloritization and sericitization)
Santa Maria Fault
Três Figueiras Fault
Potential area for Au, Cu mineralization (Chloritization and sericitization)
Diabasio dike
Conglomerates
Sandstones
Limits of Pb, Zn ores
Shafts, ramps and galleries
0 m 500
Horizontal and Vertical Scale are the same

Figura 9

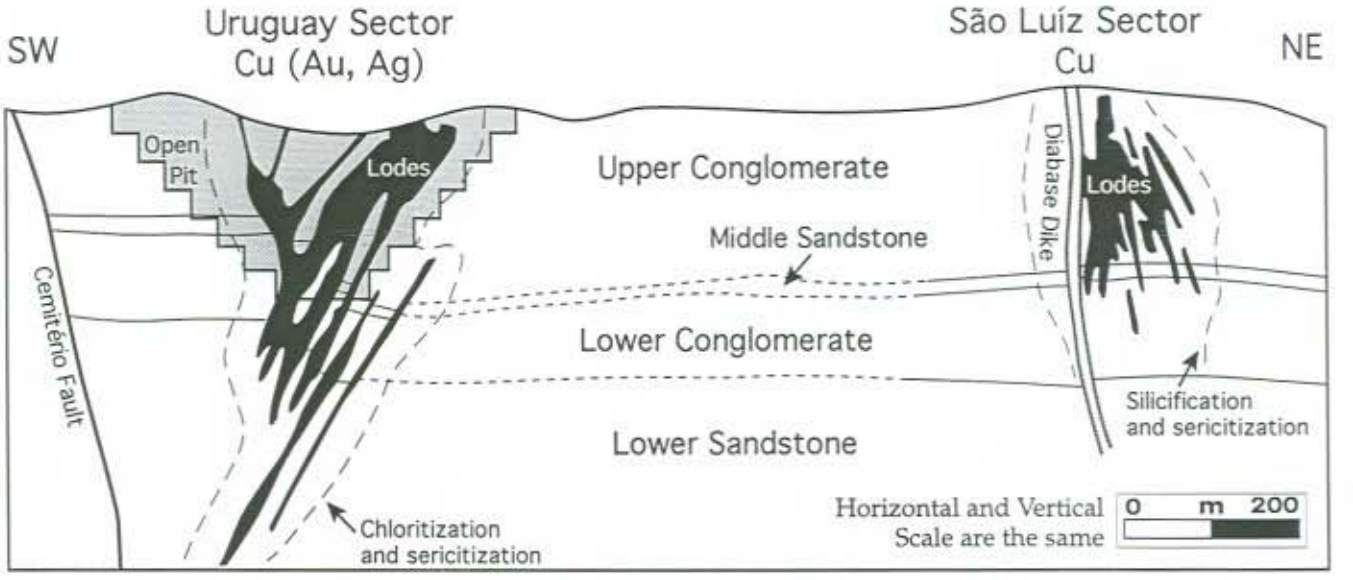
SW
Uruguay Sector
Cu (Au, Ag)
São Luíz Sector
Cu
NE
Open Pit
Lodes
Upper Conglomerate
Diabase Dike
Lodes
Middle Sandstone
Cemitério Fault
Lower Conglomerate
Silicification
and sericitization
Lower Sandstone
Chloritization
and sericitization
Horizontal and Vertical
Scale are the same
0 m 200

Figura 10

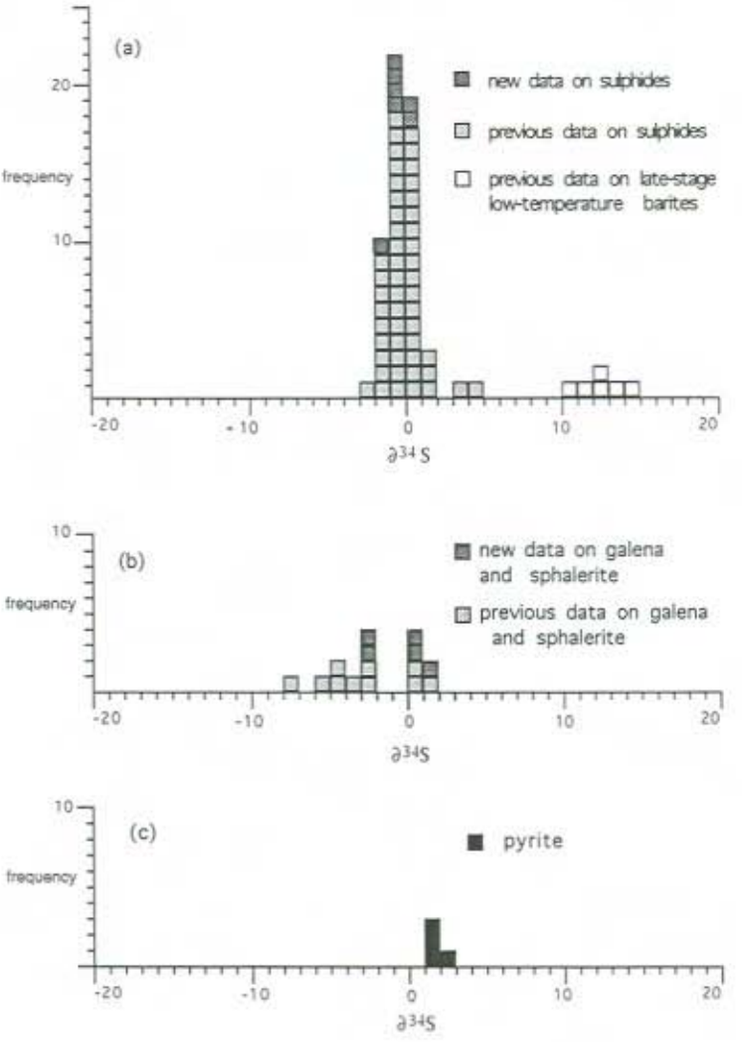
(a)
20
frequency
10
new data on sulphides
previous data on sulphides
previous data on late-stage low-temperature barites
-20
-10
0
10
20
∂34 S
10
(b)
frequency
new data on galena and sphalerite
previous data on galena and sphalerite
-20
-10
0
10
20
∂34S
10
(c)
frequency
pyrite
-20
-10
0
10
20
∂34S

Figura 11

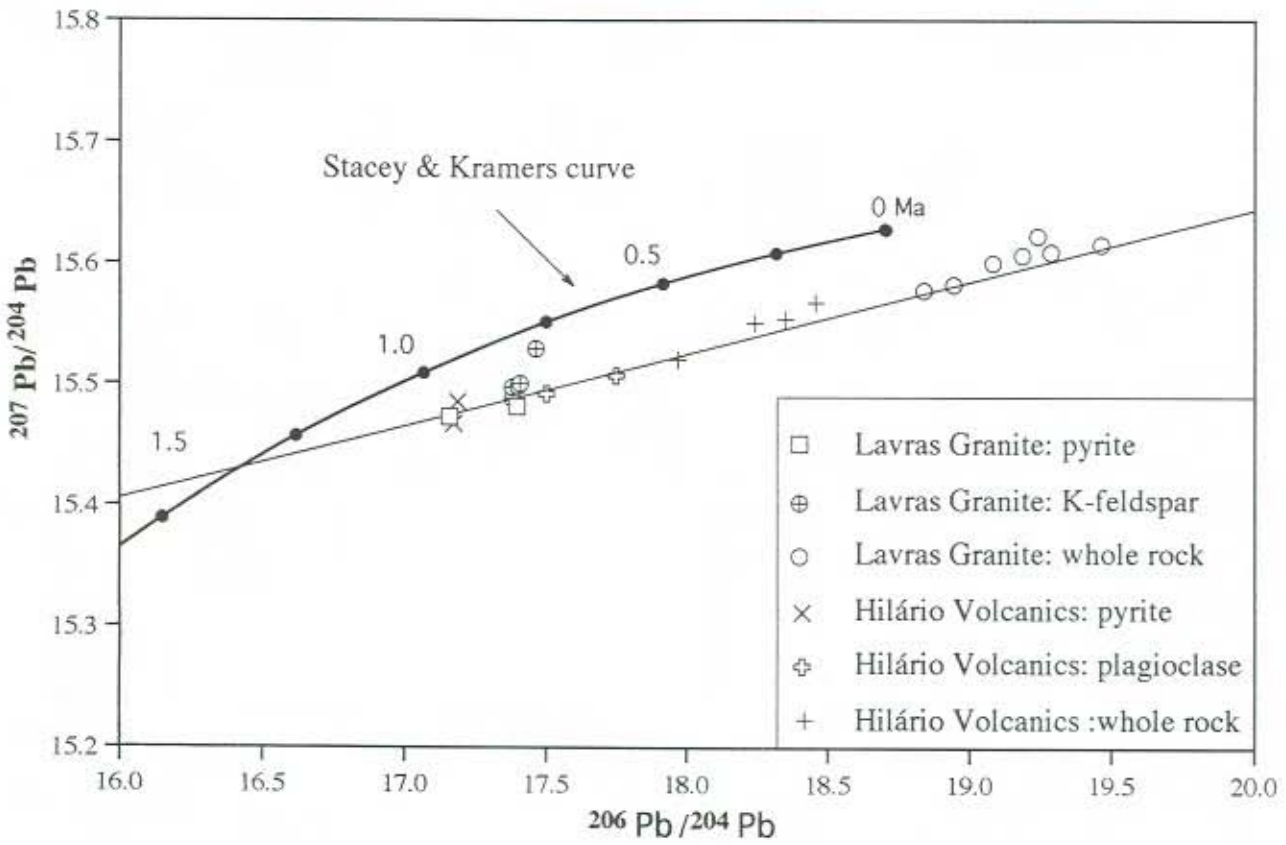
Stacey & Kramers curve
0 Ma
0.5
1.0
1.5
Lavras Granite: pyrite
Lavras Granite: K-feldspar
Lavras Granite: whole rock
Hilário Volcanics: pyrite
Hilário Volcanics: plagioclase
Hilário Volcanics :whole rock
207 Pb/204 Pb
206 Pb /204 Pb
15.8
15.7
15.6
15.5
15.4
15.3
15.2
16.0
16.5
17.0
17.5
18.0
18.5
19.0
19.5
20.0

Figura 12

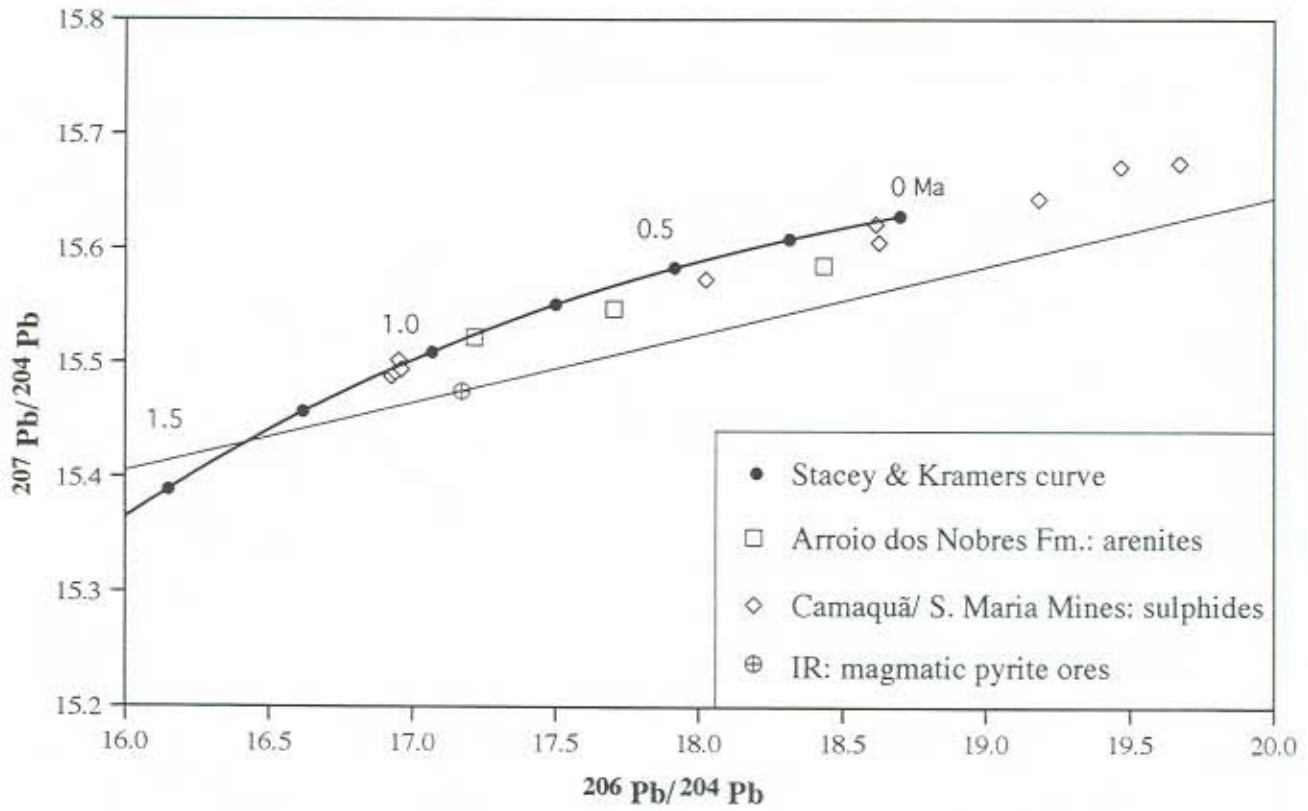
15.8
15.7
15.6
15.5
15.4
15.3
15.2
16.0
16.5
17.0
17.5
18.0
18.5
19.0
19.5
20.0
207 Pb/204 Pb
206 Pb/204 Pb
0 Ma
0.5
1.0
1.5
Stacey & Kramers curve
Arroio dos Nobres Fm.: arenites
Camaquã/ S. Maria Mines: sulphides
IR: magmatic pyrite ores

Figura 13

Table Captions

Table 1. SHRIMP U/Pb data on zircons from granodiorite central facies of Lavras Granite pluton (sample LN4Z; SHRIMP mounts n° 9616A and 9617A; errors = 1 sigma).

Table 2. SHRIMP U/Pb data on zircons from perthite-granite border facies of Lavras Granite pluton (sample LP4Z; SHRIMP mounts n° 9616B and 9617B, errors = 1 sigma).

Table 3. Sulfur and lead isotope compositions on sulphides from Camaquã-Santa Maria Deposits and Butiá and Cerro Rico Prospects. A total analytical error is ± 0.15% to each Pb-isotope ratio.

Table 4. Lead isotope compositions and SiO2 (wt %), U, Th and Pb (ppm) concentrations for Lavras Granite, Hilario Formation volcanics and Arroio dos Nobres Formation arenites whole-rocks and minerals. A total analytical error is ± 0.15% to each Pb-isotope ratio.

Tabela 1

grain-spot	U (ppm)	Th (ppm)	Th U	4f206 (%)	207* 206*	+/-	208* 206*	+/-	206* 238	+/-	207* 235	+/-	208* 232	+/-	conc (%)	207* 206* Age(Ma)	+/-	206* 238 Age (Ma)	+/-
Magmatic																			
617A.1-1	808	243	0.30	0.071	0.0601	7	0.0900	17	0.0999	11	0.8272	146	0.0299	7	101	606	27	614	7
616A.21-1	634	160	0.25	-0.004	0.0599	5	0.0790	9	0.0992	15	0.8190	147	0.0310	6	102	600	16	610	9
616A.12-1	623	141	0.23	-0.017	0.0594	5	0.0712	10	0.0981	15	0.8038	149	0.0309	7	104	582	19	604	9
616A.7-1	542	172	0.32	0.079	0.0592	7	0.0956	16	0.0979	15	0.7985	164	0.0296	7	105	573	26	602	9
616A.12-2	429	100	0.23	0.089	0.0597	7	0.0707	14	0.0979	15	0.8054	165	0.0298	8	102	591	25	602	9
616A.13-1	428	159	0.37	-0.037	0.0602	7	0.1141	17	0.0979	15	0.8130	168	0.0300	6	98	612	26	602	9
616A.5-1	839	315	0.38	0.041	0.0601	5	0.1150	13	0.0977	15	0.8100	152	0.0299	6	99	608	19	601	9
616A.5-2	785	224	0.28	0.117	0.0598	6	0.0864	14	0.0977	15	0.8050	160	0.0296	7	101	595	24	601	9
616A.6-2	439	77	0.18	-0.089	0.0605	15	0.0557	33	0.0977	15	0.8147	248	0.0309	19	97	622	53	601	9
616A.11-1	471	159	0.34	0.127	0.0586	7	0.1015	15	0.0977	15	0.7900	159	0.0294	6	109	553	25	601	9
616A.19-1	542	137	0.25	0.039	0.0592	5	0.0722	11	0.0977	15	0.7970	151	0.0278	6	105	573	20	601	9
617A.1-2	527	223	0.42	0.248	0.0583	11	0.1232	25	0.0977	11	0.7849	177	0.0285	7	111	540	40	601	6
616A.9-1	660	190	0.29	0.045	0.0594	6	0.0886	14	0.0974	15	0.7977	158	0.0300	7	103	582	23	599	9
616A.14-1	525	180	0.34	0.021	0.0596	6	0.1046	13	0.0973	15	0.7997	153	0.0297	6	101	590	21	598	9
616A.18-1	496	140	0.28	-0.016	0.0601	8	0.0852	17	0.0972	15	0.8056	171	0.0294	8	98	608	28	598	9
616A.20-1	639	201	0.31	0.099	0.0585	7	0.0944	16	0.0970	15	0.7828	161	0.0291	7	108	550	26	597	9
617A.4-2	557	217	0.39	0.039	0.0599	9	0.1150	22	0.0970	10	0.8010	159	0.0286	6	100	599	34	597	6
616A.4-1	674	204	0.30	0.025	0.0601	5	0.0924	10	0.0968	15	0.8026	146	0.0296	6	98	608	17	596	9
616A.8-1	359	74	0.21	0.081	0.0600	12	0.0646	27	0.0966	15	0.7988	218	0.0303	14	99	602	45	595	9
616A.15-1	436	158	0.36	0.095	0.0594	8	0.1061	18	0.0964	15	0.7891	172	0.0282	7	102	580	30	593	9
617A.2-1	799	231	0.29	0.065	0.0595	7	0.0867	16	0.0963	10	0.7899	136	0.0289	6	101	585	27	593	6
617A.4-1	887	275	0.31	0.041	0.0593	5	0.0930	12	0.0962	10	0.7868	116	0.0289	5	102	579	20	592	6
617A.5-1	636	273	0.43	0.029	0.0587	7	0.1309	16	0.0961	10	0.7774	128	0.0293	5	107	555	25	592	6
617A.2-2	417	174	0.42	0.463	0.0585	13	0.1150	31	0.0959	10	0.7738	205	0.0264	8	107	550	50	590	6
616A.2-1	538	189	0.35	0.262	0.0593	9	0.0886	19	0.0956	15	0.7822	176	0.0241	7	102	579	32	589	9
616A.16-1	508	153	0.30	0.058	0.0601	7	0.0947	16	0.0957	15	0.7927	163	0.0301	7	97	606	26	589	9
616A.16-2	604	234	0.39	1.851	0.0604	16	0.1197	38	0.0954	15	0.7951	260	0.0295	10	95	619	58	588	9
616A.1-1	492	173	0.35	0.177	0.0586	11	0.1075	24	0.0952	15	0.7693	193	0.0290	8	106	553	39	586	9
616A.3-1	188	75	0.40	0.627	0.0572	25	0.0676	56	0.0952	15	0.7512	357	0.0162	14	117	500	95	586	9
617A.3-1	682	203	0.30	0.009	0.0603	6	0.0902	12	0.0952	10	0.7917	118	0.0289	5	96	614	20	586	6
617A.8-2	665	217	0.33	0.131	0.0596	8	0.0955	18	0.0950	10	0.7810	144	0.0278	6	99	589	30	585	6
616A.6-1	875	322	0.37	-0.006	0.0601	4	0.1141	10	0.0947	15	0.7846	139	0.0293	5	96	607	16	583	9
617A.7-1	217	143	0.66	0.070	0.0582	14	0.2058	39	0.0947	10	0.7608	215	0.0295	7	108	539	54	583	6
616A.2-2	445	160	0.36	0.151	0.0589	8	0.1078	19	0.0945	15	0.7681	171	0.0284	7	103	564	31	582	9
616A.17-1	899	291	0.32	-0.002	0.0598	4	0.0996	8	0.0944	14	0.7785	134	0.0291	5	98	596	13	582	9
617A.6-1	633	257	0.41	-0.072	0.0605	8	0.1243	19	0.0944	10	0.7881	140	0.0289	5	93	623	28	582	6
Recent Pb-loss																			
617A.8-1	462	148	0.32	0.022	0.0598	9	0.0939	19	0.0935	10	0.7714	147	0.0274	6	96	597	31	576	6
616A.10-1	573	349	0.61	1.878	0.0602	18	0.1260	42	0.0904	14	0.7497	263	0.0187	7	92	609	64	558	8
616A.7-2	372	160	0.43	1.691	0.0605	25	0.0838	58	0.0708	11	0.5906	273	0.0138	10	71	622	90	441	7

CZ3 = 9616A, 13/05/96 (±1.53% 1 sigma, n=16); 9617A, 12/08/96 (±1.10% 1 sigma, n=16) and 31/10/96 (± 1.06% 1 sigma, n= 8)

4f206 = Proportion of Pb-206 calculated to be common Pb; %conc. = Concordance, as 100[206*/238]/t[207*/206*]

Tabela 2

grain-spot	U (ppm)	Th (ppm)	Th U	4f206 (%)	207* 206*	+/-	208* 206*	+/-	206* 238	+/-	207* 235	+/-	208* 232	+/-	%conc	207* 206* Age (Ma)	+/-	206* 238 Age (Ma)	+/-
Magmatic																			
616B.2-1	476	157	0.33	0.104	0.0584	8	0.0998	18	0.0990	15	0.7972	174	0.0300	7	112	545	30	608	9
616B.6-1	496	147	0.30	0.040	0.0602	7	0.0918	15	0.0983	15	0.8161	164	0.0305	7	99	611	24	605	9
616B.6-2	647	277	0.43	0.079	0.0595	6	0.1320	14	0.0983	15	0.8058	154	0.0303	6	103	585	21	604	9
617B.4-1	563	235	0.42	0.072	0.0599	7	0.1285	16	0.0978	10	0.8083	133	0.0301	5	100	601	24	602	6
616B.4-1	799	254	0.32	0.028	0.0604	5	0.0965	11	0.0977	15	0.8137	149	0.0296	6	97	618	18	601	9
616B.5-1	557	170	0.30	0.011	0.0595	6	0.0934	12	0.0975	15	0.8000	151	0.0299	6	103	585	20	600	9
617B.2-1	827	252	0.31	0.035	0.0599	6	0.0924	13	0.0974	11	0.8043	127	0.0295	5	100	601	21	599	6
617B.3-1	555	179	0.32	-0.114	0.0607	10	0.0999	22	0.0973	11	0.8150	168	0.0301	8	95	630	35	599	6
616B.8-1	545	174	0.32	0.055	0.0595	6	0.0990	13	0.0972	15	0.7968	155	0.0302	6	102	585	22	598	9
616B.9-1	479	154	0.32	0.106	0.0594	8	0.0953	18	0.0971	15	0.7949	173	0.0288	7	103	581	29	597	9
616B.19-1	417	131	0.31	-0.043	0.0611	8	0.0980	18	0.0970	15	0.8171	174	0.0303	7	93	642	28	597	9
617B.1-1	438	141	0.32	0.002	0.0601	5	0.0956	11	0.0970	11	0.8032	120	0.0288	5	98	606	19	597	6
616B.7-1	167	61	0.37	0.236	0.0582	12	0.1092	29	0.0966	15	0.7755	217	0.0289	9	111	538	47	595	9
617B.5-1	626	211	0.34	0.018	0.0593	9	0.1002	21	0.0968	10	0.7913	157	0.0288	7	103	579	34	595	6
616B.3-1	440	131	0.30	-0.002	0.0596	5	0.0916	11	0.0966	15	0.7942	149	0.0296	6	101	590	19	594	9
616B.10-1	485	141	0.29	0.039	0.0598	15	0.0896	35	0.0962	15	0.7937	251	0.0297	13	99	598	56	592	9
617B.7-2	349	121	0.35	0.080	0.0596	10	0.1026	23	0.0962	10	0.7908	168	0.0284	7	101	589	37	592	6
616B.13-1	467	123	0.26	0.199	0.0584	8	0.0774	17	0.0958	15	0.7707	166	0.0282	8	109	543	29	590	9
616B.14-1	592	179	0.30	-0.004	0.0606	5	0.0945	10	0.0956	15	0.7987	143	0.0299	6	94	626	16	588	9
616B.20-1	516	147	0.28	0.111	0.0596	10	0.0863	22	0.0954	15	0.7839	187	0.0290	9	100	588	36	588	9
616B.11-2	581	184	0.32	0.013	0.0595	7	0.0996	15	0.0952	15	0.7811	156	0.0299	6	100	587	24	586	9
616B.12-1	611	274	0.45	0.027	0.0598	6	0.1388	15	0.0952	15	0.7850	154	0.0295	6	98	596	23	586	9
616B.18-1	465	142	0.30	-0.013	0.0596	7	0.0913	14	0.0950	15	0.7809	156	0.0285	6	99	589	24	585	9
616B.16-1	750	219	0.29	0.056	0.0595	6	0.0879	12	0.0946	15	0.7764	148	0.0285	6	99	586	21	583	9
616B.11-1	538	190	0.35	0.003	0.0601	5	0.1104	11	0.0942	14	0.7809	142	0.0294	6	96	607	17	581	9
616B.17-1	499	142	0.29	-0.058	0.0601	10	0.0904	23	0.0937	14	0.7761	188	0.0297	9	95	605	37	578	8
616B.21-1	155	79	0.51	-0.338	0.0624	20	0.1674	49	0.0936	15	0.8056	298	0.0306	10	84	689	68	577	9
Recent Pb-loss																			
617B.6-1	775	367	0.47	0.917	0.0619	12	0.1500	29	0.0923	10	0.7874	187	0.0292	7	85	671	43	569	6
617B.1-2	607	248	0.41	0.308	0.0602	12	0.1251	28	0.0922	10	0.7649	181	0.0282	7	93	610	42	568	6
617B.7-1	809	167	0.21	3.679	0.0622	29	0.1077	66	0.0512	6	0.4387	214	0.0267	17	47	681	99	322	3

CZ3 = 9616B, 13/05/96 (±1.53% 1 sigma, n=16); 9617B, 12/08/96 (± 1.10% 1 sigma, n= 16) and 31/10/96 (± 1.06% 1 sigma, n= 8)

4f206 = Proportion of Pb-206 calculated to be common Pb; %conc. = Concordance, as 100t[206*/238]/t[207*/206*].

Tabela 3

Sample name	Mineral	Sample location	∂34S ‰ CDT	206Pb 204Pb	207Pb 204Pb	208Pb 204Pb
CB-199E.P20	Chalcopyrite I	Uruguay Sector	-0.1	19.468	15.671	40.320
CB-199E.P20	Pyrite	Uruguay Sector	0.6	19.185	15.643	39.476
CB.P-19	Pyrite	Uruguay Sector	0.0	18.626	15.605	38.933
CB.P-19	Chalcopyrite	Uruguay Sector	-0.1	18.616	15.621	39.064
CB-282A	Chalcopyrite	Uruguay Sector	-0.1	18.024	15.573	38.208
TV-211	Pyrite/Chalcopyrite II	Uruguay Sector	-1.0	19.672	15.674	39.438
TV-211-B	Bornite	Uruguay Sector	-1.8	-	-	-
MSMA-G	Galena	Santa Maria Deposit	-2.6	16.927	15.488	37.559
MSMC-G	Galena	Santa Maria Deposit	-2.1	16.950	15.502	37.625
MSB-B gn	Galena	Santa Maria Deposit	-	16.960	15.494	37.550
MSMC-Y	Sphalerite	Santa Maria Deposit	0.2	-	-	-
MSMC-S sph I	Sphalerite	Santa Maria Deposit	0.1	16.939	15.491	37.576
MSMA-S	Sphalerite	Santa Maria Deposit	1.1	-	-	-
CR-1	Pyrite	Cerro Rico Prospect	1.7	17.186	15.485	37.240
CR-2	Pyrite	Cerro Rico Prospect	1.8	17.173	15.467	37.188
BLB	Pyrite	Butiá Prospect	2.2	17.157	15.473	37.181
BLB-1	Pyrite	Butiá Prospect	1.7	17.396	15.481	37.312

Tabela 4

Samples	Unit	Material	SiO2 (%)	U (whole rock ppm)	Th	Pb	Pb206 Pb204	207Pb 204Pb	208Pb 204Pb
H2-pl	Hilario Formation	Plagioclase	-	-	-	-	17.748	15.507	37.564
HZ-pl	Hilario Formation	Plagioclase	-	-	-	-	17.501	15.492	37.380
H1-wr	Hilario Formation	Andesite	56.4	3.3	6.8	1.0	17.969	15.520	37.813
H2-wr	Hilario Formation	Andesite	56.4	4.0	9.0	1.0	18.456	15.567	38.238
H3-wr	Hilario Formation	Andesite	57.4	3.9	6.0	0.5	18.241	15.550	38.069
HZ-wr	Hilario Formation	Andesite	56.5	4.3	9.3	1.0	18.349	15.553	38.172
LN-1 kf	Lavras Granite	K-feldspar	-	-	-	-	17.400	15.498	37.304
LN4 kf	Lavras Granite	K-feldspar	-	-	-	-	17.380	15.497	37.297
LN4Z kf	Lavras Granite	K-feldspar	-	-	-	-	17.379	15.488	37.269
LT-1 kf	Lavras Granite	K-feldspar	-	-	-	-	17.408	15.500	37.323
LP-1 kf	Lavras Granite	K-feldspar	-	-	-	-	17.464	15.529	37.444
LN1 wr	Lavras Granite	Granodiorite	71.1	7.5	24	3.0	19.080	15.600	39.011
LN2 wr	Lavras Granite	Granodiorite	70.4	7.3	23	5.5	19.463	15.615	39.260
LN3 wr	Lavras Granite	Granodiorite	69.4	4.3	12	4.0	18.837	15.577	38.690
LN4 wr	Lavras Granite	Granodiorite	68.6	4.0	12	2.0	19.285	15.609	38.833
LN4Z wr	Lavras Granite	Granodiorite	68.7	3.4	12	2.0	18.943	15.582	38.674
LT1wr	Lavras Granite	Sienogranite	70.7	6.8	32	4.5	19.185	15.606	39.335
LP-1wr	Lavras Granite	Pertite granite	73.2	10	20	3.5	19.238	15.622	39.042
SMP-10	Arroio dos Nobres Formation	Arenite	64.1	1.7	8.0	1.0	17.215	15.522	37.841
SMP-15	Arroio dos Nobres Formation	Arenite	64.9	2.2	9.0	1.5	17.701	15.547	38.274
CM-7708	Arroio dos Nobres Formation	Arenite	67.0	3.3	4.8	1.5	18.433	15.585	39.122

CAPÍTULO IV

THE LINK BETWEEN HYDROTHERMAL EPIGENETIC COPPER MINERALIZATION AND THE CAÇAPAVA GRANITE OF THE BRASILIANO CYCLE IN SOUTHERN BRAZIL

Remus, M.V.D.[1]; Hartmann, L.A.[1]; McNaughton, N.J.[2]; Groves, D.I.[2]; Fletcher, I.R.[2]

[1]Centro de Estudos em Petrologia e Geoquímica, Instituto de Geociências, Universidade Federal do Rio Grande do Sul, Av. Bento Gonçalves, 9500; 91501-970, Porto Alegre, RS, Brazil

[2]Centre for Strategic Mineral Deposits, University of Western Australia, Nedlands 6907, WA, Australia.

Submetido ao Journal of South American Earth Sciences

Abstract

Base-metal deposits in the Caçapava do Sul Copper Province are hosted by both volcanosedimentary rocks of the Bom Jardim Group and by metamorphic rocks of the Passo Feio Formation, and show a spatial relationship to the Caçapava Granite. These associations have led to much controversy about the genesis of the base-metal deposits, which has been at least partly resolved by precise dating using SHRIMP (Sensitive High Resolution Ion Microprobe) U/Pb zircon studies combined with S, Pb and Sr isotope trace studies.

The Passo Feio Formation is Neoproterozoic in age and was derived from a complex continental source as shown by the presence of xenocryst zircons of Archaean, Paleoproterozoic and Neoproterozoic ages. It was metamorphosed at ca. 700 Ma. The syntectonic Caçapava Granite intruded the metamorphosed supracrustal rocks of the Passo Feio Formation at 562 Ma. It was derived from an old sialic basement

Lead-isotope data are consistent with a 562 Ma age for the base-metal sulphide deposits sited in the Passo Feio Formation. The least-radiogenic compositions lie between the field of the isotopic compositions of the Caçapava Granite and rocks of the Passo Feio Formation, suggesting that Pb in the sulphide deposits may have been derived from both sources. The Pb, like that in the Caçapava Granite and Passo Feio Formation was derived from a primitive crustal source. Sulphur isotope data from the base-metal sulphide deposits in the Passo Feio Formation are compatible with a mixed sedimentary and magmatic source.

The most logical model for ore genesis, based on the isotopic data and spatial relationships, is that magmatic metal-bearing fluids from Caçapava Granite leached metals from the Passo Feio Formation and that the deposited sulphides therefore show mixed isotopic signatures. However, there is also some isotopic evidence from the Caçapava Granite itself, which suggests assimilation of S-bearing rocks of the Passo Feio Formation during emplacement. Thus, isotopic signatures could have been inherited from assimilated metal sulphides at this stage, and deposition could have been entirely from Caçapava Granite—derived magmatic fluids.

Importantly, the inferred 562 Ma age for the deposits in the Passo Feio Formation is younger than the well-constrained age of 594 Ma for

the Camaquã/Santa Maria Deposits. Thus, the sulphides in the Passo Feio Formation cannot be the source of these deposits as previously suggested. Other isotopic data also argue against such a model.

Resumo

Os depósitos de metais-base da Província Cuprífera de Caçapava do Sul são hospedados por rochas vulcanosedimentares do Grupo Bom Jardim e por rochas metamórficas da Formação Passo Feio, estando espacialmente associados ao Granito Caçapava. Estas relações tem levantado muitas controvérsias a respeito da gênese dos depósitos de metais-base, as quais foram em parte resolvidas através de datações pelo método U/Pb via SHRIMP (Microsonda Iônica de Alta Resolução) em zircões, combinado com estudos de isótopos de S, Pb e Sr.

A Formação Passo Feio possui idade Neoproterozóica e foi derivada de uma fonte continental complexa, como evidenciado pela presença de xenocristais de zircão de idade Arqueana, Paleoproterozóica e Neoproterozóica. O metamorfismo desta unidade ocorreu há cerca de 700 Ma. O Granito Caçapava é sin-tectonico e intrudiu as rochas supracrustais metamorfisadas da Formação Passo Feio há cerca de 562 Ma. O granito foi derivado do embasamento siálico antigo.

Os dados isotópicos de Pb são consistentes com uma idade de 562 Ma para os depósitos de sulfetos de metais-base hospedados pela Formação Passo Feio. As composições menos radiogênicas localizam-se entre os campos da composição isotópica do Granito Caçapava e das rochas da Formação Passo Feio, sugerindo que o Pb nos depósitos de sulfeto pode ter sido derivado de ambas as fontes. A assinatura isotópica de Pb, encontrada no Granito Caçapava e na Formação Passo Feio, é tipica de uma fonte crustal primitiva. Os dados de isótopos de enxofre dos depósitos de sulfetos de metais-base são compatíveis com uma fonte mista, magmática-sedimentar.

O modelo mais lógico para a gênese do minério, baseado nos dados isotópicos e na associação espacial, é que os fluidos magmáticos portadores de metais do Granito Caçapava lixiviaram metais da Formação Passo Feio e em consequencia, os sulfetos depositados mostram assinatura isotópica mista. No entanto, existem também algumas evidências isotópicas que sugerem assimilação de rochas portadoras de S da Formação Passo Feio durante a intrusão do Granito

Caçapava. Em consequencia, as assinaturas isotópicas podem ter sido herdadas de sulfetos metálicos assimilados neste estágio, e a deposição ter ocorrido integralmente a partir dos fluidos magmáticos derivados do Granito Caçapava.

Significativamente, a idade inferida de 562 Ma para os depósitos na Formação Passo Feio é mais jovem que a idade de 594 Ma para os depósitos Camaquã/Santa Maria. Assim, os sulfetos na Formação Passo Feio não podem ter sido a fonte destes depósitos como previamente sugerido. Os outros dados isotópicos também contrariam este modelo.

INTRODUCTION

The copper province of Rio Grande do Sul State is located at the eastern border of the São Gabriel Block, and contains the main known Cu and Pb-Zn deposits at the Camaquã and Santa Maria Mines and the base-metal prospects of the Sul-Riograndense Shield (Figs. 1, 2). These deposits are hosted by rocks of different ages, compositions and structures. The Camaquã Cu (Au-Ag) Mines are the principal Cu deposits in the province, and are hosted by volcanosedimentary sequences of the Bom Jardim Group with an estimated age of 594 ±5Ma (Remus *et al.*, 1999).

Several mineral prospects and small deposits, spatially associated with the Caçapava Granite in the province (Fig. 2), are hosted by the Neoproterozoic Passo Feio Formation that forms the basement rocks to the Bom Jardim Group. These prospects include Cu (Au) and Pb sulphide veins and stockworks, barite, hematite veins and skarns. The origin of ore fluids and metal source(s) of these deposits has not been discussed in depth by previous workers. One important, but unresolved, question is the timing of these deposits, in particular whether they are related to one specific geotectonic cycle or to different episodes. The role of the Caçapava Granite in the genesis of these deposits is another important question. Another question concerns the possible genetic relationship of the base metal deposits, Camaquã and Santa Maria deposits, to the hydrothermal epigenetic Cu-(Au)-Fe and Pb mineralization hosted by metamorphic rocks of the Passo Feio Formation. This study considers these questions and proposes a model for the ores, which may help to identify new potential base-metal and Au deposits in the area.

Previous studies of these Cu and Pb deposits consisted mainly of field work and geochemical exploration (Gavronski, 1959; Kolling *et al.*, 1983; Feldman, *et al.*, 1983; Reischl, 1985) and some petrography (Ribeiro, 1968, 1986; Furtado, 1980). Some authors consider that the Cu mineralisation in the Passo Feio Formation could be the main source for the Camaquã deposits (e.g. Ribeiro, 1991). An alternative hypothesis is proposed that all these deposits are derived from a common regional metal source.

First, the geologic setting, geochronology, and the genesis of these deposits are summarized. Then, new SHRIMP U/Pb zircon ages, S, Sr and Pb isotope compositions of sulphides and sulphates from these deposits and prospects are presented and used to investigate possible ore-metal sources and evaluate genetic models for the different types of mineral prospects spatially related to the Caçapava Granite. New isotopic age determinations are presented for the Caçapava Granite and for the provenance and metamorphism of the Passo Feio Formation. Lead-isotope analyses of K-feldspars and whole-rocks, in combination with previous Nd and Sr isotope data, are used to constrain the source of the Caçapava Granite. The present database includes SHRIMP U-Pb ages on zircons (193 analyses), combined with Scanning Electron Microscope images of these grains using backscattered electron (BSE) and cathodoluminescence (CL) modes, 24 Pb isotopic determinations of minerals and whole-rocks, 19 sulfur isotopic determinations on sulphide minerals and three Sr isotope analyses of barites.

GEOLOGIC SETTING

The Precambrian basement in Rio Grande do Sul State is the southernmost extension of the Mantiqueira Province (Hasui *et al.*, 1975), and has four major segments (Jost and Hartmann, 1984; Soliani Jr, 1986; Fragoso Cesar *et al.*, 1986; Babinski *et al.*, 1996; Hartmann *et al.*, 1998) as shown in Figure 1. These segments have been identified using their specific petrological and tectonic associations and isotopic data, and they are bounded by NE- and NW- trending lineaments. To the east, where it is in direct contact with the 780 Ma-old Porongos schist belt, the ca. 600 Ma-old Pelotas Batholith was derived from crustal reworking of ca. 2.0 Ga-old tonalite-granodiorite and metasedimentary gneisses (Mantovani *et al.*,1987; Babinski *et al.*, 1997). The schist belt

is composed of supracrustal sequences intercalated with ca 2.0 Ga-old basement gneisses. The westernmost part of the shield contains the Taquarembó Block, an old granulite block, in the south and the São Gabriel Block, a juvenile terrain, in the north.

Passo Feio Formation

The Passo Feio Formation is a metamorphosed volcanosedimentary sequence consisting of slates, phyllites and pelitic schists, graphitic schists, marble, quartzites, metaconglomerates, calc-silicate rocks, amphibolites and subordinate metabasalts and magnesian schists (Ribeiro et al., 1966; Bitencourt, 1983), most at lower amphibolite facies. The age of the Passo Feio Formation is poorly known, but some K/Ar ages between 556 Ma (muscovites) and 666 Ma (microdiorite) were obtained by Soliani Jr (1986). The exposures of old gneisses and amphibolites, intercalated with supracrustal rocks in the southeastern part of the Passo Feio Formation, suggest that Paleoproterozoic basement (Remus *et al.*, 1966) was involved in the low-angle deformation event which affected this unit.

The sedimentary part of the Passo Feio Formation is represented by an arenaceous-pelitic-carbonate sequence. As indicated by the ocurrence of gravels and boulders of quartz and calc-silicate rocks in the beds of metarhythmites, the sequence may have been deposited from turbidity currents (Remus *et al.*, 1991). The geochemistry of metabasic rocks indicates derivation from tholeiites and alkaline-series rocks, whereas magnesian schists belong to the komatiite association (Bitencourt and Hartmann, 1984 a, b).

Regional metamorphism varies between the chlorite zone of the greenschist facies and the staurolite zone of the amphibolite facies. There are two main metamorphic events (M1 and M2) recorded in the Passo Feio Formation, locally reequilibrated in the amphibolite facies (Hartmann *et al.*, 1990). The thermal effects of the Caçapava Granite on the Passo Feio rocks is restricted to the recrystallization along contacts of its apophyses.

The activated major NE-trending transcurrent faults affecting the Passo Feio Formation and Camaquã Basin belong to the Irapuá Fault System (Ribeiro *et al.*, 1966), and represent a wrench-fault system formed during the collisional Neoproterozoic Dom Feliciano Orogeny.

Several Cu occurrences (eg. the Cioccari and Coronel Linhares Prospects) are controlled by the NE-trending Irapuá Fault System or are spatially asssociated with NW-trending transverse extensional fractures. On the west side of the Caçapava Granite, the fault zone has an inflexion to the north where the Andradas and Santa Barbara deposits are located (Fig. 2).

Camaquã Basin

The generation of the Camaquã Basin started at the end of the collisional Dom Feliciano Orogeny (630-600 Ma) and ended with the basaltic fissure eruptions of the Rodeio Velho Member at ca. 470 Ma (Remus *et al.*, 1998; Hartmann *et al.*, 1998). Deposition in the basin commenced with the Maricá Formation which was deposited directly over the Vacacaí Group and the Precambrian basement rocks of the Cambaí Complex. The Maricá Formation is made up of alluvial conglomerates and sandstones at its base, and grades upwards into marine arenaceous-pelitic arkosic rhythmites, interpreted as shallow marine sequences (Paim *et al.*, 1995).

The lowermost Bom Jardim Group depositional sequences are composed of andesitic flows and intermediate pyroclastic rocks related to the Hilario Formation of shoshonitic affinity (Nardi and Lima, 1985), more abundant in the western part of the basin. To the east, closer to the Camaquã Mines, the Bom Jardim Group is dominated by a sedimentary fraction consisting of alluvial fan conglomerates and sandstones, followed by a thick sequence of rhythmites deposited on a delta front (Paim et al., 1995). SHRIMP U-Pb in zircon dating yields an age of 594±5 Ma for the volcano-plutonic fraction of the Bom Jardim Group (Remus *et al.*, 1999).

The Santa Barbara unit consists, at its base, of acid flows and pyroclastic rocks related to the Acampamento Velho Formation. This was followed by an alluvial conglomerate facies and finally by rocks deposited from deltaic systems (Paim *et al.*, 1995). The Acampamento Velho Formation is alkaline, and may be grouped with the Saibro Suite (Hartmann and Nardi, 1982; Nardi and Bonin,1991; Lima and Nardi,1998). On the other hand, SHRIMP U-Pb zircon studies of the São Sepé Granite yielded an age of ca. 550 Ma (Remus *et al.*, 1998). This granite is

considered to be coeval with the magmatism of the Acampamento Velho Formation.

The final filling of Camaquã Basin is marked by the deposition of the Guaritas Formation, which is mostly horizontally disposed over older units. The Guaritas unit started with the basic to intermediate fissure eruptions of its Rodeio Velho Member, which are intercalated with aeolian, lacustrine and alluvial deposits at its base, and was terminated with deposits formed from alluvial fans and deltaic depositional sequences (Ribeiro *et al*, 1966 ; Paim *et al.*, 1995).

Caçapava Granite

The Caçapava granitic batholith (Leinz *et al.*, 1941; Ribeiro *et al.*,1966; Bitencourt, 1983; Sartori and Kawashita, 1985; Nardi and Bitencourt, 1989) forms an assymetrical domal structure elongated in a N-S direction (Fig. 2). Its foliation is sub-horizontal on the eastern side and in the central parts of the pluton, but dips 40-70° to the NW in the west part of the batholith.

The Caçapava batholith is composite and consists mostly of leucogranites, monzogranites and granodiorites, with minor tonalites and quartz-diorites, and intrudes the metamorphosed supracrustal sequence of the Passo Feio Formation. Biotite is the principal mafic mineral whereas hornblende is subordinate. The main accessory minerals are allanite, zircon, apatite, titanite, pyrite and magnetite and, subordinately, in the leucogranite facies, garnet, tourmaline and muscovite. Pegmatites, aplites and quartz veins with pyrite and/or hematite are common on the eastern side of the batholith, indicating relatively high fluid activity at the end of the crystallisation stage of the granite. Geochemical studies indicate a metaluminous and calc-alkaline affinity for this granite (Nardi and Bitencourt, 1989).

The age and origin of the Caçapava Granite is uncertain. Its large variations in petrographic composition (syenogranite to tonalite), its contrasting structural features (foliated and/or lineated, banded and near isotropic facies), as well as the range of K/Ar and Rb/Sr isochron ages between ca. 520 to 640 Ma (Cordani *et al.* 1974; Sartori and Kawashita, 1985; Soliani Jr., 1986; Sartori and Kawashita, 1989) of these rocks have raised intriguing questions about the origin and evolution of the batholith.

The Caçapava Granite is synchronous with the D2 shear-zone deformation episode in the area (Bitencourt, 1983; Nardi and Bitencourt, 1989; Costa *et al.*, 1995), and was derived via crustal melting processes. On the southeastern edge of pluton, the Caçapava Granite comprises thin subhorizontal sheets intruding a sequence of flat-lying marbles and dolomites that belong to the Passo Feio Formation. An assemblage of forsterite + calcite is developed in restricted parts of the marbles. The main structural features which overprint these granitic bodies are composite NE-trending, subhorizontal, mineral lineations and foliations (L>S).

ORE DEPOSITS AND PROSPECTS

The Camaquã and Santa Maria deposits

These are the major base-metal deposits hosted in the sedimentary clastic sequences of the Neoproterozoic Camaquã Basin (Fig. 2). The Camaquã deposits consist of massive veins, stockworks and disseminated ores, with chalcopyrite, pyrite, bornite, chalcocite, gold, silver and hematite, whereas the Santa Maria deposit contains disseminations and massive veins of galena and sphalerite with minor pyrite, chalcopyrite, bornite, chalcocite and native silver (Bettencourt, 1972; Badi and Gonzales, 1988, Teixeira and Gonzales, 1988; Beckel, 1990, Ribeiro, 1991 among others).

Ore reserves for the Camaquã deposits, before exhaustion, were 30.8 million tonnes averaging 1.06% Cu, with Au and Ag as the main by-products in the hematite and sulphides (Teixeira and Gonzalez, 1978). The geological reserves of the no developed Santa Maria deposit are about 33.4 million tonnes at an average of 1.44% Pb and 1.06% Zn, with Ag (12-15 g/ton) and Cu as the main by-products (Badi, 1987). A magmatic hydrothermal origin for these deposits has been confirmed based on field and isotope studies (Remus *et al.*, 1998).

Cerro dos Martins deposit

The Cerro dos Martins Deposit (Fig. 2) consists of a set of Cu-sulphide massive veins trending NW and disseminations enclosed in

siltstones, arenites, andesites and conglomerate sequences of the Bom Jardim Group. Chalcocite and bornite are the dominant ore minerals of the deposit, while chalcopyrite, pyrite, digenite, covelite, malachite and azurite are subordinate; carbonates and barite are the main gangue minerals (Flores Altamirano, 1992). Estimated ore reserves of the Cerro dos Martins deposit are 1.2 million tonnes averaging 0.8% Cu (Ribeiro, 1991).

Andradas deposit

The Andradas deposit, located on the western side of the Caçapava batholith, is spatially associated with the Santa Barbara Fault of the Irapuá Fault system. It is hosted by metavolcanosedimentary rocks of the Passo Feio Formation (Fig. 2), and comprises veins and disseminations of chalcocite, bornite and chalcopyrite with minor covelite, native copper, pyrite and digenite. The main mineralised zone trends N-S, dips to W, and is made up of four ore-bodies over a zone about one kilometer in length and around 100 m wide (Furtado, 1980; Reischl, 1985). The surface oxidation zone contains malachite, brochantite, cuprite and azurite (Furtado, 1980). This small Cu deposit has ore reserves of 4 million tonnes averaging 0.4 to 0.6% Cu (Reischl, 1985).

In drill cores in the southern part of the deposit, sulphide veinlets, with and without carbonate and quartz, crosscut the main schistosity (S1) and postdate the mineral assemblages of regional, low pressure metamorphism (M1). The host rocks of the deposit are albite-muscovite-chlorite schists, epidote-albite-muscovite-chlorite schists and meta-marls metamorphosed to the greenschist facies. Metamorphic grade increases towards the granite, reaching amphibolite facies close to the pluton. The sulphides (bornite and/or chalcopyrite, minor pyrite) generally fill fractures and voids in brecciated schists or replace the matrix of the host rocks. Because brittle fracture and void spaces are common, deposition of these sulphides occurred at shallow levels. Chalcocite occurs mainly as very fine-grained disseminations in the rock matrix .

In the northern part of the deposit, the ores are controlled by N-S and NNE-trending high-angle W-dipping faults. Surface ocurrences consist of veins of chalcocite (+ malachite and cuprite) which fill

fractures, are disseminated, or occur in places, as pods in zones of intensely cataclastically deformed and brecciated rocks. The faults also control the location of andesitic dikes which remobilized sulphides as they crosscut primary chalcocite veinlets.

Santa Bárbara deposit

The Santa Bárbara deposit (Fig. 2) is located to the NW of the Caçapava Granite and is sited in the metamorphic rocks of the Passo Feio Formation. It comprises several barite veins which contain chalcopyrite, minor pyrite, bornite, covellite and gold, with quartz- and some carbonate-filled fractures and faulted schists and felsic dikes. The veins trend N-S to N20W and dip subvertically. They cut the schistosity (S1) and therefore postdate the M1 regional greenschist facies metamorphism in this area. The mineralised zones are up to 500 m in length, in which the barite veins have a maximum width of one meter. Gold distribution along veins is irregular, but reaches 25 ppm (Remus and Hartmann, 1997). The wall rocks consist of albite-carbonate-chlorite schists, tourmaline-muscovite-albite-chlorite schists, meta-tuffs, meta-marls and altered dacitic and andesitic dikes. The deposit is cut by twelve, N-S oriented Mesozoic diabase dikes.

Faxinal prospect

The Faxinal prospect (Fig. 2) consists of several meter long and decimeter wide, NE-trending quartz veins, enclosed in meta-marls and spatially associated with NE-trending faults. The prospect contains galena and minor chalcopyrite and pyrite. The quartz veins have comb structures and at least two stages of quartz generation are recognized.

Coronel Linhares prospect

This prospect (Fig. 2) is located on the eastern side of the Caçapava Granite batholith, and consists of chalcopyrite, pyrite, marcasite and invisible gold hosted by carbonate and/or chlorite gangue.

The ore occurs near contacts between the granitic apophyses and marbles, as reefs and elongated linear bodies, which are structurally controlled by a NE-plunging sub-horizontal lineation or as stockworks and irregular bodies, controlled by NW-trending extensional fractures, which replace the carbonate wallrocks along breccia zones. These deposits are skarns, which are related to granitic intrusion during the second deformation (D2) and metamorphic (M2) phases. Strong magnesium metasomatism progressively transforms the biotite-granodiorite sheets into a plagioclase-chlorite-rich rock, and produces a chlorite rock along the contacts with dolomitic marble. The granite sheets and apophyses from the Caçapava Granite may have assimilated sulfur and magnesium from sulphide bearing country rocks and produced strong chloritic alteration and sulphur saturation in the fluids. This indicates contemporaneity between mineralization, alteration and intrusion of the Caçapava Granite.

Cioccari prospect

The Cioccari prospect (Fig. 2), situated 4 Km to the south of Coronel Linhares, occurs in dolomitic marbles of the Passo Feio Formation and consists of a mineralised zone 150 m long and 1.5 m wide made up of several thin veins of massive chalcopyrite, minor pyrite, invisible gold, Cu oxides, calcite, talc, serpentine, tremolite and quartz. These veins form a network, which crosscut the S1 foliation of the marbles and dolomites and postdate the regional metamorphism (M1). Sulphides replace the carbonate minerals in the host rocks. The ore minerals are controlled by a subvertically-dipping fracture zone which is oriented NW. Gold is irregularly distributed in the lodes, and can reach 23 ppm (Remus & Hartmann, 1997).

As indicated by structural features, the sulphide veins of the Cioccari Prospect, chalcopyrite, pyrite and gold located on the eastern side of batholith, were all mobilized during intrusion of the Caçapava Granite.

METHODOLOGY

Geological field mapping was carried out over the entire metamorphic belt at a 1:50,000 scale, and a more detailed 1:10,000 survey was made of the area closer to the mineral deposits and prospects. Structural controls were established, and rock and ore samples collected for laboratory studies. Approximately three hundred thin sections and one hundred polished sections of ores were studied in the entire metamorphic belt and its contained deposits and prospects, followed by rock geochemistry and electron microprobe analyses of minerals (Hartmann *et al*; 1990; Remus and Hartmann, 1997).

In the present investigation, rock samples were collected from the mineral deposits and prospect sites (Fig. 2) and from the Caçapava Granite. Samples weighing one kilogram were collected for Pb isotopic studies, and about forty kilograms of a muscovite-albite-chlorite schist of the Passo Feio Formation, from the creek close to the Santa Barbara deposit, were collected for zircon studies, because the rock is poor in this mineral. Twenty kilograms of a dacite dike from the Passo Feio Formation were collected from the walls of lodes of the Santa Barbara deposit (Fig. 2) for zircon studies. Only five kilograms of granite were necessary for zircon separation. Feldspars and zircons were separated by conventional magnetic and heavy liquid procedures. Ore sulphides were collected from mineral deposits and prospects for sulphide S-Pb isotope studies. Individual coarse-grained sulphides were separated by hand picking and analysed using procedures outlined in Ho *et al.* (1994).

Zircon geochronology was undertaken on two samples to determine the ages of the provenance and metamorphism of host rocks to mineralization from the Passo Feio Formation, and in one sample of Caçapava Granite to define its magmatic age. SHRIMP investigations of zircons were undertaken at Curtin University and follow the procedures of Compston *et al.* (1984) and Smith *et al.* (1998). Scanning electron microscope images of grains were obtained using backscattered electron (BSE) and cathodoluminescence (CL) modes at the Centre for Microscopy and Microanalysis, University of Western Australia.

Rocks for isotopic analyses and conventional geochemistry were crushed and milled in an agate mortar to minimise contamination. The concentration of U, Th and Pb (ppm) was determined in whole rocks using inductively coupled plasma mass spectrometery (ICP-MS)

available commercially through Genalyses Laboratory Services Pty. Ltd. (Perth, Australia). The SiO_2 (wt. %) was determined in whole rocks by the XRF method at Analabs Pty. Ltd. (Perth, Australia). Strontium was separated using Eichrom Sr-spec resin and Pb was extracted by ion exchange chromatography using HBr at the Lead-free Laboratory, University of Western Australia. Strontium and Pb isotopic measurements were made on a VG354 multicollector mass spectrometer housed at Curtin University of Technology, Perth, Western Australia. Sulfur isotopic analyses were performed in the stable isotope laboratories at the Australia National University (Canberra, Australia).

SHRIMP U-Pb ZIRCON AGES

Metasedimentary rock from the Passo Feio Formation: One sample (sample CERR-wr) of albite-muscovite-chlorite schist, with minor tourmaline, pyrite, magnetite and carbonate, was collected in a creek close to the Santa Barbara deposit (Fig. 2). The outcrop is located near E = 258650 m and N = 6631550 m of the UTM reference frame. Sixty six SHRIMP spot analyses were obtained on 55 zircon grains separated from this sample (Table 1). BSE and CL studies, combined with SHRIMP U-Pb ages, allow the definition of four distinct zircon populations which are shown on the concordia diagrams of Figures 3 and 4. The oldest zircon grains are Archaean. The concordant Archaean zircon spot (529B.5-2) is a partially corroded xenocryst and included in a rounded Paleoproterozoic grain (spot 529.5-1; Fig. 5 C-D). Two populations are Paleoproterozoic. The older is represented by seven spots on six zircons. These include rounded grains typical of sedimentary transport (Fig. 5 E-F); euhedral and circular shapes with internal oscillatory and complex zoning also occur. Three most concordant analyses yield a $^{207}Pb/^{206}Pb$ age of 2468±22 Ma. As indicated by the age and morphology of this population, the most probable source rock of these zircons is the Neto Rodrigues Gneiss (Remus *et al.*, 1996). Ten analyses were obtained on seven grains of the younger Paleoproterozoic population, which is composed of rounded grains which have elliptical or spherical shapes, denoting strong sedimentary reworking. The internal morphology of these zircons shows sector, oscillatory and complex zoning. Four most concordant analyses yield a $^{207}Pb/^{206}Pb$ age of 2053±46 Ma. The source

area of these zircons may be the Santa Maria Chico Granulitic Complex, which formed during the Transamazonian Orogenic Cycle (Hartmann, 1998).

Fourty six analyses were done on 39 zircon grains of the Neoproterozoic population. These zircons have euhedral and rounded external shapes, with internal morphology showing oscillatory and sector zoning and, rarely, complex zonation with distinct rims and cores. This population shows a data array on the concordia diagram of Figure 4, with a range in $^{206}Pb/^{238}U$ ages from 908 to 774 Ma (Table 1). Several zircon grains of that inherited population have rounded shapes, indicating reworking during a sedimentary cycle, and occur together with euhedral grains with a similar range of ages (Fig. 5 I-J). The source rocks of zircon were most probably the diorites and tonalites of the Cerro Mantiqueiras region studied by Leite *et al.* (1998). Zircon $^{206}Pb/^{238}U$ ages in the range of 674 to 560 Ma (Fig. 4) probably reflect the tectonic event in which the syntectonic Caçapava Granite was intruded at ca. 560 Ma (see below). Younger ages are often from zircons with high-U and are considered to be related to Pb-loss from radiation-damaged areas during modern weathering.

Dacite dyke from the Passo Feio Formation: A deformed dacite dyke, the other sample of the Passo Feio Formation, was collected in the wall rocks of the Santa Barbara deposit (Fig. 2), near E = 258240 m and N = 6632000 m of the UTM reference frame, and has two distinct inherited zircon populations. The older one consists of four rounded or broken early Archaean grains (Fig. 6). BSE and CL images reveal a normal igneous zonation, with some grains affected by recrystallization along the rim or in domains (Fig. 5 A-B). The four low-U analyses yield a $^{207}Pb/^{206}Pb$ age of 3222±13 Ma .

Thirty analyses on 23 zircons of the Neoproterozoic population have a spread in $^{206}Pb/^{238}U$ ages between 947 and 190 Ma (Fig. 7 and Table 2). The majority of grains have a distinct texture of zoned cores with a massive rim. Cores have normal and oscillatory igneous zonation and rare complex patterns. Inherited cores have $^{206}Pb/^{238}U$ ages in the range of 885 to 715 Ma. These zircons are interpreted as xenocrysts because some grains are broken (reworked) and overgrown by massive rims due to the metamorphic episode. The most probable source for these zircons was the plutonic and volcanic rocks of the São Gabriel Block, namely diorites and TTG associations from the Cerro

Mantiqueiras region (Leite *et al.*, 1998) and acid to intermediate volcanics from the Bossoroca Volcanic Arc (Remus *et al*, 1998). Spot 682A.9-2 has high common Pb (Fig. 7), hence the 947 Ma date is not considered to be the age of a geologic event in the Shield. The massive rims are 10 μm wide, at most, and have a very distinctive bright color in the CL images (Fig. 5 G-H). The rims overgrow indistinctly euhedral or broken grains, and are interpreted as the effect of metamorphic recrystallisation or new zircon growth overgrowing the inherited reworked igneous grains. One spot located between the massive rim and zoned core domain on grain 682A.3 (Fig. 5 G-H) yields a $^{206}Pb/^{238}U$ age of 685±12 Ma, a value that is very close to the regional metamorphic event defined for the Campestre Formation at ca. 700 Ma (Remus *et al.*, 1998b) located a few tens of kilometers to the west. The opening of the Passo Feio basin probably occurred at ca. 760 Ma, as indicated by the contemporaneous Campestre Formation volcanism. The closure of the basin is represented by tangential deformation and regional metamorphism (M1) at ca. 700 Ma. Younger discordant zircon ages are related to the tectonic event in which the Caçapava Granite intruded and shear zone development at 562 Ma (see below) and to modern Pb-loss.

Caçapava Granite: One sample of the gray foliated-facies granodiorite of the Caçapava Granite, collected in the Cioccari quarry along the eastern side of batholith (Fig. 2 - Cioccari Prospect), near E = 268900 m and N= 6620000 m of the UTM reference frame, was selected for study. The zircons within this sample are included in plagioclase, quartz and biotite. Where accessory allanite is present, zircons are preferentially included in that mineral, especially in granodiorite samples from the central part of the batholith.

Three distinct zircon age populations in the sample are shown on the concordia diagrams of Figures 8 and 9 and in Table 3. Two populations are Paleoproterozoic xenocrysts and the younger one is a Neoproterozoic magmatic population. A magmatic $^{206}Pb/^{238}U$ age of 562±8 Ma is obtained from the cores and rims of 18 out of 83 colorless or yellowish, euhedral, prismatic grains and long prismatic, zoned zircon grains. The majority of the zircons have apatite and magnetite inclusions. BSE and CL images show a strong oscillatory zonation in both the core and rim regions of these grains (Fig. 10 A to F). Sixty three of 83 analysed grains have a range of discordant younger ages (Fig. 9), largely from rim domains, which trend to higher U (up to 6284 ppm), Th (up to 3553 ppm) and common Pb corrections, relative to the

core regions (Table 3). These younger zircon domains all have darker colors when viewed under a conventional petrographic microscope in plane polarized light. Some thin bands are also dark in BSE and CL images, and represent metamict domains. The youngest $^{206}Pb/^{238}U$ age of 187±3 Ma is obtained in the rim region of grain 520A.5-1 (Fig.10 E-F), in which there are thin dark bands in both CL and BSE images, typical of metamictized zircon. Two slightly older analyses show the same morphologic characteristics as the magmatic population, but are distinctly older than 562±8 Ma (Fig. 9) and indicate a xenocrystic origin.

The Paleoproterozoic xenocrysts are grouped into two distinct populations (Fig. 8). The older is represented by two short prismatic zircon grains (519A.4; 520A.8) which have discordant $^{207}Pb/^{206}Pb$ ages varying between 2399 and 2108 Ma. The younger Paleoproterozoic population is represented by four xenocrysts (519A.1; 519A.8; 519A.10; 520A.37). The maximum concordant $^{207}Pb/^{206}Pb$ age of ca. 2050 Ma is interpreted as the real age of xenocryst zircons, while the younger values (Table 3) are attributed to Pb-loss due to emplacement of the Caçapava Granite and the related shear zone development. Paleoproterozoic xenocrysts are partially preserved as cores in the discordant euhedral Neoproterozoic magmatic grains from the Caçapava Granite (Fig. 10 G-H), or occur as free zircon grains (Fig. 10 I-J).

SHRIMP U-Pb zircon dating of a monzogranite facies, located on the SE edge of batholith (Leite *et al.*, 1998), indicates a magmatic age of 540 Ma and 560 Ma for xenocrysts for the protolith of these rocks. We interpret the 540 Ma age as reflecting Pb-loss from a ~562 Ma magmatic zircon population. The zircons are interpreted to have lost varying amounts of Pb, and as with the gray phase of the Caçapava Granite, it is difficult to distinguish the real age of the magmatic episode. The main cause of Pb-loss could be related to radiation damage in high U domains of zircons, mainly in edge zones of grains.

The concordia diagram on Figure 11 summarizes those magmatic and tectono-metamorphic events in the São Garbriel Block during the Brasiliano Cycle which are registered in inherited and/or recrystallized zircons of the Passo Feio Formation and Caçapava Granite samples.

SULPHUR ISOTOPES

The sulphur isotopic compositions of sulphides and sulphates are used as tracers to determine the source of the element itself, or as a paleothermometer, both of which are useful for interpreting the origin of mineral deposits (Ohmoto, 1972; Ohmoto and Rye, 1979). Three sulphur reservoirs with distinctive $\partial^{34}S$ have been proposed: mantle derived sulphur with values in the range of -3 to +3‰ CDT; 1) seawater sulphur where values are positive, vary with time, and are today around +20‰ CDT; and 3) sedimentary sulphur (strongly reduced) with large negative values (Claypool *et al.*, 1980; Chaussidon *et al.*, 1990; Ohmoto *et al.* 1990).

The $\partial^{34}S$ of sulphides (galena, pyrite, chalcopyrite, chalcocite and bornite) from the deposits and prospects spatially associated with the Caçapava Granite vary from -15.2‰ to +10.8‰ CDT (Table 4). This large range of values suggests that at least two sulphur reservoirs are involved in the source of ore fluids.

The sulphides of the the Andradas deposit have a $\partial^{34}S$ range +2.1‰ to -11.2‰ (Fig. 12a). The slightly positive (+0.2‰ to +2.1‰) values are from primary chalcocites from the northern part of the deposit, and suggest a magmatic origin for the sulphur. However, chalcopyrites and bornites from the southern part of the Andradas deposit have negative values in the range of -3.9‰ to -11.2‰, consistent with a sedimentary component in the source of sulphur. The total sulfur isotopic composition of sulphides from the Andradas deposits could be explained by mixing between fluids from a magmatic source (Caçapava Granite) and reduced sulphur derived from leaching of metasedimentary host rocks of the Passo Feio Formation (pyritic and graphitic phyllites/schists).

Two pairs of contemporaneous samples of barite-chalcopyrite from barite-chalcopyrite ± pyrite-bornite veins of the Santa Barbara deposit have $\partial^{34}S$ values of +7.6‰ to +8.5‰ for barites and -13.4‰ to -15.5‰ for chalcopyrite (Fig. 12b). This range of compositions indicates isotope fractionation from an oxidizing fluid during ore deposition. Geothermometric calculations, based on S-isotopic fractionation between barite-chalcopyrite pairs (Ohmoto and Rye, 1979), yield a temperature of 288 to 304±10°C for deposition of these massive veins.

The homogeneity of $\partial^{34}S$ values for analysed barites and chalcopyrites of the Santa Barbara deposit suggests that physico-

chemical conditions did not significantly change during ore deposition. Since the studied vein system was formed within the barite-chalcopyrite-pyrite stability field at relatively high SO_4/H_2S ratios, the $\partial^{34}S_{fluid}$ should be close to $\partial^{34}S_{barite}$ (~8.5‰). This $\partial^{34}S$ value is compatible with a fluid-source contribution from the marine metasedimentary host rocks of the Passo Feio Formation. However, the Sr isotopic composition of barites (see below) indicate some ore-fluid participation from the Caçapava Granite magma, which may have contributed with some sulphur during leaching of the metasedimentary country rocks.

The Coronel Linhares and Cioccari Prospects have positive $\partial^{34}S$ values for sulphides in the range of +3.9‰ to +10.8‰ (Fig.12c). The pyrites and chalcopyrites from the first prospect have very homogeneous values between +3.9‰ to +4.9‰, and indicate a magmatic source for sulfur, with a minor contribution from the marine, dolomitic-marble wall rocks. The granite sheets and apophyses from the Caçapava Granite are interpreted to have assimilated sulfur and magnesium from dolomitic marbles and produced strong chloritic alteration and sulphur saturation in the fluids, as discussed in previuos section. This acid sulphur-saturated solution precipitated chalcopyrite and pyrite along the contacts of the chlorite-altered granite sheets and marbles due to neutralization of acid solution by carbonate wall rocks (cf. Lu *et al.*, 1992).

The two chalcopyrite samples from the Cioccari Prospect also have homogeneous but higher values for $\partial^{34}S$, both around +10‰. Here, the hydrothermal silica-sulfur aqueous solutions are interpreted to have infiltrated into the dolomitic marble along NW-trending fractures, dissolving and producing new space and consequently enhancing permeability and fluid flux into the country rocks. The dissolution and assimilation of sulfur from marine dolomitic marbles would increase $\partial^{34}S$ values. The calcium and magnesium silicate alteration- mineralogy (talc, tremolite and serpentine) are interpreted to have formed by reaction of SiO2 and H2O from the ore fluids with wall rock carbonates due to the consumption of H^+ ion by the carbonates and consequent sulphide precipitation. Thus, the fluid-wall rock reactions of the Cioccari deposit can be represented by neutralization due to reaction of acid solutions by dolomite.

One galena sample from Faxinal Prospect has a $\partial^{34}S$ of -4.3‰ (Fig. 12c), which could represent a mixing between hydrothermal magmatic

fluids from Caçapava Granite and reduced sulfur from pyritic metamarl wall rocks.

LEAD AND STRONTIUM ISOTOPES AND SOURCE OF MINERALISATIONS

Lead isotope studies of ore-gangue minerals can provide helpful information about the genesis of ore metal deposits by constraining the source rock(s) of these elements. Galenas and potassium feldspars are the best minerals for estimation of the initial Pb isotope ratios of ores and magmas, because they have very low U/Pb ratios and ideally do not change their Pb isotope composition with time. The low-Pb sulphides, on the other hand, may provide information about the initial Pb isotope ratios if the age of mineralisation is known because additions of radiogenic Pb should be constrained to an isochron which includes the initial Pb composition (Gulson *et al.*, 1983; Ho *et al.*, 1994; Bierlein and McNaughton, 1998). The Pb-isotope systematics have been used extensively by many authors (Doe and Stacey 1974; Doe and Zartmann, 1979; McNaughton and Bickle,1987; Ho *et al.*, 1994; Carr and Dean, 1995; McNaughton and Groves, 1996, among others). Because galena is present only in the Faxinal Prospect in this region, ten samples of pyrite, chalcopyrite, chalcocite and bornite were also analysed.

For sulphates, the isotopic ratios of strontium in barites can be used as a tool to constrain the source of ore fluids, because they have very low Rb concentrations (Lange *et al.*, 1983; Barbieri *et al.*, 1987; Canals and Cardelach, 1993; Galindo *et al.*, 1994).

Caçapava Granite

The petrographic and chemical variations within the Caçapava Granite have been related mainly to fractional crystallization processes (Nardi and Bitencourt, 1989). Sartori and Kawashita (1989) demonstrated a large variation in the initial $^{87}Sr/^{86}Sr$ ratios of rocks of the batholith and interpreted it as reflecting the isotopic heterogeneity of the source region. Such isotopic variations across the batholith are also evident from distinct variation in εNd isotopic values of -10 and -19 for t = 600 Ma (Babinski *et al.*, 1996).

Lead isotopic data from K-feldspars (n=5) and whole-rocks (n=4) from the Caçapava Granite are shown in a common Pb diagram on Figure 13 and listed in Table 5. The K-feldspars plot in a small, but significant, range potentially indicating different initial ratios and a heterogeneous crustal source for the Caçapava Granite. Although these variation could also be related to *in-situ* uranium decay, the wide strong variation in initial Sr and Nd isotopic compositions favours the heterogeneous source hypothesis. These isotopic results and the SHRIMP data from zircon xenocrysts suggest that the source of the Caçapava batholith was contituted by complex and heterogeneous crustal material of variable nature and age.

Copper and lead deposits and prospects

The ocurrence of several Cu-Au deposits located close to the granite suggest that the Caçapava Granite may have been the main metal source, or heat source which mobilized metals from the wallrocks of Passo Feio Formation. In the following section, the Pb isotope composition of the ore sulphides are compared to the compositional field of Pb of K-feldspars from the Caçapava Granite which represent the range of initial ratios of that magma, and to the plagioclase, amphibolite, metamarls and albite-chlorite schist from Passo Feio Formation (Fig. 13) to elucidate the source of Pb in the ores.

Field relationships indicate that the Caçapava Granite is intrusive into the Passo Feio Formation, and that granite apophyses and related fluids caused mineral transformations in the host rocks. In the Coronel Linhares Prospect, there is a close spatial association between sulphides and altered granite, and structural relationships show that the sulphides were deposited during granite emplacement. The sulphur saturation of the granite magma is interpreted to be due to wall rock assimilation during emplacement, with neutralization of the acid magmatic fluids causing precipitation of Cu and Fe sulphides. These copper and Fe-sulphides (and Au) could be derived from a mixed source involving at least two components: fluids derived from the Caçapava Granite and from metasedimentary rocks such as metamarls and related para-amphibolites of the Passo Feio Formation.

The Pb-isotopic composition of pyrites, chalcopyrites, bornites and chalcocites from the deposits and prospects of this study are

plotted on a common Pb diagram in Figure 14 and presented in Table 4. Also plotted in Figure 14 is the Pb isotopic composition of a galena sample hosted by metamarls, collected from the Faxinal Prospect which is located a few kilometres north of the Coronel Linhares Prospect. The compositional field of Pb from K-feldspars, representing the range of initial ratios of the Caçapava Granite, together with the compositional field of amphibolites of the Passo Feio Formation, are shown for comparison. The Pb isotope compositions of sulphides from all the deposits are very consistent. They have a wide scatter in 206Pb/204Pb (16.555 to 20.267) and correlated variations in 207Pb/204Pb (15.443 to 15.687). The least-radiogenic sulphide samples from the prospects represent the best estimates of initial ratios and fall between the fields of the Caçapava Granite and the amphibolites. The linear array defined by the sulphides is subparallel to the 562 Ma reference isochron of the Caçapava Granite (age defined by SHRIMP U-Pb zircon studies). This trend also includes the composition of albite-chlorite schists, plotted in figure 13, and suggests that Pb in the metamorphic rocks of the Passo Feio Formation and the ore sulphides have a similar source.

The least-radiogenic Cu-Fe sulphides are the pyrites and chalcopyrites from the Coronel Linhares and Cioccari prospects, which have similar initial Pb-isotopic ratios to the galena from Faxinal prospect. This suggests that the isotopic compositions of these low-Pb sulphides provide approximate estimates for the initial Pb-isotope ratios of the ore system. The very primitive initial Pb-isotope composition of these sulphides, compared to the Stacey and Kramers (1975) growth curve is compatible with a metal source from a depleted continental crust.

Chalcopyrites and bornites from the Andradas deposit have a radiogenic Pb-isotopic compositions but overlap the 562 Ma reference isochron for the Passo Feio Formation, implying a similar source (Fig. 14).

The lead contents of chalcopyrites and barites, the main minerals in the ores of the Santa Barbara deposit, are very low, which makes it difficult to determine their initial isotopic composition. The one analysed sample of Santa Barbara chalcopyrite plotted in the common Pb diagram of Figure 14 adheres well with the 562 Ma reference isochron for the Passo Feio Formation, suggesting that this ore had a similar Pb source to the others.

As shown by the common Pb diagram of Figure 14, the origin of Pb in sulphides from studied mineralisations is compatible with a Pb source largely from the metasedimentary rocks of Passo Feio Formation, with or without contributions from the Caçapava Granite or amphibolites. The field and isotopic evidence also suggest assimilation of S-bearing rocks of the Passo Feio Formation during Caçapava Granite emplacement. Thus, isotopic signatures of Coronel Linhares and Cioccari sulphides could have been inherited from assimilated metal sulphides at this stage, and deposition could have been entirely from Caçapava Granite—derived magmatic fluids. In the Andradas and Santa Barbara deposits, leaching of chlorite schists is favoured instead of metal sulphides assimilation and deposition entirely from granite-derived fluids. Copper sulphide mineralisations from prospects and deposits of the Passo Feio Formation have previously been postulated to be the detrital source for metals of the Camaquã and Santa Maria deposits (Ribeiro, 1991) However, the interpreted 562 Ma age of these deposits is younger than the well-constrained 594 Ma age for Camaquã/Santa Maria deposits (Remus et al, 1998; 1999). Additionally, the sulfur isotope signatures of deposits hosted by the Passo Feio Formation are distinct from those of the Camaquã/Santa Maria ores. However, the Pb-isotope signature of both systems is compatible with a very depleted crustal source, suggesting that the ultimate source of the metals could be the same crust.

Strontium from the Santa Barbara Deposit

The Sr isotopic compositions of barites from barite+chalcopyrite± pyrite±bornite veins of the Santa Barbara deposit show a limited range between 0.70652 and 0.70688 (Table 6). However, these variations are larger than analytical error (±0.00010 at 95% confidence level), and suggest small differences in the isotopic composition of the hydrothermal fluid with time and space. These values are close to, but slightly higher than, the acceptable range of 0.70328 to 0.70554 in the Caçapava Granite (Sartori & Kawashita, 1989). The higher ratio of 0.70728 recorded by these authors corresponds to a 543±23 Ma age, which is clearly not the accepted age, and the ratio is then discarded. The Sr-isotope composition of barites requires a more radiogenic source component than Caçapava Granite. These results suggest that Sr

from Santa Barbara barites was derived from a mixed source involving fluids from the Caçapava Granite and another, more radiogenic component, possibly related to rocks of the Passo Feio Formation.

CONCLUSIONS

1. SHRIMP U-Pb zircon dating, combined with CL and BSE studies, of the Passo Feio Formation show it to have a Neoproterozoic age. The supracrustal rocks of the Passo Feio Formation were affected by regional dynamothermal metamorphism at ca. 700 Ma, and have distinct inherited Archaean, Paleoproterozoic and Neoproterozoic zircon populations implicating a complex continental source.

2. The Caçapava Granite, emplaced syn-tectonically during a D2 transcurrent deformation event, intruded into the supracrustal sequences of the Passo Feio Formation at 562 Ma, as shown by SHRIMP U-Pb zircon dating. Strontium, Nd and Pb isotopes indicate a heterogeneous, old, sialic basement source for the Caçapava Granite.

3. Sulphides from mineral deposits of the Caçapava do Sul Copper Province show a significant spread in Pb isotopic ratios parallel to the 562 Ma reference isochron, with the least-radiogenic samples representing the best estimate of initial ratios. The least-radiogenic samples fall between the fields for amphibolites of the Passo Feio Formation and the Caçapava Granite and overlap with chloritic metasedimentary rocks, which strongly suggests that Pb and other metals were derived from leaching of host rocks during Caçapava Granite magmatism at 562 Ma.

4. The least-radiogenic Pb-isotope compositions are from pyrites and chalcopyrites from the Coronel Linhares and Cioccari prospects, which have similar value to galena from the Faxinal prospect. The Pb appears to have been derived from a very primitive crustal source.

5. Sulphides from the Andradas and Santa Bárbara deposits have radiogenic Pb-isotopic compositions lying close to the 562 Ma isochron, which lie between the fields for the Caçapava Granite and the amphibolites of the Passo Feio Formation. The S isotope composition of sulphides is compatible with a sedimentary source, with some contribution from a magmatic source. Strontium isotope ratios of the Santa Bárbara barites also implied a mixed source, potentially

involving the Caçapava Granite and a more radiogenic component related to rocks of the Passo Feio Formation.

6. In combination, isotopic (S, Pb) results and geochronological data indicate that Cu sulphide deposits hosted by the Passo Feio Formation could not be the main source for mineralization in the Camaquã and Santa Maria deposits, although both could share a similar deep crustal Pb source.

More important than any of the above specific conclusions is the significance of the systematic application of SHRIMP U-Pb analyses which establish the geochronological framework of mineralization, magmatism and metamorphism, without which interpretations would have been severely restricted.

Acknowledgments

This paper is part of the Ph.D. thesis of the first author on the Copper Province of Rio Grande do Sul. Funding by CNPq - National Research Council of Brazil (Grant 201393/94-8) is acknowledged. Mr. Marion Dahl (UWA - Australia) is thanked for help with the analytical procedures. Dra. Tamar Galembeck (UNESP-SP) is thanked for the preliminary zircon sample preparation. Paul Potter reviewed the English version of the paper. Zircons were analysed on the SHRIMP II operated by a consortium consisting of Curtin University of Technology, the Geological Survey of Western Australia and the University of Western Australia, with the support of the Australian Research Council.

REFERENCES

Babinski, M., Chemale Jr. F., Hartmann, L.A., Van Schmus, W.R. and Silva L.C. (1996) Juvenile accretion at 750-700 Ma in southern Brazil. *Geology*, 24 (5), 439-442.

Babinski, M., Chemale Jr. F., Van Schmus, W.R., Hartmann, L.A. and Silva L.C. (1997) U-Pb and Sm-Nd geochronology of the Neoproterozoic granitic-gneissic Dom Feliciano Belt, southern Brazil. *Journal of South American Earth Sciences*, 10 (3-4), 263-274.

Badi, W.S.R. (1987) *Relatório final de pesquisa.* Unpublished final report, Companhia Brasileira do Cobre, Porto Alegre, RS, 98 p.

Badi, W.S.R. and Gonzalez, A.P. (1988) Jazida de metais básicos de Santa Maria, Caçapava do Sul-RS. In: *Principais Depositos Minerais do Brasil*, Schobbenhaus, C. and Silva Coelho, C.E. (eds.) DNPM/CVRD, Rio de Janeiro, 3, 157-170.

Barbieri, M., Bellanca, A., Neri, R. and Tolomeo, L. (1987) Use of strontium isotopes to determine the sources of hydrothermal fluorite and barite from northwestern Sicily (Italy). *Chemical Geology* 66, 273-278.

Bettencourt, J.S. (1972). *A Mina de cobre de Camaquã, Rio Grande do Sul*. Unpublished Ph.D. Thesis, 175p. Universidade de São Paulo, São Paulo - Brazil.

Bettencourt, J.S. (1976) Mineralogie, inclusions fluides et isotopes stables d'oxygene et de soufre de la mine de cuivre de Camaquã - RS. (une ètude preliminaire). In: Congresso Brasileiro de Geologia, 29, Ouro Preto-MG, SBG, *Anais* 2, 409-423.

Bierlein, F.P. and McNaughton, N.J. (1998) Pb isotope fingerprinting of mesothermal gold deposits from central Victoria, Australia: implications for ore genesis. *Mineralium Deposita*, 33, 633-638.

Bitencourt, M.F. (1983) *Geologia, petrologia e estrutura dos metamorfitos da região de Caçapava do Sul, RS.*, Unpublished M.Sc. Thesis, 161p. Universidade Federal do Rio Grande do Sul, Porto Alegre, RS - Brazil.

Bitencourt, M.F. and Hartmann, L.A. (1984a) Reconhecimento geoquímico dos xistos magnesianos da região do Passo Feio, Caçapava do Sul, RS. In: Congresso Brasileiro de Geologia, 33, Rio de Janeiro, SBG, *Anais* 6, 2607-2614.

Bitencourt, M.F. and Hartmann, L.A. (1984b) Geoquímica das rochas anfibolíticas da região de Caçapava do Sul, RS. Parte I: caracterização geológica e petrográfica, elementos maiores e menores. In: Congresso Brasileiro de Geologia, 33, Rio de Janeiro, SBG, *Anais* 9, 4253-4265.

Camozzato, E. (1987) Folha Cachoeira do Sul SH.22-Y-A, Região Sul. In: *Projeto mapas metalogenéticos e de previsão de recursos minerais*, CPRM-DNPM. Ed. Siqueira, L.P. Texto e Mapas, Brasília, DNPM.

Canals, A. and Cardelach, E. (1993) Strontium and sulphur isotope geochemistry of the low temperature barite-fluorite veins of the Catalonian Coastal Ranges (NE Spain): a fluid mixing model and age constraints. *Chemical Geology*,104, 269-280.

Carr, G.R., Dean, J.A., Suppel. D.H. and Heithersay, P.S. (1995) Precise lead isotope fingerprinting of hydrothermal activity associated with Ordovician to Carboniferous metallogenic events in Lachlan Fold Belts of New South Wales. *Economic Geology,* 90, 1467-1505.

Chaudisson, M. and Lorand, J.P. (1990) Sulphur isotope composition of orogenic spinel lherzolite massifs from Ariege (N.E. Pyrinees, France): An ion microprobe study. *Geochimica Cosmochimica Acta.*, 54, 2835-2846.

Claypool, G.E, Holster, W.T., Kaplan, I.R., Sakai, H. and Zak, I. (1980) The age curves of sulfur and oxygen isotopes in marine sulfate and their mutual interpretation. *Chemical Geology*, 28, 199-260.

Compston, W., Williams, I.S. and Meyer, C. (1984) U-Pb geochronology of zircons from Lunar breccia 73217 using a sensitive high-mass resolution ion microprobe. *J. Geophys. Res.*, 89 Suppl.: B525-B534.

Cordani, U.G., Halpern, N. and Berenholc, M. (1974) Idades radiométricas de rochas do Escudo Sul-riograndense e sua significação tectonica. *X Carta do Brasil ao Milionésimo* . Folha de Porto Alegre, DNPM.

Costa, A.F.U, Fernandes, L.A.D., Shukowsky, W., Nardi, L.V.S. and Bitencourt, M.F. (1995) Teste dos modelos tectônicos e de posicionamento do Complexo Granítico de Caçapava do Sul, através de estudos de modelagem gravimétrica 3-D. *Revista Brasileira de Geofísica,* 13(2), 91-101.

Doe, B.R. and Stacey, J.S. (1974) The application of Pb isotopes to the problems of ore genesis and ore prospect evaluation. A review. *Economic Geology*, 69, 757-776.

Doe, B.R and Zartmann, R.E. (1979) Plumbotectonics: The Phanerozoic. In *Geochemistry of hydrothermal ore deposits.* ed. Barnes, H.L., pp. 22-70, Wiley, New York, USA.

Feldman, E., Reischl, J.L., Kolling, S.L. and Jost, H. (1983) Pb and Zn estratiforme na sequencia vulcano-sedimentar do Passo Feio-RS. Simpósio Sul-Brasileiro de Geologia, 1, Porto Alegre, RS, *Atas*, 322-335.

Fragoso César A.R.S., Figueiredo M.C.H., Soliani Jr E. and Faccini U.F. (1986) O Batólito de Pelotas (Proterozóico Superior/Eo-Paleozóico) no Escudo do Rio Grande do Sul. In: Congresso Brasileiro de Geologia, 34, Goiânia, GO. *Anais*, 3, 167-191.

Furtado, S.M.A. (1980) *Contribuição aos estudos petrológico, geoquímico e metalogenético da ocorrência cuprífera de Cerro dos Andradas,*

Caçapava do Sul -RS. Unpublished M.Sc. Thesis, 163p. Universidade Federal do Rio Grande do Sul, Porto Alegre -RS.

Galindo, C., Tornos, F., Darbyshire, D.P.F. and Casquet, C. (1994) The age and origin of the barite-fluorite (Pb-Zn) veins of the Sierra del Guadarrama (Spanish Central System, Spain): a radiogenic (Nd, Sr) and stable isotope study. *Chemical Geology,*112, 351-364.

Gavronski, E.F. (1959) *Relatório sobre a prospecção das ocorrências de cobre do Cerro dos Andrades, Primavera e Santa Bárbara no munícipio de Caçapava do Sul, RS, Brasil.* Divisão de Fomento da Produção Mineral, Brazil, 95p.

Gulson, B.L., Perkins, W.G. and Mizon, K.J. (1983) Lead isotope studies bearing on the genesis of copper ore bodies at Mount Isa, Queensland. *Economic Geology* , 78, 1466-1504.

Hartmann, L.A. (1998) Deepest Exposed Crust of Brazil - Geochemistry of Paleoproterozoic depleted Santa Maria Chico Granulites. *Gondwana Research*, 1 (3/4), 331-341.

Hartmann, L.A., Silva, L.C., Remus, M.V.D., Leite, J.A. and Philipp, R.P. (1998) Evolução geotectônica do Sul do Brasil e Uruguai entre 3,3 Ga e 470 Ma. Congresso Uruguayo de Geologia, 2, Punta Del Este, *Anais*, 277-284.

Hartmann, L.A., Tindle, A., and Bitencourt, M.F. (1990) O metamorfismo de fácies anfibolito no Complexo Passo Feio, RS com base em química dos minerais. *Pesquisas*, 17 (1-2), 62-71.

Hasui, Y., Carneiro, C. D. R. and Coimbra, A.M. (1975) The Ribeira Folded Belt. *Revista Brasileira de Geociências*, 5 (4), 257-266.

Ho, S.E., McNaughton, N.J. and Groves, D.I. (1994) Criteria for determining initial lead isotopic compositions of pyrite in Archaean lode-gold deposits: A case study at Victory, Kambalda, Western Australia. *Chemical Geology*, 111, 57-84.

Jost, H. and Hartmann, L.A. (1984) Província Mantiqueira - Setor meridional. In: *O Pré-Cambriano do Brasil,* eds. Almeida F.F.M., Hasui, Y., pp. 345-367. Edgard Blücher, São Paulo, Brazil.

Kolling, S.L., Reischl, J. L. and Feldmann, E. (1983) Ocorrência de cobre com controle estratiforme na Formação Vacacaí, área Picada dos Tocos, Caçapava do Sul-RS. In: Simpósio Sul-Brasileiro de Geologia, 1, Porto Alegre-RS,*Atas,* 336-352.

Lange, S., Choudhuri, S. and Clares, N. (1983) Strontium isotope evidence for the origin of barites and sulphides from the Mississippi Valley-

type ore deposits in southeast Missouri. *Economic Geology,* 78, 1255-1261.

Leinz, V., Barbosa, A.F. and Teixeira, E. (1941) Mapa geológico de Caçapava-Lavras. Secretaria da Agricultura Indústria e Comércio, *Boletim.* 90, 1-39.

Leite, J.A.D., Hartmann, L.A., McNaughton, N.J. and Chemale Jr, F. (1998) SHRIMP U/Pb zircon geochronology of Neoproterozoic juvenile and crustal-reworked terranes in southernmost Brazil. *International Geology Reviews*, 40, 688-705.

Lu, C., Reed, M.H. and Misra, K.C. (1992) Zinc-lead skarn mineralization at Tin Creek, Alaska: Fluid inclusion and skarn-forming reactions. *Geochimica et Cosmochimica Acta*, 56, 109-119.

Mantovani, M.S.M., Hawkesworth, C.J. and Basei, M.A.S. (1987) Nd and Pb isotope studies bearing on the crustal evolution of southeastern Brazil. *Revista Brasileira de Geociências*, 17 (3), 263-268.

McNaughton, N.J. and Bickle, M.J. (1987) K-feldspar Pb-Pb isotope systematics of post-kinematic granitoid intrusions of the Diemals area, central Yilgarn Block, Western Australia: *Chemical Geology*, 66, 193-208.

McNaughton, N.J and Groves, D.I. (1996) A review of Pb-isotope constraints on the genesis of lode-gold deposits in the Yilgarn Craton, Western Australia. *Journal of the Royal Society of Western Australia,* 79, 123-129.

Nardi, L.V.S. and Bitencourt, M.F. (1989) Geologia, petrologia e geoquímica do Complexo Granitico de Caçapava do Sul, RS. *Revista Brasileira de Geociências* 19 (2), 153-169.

Nardi, L.V.S. and Bonin, B. (1991) Post-orogenic and non-orogenic alkaline associations: the Saibro Intrusive Suite, southern Brazil- a case study. *Chemical Geology*, 92, 192-212.

Nardi, L.V.S. and Lima. E.F. (1985) A associação shoshonítica de Lavras do Sul, RS. *Revista Brasileira de Geociências,* 15 (2),139-146.

Ohmoto, H., Kaiser, C.J. and Geer, K.A. (1990) Systematics of sulphur isotopes in recent marine sediments and ancient sediment-hosted basemetal deposits. In: *Stable Isotopes and Fluid Processes in Mineralization*,, Herbert, H. K. & Ho, S. E. (eds). Perth: University of Western Australia Publication, 23, 70-120.

Ohmoto, H. and Rye, R.O. (1979) Isotopes of sulfur and carbon. In: *Geochemistry of hydrothermal ore deposits.* ed. Barnes, H.L., pp. 509-567, Wiley, New York, USA.

Paim, P.S.G., Lopes, R.C. and Chemale Jr., F. (1995) Aloestratigrafia, sistemas deposicionais e evolução paleogeográfica da Bacia do Camaquã - Vendiano Superior/Ordoviciano inferior. In: Simpósio Sul Brasileiro de Geologia, 6, SBG, Porto Alegre, *Boletim de Resumos Expandidos*, 39-50.

Reischl, J.L. (1985) *Ocorrência Andradas Sul*. Unpublished final report, Companhia Brasileira do Cobre, Porto Alegre, RS, 37p.

Remus, M.V.D. and Hartmann, L.A. (1997a) Caracterização do minério do Depósito Santa Bárbara-Rosso, Caçapava do Sul - RS. In: *Caracterização de Minérios e Rejeitos de Depósitos Minerais Brasileiros*. DNPM/DIREX, PADCT/GTM - Ministério das Minas e Energia, Brasília-DF, Resumos Expandidos, 91-98.

Remus, M.V.D., Hartmann; L.A., McNaughton, N.J., Groves, D.I , Reischl, J.L., and Dorneles; N.T (1998a) The Camaquã Cu (Au-Ag) and Santa Maria Pb-Zn (Cu-Ag) Mines of Rio Grande do Sul, southern Brazil — is their mineralization syngenetic, diagenetic or magmatic hydrothermal? *Workshop: Depósitos Minerais Brasileiros de Metais Base,* Salvador, BA, Brazil, 58-67.

Remus, M.V.D., Hartmann, L. A. and Ribeiro, M. (1991) Nota sobre a geologia dos metamorfitos de pressão intermediária e granitóides associados da região de Pinheiro Machado/RS. *Acta Geológica Leopoldensia*, XIV (34), 175-190.

Remus, M.V.D., McNaughton, N.J., Hartmann, L.A. and Fletcher, I.R. (1997b). Zircon SHRIMP U/Pb dating and Nd isotope data of granitoids of the São Gabriel Block, southern Brazil: evidence for an Archaean/Paleoproterozoic basement. In: Second International Symposium on Granite and Associated. Mineralisation. Salvador, BA-Brazil. *Extended Abstracts*, 271-272.

Remus, M.V.D., McNaughton, N.J., Hartmann, L.A. and Groves, D.I. (1996) SHRIMP U/Pb zircon dating at 2448 Ma of the oldest igneous rock in Southern Brazil: identification of the westernmost border of the Dom Feliciano Belt. In: *Symposium on Archaean Terranes of the South America Plataform*. Brasília-DF. Extended Abstracts, 67-70.

Remus, M.V.D., McNaughton, N.J., Hartmann, L.A., Koppe, J.C., Fletcher, I.R.; Groves D.I. and Pinto, V.M. (1998b) Gold in the Neoproterozoic juvenile Bossoroca Volcanic Arc of southernmost Brazil: isotopic constraints on timing and sources. *Journal of South American Earth Sciences* (submitted).

Ribeiro, M. (1968) Investigação preliminar sobre a gênese de algumas ocorrências cupríferas da folha de Bom Jardim. Congresso Brasileiro de Geologia, 22, Belo Horizonte, SBG, *Anais*, 65-73.

Ribeiro, M. (1986) O metamorfismo dos campos termais do Escudo Sul-Riograndense. *Iheringia, Série Geológica,* 11, 15-28.

Ribeiro, M., Bocchi, P.R., Figueiredo Filho, P.M. and Tessari, R.I. (1966) Geologia da quadrícula de Caçapava do Sul, RS, Brasil. *Boletim da Divisão de Geologia e Mineralogia*, DPM-DNPM,127, 1-232.

Ribeiro, M. J. (1991) *Sulfetos em sedimentos detríticos Cambrianos do Rio Grande do Sul, Brasil.* Unpublished Ph.D. Thesis, 416p. Universidade Federal do Rio Grande do Sul, Porto Alegre, RS, Brazil.

Sartori, P.L.P. and Kawashita, K. (1985) Petrologia e geocronologia do batólito granítico de Caçapava do Sul - RS. In: Simpósio Sul-Brasileiro de Geologia, 2, Florianópolis, SC, SBG, *Atas* , 102-115.

Sartori, P.L.P. and Kawashita, K. (1989) Petrologia e geocronologia do stock granítico Santos Ferreira e sua correlação com o batólito de Caçapava do Sul, RS. *Acta Geológica Leopoldensia,* Simpósio Sul-Brasileiro de Geologia, 4, Porto Alegre, RS, SBG, XII (29), 131-142.

Smith, J.B., Barley, M.E., Groves, D.I., Krapez, B., McNaughton, N.J., Bickle M.J. and Chapman, H.J. (1998) The Scholl Shear Zone, West Pilbara; evidence for a domain boundary structure from the integrated tectonostratigraphic analyses, SHRIMP U-Pb dating and isotopic and geochemical data of granitoids. *Precambrian Research,* 88, 143-171.

Soliani, Jr E. (1986) *Os dados geocronológicos do Escudo Sul-Riograndense e suas implicações de ordem geotectônica.* Unpublished Ph.D. Thesis, 239p. Universidade de São Paulo, São Paulo, Brazil.

Stacey, J.S. and Kramers, J.D. (1975) Approximation of terrestrial lead isotope evolution by a two stage model. *Earth Planetary Science Letters,* 26, 207-221.

Teixeira, G. and Gonzales, M.A. (1988) Minas do Camaquã, município de Caçapava do Sul, RS. In: *Principais Depósitos Minerais do Brasil*, eds. Schobbenhaus, C. and Silva Coelho, C.E. 3, 33-41. DNPM/CVRD, Rio de Janeiro, Brazil.

Figure Captions

Fig. 1 Schematic geotectonic map showing the regional setting of the Caçapava Copper District in the Sul-Riograndense Shield (after Jost & Hartmann, 1984; Soliani Jr, 1986; Fragoso Cesar et al., 1986; Babinski et al.,1996).

Fig. 2 Geological map of the Caçapava Copper District showing the main base-metal deposits and prospects (modified from Ribeiro & Carraro, 1971; Camozzato, 1987).

Fig. 3 Concordia diagram of all zircon populations from the albite-muscovite-chlorite schist from the Passo Feio Formation (sample CERR; SHRIMP mounts nº 9528C, and 9529A and B; errors boxes = 1 sigma). The four zircon populations represent Archaean, and Proterozoic inheritance and Neoproterozoic magmatism. The most probable provenances for Paleoproterozoic zircons are also shown.

Fig. 4 Concordia diagram of Neoproterozoic zircon populations from albite-muscovite-chlorite schist (sample CERR; SHRIMP mounts nº 9528C, and 9529A and B; errors boxes = 1 sigma) from the Passo Feio Formation (from Fig. 3). The oldest population (unfilled pattern) is inherited from São Gariel Block rocks, most probably from the Passinho Diorite studied by Leite et al. (1998). The spread in $^{206}Pb/^{238}U$ ages of that population may be related to Pb-loss due to a metamorphic event in the area at ca. 700 Ma (see Fig. 11). Also shown are the zircons from populations with Pb-loss due to the Caçapava Granite intrusion, shearing and metamorphism at ca. 560 Ma (stippled pattern) and to modern weathering (gray pattern).

Fig. 5 SEM images of sectioned zircons from albite-muscovite-chlorite schist (A to F) and dacite dike (G to J) of the Passo Feio Formation. On the left are the BSE

(backscattered electron) images, whereas CL (cathodoluminescence) images of the same grain are shown on the right. Circles and marks indicate areas of analyses; scale bar is 10 μm. The inherited complex zircon in images A and B (grain 529B.5) shows a partially corroded euhedral Archean grain preserved as a core in a Paleoproterozoic rounded grain. Zircon in C-D image (grain 529.B-1) shows an internal igneous zonation and an external morphology suggestive of sedimentary recycling. The zircon images E-F (grain 529.B-3) shows internal igneous sector zoning and an external rounded shape indicating sedimentary recycling. New external faces (lower left) are due to younger metamorphic overgrowth on the detrital grain. The early-Archean inherited zircon G-H (grain 682A.27) shows an internal igneous zonation affected by recrystallization in domains (bottom right); rounding is suggestive of sedimentary processes. The composit zircon in image I-J (grain 682A.3) shows an internal igneous oscillatory zonation overgrown by a younger massive metamorphic rim.

Fig. 6 Concordia diagram of all zircon populations from the dacite dike from the Passo Feio Formation (sample SBG; SHRIMP mount nº 9682A; errors boxes = 1 sigma). The inherited Archean population are the oldest zircons identified in the Sul-Riograndense Shield (grain 682-A.27).

Fig. 7 Concordia diagram of Neoproterozoic zircon populations in the dacite dike (sample SBG; SHRIMP mount nº 9682A; errors boxes = 1 sigma) from the Passo Feio Formation (from Fig. 6). The oldest Neoproterozoic population (unfilled pattern) is interpreted to be inherited from São Gabriel Block rocks, including diorites and TTG associations of the Cerro da Mantiqueiras region studied by Leite et al. (1998), and from acid volcanic rocks from Bossoroca Volcanic Arc (Remus et al, submitted). The black pattern represent inherited igneous zircons affected by regional dynamothermal metamorphism at ca. 700 Ma. The concordant analysis is from a

composite grain (682A.3) shown in I-J images of Figure 5. The light gray pattern population represent zircons that have lost lead due to modern weathering.

Fig. 8 Concordia diagram of zircon populations from the gray-foliated granodiorite facies of the Caçapava Granite batholith (sample FS-5; SHRIMP mounts 9519A and 9520A; errors boxes = 1 sigma). The Paleoproterozoic populations are inherited xenocrysts and the Neoproterozoic zircon group is magmatic. The most probable provenances of Paleoproterozic xenocryst populations are also shown.

Fig. 9 Concordia diagram of the Neoproterozoic zircon populations from the gray-foliated granodiorite facies (sample FS-5; SHRIMP mounts 9519A and 9520A; error boxes = 1 sigma) of Caçapava Granite batholith (from Fig. 8). The oldest zircon group (gray pattern) defines the magmatic age of the granite and is shown in the insert. Two older analyses (stippled pattern) represent xenocrysts, probably partially reset by the magmatic event. The younger ages (unfilled pattern) are from spots in the generally high U-Th rims of magmatic zircons, including high common-Pb grains, and define a trend to the origin of the graph, which is interpreted as Pb-loss due to modern weathering.

Fig. 10 SEM images of sectioned zircons from the gray-foliated granodiorite facies of the Caçapava Granite batholith; backscattered electron images on the left and cathodoluminescence images on the right. Zircons from images A-B (grain 520A.30) and C-D (grain 520A.36) belong to the magmatic population and show concordant ages in the core region and discordant ages in the rims. Zircon in image E-F (grain 520A.5) shows an igneous oscillatory zoning texture both in the core and the rim regions; it has a concordant magmatic age in the core (normal U and Th contents) but a discordant and very young age in the rim (high U and Th contents). Thin dark bands on the rims, both in BSE and CL images, are metamict domains. In image G-F (grain 519A.10), a Paleoproterozoic zircon xenocryst is preserved as a core in the

magmatic grain. The analysed sites (circles in image G-F) of the xenocryst show partial resetting by the magma of the Caçapava Granite. The Paleoproterozoic xenocryst zircon of image I-J (grain 520A.37) shows rounding suggestive of sedimentary recycling before incorporation into the magma.

Fig. 11 Summary of magmatic and tectonic-metamorphic events related to the Brasiliano Cycle in the São Gabriel Block, as registered in zircons of the Passo Feio Formation and Caçapava Granite. The oldest event is represented by detrital zircons from the Passinho Diorite (Leite et al, 1998). Opening of the basin into which Passo Feio Formation was deposited probably occurred at ca. 760 Ma, synchronous with Campestre Formation volcanism (Remus et al., 1998). The closure of the Passo Feio basin and regional dynamothermal metamorphism was at ca. 700 Ma, during TTG magmatism, regional metamorphism and gold deposition in the Bossoroca Volcanic Arc (Remus et al., 1998). The syntectonic Caçapava Granite intruded the supracrustal rocks of the Passo Feio Formation at ca. 560 Ma, during shear zone deformation, and initiated Cu, Pb (Au) sulphide mineralisation.

Fig. 12a $\partial^{34}S‰$ CDT of chalcopyrite, bornite and chalcocite from the Andradas deposit.

Fig. 12b $\partial^{34}S‰$ CDT of chalcopyrite and barite from the Santa Barbara deposit.

Fig. 12c $\partial^{34}S‰$ CDT of pyrite and chalcopyrite from the Coronel Linhares and Cioccari prospects and a galena sample from the Faxinal Prospect.

Fig. 13 Lead isotopic composition of K-feldspar and whole-rocks from the Caçapava Granite and amphibolites, chlorite schists and plagioclase from the Passo Feio Formation. Growth curve of Stacey & Kramers (1975) is shown for comparison.

Fig. 14 Lead isotopic composition of low-Pb sulphides from the Andradas, Santa Barbara, Coronel Linhares and Cioccari deposits and galena from the Faxinal Prospect, in relation to the crustal Pb-evolution model of Stacey & Kramers (1975). Also shown are the fields for the Caçapava Granite, and amphibolites and schists of the Passo Feio Formation. The sulphides show a spread in lead isotopic ratios parallel to the 562 Ma isochron, with the least-radiogenic samples representing the best estimate of initial ratios. The least-radiogenic samples fall between the fields for the amphibolites and Caçapava Granite, and are compatible with Pb derived from the schists, suggesting that Pb was derived from leaching of schists, with possible contributions from the amphibolites and Caçapava Granite during the magmatism at 562 Ma.

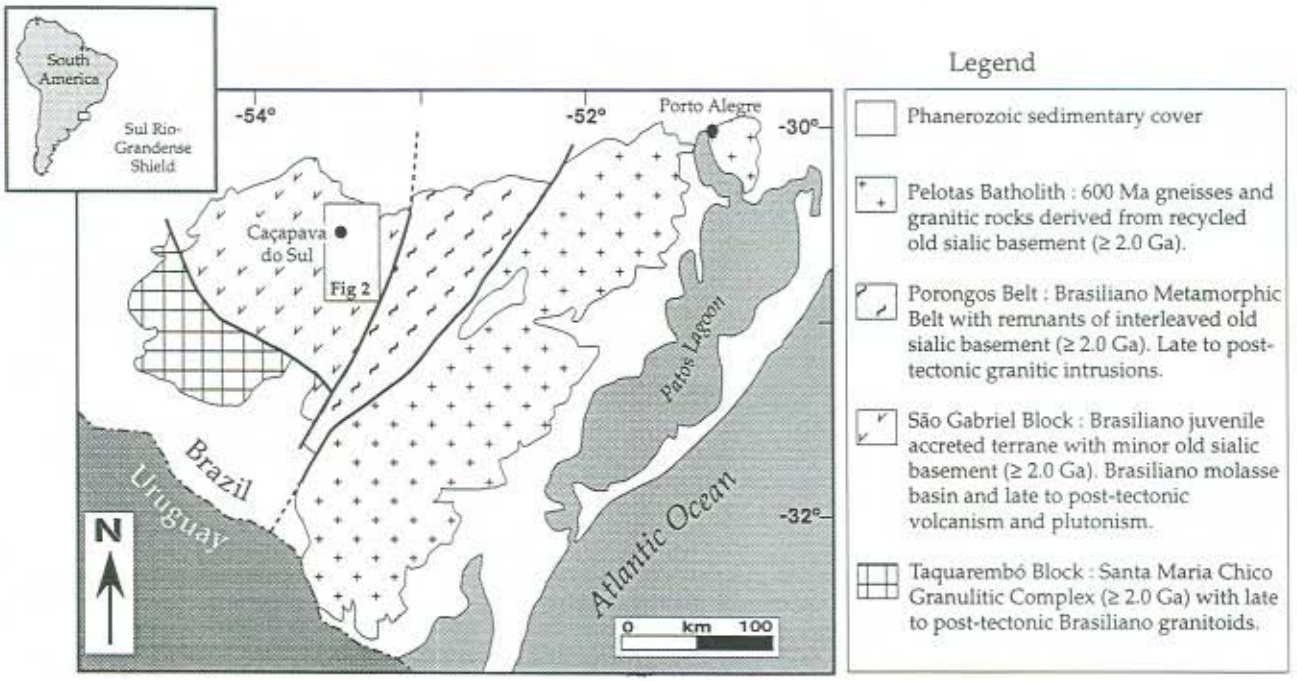
South America
Sul Rio-Grandense Shield
-54°
-52°
-30°
-32°
Porto Alegre
Caçapava do Sul
Fig 2
Patos Lagoon
Brazil
Uruguay
Atlantic Ocean
N
0 km 100
Legend
Phanerozoic sedimentary cover
Pelotas Batholith : 600 Ma gneisses and granitic rocks derived from recycled old sialic basement (≥ 2.0 Ga).
Porongos Belt : Brasiliano Metamorphic Belt with remnants of interleaved old sialic basement (≥ 2.0 Ga). Late to post-tectonic granitic intrusions.
São Gabriel Block : Brasiliano juvenile accreted terrane with minor old sialic basement (≥ 2.0 Ga). Brasiliano molasse basin and late to post-tectonic volcanism and plutonism.
Taquarembó Block : Santa Maria Chico Granulitic Complex (≥ 2.0 Ga) with late to post-tectonic Brasiliano granitoids.

Figura 1

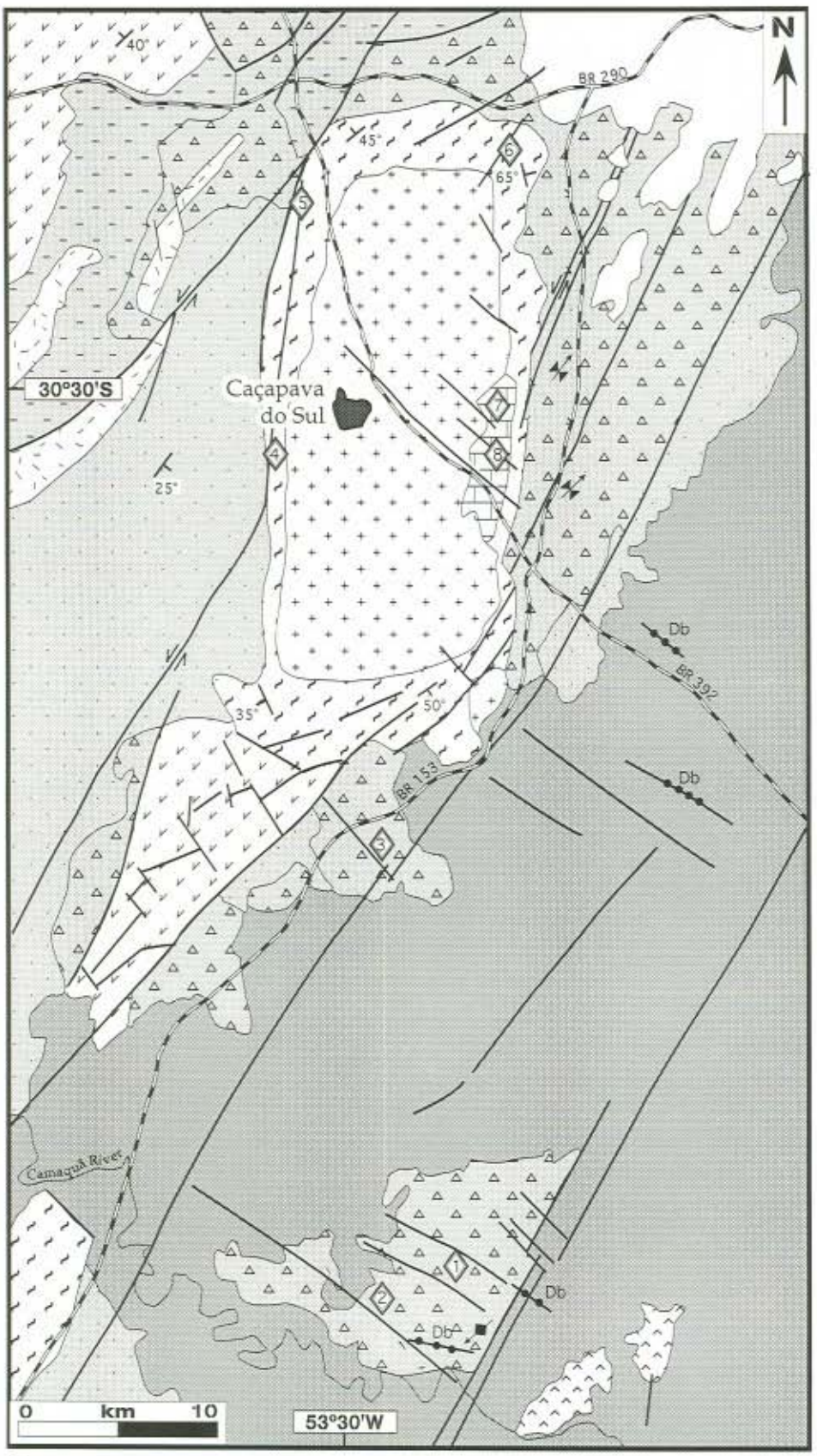

Federal Road
Synform
Antiform
Strike and dip
Fault
Diabase dykes

Paraná Basin

Early Paleozoic
Guaritas Formation
aeolian and lacustrine facies

Rodeio Velho Member (470 Ma)
volcanic andesitic and basic flows

Santa Bárbara Formation
alluvial fans and deltaic facies

Acampamento Velho Formation
acid volcanic rocks

Caçapava Granite (562 Ma)
granodiorite to syenogranite

Neoproterozoic
Bom Jardim Group (594 Ma)
volcano (shoshonitic)-sedimentary clastic sequence

Maricá Formation
marine turbidite and alluvial fans

Vacacaí Group (757 Ma)
juvenile volcanic-arc related rocks

Passo Feio Formation
meta-volcanosedimentary rocks

marble, metamarls

◇ Deposits and prospects

1 - Camaquã Mine - Cu, Au
2 - Santa Maria Deposit - Cu, Pb, Zn, Ag
3 - Cerro dos Martins Deposit - Cu
4 - Andradas Deposit - Cu
5 - Santa Bárbara Deposit - Cu, Au
6 - Faxinal Prospect - Pb, Cu
7 - Coronel Linhares Prospect - Cu, Au
8 - Cioccari Prospect - Cu, Au

Figura 2

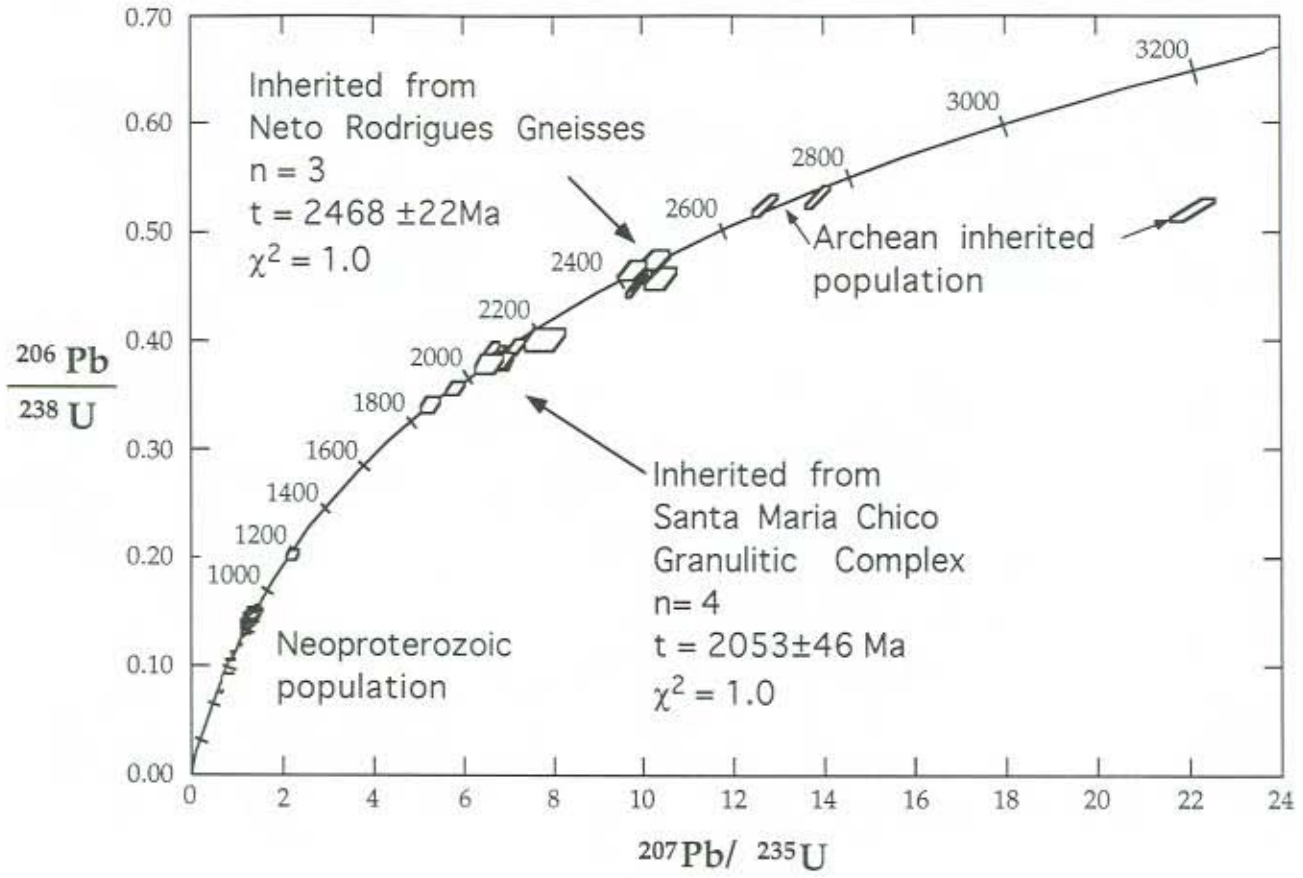
Inherited from
Neto Rodrigues Gneisses
n = 3
t = 2468 ±22Ma
χ² = 1.0
Archean inherited
population
Inherited from
Santa Maria Chico
Granulitic Complex
n= 4
t = 2053±46 Ma
χ² = 1.0
Neoproterozoic
population
206 Pb / 238 U
207 Pb/ 235 U
0.70
0.60
0.50
0.40
0.30
0.20
0.10
0.00
0
2
4
6
8
10
12
14
16
18
20
22
24
1000
1200
1400
1600
1800
2000
2200
2400
2600
2800
3000
3200

Figura 3

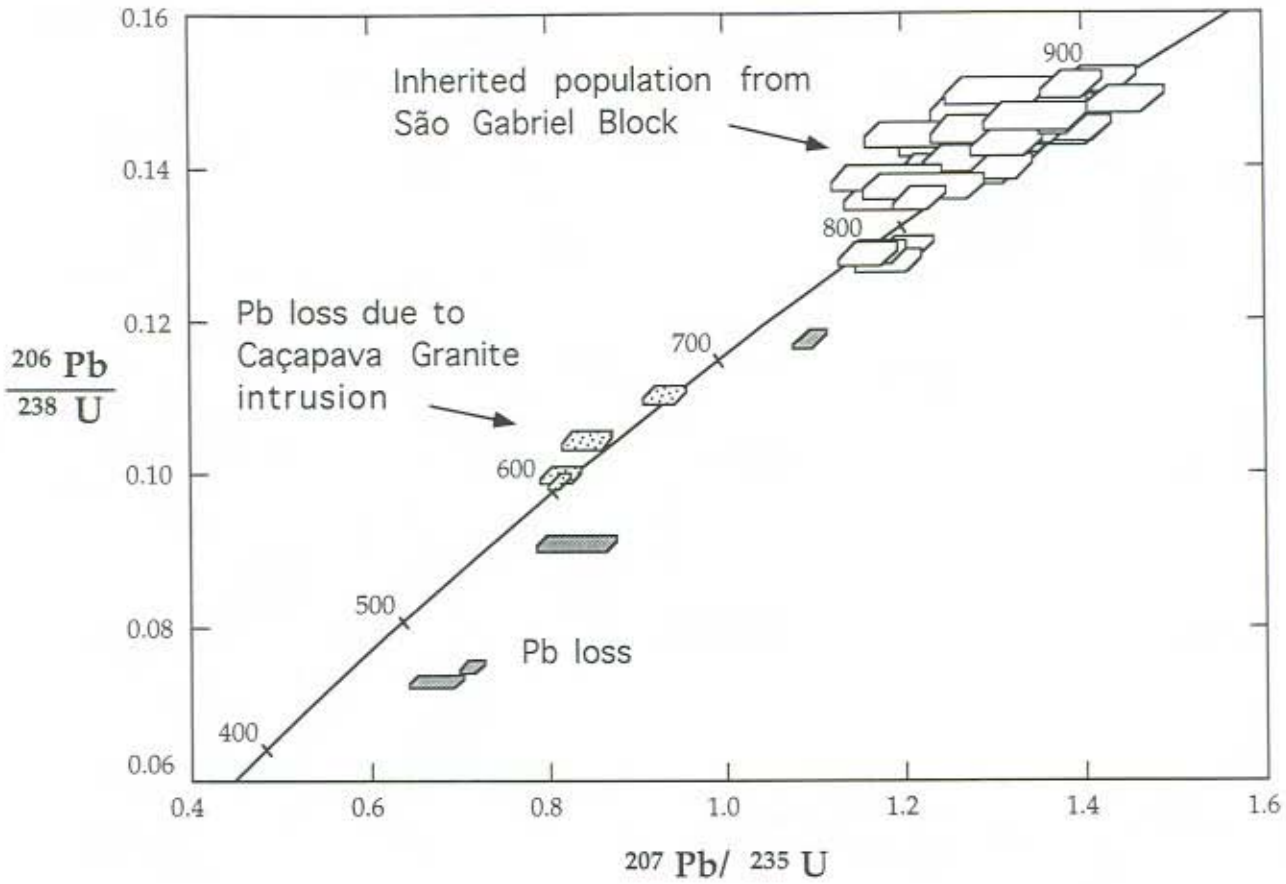
Inherited population from
São Gabriel Block
Pb loss due to
Caçapava Granite
intrusion
Pb loss
900
800
700
600
500
400
0.16
0.14
0.12
0.10
0.08
0.06
0.4
0.6
0.8
1.0
1.2
1.4
1.6
206 Pb / 238 U
207 Pb/ 235 U

Figura 4

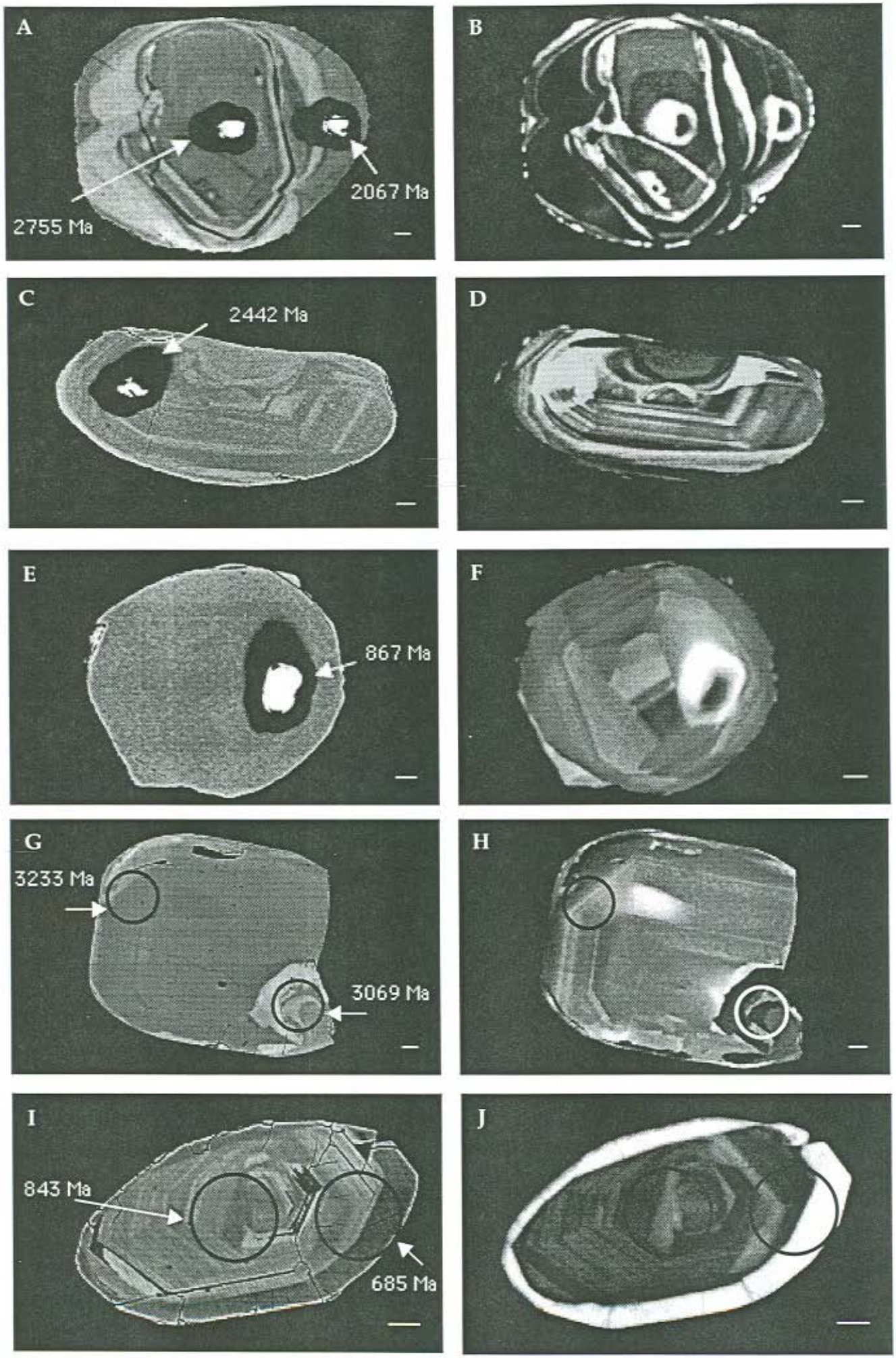
A
2755 Ma
2067 Ma
B
C
2442 Ma
D
E
867 Ma
F
G
3233 Ma
3069 Ma
H
I
843 Ma
685 Ma
J

Figura 5

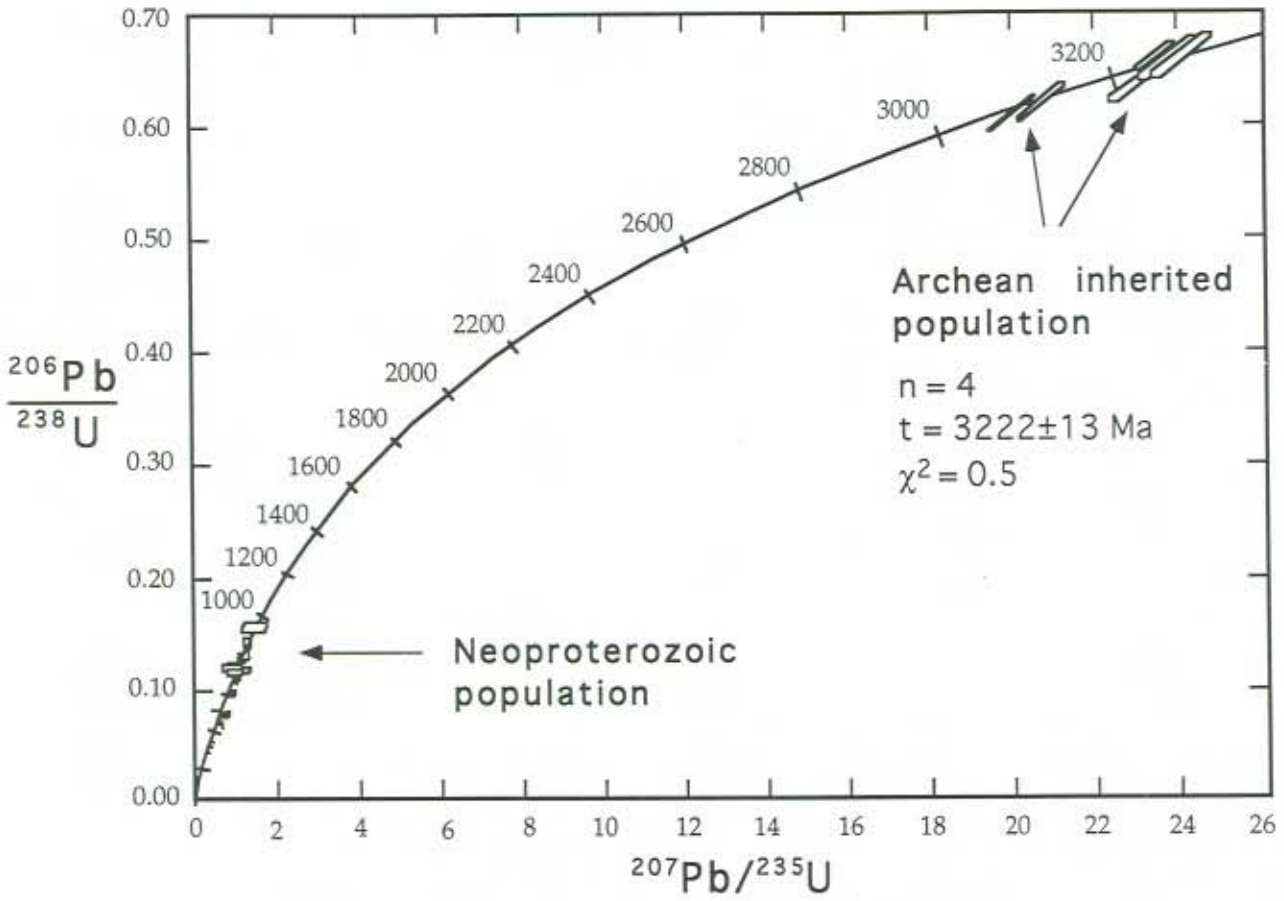
0.70
0.60
0.50
0.40
0.30
0.20
0.10
0.00
206Pb/238U
0
2
4
6
8
10
12
14
16
18
20
22
24
26
207Pb/235U
1000
1200
1400
1600
1800
2000
2200
2400
2600
2800
3000
3200
Archean inherited population
n = 4
t = 3222±13 Ma
χ2 = 0.5
Neoproterozoic population

Figura 6

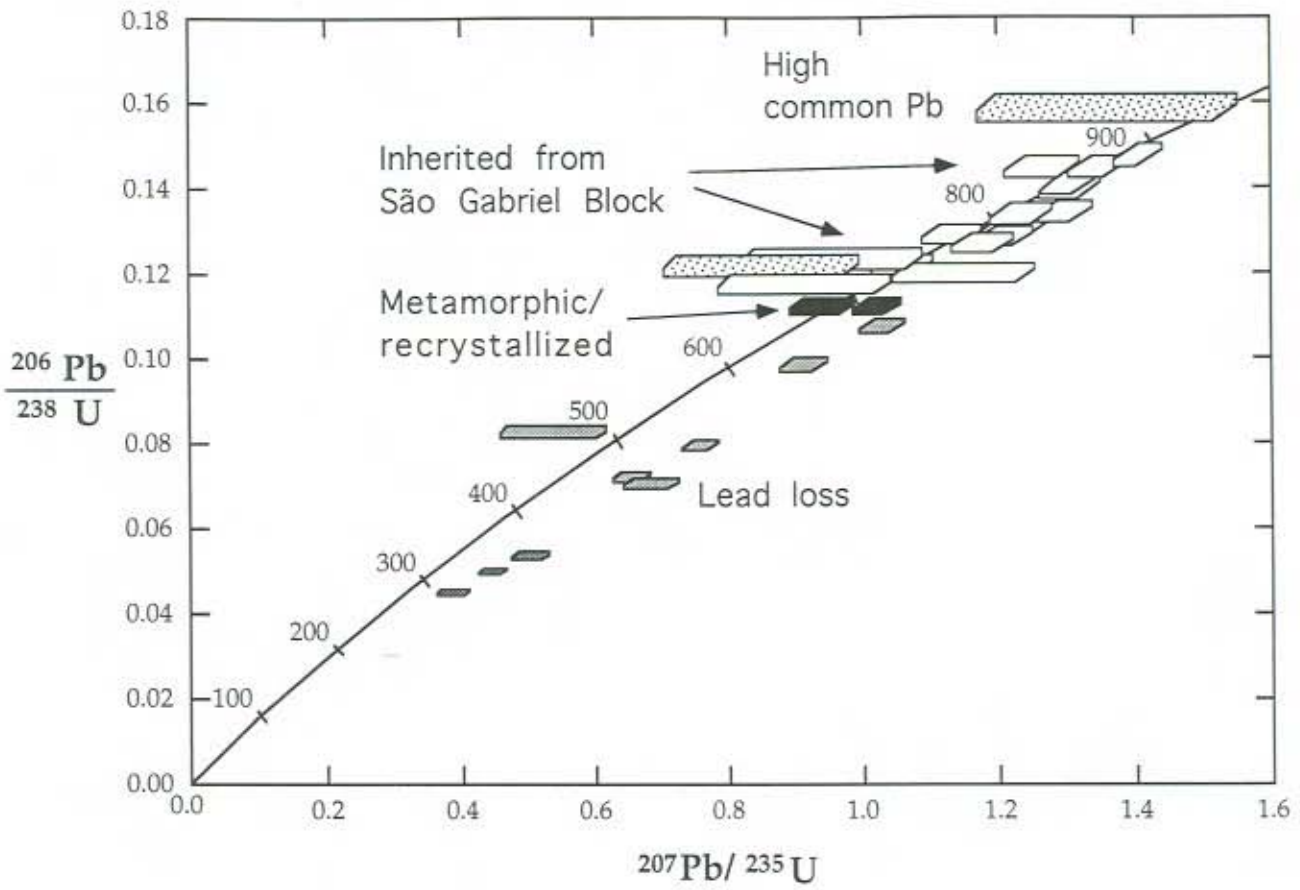
High
common Pb
Inherited from
São Gabriel Block
Metamorphic/
recrystallized
Lead loss
900
800
600
500
400
300
200
100
0.18
0.16
0.14
0.12
0.10
0.08
0.06
0.04
0.02
0.00
0.0
0.2
0.4
0.6
0.8
1.0
1.2
1.4
1.6
206 Pb / 238 U
207 Pb / 235 U

Figura 7

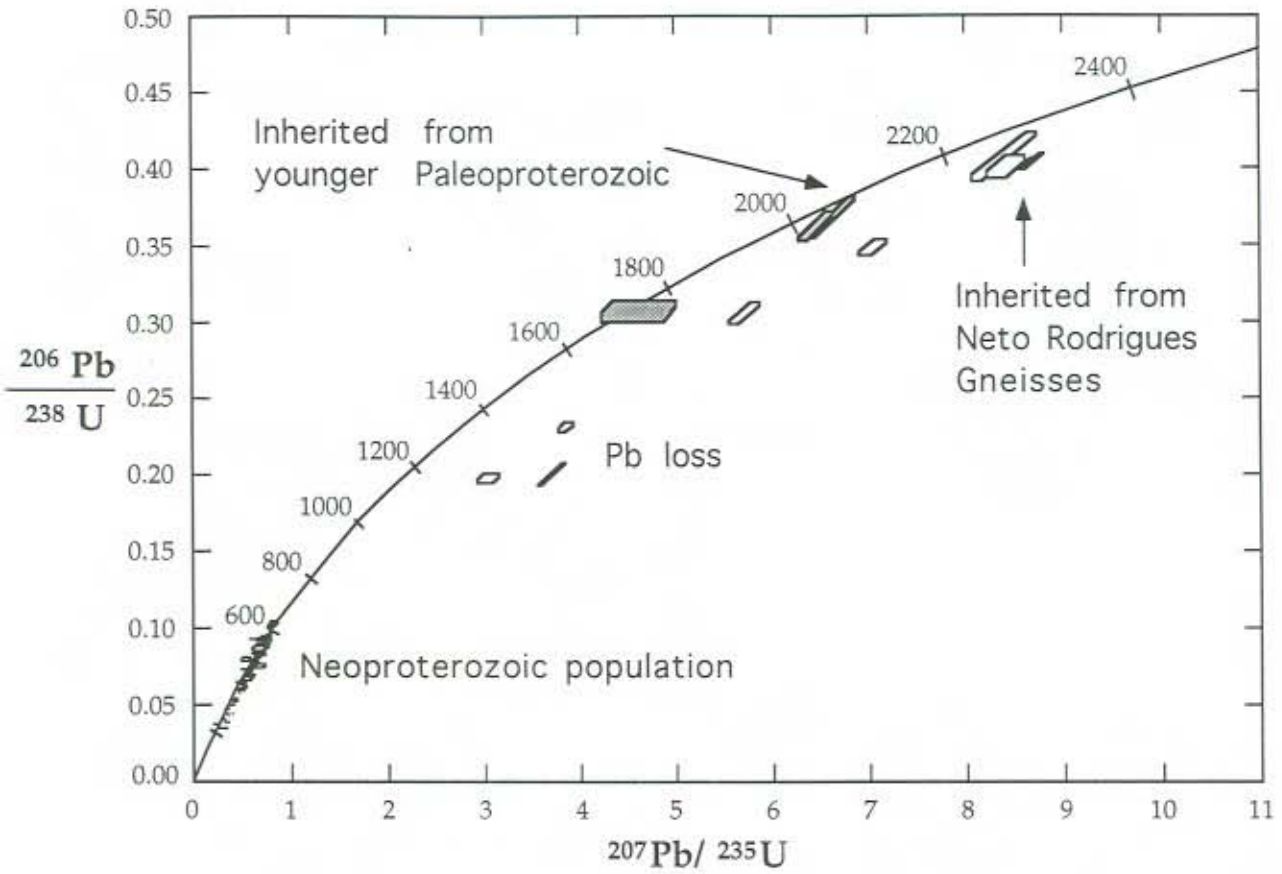
0.50
0.45
0.40
0.35
0.30
0.25
0.20
0.15
0.10
0.05
0.00
206 Pb / 238 U
0
1
2
3
4
5
6
7
8
9
10
11
207Pb/ 235U
2400
2200
2000
1800
1600
1400
1200
1000
800
600
Inherited from younger Paleoproterozoic
Inherited from Neto Rodrigues Gneisses
Pb loss
Neoproterozoic population

Figura 8

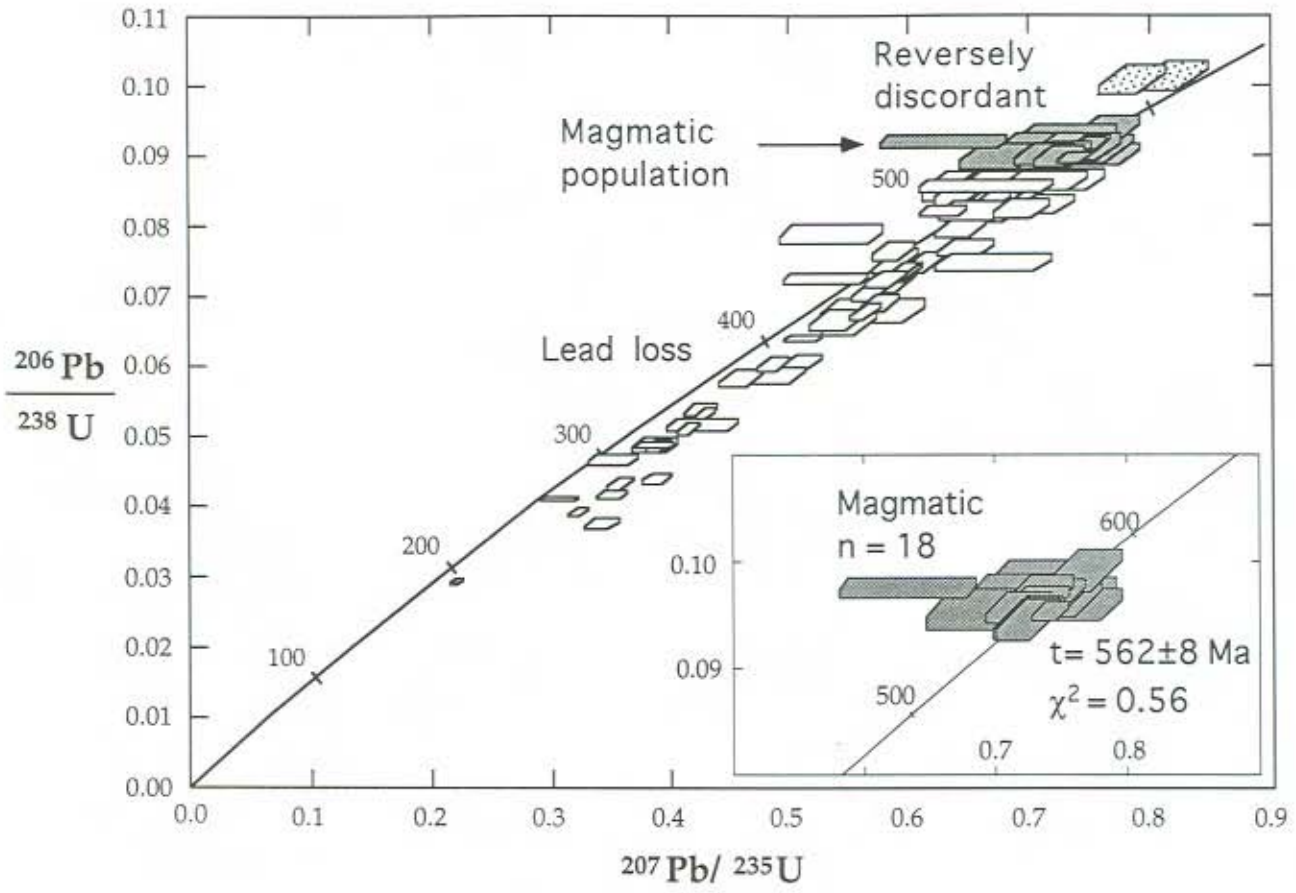
Reversely
discordant
Magmatic
population
Lead loss
Magmatic
n = 18
t= 562±8 Ma
χ² = 0.56
206 Pb / 238 U
207 Pb/ 235 U

Figura 9

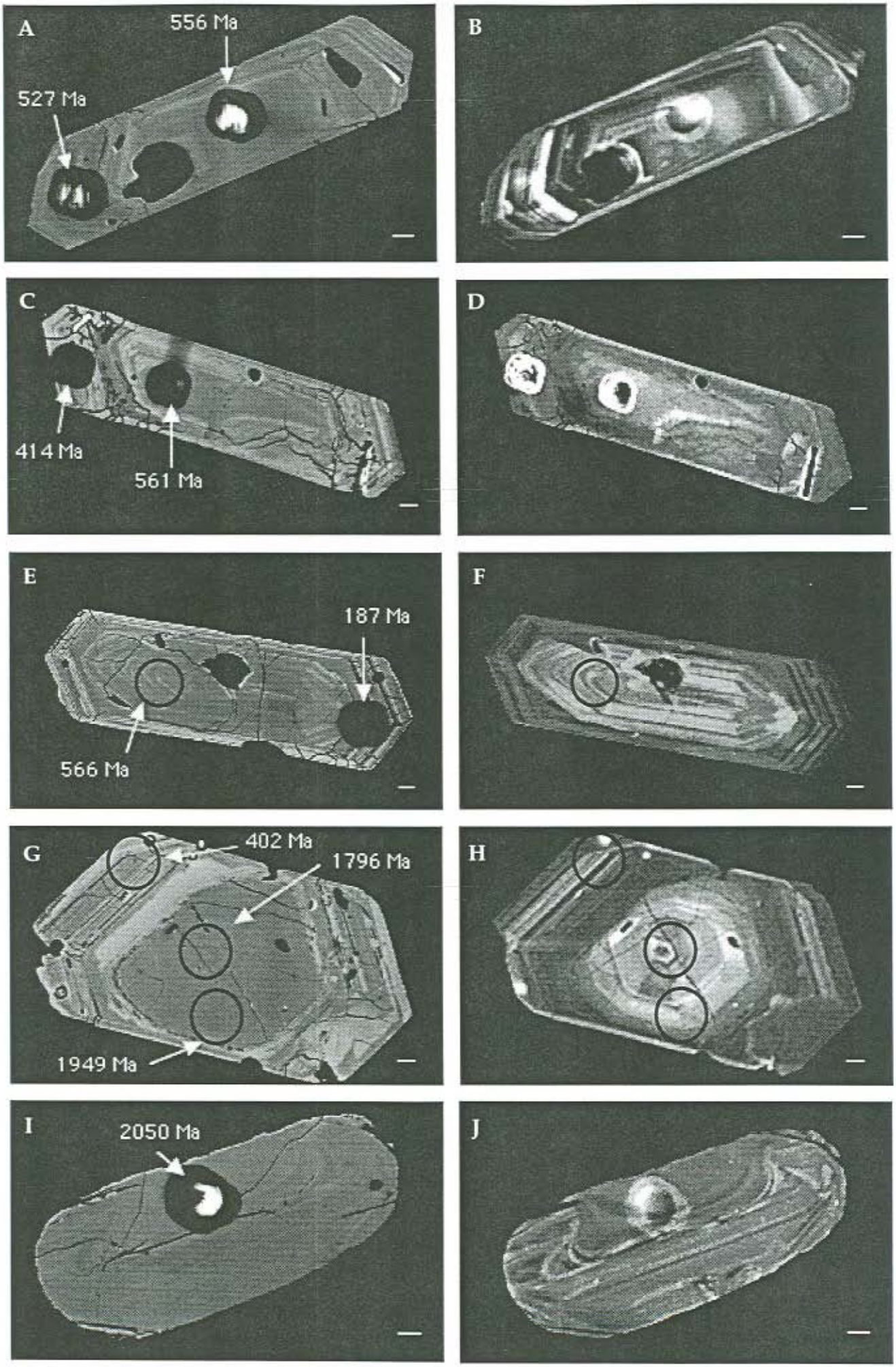
A
556 Ma
527 Ma
B
C
414 Ma
561 Ma
D
E
187 Ma
566 Ma
F
G
402 Ma
1796 Ma
1949 Ma
H
I
2050 Ma
J

Figura 10

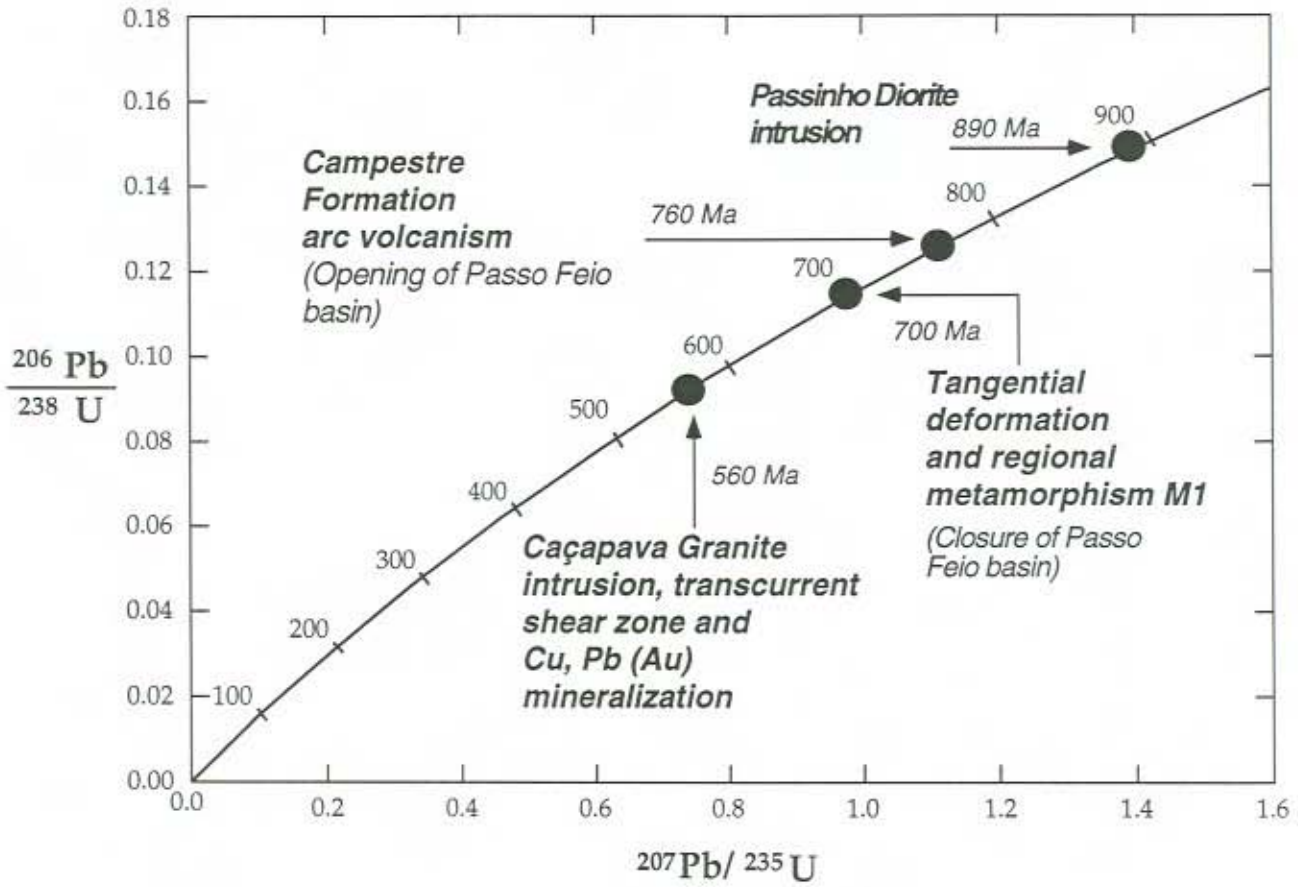
Passinho Diorite intrusion
890 Ma
900
800
760 Ma
Campestre Formation arc volcanism
(Opening of Passo Feio basin)
700
700 Ma
600
500
560 Ma
Tangential deformation and regional metamorphism M1
(Closure of Passo Feio basin)
400
300
200
100
Caçapava Granite intrusion, transcurrent shear zone and Cu, Pb (Au) mineralization
0.18
0.16
0.14
0.12
0.10
0.08
0.06
0.04
0.02
0.00
0.0
0.2
0.4
0.6
0.8
1.0
1.2
1.4
1.6
206 Pb / 238 U
207 Pb/ 235 U

Figura 11

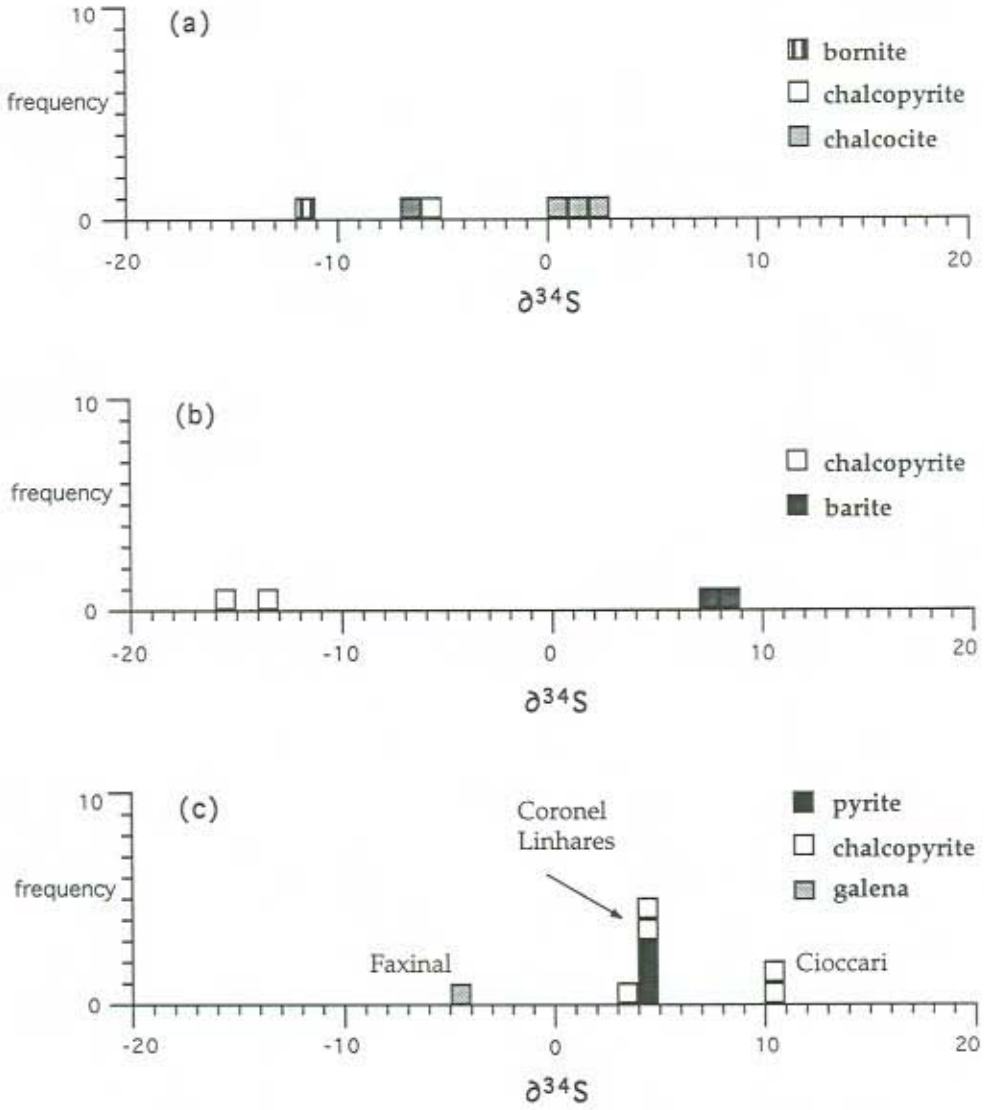
(a)
bornite
chalcopyrite
chalcocite
frequency
10
0
-20
-10
0
10
20
∂34S
(b)
chalcopyrite
barite
frequency
10
0
-20
-10
0
10
20
∂34S
(c)
Coronel
Linhares
pyrite
chalcopyrite
galena
Faxinal
Cioccari
frequency
10
0
-20
-10
0
10
20
∂34S

Figura 12

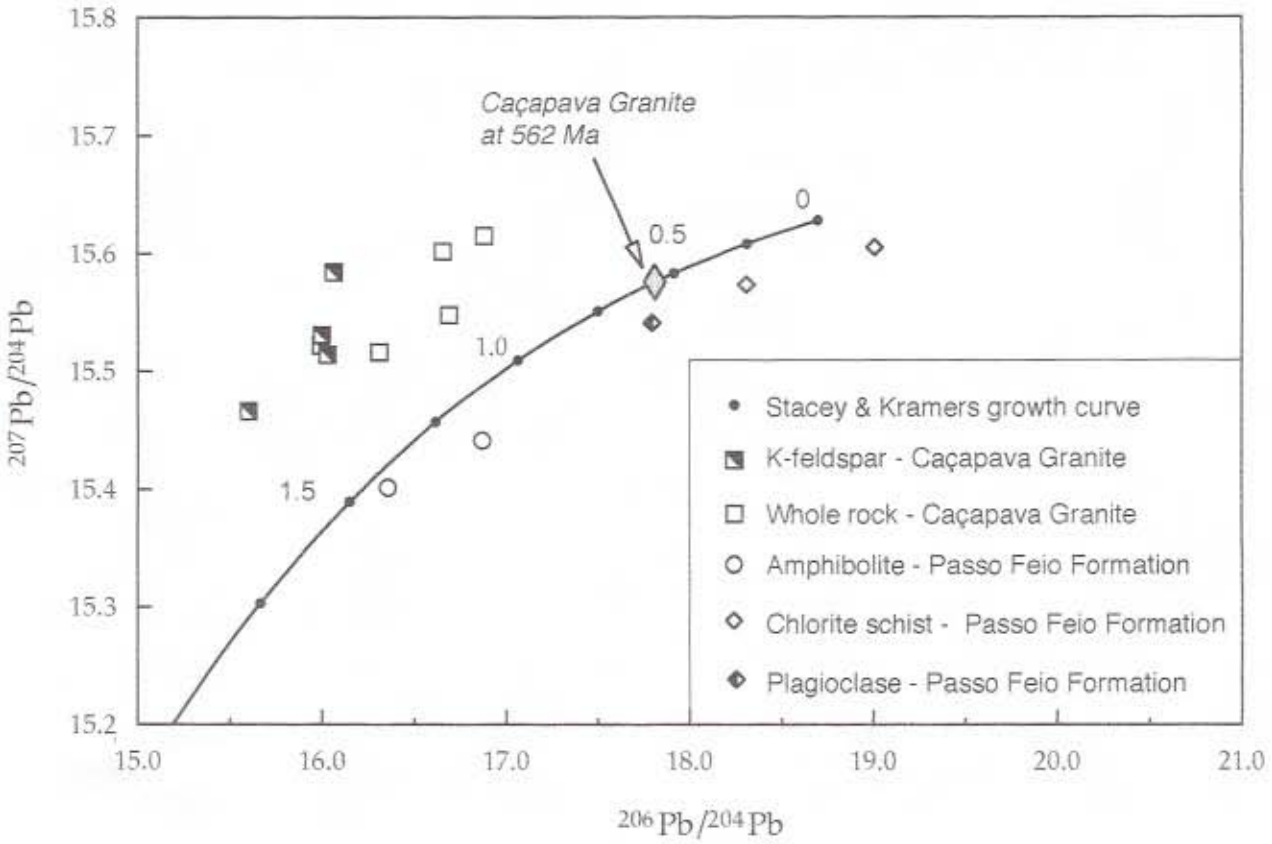
Caçapava Granite
at 562 Ma
0
0.5
1.0
1.5
Stacey & Kramers growth curve
K-feldspar - Caçapava Granite
Whole rock - Caçapava Granite
Amphibolite - Passo Feio Formation
Chlorite schist - Passo Feio Formation
Plagioclase - Passo Feio Formation
15.8
15.7
15.6
15.5
15.4
15.3
15.2
15.0
16.0
17.0
18.0
19.0
20.0
21.0
207Pb/204Pb
206Pb/204Pb

Figura 13

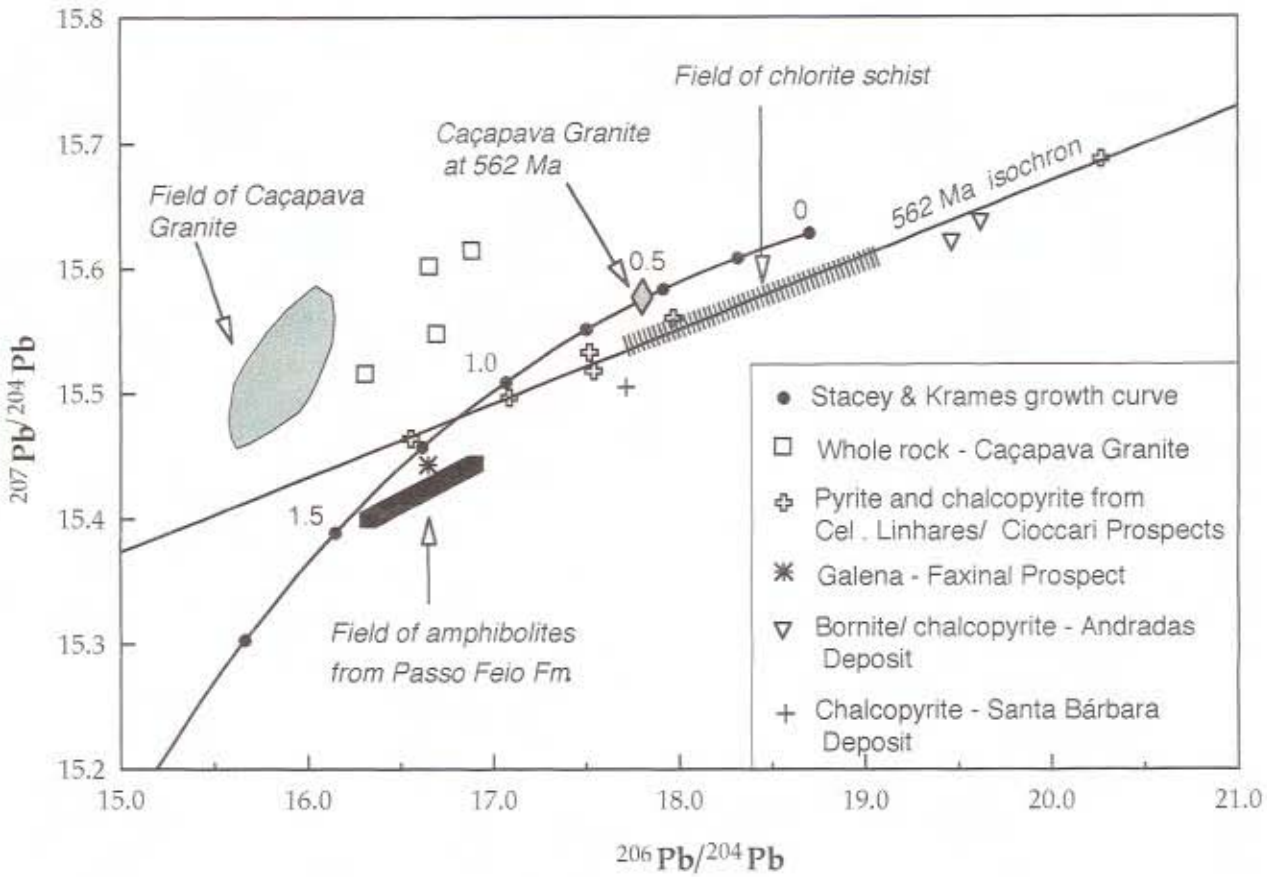
Field of chlorite schist
Caçapava Granite at 562 Ma
Field of Caçapava Granite
562 Ma isochron
0
0.5
1.0
1.5
Field of amphibolites from Passo Feio Fm
Stacey & Krames growth curve
Whole rock - Caçapava Granite
Pyrite and chalcopyrite from Cel . Linhares/ Cioccari Prospects
Galena - Faxinal Prospect
Bornite/ chalcopyrite - Andradas Deposit
Chalcopyrite - Santa Bárbara Deposit
15.8
15.7
15.6
15.5
15.4
15.3
15.2
15.0
16.0
17.0
18.0
19.0
20.0
21.0
207Pb/204Pb
206Pb/204Pb

Fig. 14

Table Captions

Table 1 SHRIMP U/Pb data on zircons from albite-muscovite-chlorite schist from the Passo Feio Formation (sample CERR; SHRIMP mounts nº 9528C, and 9529A and B; errors = 1 sigma)

Table 2 SHRIMP U/Pb data on zircons from dacitic dike of the Passo Feio Formation (sample SBG; SHRIMP mount nº 9682A; errors = 1 sigma)

Table 3 SHRIMP U/Pb on zircons from the gray-foliated granodiorite facies of the Caçapava Granite (sample FS-5; SHRIMP mounts 9519A and 9520A; errors = 1 sigma)

Table 4 $\partial^{34}S‰$ CDT and lead isotope data for sulphides and barites from base-metal deposits in the Passo Feio Formation. A total analytical error is ± 0.15% to each Pb-isotope ratio.

Table 5 Lead isotope compositions and SiO2 (wt %), U, Th and Pb (ppm) concentrations for Caçapava Granite and Passo Feio Formation whole-rocks and minerals. A total analytical error is ± 0.15% to each Pb-isotope ratio.

Table 6 Strontium isotope composition of barites from the Santa Bárbara deposit. The values are measured ratios and the analycal error is ±0.00010.

Table 1

grain-spot	U (ppm)	Th (ppm)	Th U	4f206 (%)	207*/206*	+/-	208*/206*	+/-	206*/238	+/-	207*/235	+/-	208*/232	+/-	conc. %	207*/206* Age (Ma)	+/-	206*/238 Age (Ma)	+/-
Archaean inherited																			
529B.5-2	195	116	0.60	0.054	0.1915	11	0.1557	11	0.5297	61	13.9827	1876	0.1382	20	99	2755	9	2740	26
528C.33-1	89	36	0.41	0.295	0.1777	12	0.1089	20	0.5226	65	12.8021	1895	0.1394	33	103	2631	11	2710	28
Inherited from Neto Rodrigues Gneisses																			
529B.13-1	31	28	0.89	0.493	0.1665	27	0.2446	44	0.4555	65	10.4574	2415	0.1246	31	96	2523	28	2419	29
528C.7-1	266	186	0.70	0.092	0.1628	5	0.1674	9	0.4673	54	10.4899	1299	0.1117	15	99	2485	6	2472	24
528C.12-1	222	16	0.07	0.052	0.1618	6	0.0195	7	0.4468	52	9.9677	1258	0.1217	46	96	2475	6	2381	23
528C.6-1	84	101	1.20	0.154	0.1616	11	0.2955	25	0.4601	57	10.2494	1526	0.1133	18	99	2472	11	2440	25
528C.27-1	201	196	0.97	0.095	0.1603	6	0.2630	13	0.4516	53	9.9832	1280	0.1223	17	98	2459	7	2402	23
529B.1-1	67	62	0.92	0.079	0.1587	24	0.2488	45	0.4723	59	10.3339	2151	0.1278	30	102	2442	26	2494	26
529B.18-1	38	38	0.99	0.25	0.1538	23	0.2657	37	0.4624	64	9.8081	2117	0.1243	27	103	2389	25	2450	28
Inherited from Santa Maria Chico Granulitic Complex																			
529B.19-1	16	8	0.51	-0.395	0.1411	47	0.1644	89	0.4001	63	7.7820	3022	0.1279	75	97	2241	58	2169	29
529B.8-1	134	24	0.18	-0.032	0.1344	15	0.0521	19	0.3780	44	7.0036	1195	0.1124	45	96	2156	19	2067	21
529B.8-2	77	22	0.28	0.144	0.1334	17	0.0775	23	0.3916	46	7.2039	1310	0.1079	35	99	2143	22	2130	21
529B.15-1	32	39	1.21	-0.13	0.1297	32	0.3356	67	0.3804	54	6.8028	2044	0.1052	27	99	2094	44	2078	25
529B.5-1	174	48	0.28	0.039	0.1277	11	0.0748	14	0.3867	44	6.8088	1037	0.1049	24	102	2067	15	2107	21
529B.15-2	28	31	1.11	-0.152	0.1261	35	0.3194	71	0.3772	54	6.5588	2125	0.1085	31	101	2045	48	2063	25
529B.7-1	71	139	1.95	0.007	0.1244	15	0.5445	37	0.3892	47	6.6771	1200	0.1085	16	105	2021	21	2119	22
529B.7-2	64	53	0.82	0.333	0.1196	22	0.2277	41	0.3535	43	5.8288	1360	0.0976	22	100	1950	33	1951	20
529.11-1	30	21	0.67	0.11	0.1125	17	0.1904	46	0.3392	47	5.2598	1518	0.0957	28	102	1840	43	1883	23
529B.2-1	83	40	0.48	0.159	0.0794	27	0.1459	54	0.2017	24	2.2089	818	0.0608	24	100	1183	66	1184	13
Inherited from São Gabriel Block																			
529B.4-1	148	127	0.86	0.16	0.0682	17	0.2580	38	0.1512	17	1.4206	413	0.0455	9	104	873	53	908	10
529A.22-2	187	215	1.15	0.074	0.0670	13	0.3427	33	0.1504	18	1.3893	343	0.0448	7	108	838	42	903	10
528C.32-1	101	46	0.46	1.529	0.0637	29	0.1205	68	0.1496	18	1.3147	646	0.0394	23	123	733	98	899	10
529.12-1	75	58	0.78	0.014	0.0707	18	0.2382	35	0.1486	18	1.4491	422	0.0454	9	94	950	51	893	10
528C.3-2	337	210	0.62	0.073	0.0685	6	0.1645	16	0.1474	17	1.3922	215	0.0388	6	100	884	19	886	9
528C.29-1	136	89	0.66	1.055	0.0630	22	0.1916	52	0.1474	17	1.2809	485	0.0429	13	125	709	73	886	10
529B.17-1	182	124	0.68	0.171	0.0675	14	0.2008	30	0.1473	18	1.3708	353	0.0433	8	104	854	44	886	10
528C.22-1	349	316	0.91	0.091	0.0681	7	0.2743	20	0.1472	17	1.3824	220	0.0446	6	102	872	20	885	9
529A.23-1	81	47	0.57	0.292	0.0670	26	0.1614	54	0.1462	18	1.3497	571	0.0411	15	105	836	81	880	10
528C.8-1	147	82	0.56	0.524	0.0655	16	0.1613	37	0.1458	17	1.3170	365	0.0420	11	111	791	50	877	10
529A.22-1	387	309	0.80	0.165	0.0687	10	0.2477	21	0.1456	17	1.3800	270	0.0450	7	98	891	29	876	10
528C.21-1	144	70	0.49	0.149	0.0680	14	0.1507	34	0.1448	17	1.3579	346	0.0446	12	100	869	44	872	9
528C.13-1	86	33	0.38	0.3	0.0694	22	0.1131	50	0.1447	17	1.3853	487	0.0434	20	96	911	65	871	10
528C.23-1	152	113	0.74	0.205	0.0702	12	0.2244	32	0.1447	17	1.4013	313	0.0437	9	93	935	36	871	9
529.10-1	119	80	0.67	0.214	0.0639	18	0.1995	39	0.1445	18	1.2732	413	0.0431	10	118	738	61	870	10
528.19-2	102	60	0.59	0.333	0.0692	22	0.1870	54	0.1443	17	1.3770	493	0.0456	15	96	904	67	869	10
528C.30-1	229	138	0.61	0.129	0.0684	11	0.1860	26	0.1443	17	1.3617	277	0.0444	8	99	882	32	869	9
529B.3-1	60	30	0.50	1.026	0.0627	41	0.1375	88	0.1439	17	1.2440	849	0.0392	26	124	697	140	867	10
528.19-1	198	196	0.99	0.128	0.0683	10	0.2976	29	0.1433	16	1.3502	264	0.0431	7	98	878	30	863	9
528.18-1	241	186	0.77	0.352	0.0671	12	0.2392	30	0.1431	16	1.3233	290	0.0445	8	103	840	36	862	9
528C.24-1	88	53	0.60	0.945	0.0634	24	0.1728	58	0.1429	17	1.2495	520	0.0411	15	119	723	81	861	10
529B.14-1	135	97	0.72	0.314	0.0669	18	0.2149	37	0.1428	17	1.3172	400	0.0427	9	103	834	55	861	10
528C.2-1	169	55	0.33	0.159	0.0680	14	0.0986	32	0.1421	16	1.3318	337	0.0430	15	99	867	44	857	9
528C.11-1	131	82	0.63	0.222	0.0675	14	0.1941	35	0.1407	16	1.3102	322	0.0436	10	99	855	42	849	9
529.9-2	145	135	0.93	0.192	0.0650	17	0.2674	37	0.1407	17	1.2617	372	0.0405	8	110	775	54	849	10
528C.26-1	116	42	0.36	0.323	0.0679	17	0.1122	39	0.1398	17	1.3087	382	0.0438	17	98	865	53	844	9
528C.25-1	80	43	0.54	0.442	0.0650	27	0.1634	63	0.1396	17	1.2518	550	0.0420	17	109	775	86	842	10
528C.14-1	167	110	0.66	0.242	0.0679	13	0.2047	33	0.1391	16	1.3027	306	0.0434	9	97	865	40	840	9
529B.20-1	71	78	1.10	0.698	0.0621	31	0.3188	73	0.1383	17	1.1834	622	0.0402	11	123	677	106	835	10
528C.4-1	261	172	0.66	0.108	0.0674	8	0.1687	20	0.1375	16	1.2782	221	0.0352	6	98	850	24	831	9
529B.20-2	74	103	1.39	0.678	0.0647	34	0.4126	84	0.1372	17	1.2250	674	0.0407	10	108	766	110	829	10
528C.15-1	131	94	0.72	0.636	0.0631	17	0.2158	42	0.1361	16	1.1843	359	0.0407	10	116	712	57	823	9
528C.16-1	74	49	0.65	0.879	0.0635	26	0.1889	63	0.1358	16	1.1891	524	0.0392	14	113	725	87	821	9
529B.21-2	221	140	0.64	-0.021	0.0652	13	0.1900	26	0.1357	16	1.2200	295	0.0405	8	105	781	41	820	9
528.17-1	205	151	0.73	0.542	0.0676	14	0.2266	35	0.1294	15	1.2052	300	0.0399	8	92	855	43	784	8
529B.9-1	209	252	1.21	0.785	0.0659	17	0.3767	43	0.1288	15	1.1701	352	0.0402	66	97	804	56	781	8
529B.21-1	219	111	0.51	0.085	0.0657	16	0.1529	33	0.1284	15	1.1628	334	0.0386	10	98	796	52	779	9
528.17-2	270	364	1.35	1.659	0.0674	19	0.4231	49	0.1276	15	1.1853	369	0.0401	7	91	849	57	774	8
Pb-loss due to Caçapava Granite intrusion																			
528C.28-1	208	85	0.41	0.371	0.0615	14	0.1278	33	0.1102	13	0.9339	249	0.0346	10	103	655	49	674	7
528C.1-1	158	154	0.97	0.488	0.0588	18	0.2793	48	0.1043	12	0.8450	283	0.0299	6	114	559	66	639	7
528C.20-1	197	83	0.42	0.324	0.0593	15	0.1278	35	0.0997	11	0.8149	233	0.0301	9	106	578	54	613	7
528C.31-1	666	355	0.53	0.115	0.0596	6	0.1663	15	0.0989	11	0.8132	129	0.0308	5	103	590	22	608	6
Pb-loss due to modern weathering																			
528C.9-1	331	200	0.61	0.175	0.0677	8	0.1745	21	0.1174	13	1.0968	194	0.0338	6	83	861	26	716	8
528C.5-1	110	190	1.72	1.053	0.0664	35	0.4316	92	0.0908	11	0.8313	464	0.0228	6	68	819	111	560	6
529B.6-1	1494	1094	0.73	1.457	0.0693	11	0.2210	25	0.0746	8	0.7130	147	0.0225	4	51	908	33	464	5
528C.10-1	459	456	0.99	4.106	0.0669	29	0.3541	70	0.0728	8	0.6720	306	0.0259	6	54	836	89	453	5

CZ3 = 9528C, 06/12/95 (±1.11% 1 sigma, n=11) and 9529A and B, 30/12/95 (± 1.18% 1 sigma, n= 5)

4f206 = Proportion of Pb-206 calculated to be common Pb; %conc. = Concordance, as 100t[206*/238]/t[207*/206*].

Table 2

grain-spot	U (ppm)	Th (ppm)	Th U	4f206 (%)	207*/206*	+/-	208*/206*	+/-	206*/238	+/-	207*/235	+/-	208*/232	+/-	conc %	207*/206* Age (Ma)	+/-	206*/238 Age (Ma)	+/-
Archean inherited																			
82A.27-1	121	74	0.61	0.226	0.2577	15	0.1567	22	0.6691	129	23.7716	4941	0.1712	45	102	3233	9	3302	50
82A.18-2	121	80	0.66	0.071	0.2558	13	0.1682	19	0.6622	127	23.3592	4784	0.1677	41	102	3221	8	3276	49
82A.18-1	130	81	0.63	0.084	0.2556	13	0.1604	18	0.6457	123	22.7569	4606	0.1655	40	100	3220	8	3211	48
82A.19-1	116	68	0.59	0.032	0.2551	13	0.1529	17	0.6672	130	23.4630	4884	0.1740	44	102	3216	8	3295	50
82A.12-1	296	37	0.13	0.082	0.2367	8	0.0327	8	0.6267	114	20.4560	3869	0.1627	52	101	3098	5	3136	45
82A.27-2	810	122	0.15	0.011	0.2324	5	0.0402	3	0.6165	110	19.7539	3592	0.1652	34	101	3069	3	3096	44
Partially reset xenocryst																			
82A.9-2	91	88	0.97	2.127	0.0627	85	0.1494	200	0.1582	33	1.3677	1922	0.0244	33	136	698	294	947	18
Inherited from São Gabriel Block																			
82A.15-1	299	147	0.49	0.111	0.0696	11	0.1462	26	0.1472	26	1.4126	360	0.0439	12	97	917	33	885	15
82A.25-1	165	108	0.66	0.836	0.0639	23	0.1851	57	0.1444	27	1.2720	546	0.0408	15	118	738	78	870	15
82A.28-1	220	96	0.44	0.128	0.0680	16	0.1296	37	0.1445	26	1.3541	425	0.0427	15	100	867	49	870	15
82A.9-1	220	128	0.58	0.298	0.0676	15	0.1654	37	0.1404	26	1.3092	402	0.0399	12	99	857	47	847	14
82A.3-2	242	137	0.57	0.339	0.0681	18	0.1628	43	0.1397	25	1.3126	444	0.0401	13	97	873	55	843	14
82A.24-1	266	158	0.59	0.156	0.0705	17	0.1774	40	0.1341	24	1.3040	413	0.0400	12	86	944	49	811	14
82A.31-1	252	186	0.74	0.514	0.0674	20	0.1777	47	0.1335	24	1.2409	451	0.0321	11	95	851	61	808	14
82A.7-1	293	979	3.34	0.911	0.0684	22	0.2274	53	0.1305	24	1.2310	476	0.0089	3	90	881	66	791	13
82A.4-2	343	304	0.88	0.506	0.0679	14	0.1918	36	0.1296	23	1.2133	359	0.0281	7	91	866	44	786	13
82A.6-1	299	187	0.62	0.809	0.0641	20	0.1471	47	0.1289	23	1.1382	433	0.0304	11	105	744	66	781	13
82A.9-1b	237	216	0.91	0.276	0.0688	19	0.1725	45	0.1282	23	1.2167	422	0.0243	8	87	893	56	778	13
82A.21-1	196	133	0.68	0.589	0.0678	21	0.1224	49	0.1267	23	1.1849	449	0.0228	10	89	864	64	769	13
82A.10-2	64	1	0.01	1.004	0.0566	78	-0.0076	177	0.1230	25	0.9599	1362	-0.0839	-1956	157	476	308	748	14
82A.8-1	220	40	0.18	0.491	0.0634	22	0.0338	49	0.1218	22	1.0653	445	0.0225	33	103	722	75	741	13
82A.22-1	51	1	0.01	2.82	0.0510	84	-0.0304	191	0.1215	26	0.8544	145	-0.3521	-2243	306	241	292	739	15
82A.10-1	87	0	0.00	-0.62	0.0700	61	0.0221	137	0.1198	24	1.1568	1057	0.6837	4328	78	930	179	729	14
82A.26-1	81	1	0.02	1.897	0.0569	77	-0.0139	175	0.1172	24	0.9190	1282	-0.1014	-1281	147	486	302	715	14
Metamorphic/recrystallized																			
82A.3-1	241	199	0.83	1.424	0.0612	27	0.1660	65	0.1121	20	0.9461	474	0.0225	10	106	646	96	685	12
82A.23-1	383	320	0.84	0.976	0.0666	18	0.1653	43	0.1119	20	1.0270	352	0.0221	7	83	825	57	684	12
Recent lead-loss																			
82A.17-2	316	226	0.72	0.561	0.0700	19	0.1659	45	0.1072	19	1.0347	354	0.0249	8	71	929	55	656	11
82A.2-1	312	143	0.46	5.357	0.0476	68	0.1463	16	0.0824	16	0.5403	795	0.0263	29	659	77	194	510	9
82A.29-1	381	575	1.51	0.872	0.0698	21	0.1978	52	0.0793	14	0.7632	285	0.0104	3	53	924	63	492	8
82A.4-1	564	888	1.57	1.948	0.0664	25	0.2205	60	0.0718	13	0.6581	288	0.0101	3	55	820	79	447	8
82A.17-1	238	397	1.67	1.644	0.0711	39	0.1895	92	0.0702	13	0.6883	412	0.0080	4	46	961	112	437	8
82A.5-1	621	835	1.34	3.708	0.0686	35	0.0775	81	0.0534	10	0.5052	285	0.0031	3	38	885	106	336	6
82A.30-1	584	148	0.25	3.552	0.0632	38	0.0272	88	0.0446	8	0.3887	255	0.0048	15	39	716	129	281	5
82A.13-1	539	940	1.74	2.113	0.0715	43	0.3729	110	0.0299	5	0.2943	192	0.0064	2	20	972	124	190	3

CZ3 = 01/01/97 (±1.76% 1 sigma, n=17)

4f206 = Proportion of Pb-206 calculated to be common Pb; %conc. = Concordance, as 100t[206*/238]/t[207*/206*].

Table 3

grain-spot	U (ppm)	Th (ppm)	Th U	4f206 (%)	207* 206*	+/-	208* 206*	+/-	206* 238	+/-	207* 235	+/-	208* 232	+/-	conc %	207* 206* Age (Ma)	+/-	206* 238 Age (Ma)	+/-
Inherited from Neto Rodrigues Gneisses																			
19A.4-4	262	104	0.40	0.046	0.1548	7	0.1053	11	0.4019	40	8.5777	99	0.1064	17	91	2399	8	2178	18
19A.4-1	882	396	0.45	-0.009	0.1538	4	0.1208	5	0.4051	38	8.5914	859	0.1091	12	92	2389	4	2193	17
19A.4-2	128	75	0.59	0.398	0.1498	15	0.1279	29	0.4021	42	8.3053	1257	0.0876	23	93	2344	16	2179	19
19A.4-1a	182	54	0.30	0.398	0.1451	9	0.0758	17	0.4122	102	8.2473	2175	0.1045	35	97	2289	11	2225	47
19A.4-3	234	98	0.42	0.542	0.1443	12	0.1163	23	0.3498	35	6.9577	943	0.0976	23	85	2279	14	1934	17
20A.8-1	169	75	0.45	0.033	0.1327	12	0.1358	17	0.3080	51	5.6349	1109	0.0939	20	81	2134	15	1731	25
19A.4-2a	1205	638	0.53	0.132	0.1307	4	0.1471	8	0.2018	50	3.6380	917	0.0561	14	56	2108	5	1185	27
Inherited from Transamazonian																			
19A.1-1	223	97	0.43	0.069	0.1269	7	0.1230	12	0.3717	92	6.5038	1686	0.1052	28	99	2056	9	2037	43
20A.37-1	226	25	0.11	0.043	0.1265	9	0.0299	9	0.3647	61	6.3624	1188	0.0988	35	98	2050	12	2005	29
19A.10-1	187	80	0.43	0.327	0.1195	12	0.1496	25	0.2311	23	3.8065	574	0.0812	17	69	1949	18	1340	12
19A.10-2	262	95	0.36	2.124	0.1098	23	0.1425	52	0.1976	19	2.9918	729	0.0775	30	65	1796	38	1162	10
19A.8-1	22	36	1.66	1.388	0.1047	56	0.4770	146	0.3096	48	4.4703	2550	0.0892	33	102	1710	98	1739	24
Partially reset xenocrysts																			
20A.42-1	429	187	0.44	0.453	0.0586	15	0.1294	31	0.1020	22	0.8248	290	0.0304	10	113	553	56	626	13
20A.43-1	371	90	0.24	0.092	0.0565	14	0.0676	27	0.1015	22	0.7909	276	0.0284	13	132	473	56	623	13
Magmatic																			
20A.29-4	174	149	0.86	0.074	0.0593	17	0.2594	38	0.0941	20	0.7697	285	0.0285	8	100	579	60	580	12
20A.41-1	107	89	0.83	0.343	0.0573	30	0.2546	69	0.0931	20	0.7353	433	0.0287	10	114	502	115	574	12
19A.7-4	209	76	0.36	1.606	0.0497	41	0.0926	94	0.0925	9	0.6339	529	0.0237	24	315	181	180	570	6
20A.1-1	340	211	0.62	0.186	0.0594	11	0.1919	22	0.0920	15	0.7544	193	0.0285	6	97	583	38	568	9
20A.18-1	547	288	0.53	0.116	0.0594	9	0.1556	17	0.0918	15	0.7520	174	0.0272	5	97	583	31	566	9
20A.5-2	281	220	0.78	0.200	0.0580	16	0.2331	36	0.0917	20	0.7333	269	0.0273	7	107	530	60	566	12
20A.40-1	145	146	1.00	0.372	0.0577	38	0.2913	90	0.0918	20	0.7295	528	0.0266	10	109	517	146	566	12
20A.46-1	447	187	0.42	0.275	0.0608	14	0.1280	29	0.0916	19	0.7673	257	0.0280	9	89	632	50	565	12
20A.7-2	275	268	0.97	0.598	0.0583	16	0.3030	38	0.0912	15	0.7330	245	0.0284	6	104	540	59	563	9
20A.36-2	274	126	0.46	2.071	0.0610	24	0.1499	53	0.0909	15	0.7639	340	0.0295	12	88	638	85	561	9
20A.25-1	273	166	0.61	0.279	0.0575	16	0.1892	36	0.0907	15	0.7187	249	0.0282	7	110	511	62	559	9
20A.3-2	304	227	0.75	0.178	0.0586	13	0.2243	29	0.0903	15	0.7303	212	0.0271	6	101	553	48	558	9
20A.13-2	134	184	1.38	0.491	0.0551	28	0.4105	71	0.0905	19	0.6875	391	0.0270	8	134	417	112	558	11
19A.7-1	286	169	0.59	0.015	0.0597	9	0.1826	25	0.0903	8	0.7428	138	0.0278	5	94	592	32	557	5
20A.30-2	311	122	0.39	0.239	0.0589	13	0.1161	26	0.0900	15	0.7314	217	0.0267	8	98	565	49	556	9
20A.30-4	408	134	0.33	0.143	0.0586	12	0.0980	21	0.0899	19	0.7270	224	0.0269	8	100	553	43	555	11
20A.18-2	404	205	0.51	0.210	0.0586	14	0.1576	28	0.0896	19	0.7235	241	0.0278	8	100	552	51	553	11
20A.39-2	419	234	0.56	0.291	0.0588	14	0.1666	28	0.0895	19	0.7260	240	0.0267	7	98	561	50	553	11
Modern lead-loss																			
20A.39-1	545	331	0.61	0.013	0.0588	7	0.1922	15	0.0883	15	0.7164	157	0.0279	5	97	561	28	546	9
20A.31-1	382	127	0.33	0.225	0.0576	11	0.1010	22	0.0881	15	0.7001	191	0.0269	7	106	515	43	545	9
20A.20-1	501	134	0.27	0.265	0.0595	10	0.0850	18	0.0878	14	0.7194	177	0.0280	8	93	584	36	542	9
20A.44-1	477	272	0.57	0.426	0.0582	15	0.1595	31	0.0874	19	0.7020	244	0.0245	7	100	538	55	540	11
20A.29-2	125	96	0.77	0.272	0.0612	24	0.2301	53	0.0871	14	0.7351	326	0.0260	8	83	647	84	538	9
20A.34-2	161	114	0.71	0.566	0.0600	26	0.2262	58	0.0870	14	0.7189	344	0.0276	9	89	602	93	538	9
20A.1-3	229	229	1.00	0.205	0.0583	24	0.3009	56	0.0868	19	0.6980	334	0.0261	7	99	543	88	536	11
20A.41-2	308	150	0.49	1.936	0.0576	29	0.1435	65	0.0863	19	0.6856	397	0.0254	13	104	514	112	534	11
19A.2-2	263	139	0.53	0.729	0.0560	17	0.1495	40	0.0863	21	0.6668	273	0.0244	9	118	453	66	534	13
19A.3-2	107	14	0.14	0.700	0.0558	36	0.0299	80	0.0863	21	0.6642	479	0.0191	52	120	445	144	534	13
19A.7-3	118	81	0.69	0.386	0.0563	45	0.2054	109	0.0863	9	0.6692	553	0.0258	14	115	463	179	533	5
20A.24-1	412	323	0.78	0.237	0.0582	11	0.2495	25	0.0858	14	0.6887	184	0.0273	5	99	538	42	530	8
20A.30-3	481	255	0.53	3.855	0.0566	28	0.1547	63	0.0852	18	0.6643	376	0.0248	11	111	474	110	527	11
20A.34-1	421	264	0.63	0.651	0.0578	14	0.1950	31	0.0846	14	0.6744	209	0.0263	6	100	524	53	523	8
20A.15-1	543	293	0.54	0.195	0.0582	9	0.1645	19	0.0840	14	0.6742	162	0.0256	5	97	537	34	520	8
20A.17-1	876	282	0.32	0.560	0.0605	9	0.1079	19	0.0839	14	0.7005	168	0.0281	7	83	623	33	520	8
20A.19-1	286	111	0.39	0.233	0.0581	16	0.1229	32	0.0840	14	0.6736	224	0.0265	8	97	535	59	520	8
20A.27-1	155	64	0.41	-0.020	0.0623	17	0.1430	30	0.0836	14	0.7184	238	0.0290	8	76	684	57	518	8
20A.30-1	392	181	0.46	1.031	0.0610	16	0.1509	35	0.0830	14	0.6983	233	0.0272	8	80	639	58	514	8
20A.34-3	463	296	0.64	0.970	0.0593	18	0.1912	40	0.0829	18	0.6775	268	0.0248	7	89	578	67	513	11
20A.35-2	206	127	0.62	1.165	0.0579	24	0.1812	52	0.0826	14	0.6596	303	0.0242	8	97	527	89	511	8
19A.7-2	450	220	0.49	0.746	0.0557	16	0.1413	39	0.0825	8	0.6334	201	0.0238	7	116	439	65	511	5
20A.13-1	471	201	0.43	1.292	0.0587	16	0.1239	34	0.0800	13	0.6479	215	0.0233	7	89	557	59	496	8
20A.16-1	225	89	0.40	3.941	0.0494	37	0.1114	83	0.0792	13	0.5394	426	0.0223	17	295	167	167	491	8
20A.23-2	288	225	0.78	0.990	0.0612	19	0.2199	43	0.0773	13	0.6519	245	0.0218	6	74	645	68	480	8
20A.28-1	653	208	0.32	0.681	0.0558	12	0.1022	25	0.0768	13	0.5911	171	0.0247	7	107	444	49	477	8
19A.3-1	473	257	0.54	0.358	0.0571	11	0.1538	26	0.0754	19	0.5937	195	0.0214	6	94	496	42	469	11
20A.2-1	270	128	0.47	6.734	0.0651	43	0.2051	98	0.0751	13	0.6750	478	0.0325	17	60	779	140	467	8
20A.15-3	812	401	0.49	0.504	0.0595	11	0.1533	24	0.0751	16	0.6169	187	0.0234	6	80	587	42	467	10
20A.6-1	6284	3553	0.57	0.693	0.0596	3	0.1848	7	0.0737	12	0.6057	109	0.0241	4	78	591	12	458	7
20A.25-2	601	332	0.55	0.094	0.0589	10	0.1889	20	0.0736	16	0.5982	171	0.0252	6	81	565	37	458	9

cont.. Table 3

grain-spot	U (ppm)	Th (ppm)	Th U	4f206 (%)	207* 206*	+/-	208* 206*	+/-	206* 238	+/-	207* 235	+/-	208* 232	+/-	conc %	207* 206* Age (Ma)	+/-	206* 238 Age (Ma)	+/-
20A.29-1	591	335	0.57	0.701	0.0583	12	0.1581	27	0.0728	12	0.5854	167	0.0203	5	84	541	46	453	7
19A.8-2	325	124	0.38	1.737	0.0533	34	0.0987	79	0.0728	7	0.5347	354	0.0189	15	133	340	146	453	4
20A.1-2	519	222	0.43	0.647	0.0590	15	0.1256	31	0.0725	15	0.5899	209	0.0213	7	80	567	56	451	9
20A.15-2	911	352	0.39	0.701	0.0584	11	0.1118	24	0.0712	15	0.5731	176	0.0206	6	82	544	43	443	9
20A.3-1	2045	309	0.15	5.705	0.0606	13	0.0585	29	0.0694	11	0.5801	168	0.0269	14	69	627	47	432	7
19A.6-1	338	122	0.36	5.098	0.0609	43	0.1303	100	0.0683	17	0.5732	447	0.0246	20	67	635	153	426	10
20A.14-1	1214	229	0.19	0.323	0.0604	8	0.0641	14	0.0682	11	0.5674	125	0.0232	6	69	617	28	425	7
20A.2-2	405	232	0.57	0.796	0.0589	20	0.1579	42	0.0670	14	0.5437	228	0.0185	6	74	563	73	418	9
19A.2-1	393	225	0.57	0.920	0.0604	19	0.1751	45	0.0665	16	0.5542	233	0.0203	7	67	620	67	415	10
20A.36-1	624	221	0.35	11.707	0.0604	42	0.1598	95	0.0664	11	0.5530	405	0.0299	18	67	618	150	414	7
19A.10-3	567	202	0.36	0.903	0.0581	17	0.0983	39	0.0643	6	0.5154	163	0.0177	7	75	534	64	402	4
20A.29-3	893	580	0.65	1.171	0.0612	16	0.1825	35	0.0607	13	0.5126	184	0.0171	5	59	647	57	380	8
20A.32-1	1034	316	0.31	1.146	0.0586	12	0.0974	24	0.0606	10	0.4901	134	0.0194	6	69	553	43	379	6
20A.34-4	694	249	0.36	1.691	0.0608	22	0.1325	48	0.0591	13	0.4953	219	0.0218	9	58	633	78	370	8
20A.2-3	776	399	0.51	1.373	0.0573	18	0.1535	38	0.0587	13	0.4635	183	0.0176	6	73	501	67	368	8
20A.7-1	537	328	0.61	0.890	0.0576	15	0.1702	33	0.0540	9	0.4287	139	0.0150	4	66	515	57	339	5
20A.26-1	1803	725	0.40	0.607	0.0586	8	0.1417	16	0.0534	9	0.4313	97	0.0188	4	61	551	29	335	5
20A.35-1	501	308	0.62	8.479	0.0601	40	0.1978	91	0.0519	9	0.4306	305	0.0167	8	54	608	144	326	5
20A.23-1	1714	873	0.51	0.852	0.0591	9	0.1276	19	0.0514	8	0.4186	99	0.0129	3	57	570	32	323	5
20A.38-2	1886	765	0.41	1.596	0.0583	11	0.1377	24	0.0489	8	0.3928	105	0.0166	4	57	540	42	308	5
20A.7-3	806	585	0.73	2.699	0.0578	26	0.2154	58	0.0490	10	0.3900	201	0.0145	5	59	521	97	308	6
19A.9-2	677	249	0.37	1.314	0.0578	22	0.1425	53	0.0489	5	0.3898	160	0.0190	7	59	522	85	308	3
20A.38-1	675	244	0.36	6.067	0.0549	30	0.1434	68	0.0469	8	0.3546	211	0.0186	9	73	407	123	295	5
20A.11-1	1557	2455	1.58	2.786	0.0643	17	0.4461	42	0.0442	7	0.3917	131	0.0125	2	37	752	57	279	4
20A.44-2	2220	867	0.39	1.226	0.0601	12	0.1242	26	0.0435	9	0.3605	112	0.0138	4	45	607	44	275	6
20A.33-1	1336	264	0.20	3.428	0.0614	20	0.0567	44	0.0418	7	0.3539	137	0.0120	10	40	654	71	264	4
19A.9-1	996	231	0.23	1.665	0.0543	26	0.0964	59	0.0413	4	0.3090	152	0.0172	11	68	382	106	261	2
20A.12-1	5017	939	0.19	3.765	0.0596	10	0.0696	23	0.0395	7	0.3248	82	0.0147	5	42	588	38	250	4
20A.11-2	1219	2451	2.01	2.197	0.0663	24	0.5808	61	0.0377	8	0.3443	151	0.0109	3	29	816	75	238	5
20A.22-1	1685	333	0.20	17.464	0.0483	42	0.0736	96	0.0362	6	0.2415	221	0.0135	18	199	116	155	229	4
20A.45-1	1257	471	0.37	32.662	0.0638	83	0.2324	189	0.0342	8	0.3009	404	0.0212	18	29	736	277	217	5
20A.5-1	3317	1789	0.54	1.016	0.0550	9	0.1537	18	0.0294	5	0.2231	53	0.0084	2	46	410	35	187	3

CZ3 = 9519A, 05/01/96 (± 2.46% 1 sigma, n=10) 31/10/96 (± 0.92% 1 sigma, n= 8); 9520 A, 03/10/95 (±1.64% 1 sigma, n= 13) 01/08 96 (±2.12%, n= 13)
4f206 = Proportion of Pb-206 calculated to be common Pb; %conc. = Concordance, as 100t[206*/238]/t[207*/206*].

Table 4

Sample name	Sample location	Mineral	δ34S ‰ CDT	206Pb 204Pb	207Pb 204Pb	208Pb 204Pb	Occurrence
A2- 70.35	Andradas	Bornite	-6.3	19.465	15.62	37.655	Massive vein in albite-chlorite schist
A2-74.3	Andradas	Bornite	-11.2	-	-	-	Massive vein in albite-chlorite schist
A2-81.4	Andradas	Chalcopyrite	-5.7	19.619	15.636	40.127	Massive vein in albite-chlorite schist
AGAL-N	Andradas	Chalcocite	2.1	-	-	-	Cataclastic zone
AND-GE	Andradas	Chalcocite	0.2	-	-	-	Cataclastic zone
AND-TR	Andradas	Chalcocite	2.0	-	-	-	Cataclastic zone
GAL-II-7	Santa Barbara	Chalcopyrite	-13.4	-	-	-	Barite-chalcopyrite vein
GAL II-5 cpy	Santa Barbara	Chalcopyrite	-15.2	17.716	15.505	37.914	Barite-chalcopyrite vein
GAL-II-6	Santa Barbara	Barite	8.5	-	-	-	Barite-chalcopyrite vein
GAL-II-5	Santa Barbara	Barite	7.6	-	-	-	Barite-chalcopyrite vein
FAX	Faxinal	Galena	-4.3	16.649	15.443	37.14	Quartz vein in metamarl
DLF-I2 py	Coronel Linhares	Pyrite	4.7	20.267	15.687	42.041	Skarn - contact between altered granite and marble
DLF-I2-cpy	Coronel Linhares	Chalcopyrite	4.4	17.538	15.518	38.39	Skarn - contact between altered granite and marble
DLF	Coronel Linhares	Chalcopyrite	4.7	17.083	15.497	37.671	Skarn - contact between altered granite and marble
DLF-1	Coronel Linhares	Pyrite	4.9	-	-	-	Skarn - contact between altered granite and marble
CEL-PC py	Coronel Linhares	Pyrite	4.1	17.516	15.533	36.817	Skarn in marble
CEL-PC cpy	Coronel Linhares	Chalcopyrite	3.9	17.971	15.56	38.391	Skarn in marble
FSI-3	Cioccari Prospect	Chalcopyrite	10.8	-	-	-	Vein in marbles
FS-1	Cioccari Prospect	Chalcopyrite	10.7	16.555	15.464	37.113	Vein in marbles

Table 5

Sample	Unit	Material	SiO2 (%)	U (whole rock ppm)	Th	Pb	206Pb 204Pb	207Pb 204Pb	208Pb 204/Pb
FS-5	Caçapava Granite	K-feldspar	-	-	-	-	15.602	15.466	36.497
PG	Caçapava Granite	K-feldspar	-	-	-	-	15.991	15.522	36.533
PG-R	Caçapava Granite	K-feldspar	-	-	-	-	15.997	15.531	36.553
E	Caçapava Granite	K-feldspar	-	-	-	-	16.027	15.514	36.574
F	Caçapava Granite	K-feldspar	-	-	-	-	16.064	15.584	36.760
FS-5 wr	Caçapava Granite	Granodiorite	70.2	2.4	8.3	1.5	16.655	15.602	37.182
PG-wr	Caçapava Granite	Leucogranite	76.2	2.6	12	5.0	16.310	15.516	36.684
E-wr	Caçapava Granite	Monzogranite	72.1	3.2	12.3	2.0	16.692	15.548	37.279
F-wr	Caçapava Granite	Monzogranite	72.4	4.7	10	2.5	16.882	15.615	37.219
B-plag	Passo Feio Formation	Plagioclase	-	-	-	-	17.793	15.541	37.436
A-wr	Passo Feio Formation	Chlorite schist	60.9	2.1	5.5	1.0	18.312	15.573	38.385
B-wr	Passo Feio Formation	Chlorite schist	58.0	1.5	5.1	1.0	19.006	15.605	39.188
CAC-wr	Passo Feio Formation	Metamarl	47.9	0.2	0.4	1.0	16.869	15.441	37.093
PT-02wr	Passo Feio Formation	Amphibolite	49.3	1.0	3.5	2.0	16.353	15.401	36.612

Table 6

Barite samples	7200	GAL-II-1	GAL-II-4
$^{87}Sr/^{86}Sr$	0.70652	0.70688	0.70653